LEWIS ACID PROPERTIES OF THE XeF^+ CATION

AND

ITS ADDUCTS WITH ORGANIC NITROGEN BASES

By

ADEL ABBAS AHMED EMARA, B.Sc., M.Sc.

A Thesis

Submitted to the School of Graduate Studies

in Partial Fulfilment of the Requirements

for the Degree

Doctor of Philosophy

McMaster University

November 1991

LEWIS ACID PROPERTIES OF THE XeF^+ CATION AND ITS ADDUCTS WITH ORGANIC NITROGEN BASES

DOCTOR OF PHILOSOPHY (1991) McMASTER UNIVERSITY

(Chemistry) Hamilton, Ontario

TITLE: Lewis Acid Properties of the XeF^+ Cation and Its Adducts with Organic Nitrogen Bases

AUTHOR: Adel Abbas Ahmed Emara, B.Sc., M.Sc. (Ain-Shams University)

SUPERVISOR: Professor G.J. Schrobilgen

NUMBER OF PAGES: xxiii, 300

ABSTRACT

This Thesis describes the syntheses and spectroscopic characterization of noble-gas compounds containing Xe-N bonds in solution by multinuclear magnetic resonance (multi-NMR) spectroscopy and in the solid state by low-temperature Raman spectroscopy.

The present work represents an extension of noble-gas chemistry, and in particular, the synthesis of novel xenon-nitrogen bonded compounds. The key synthetic approach involves the interaction of the Lewis acid XeF^+ with an organic nitrogen Lewis base, where the organic nitrogen base must be resistant to oxidation by the XeF^+ cation. Hydrogen cyanide, alkyl nitriles, perfluorophenyl nitrile and perfluoropyridine derivatives were investigated as potential ligands for xenon(II). The electron lone pairs of nitriles and perfluoropyridines have been shown to interact with the Lewis acid XeF^+ resulting in the cations $RC{\equiv}N\text{-}XeF^+$ (R = H, CH_3, CH_2F, CH_2Cl, C_2H_5, CH_2FCH_2, *n*-C_3H_7, $CH_2FCH_2CH_2$, CH_3CHFCH_2, $CHF_2CH_2CH_2$, $CH_3CF_2CH_2$, *n*-C_4H_9, $CH_3CHFCH_2CH_2$, $(CH_3)_2CH$, $(CH_3)_3C$, $FCH_2C(CH_3)H$, $ClCH_2C(CH_3)H$ and C_6F_5) and $R_FC_5F_4N\text{-}XeF^+$ (R_F = F, 2-CF_3, 3-CF_3, 4-CF_3). These cations have been characterized in HF and/or BrF_5 by ^{129}Xe, ^{19}F, ^{15}N, ^{14}N, ^{13}C and ^1H NMR spectroscopy and in the solid state by low-temperature Raman spectroscopy.

The hydrogen cyanide, alkyl nitriles and perfluorophenyl nitrile adducts represent the first examples of xenon bonded to nitrogen that is formally sp hybridized. The perfluoropyridine adducts are the first examples of xenon bonded to aromatic rings.

The thermal stabilities of $RC{\equiv}N\text{-}XeF^{+}AsF_6^{-}$ salts have been examined by warming HF solutions of $RC{\equiv}N$ (R = H, CH_3, C_2H_5, *n*-C_3H_7 and *n*-C_4H_9) and $XeF^{+}AsF_6^{-}$ for several hours at room temperature. The stabilities of $RC{\equiv}N\text{-}XeF^{+}AsF_6^{-}$ salts with respect to alkyl chain fluorination depend on the chain-length of the alkyl group, decreasing in the order: *n*-$C_4H_9C{\equiv}N$ > *n*-$C_3H_7C{\equiv}N$ > $HC{\equiv}N$ > $C_2H_5C{\equiv}N$ > $CH_3C{\equiv}N$.

The decomposition products of $HC{\equiv}N\text{-}XeF^{+}$ have been characterized by ^{1}H, ^{13}C, ^{15}N, ^{14}N and ^{19}F NMR spectroscopy, for natural abundance, 99.3% ^{13}C-enriched $[^{13}C]HC{\equiv}N\text{-}XeF^{+}AsF_6^{-}$ and 99.7% ^{15}N-enriched $[^{15}N]HC{\equiv}N\text{-}XeF^{+}AsF_6^{-}$. Among the decomposition products that were identified were CF_3H, CF_4, $CF_3NH_3^{+}$, $CF_2{=}NH_2^{+}$ and $HFC{=}NH_2^{+}$. The NMR spectra of $HC{\equiv}N$ recorded at -15 °C in HF after warming for 7 days at room temperature indicate that one species, $CHF_2NH_3^{+}$, was formed, which presumably arises from the stepwise addition of HF.

The solvolytic behaviors of the adduct salts, $RC{\equiv}N\text{-}XeF^{+}AsF_6^{-}$, have also been studied in anhydrous HF solvent. The decompositions of the nitrile adduct cations $CH_3(CH_2)_nC{\equiv}N\text{-}XeF^{+}$ (n = 0 - 3) have been monitored in HF solution by multi-NMR spectroscopy. The rate of fluorination of the alkyl chain was shown to increase with increasing chain length, where the degree of fluorination increases at the alkyl carbons in the order $\beta < \gamma < \delta$, with no fluorination being observed at the α-carbon. A parallel study of the alkyl nitriles $RC{\equiv}N$ (R = CH_3, C_2H_5, *n*-C_3H_7 and *n*-C_4H_9) in HF showed the fluorination products are significantly different. The reaction mechanisms of the fluorination reactions have been proposed, i.e., the former is a radical-substitution reaction and the latter is an addition reaction and dimerization.

ACKNOWLEDGEMENTS

I wish to express my gratitude to Prof. G.J. Schrobilgen, for his enthusiasm, interest and guidance throughout the course of this study.

The interest and help shown by Prof. R. Bell and Dr. J. Barbier, who both served on my Ph.D. supervisory committee, is gratefully acknowledged.

I gratefully acknowledge Dr. D.W. Hughes, Mr. B. Sayer and Mr. J.I.A. Thompson for their instruction and technical assistance on the NMR spectrometers.

I am also grateful to the many people I have come to know during my stay at McMaster. I will always remember their friendship and hospitality with pleasure. In particular, I wish to thank Dr. Már Björgvinsson, Ms. Jónína Valsdóttir, Mr. Kenneth M. Mitchell, Dr. Jeremy C.P. Sanders, Dr. Hélène P. Mercier, Mr. Hosen Alarabi, Mr. J. Marc Whalen and Mrs. Carol Dada.

I gratefully acknowledge the financial support of the Department of Chemistry in the form of scholarships and teaching assistantships (1986 - 1991) and the Provincial Government of Ontario for tuition fee waivers (1987 - 1990).

TABLE OF CONTENTS

LIST OF TABLES

LIST OF FIGURES

CHAPTER 1

INTRODUCTION

GENERAL BACKGROUND

The elements that comprise Group VIII (18) of the periodic table were, until 1962, inappropriately termed the "inert gases". The discovery of the first true compound of a noble-gas, namely, $Xe^{+}PtF_6^{-}$ by Bartlett[1] made the term "inert" immediately obsolete. Since then, the Group VIII elements have been more justifiably called the noble-gas elements and aside from He, Ne and Ar, form compounds with highly electronegative elements or ligands.

It was quickly realized that KrF_2 and the fluorides and oxofluorides of xenon bear remarkable similarities in their chemical and structural properties to those of the neighboring halogen fluorides and oxofluorides. As various spectroscopic techniques such as X-ray crystallography, vibrational spectroscopy and multinuclear magnetic resonance spectroscopy began to be applied, the structures and bonding of the compounds were elucidated and analogies to the halogen compounds strengthened. There are several excellent reviews available which cover most of the developments in the field of noble-gas chemistry except those from 1984 to the present.[2-6] Those areas not previously reviewed are briefly summarized in this Chapter in order to put the present work into

perspective.

The valence shell electron pair repulsion rules[7] have proven to be a useful tool for predicting the structures of the binary fluorides, oxides and the oxofluorides as well as their cationic and anionic derivatives.[3] For compounds with coordination numbers of six or less (including nonbonding electron pairs) this model predicts, successfully, the correct geometry. The geometries of compounds having coordination numbers exceeding six are also predicted as can be seen for XeF_6 (AX_6E) in the gas phase, a distorted octahedron;[8,9] XeF_5^- (AX_5E_2), pentagonal planar;[10] IOF_6^-, $TeOF_6^{2-}$ [11] and IF_7 (AX_7),[12] pentagonal bipyramidal and TeF_8^{2-} [11] and IF_8^{2-} (AX_8), square antiprismatic.

The ability of electronegative elements to form bonds to xenon in isolable compounds is now established for fluorine, oxygen, nitrogen and carbon. In addition to the simple fluorides of xenon XeF_2,[13] XeF_4 [14] and XeF_6[15] and the oxofluorides $XeOF_2$,[16] XeO_2F_2 [17] and $XeOF_4$,[18] a number of fluoride and oxofluoride xenon "adducts" are known. The neutral compounds can behave as fluoride ion donors in the presence of a strong fluoride ion acceptor or, with the exception of XeF_2, can behave as a fluoride ion acceptor towards an appropriate fluoride ion donor. The fluoride acceptor properties of high-valent xenon fluorides is illustrated by the recent preparation of XeF_5^-.[10] The formation of complexes as salt-like species containing well-defined cations or anions should, however, be approached with a certain amount of caution. This is particularly well illustrated with xenon difluoride adducts which span the gamut of complexes from salt-like species such as $XeF^+Sb_2F_{11}^-$,[19] to covalent adducts like $XeF_2.XeOF_4$.[3] In the latter, the components preserve their molecular identities and dimensions and the adduct is clearly covalent, but

even in the former the relatively short Xe...F bridge distance (2.34 Å) between the XeF^+ cation and the $Sb_2F_{11}^-$ anion, a weak fluoride-ion-base anion, implies considerable covalent character (cf. van der Waals contact distance, 3.50 Å).

The criteria which have been drawn upon in assuming the degrees of covalent bonding in noble-gas compounds are based mainly on bond distances obtained from X-ray crystal structure determinations, stretching frequencies of both terminal and bridging fluorine bonds and ^{19}F and ^{129}Xe NMR chemical shift data. Clear correlations exist among all of these. The NMR evidence (^{129}Xe chemical shifts, ^{19}F chemical shifts and ^{129}Xe-^{19}F coupling constants) provide an internally consistent picture of the electronic structure of the covalent xenon compounds. Schrobilgen *et al.*[20] have shown that the empirical plot of xenon chemical shifts *versus* the fluorine chemical shifts of the terminal fluorine on Xe(II) for species containing fluorine-bridges are near linear (Figure 1.1) and that XeF groups bonded to a ligand through oxygen constitute a separate near linear plot with the two plots converging near XeF^+. There are also smooth curves correlating $^1J(^{129}Xe$-$^{19}F)$ values and ^{19}F chemical shifts for all oxidation states of xenon (Figure 1.2).[21] The covalent nature of the Xe-F bond is seen to increase with increasing ^{129}Xe and decreasing ^{19}F chemical shifts and also correlates with the decrease in bond length observed for the Xe(II) species with increasing XeF^+ character. The latter trends are further corroborated by trends in Xe-F stretching frequency, which increase with increasing XeF^+ character.[21] However, a study of the ^{129}Xe resonance is of particular value from the stand point of some structural considerations, especially when only one fluorine directly bonded to xenon is present. Thus, based on their multiplicities and relative

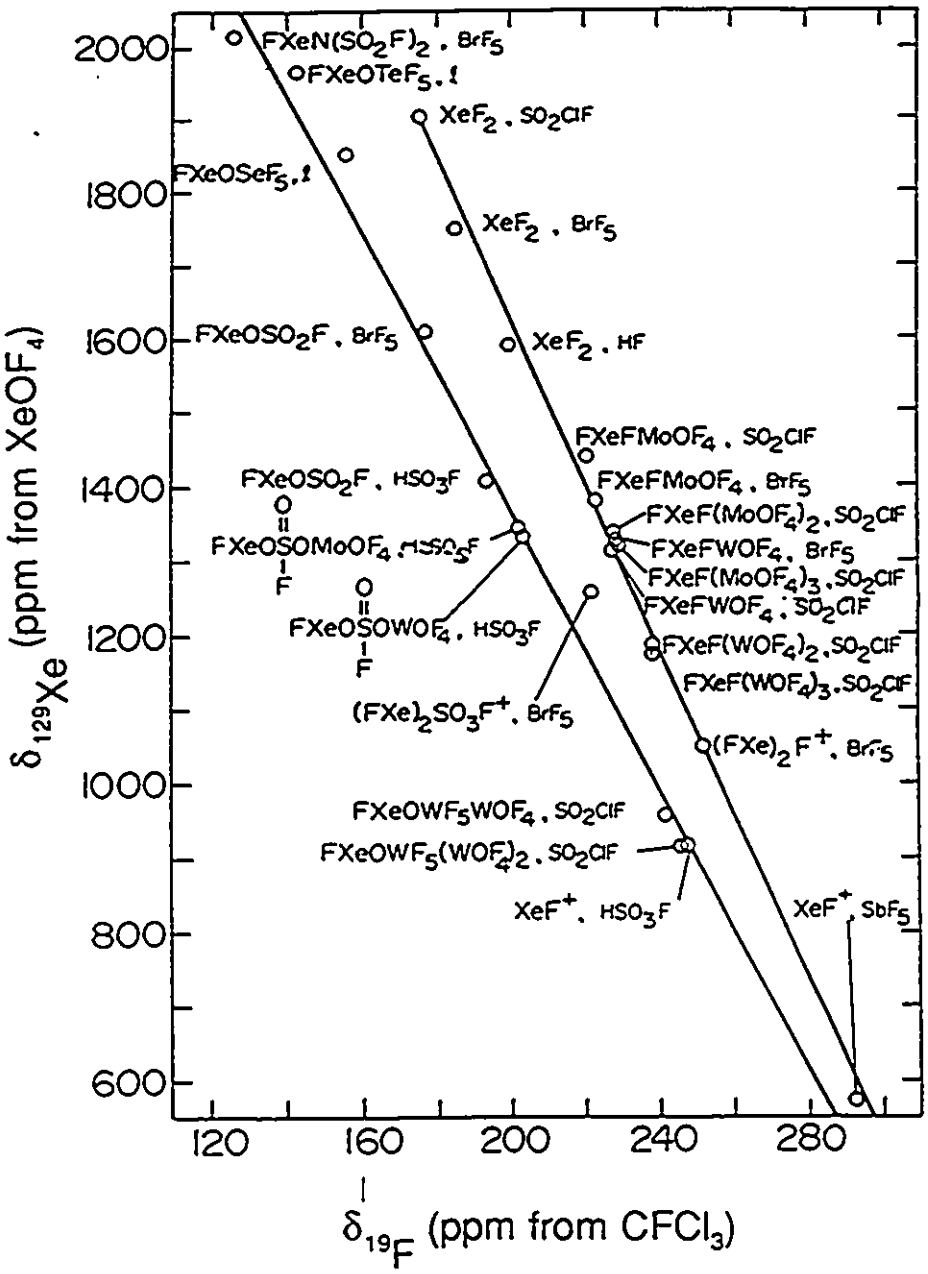

Figure 1.1 Empirical plot of ^{129}Xe chemical shifts *versus* ^{19}F chemical shifts of the terminal fluorine on xenon for some Xe(II) species containing F-bridges (upper line) and O-bridges (lower line). From ref.(20).

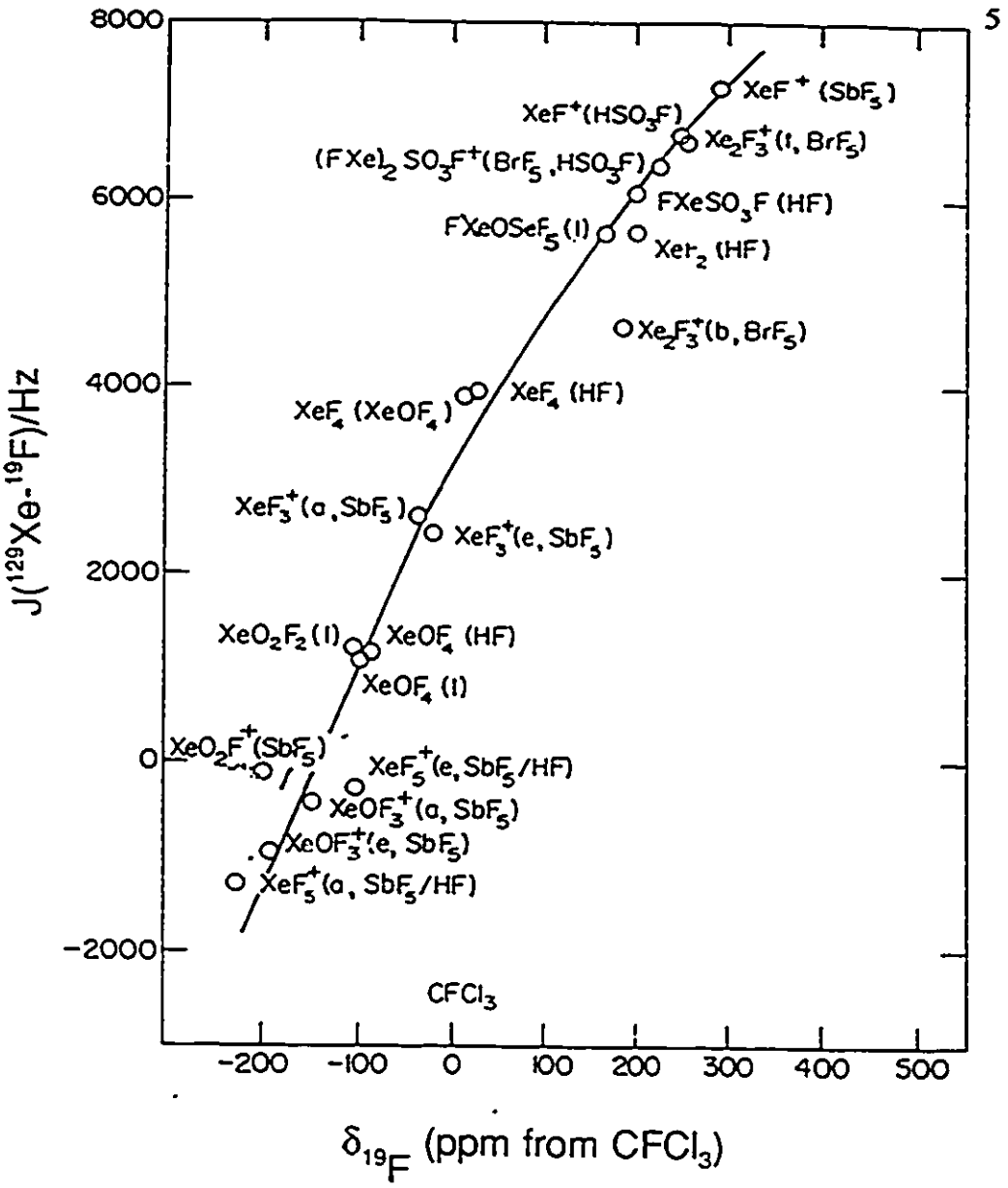

Figure 1.2 Correlation of ^{19}F chemical shifts and $J(^{129}Xe\text{-}^{19}F)$ coupling constants for some xenon compounds. The solvent medium conditions are given in parantheses after the molecular formula. a, axial; e, equatorial; b, bridging; t, terminal; l, neat liquid. From ref. (21).

intensities, the observed splittings arising from $^1J(^{129}Xe\text{-}^{19}F)$ can be used to confirm the structures of species such as XeO_2F_2, XeF_4, $XeOF_4$, $(FXe)_2F^+$ and $(FXe)_2SO_3F^+$.

(A) XENON FLUORIDE ADDUCTS

The compounds XeF_2 and XeF_6 form stable complexes with a number of fluoride-ion acceptors having compositions $2XeF_n.MF_5$, $XeF_n.MF_5$ and $XeF_n.2MF_5$ (n = 2 or 6).[3] Both salt and fluorine-bridged formulations have been suggested to explain the bonding in these adducts. However, it is clear that xenon difluoride-metal pentafluoride adducts have vibrational spectra which can be interpreted on the basis of the ionic formulations $XeF^+M_2F_{11}^-$, $XeF^+MF_6^-$ and $Xe_2F_3^+MF_6^-$. There is, however, a considerable amount of covalent interaction between the cation and anion by means of Xe...F-M bridges.[22-24] It has also been established that the degree of ionic character in the adducts is dependent upon the Lewis acid properties of the pentafluoride.[25-27]

The pseudo-octahedral XeF_5^+ cation (C_{4v}) is amply confirmed in the solid phase. In fact, XeF_5^+ has been established in a number of adducts through detailed single crystal structure determinations on, namely, $XeF_5^+RuF_6^-$,[28] $XeF_5^+PtF_6^-$ [29,30] and $(XeF_5^+)_2PdF_6^{2-}$ [31] as well as less comprehensive data on $XeF_5^+BF_4^-$,[29] $XeF_5^+AuF_6^-$ [29] and $XeF_5^+UF_6^-$.[32]

The $Xe_2F_{11}^+$ ion consists of two XeF_5^+ groups joined by a common fluoride ion (fluorine bridge). The XeF_5 adducts which contain the $Xe_2F_{11}^+$ cation are: $2XeF_6.RuF_5$, $2XeF_6.IrF_5$,[33] $2XeF_6.PtF_5$,[34] $2XeF_6.AuF_5$,[35-37] $2XeF_6.PF_5$,[29,34,38], $2XeF_6.AsF_5$,[29,33,38] $2XeF_6.SbF_5$,[36] $4XeF_6.PdF_4$[35] and $(Xe_2F_{11}^+)_2NiF_6^{2-}$.[39] The ionic description $(XeF_5)^+F^-(XeF_5)^+$

thus appears to provide a fairly good description of the species, although a certain measure of covalency in terms of $(XeF_5^+)XeF_6$ should be introduced as suggested by departure of the Xe-F-Xe angle (169.2°) from linearity. The interatomic bridging distances are 2.21 and 2.26 Å, respectively.

The corresponding chemistry of XeF_4 is considerably more sparse. The only adducts which have been isolated at room temperature are $XeF_4.SbF_5$,[40-42] $XeF_4.2SbF_5$,[40,43] $XeF_4.BiF_5$ and $XeF_4.2BiF_5$.[44] As a result, it has been concluded the XeF_4 is a much weaker fluoride-ion donor and that fluoride ion donor abilities among the binary xenon fluorides decrease in the order $XeF_6 > XeF_2 >> XeF_4$.[7] However, the relative order of fluoride ion donor abilities of XeF_2 and XeF_4 has been disputed. Using as criteria: (a) the average length of the Xe...F bridge, which decreases in the series $[F_5Xe]^+$...F, $[F_3Xe]^+$...F and $[FXe]^+$...F, (b) the directionality of the secondary bridge bonds, which form in directions which avoid both the bonding pairs and the presumed location of nonbonding pairs in the xenon valence shell of the cations, and (c) the number of bridge bonds, which increases with decreasing strength of the bridge bonds, the fluoride ion acceptor abilities of the cations increase in the order $XeF_5^+ < XeF_3^+ < XeF^+$.[43]

(B) COVALENT DERIVATIVES OF XENON(II) IN WHICH XENON IS BONDED TO A SECOND ROW ELEMENT OTHER THAN FLUORINE

(i) Xenon-Oxygen Bonded Compounds

The ligand groups which form xenon-oxygen bonds are $-OSO_2F$,[45,46] $-OTeF_5$,[47-54] $-OPOF_2$,[47-55] $-OSeF_5$,[56,57] $-OClO_3$,[45,46] $-OCOCF_3$,[50,58] $-OSO_2CF_3$,[46] $-ONO_2$ [59] and $-OIOF_4$.[60]

Each of these groups exists in the form of a moderate to strong monoprotic acid (i.e., $HOSO_2F$, $HOTeF_5$, $HOIOF_4$) and, in addition, the effective group electronegativities of these groups are very high and, in some cases, approach that of fluorine itself. Table 1.1 summarizes all the known neutral covalent oxygen ligand-group derivatives of xenon and their physical properties. From inspection of Table 1.1 it is evident that the $-OTeF_5$ group is second only to oxygen and fluorine in its ability to stabilize the +4 and +6 oxidation states of xenon.

The thermal stability of ligand-group derivatives of xenon vary, but in any case, are less stable than those of their corresponding binary fluorides or oxofluorides. This fact is clearly illustrated by comparing the decomposition temperatures for XeF_4 (330 °C) and $Xe(OTeF_5)_4$ (72 °C). The vast difference presumably arises from the fact that the peroxide $F_5TeO\text{-}OTeF_5$ is formed much more readily than F_2 (equations (1.1) and (1.2)) as well as the relative bond strengths, i.e., Xe-O < Xe-F.

$$XeF_4 \xrightarrow{300\text{-}600\ ^\circ C} XeF_2 + F_2 \qquad (1.1)$$

$$Xe(OTeF_5)_4 \xrightarrow{72\ ^\circ C} Xe(OTeF_5)_2 + F_5TeO\text{-}OTeF_5 \qquad (1.2)$$

Furthermore, the thermal stabilities of xenon(II) derivatives increase in the order $-OSO_2F$ < $-OSeF_5$ < $-OTeF_5$, and are consistent with the decreasing stabilities of the corresponding peroxides. This trend is exemplified by the $-OClO_3$ and $-OCOCF_3$ derivatives of xenon(II). Whereas $Xe(OClO_3)_2$ decomposes above -20 °C and $Xe(OCOCF_3)_2$ detonates above -20 °C, the corresponding decomposition products, Cl_2O_7 and $CF_3OCO\text{-}OCOCF_3$,

Table 1.1

Known Oxygen Ligand-Group Derivatives of Xenon and Their Physical Properties

Oxidation State	Compound	Form	Remarks	Ref.
II	$FXeOTeF_5$	Pale-yellow liquid	m.p. = -24 °C, b.p. 53 °C	(47)
	$FXeOSO_2F$	White solid	m.p. = 36.6 °C Yellow-green	(45)
	$Xe(OTeF_5)_2$	White solid	m.p. = 35-37 °C	(48)
	$Xe(OSO_2F)_2$	Yellow solid	m.p. = 43-45 °C	(45)
	$FXeOPOF_2/Xe(OPOF_2)_2$	Pale-yellow solids	decomposes at room temperature	(55)
	$FXeOClO_3$	White solid	m.p. = 16.5 °C	(46)
	$Xe(OClO_3)_2$	Pale-yellow solid	decomposes above -20 °C	(45)
	$FXeOCOCF_3/Xe(OCOCF_3)_2$	Pale-yellow solids	explode above -20 °C	(50)
	$FXeOSO_2CF_3$	Yellow solid at 0 °C	decomposes slowly at 0 °C	(46)
	$FXeOSeF_5$	Pale-yellow liquid	m.p. = -13 °C	(56)
	$Xe(OSeF_5)_2$	Yellow solid	m.p. = 69 °C	(56)
	$FXeONO_2/Xe(NO_2)_2$ [a]	[Red-brown solids]	decompose rapidly at RT	(59)
	$FXeOIOF_4$	Light yellow liquid at RT	m.p. = -5 - 0 °C	(60)
	$Xe(OIOF_4)_2$	Pale-yellow solid at RT	decompose at RT under vacuum	(60)
IV	$Xe(OTeF_5)_4$	Pale-yellow solid	m.p. = 72 °C with decomposition	(51)
VI	$OXe(OTeF_5)_4$	White solid	m.p = 56 °C	(52)
	$O_2Xe(OTeF_5)_2$	White solid	decomposes above 0 °C	(54)
	$[Xe(OTeF_5)_6]$ [b]	Red/violet solid at -40 °C	m.p. = -10 °C	(52)

a Evidence for $FXeONO_2$ is based on decomposition products only.[59]

b Evidence for $Xe(OTeF_5)_6$ is based on decomposition products[52] and preliminary X-ray analysis.[53]

are stable up to their boiling points, (Cl_2O_7 b.p. = 82 °C,[61] $CF_3CO\text{-}OCOCF_3$ b.p. = 40 °C[62]) if not shocked.

(ii) Xenon-Nitrogen Bonded Compounds

Meinert and Rüdiger[59] studied the reaction of XeF_2 in $CH_3C{\equiv}N$ with 2,2′-bipyridine to form a 1:2 complex which was characterized by infrared spectroscopy, however, no convincing physical evidence has been given in support of the formation of Xe-N bonded species.

Compounds containing xenon-nitrogen bonds have been reported relatively recently and include neutral species $FXeN(SO_2F)_2$,[64,65,66] $Xe[N(SO_2F)_2]_2$[65,67] and $Xe[N(SO_2CF_3)_2]_2$[68] and the cations $XeN(SO_2F)_2^+$ [69] and $F[XeN(SO_2F)_2]_2^+$.[65,69,70]

Under very carefully controlled conditions, $HN(SO_2F)_2$ and XeF_2 react to form $FXeN(SO_2F)_2$ (equation (1.3)).

$$XeF_2 + HN(SO_2F)_2 \xrightarrow[4\ \text{days}]{CF_2Cl_2,\ 0\ ^\circ C} FXeN(SO_2F)_2 + HF \qquad (1.3)$$

An X-ray single crystal study has shown that the solid consists of $FXeN(SO_2F)_2$ molecules[64] of molecular point symmetry C_2 in which the xenon atom of the Xe-F group is bonded to the nitrogen (illustrated in Figure 1.3). This structure gives the first definitive proof for the existence of a stable xenon-nitrogen bond.[64] Using the bond order-bond length relationship of Pauling for the calculation of terminal Xe-F order, the Xe-F bond of $FXeN(SO_2F)_2$ has a bond order of 0.59 compared to ½ for XeF_2 making the

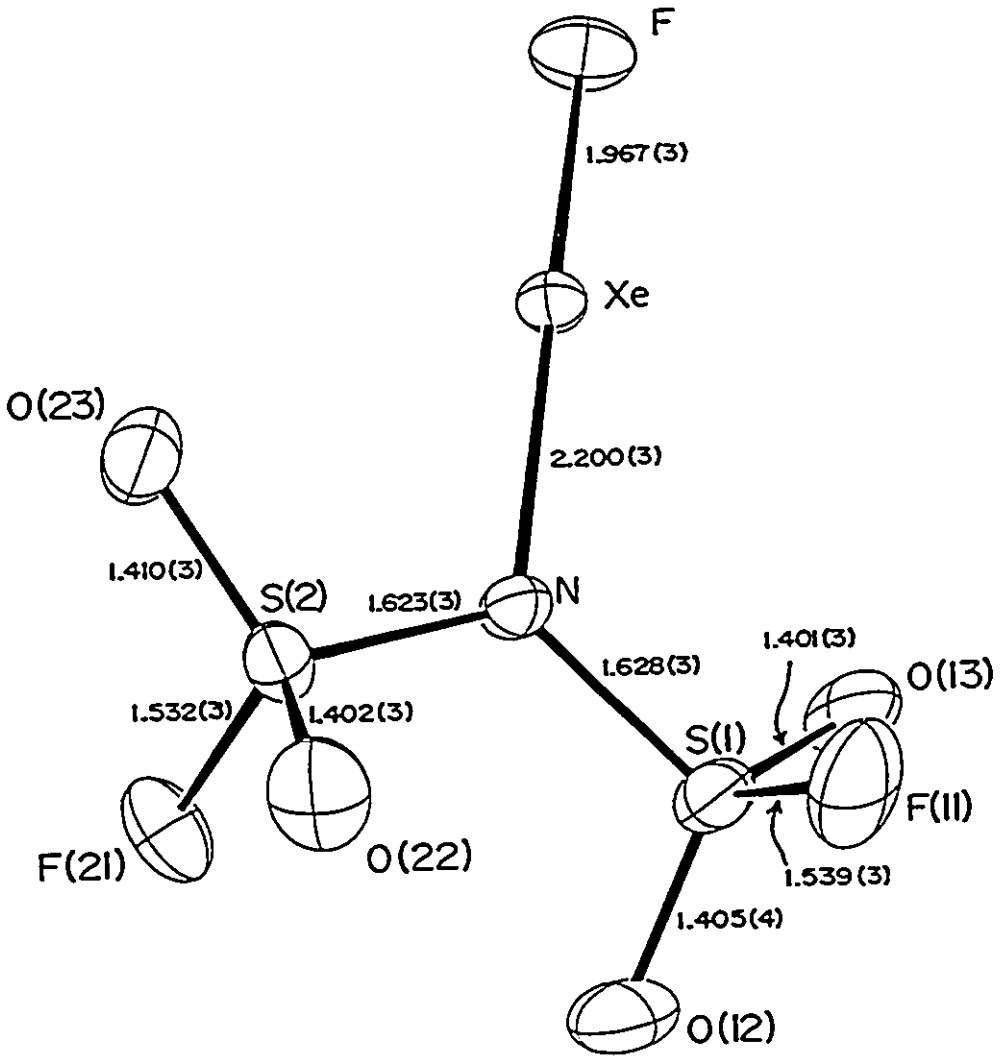

Figure 1.3 X-ray crystal structure of $FXeN(SO_2F)_2$.[64]

Xe-F bond of $FXeN(SO_2F)_2$ the most XeF_2-like bond encountered thus far. As has been proposed for other xenon(II) compounds, the bonding description of $FXeN(SO_2F)_2$ can be represented as a resonance hybrid of valence bond Structures I and II. This result for the Xe-F bond order implies that valence bond Structure I only has a 59 : 41 dominance over

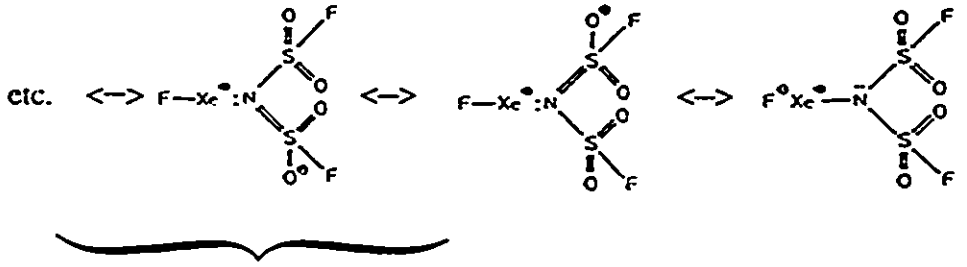

I II

valence bond Structure II. The Xe-F stretching mode in the Raman spectrum of the solid at 506 cm^{-1} is the lowest value of ν(XeF), observed thus far for an F-Xe-Y[64] type structure which is less than those observed in $FXeOSO_2F$ (528 cm^{-1})[25] and $FXeOTeF_5$ (520 cm^{-1}).[50] In view of the very small shift from the value of the XeF stretching frequency in XeF_2 (497 cm^{-1}), the increase in the amount of Xe-F$^+$ character relative to that of XeF_2 must be very small (if XeF_2 is represented as $F\text{-}Xe^+F^- \longleftrightarrow F^-XeF^+$). A similar conclusion can be drawn from ^{19}F and ^{129}Xe data. The similarity of $FXeN(SO_2F)_2$ and XeF_2 chemical shifts relative to those in other xenon(II) compounds is a clear indication that the bonding in the F-Xe-N moiety is similar to that in XeF_2 itself.

The compound, $Xe[N(SO_2F)_2]_2$, was formed under similar conditions used to form $FXeN(SO_2F)_2$, but a 2:1 ratio of $HN(SO_2F)_2$ to XeF_2 was used instead (equation (1.4)).[64]

$$XeF_2 + 2\ HN(SO_2F)_2 \xrightarrow[0\ ^\circ C]{CF_2Cl_2} Xe[N(SO_2F)_2]_2 + 2\ HF \qquad (1.4)$$

The white solid, $Xe[N(SO_2F)_2]_2$, melts near room temperature with rapid decomposition according to equation (1.5).

$$Xe[N(SO_2F)_2]_2 \longrightarrow Xe + [N(SO_2F)_2]_2 \qquad (1.5)$$

A ligand transfer reagent has also been used in the preparation of an Xe-N bonded derivative. DesMarteau and Foropoulos[68] have shown that by reacting the silylimide precursor $Me_3SiN(SO_2CF_3)_2$, prepared according to equation (1.6), with XeF_2 (equation (1.7)) the Xe-N bonded product $Xe[N(SO_2CF_3)_2]_2$ is obtained in high yield. In addition, the formation of HF, which is a major problem in acid displacement reactions of the type illustrated by equations (1.3 and 1.4) is eliminated by this approach.

$$Me_3SiH + (CF_3SO_2)_2NH \xrightarrow{-196\ \text{to}\ 22\ ^\circ C} Me_3SiN(SO_2CF_3)_2 + H_2 \qquad (1.6)$$

$$2\ Me_3SiN(SO_2CF_3)_2 + XeF_2 \xrightarrow[CF_2Cl_2]{-22\ \text{to}\ 10\ ^\circ C} Xe[N(SO_2CF_3)_2]_2 + 2\ Me_3SiF \qquad (1.7)$$

Equation (1.7) represents the only method where a metathesis reaction, apart from HF

metathesis (acid displacement) has been used to prepare a xenon-nitrogen derivative.

The first xenon-nitrogen adduct with a Lewis acid reported possessed the stoichiometry $2FXeN(SO_2F)_2.AsF_5$ and was postulated to have the ionic formulation $F[XeN(SO_2F)_2]_2^+AsF_6^-$.[65,69] It was prepared according to equations (1.8) and (1.9).

$$FXeN(SO_2F)_2 + AsF_5 \xrightarrow{78\ ^\circ C} XeN(SO_2F)_2^+AsF_6^- \qquad (1.8)$$

$$2\ XeN(SO_2F)_2^+AsF_6^- \xrightarrow[\text{vacuum}]{23\ ^\circ C} F[XeN(SO_2F)_2]_2^+AsF_6^- + AsF_5 \qquad (1.9)$$

The $F[XeN(SO_2F)_2]^+$ cation was postulated to be fluorine bridged and its pale yellow AsF_6^- salt appears to be stable at room temperature. The yellow solid, $XeN(SO_2F)_2^+AsF_6^-$, is unstable at room temperature, whereas the $XeN(SO_2F)_2^+Sb_3F_{16}^-$ salt can be isolated from SbF_5 solvent according to equation (1.10).

$$F[XeN(SO_2F)_2]_2^+AsF_6^- + 3\ SbF_5 \xrightarrow[0\ ^\circ C]{SbF_5} 2\ XeN(SO_2F)_2^+Sb_3F_{16}^- + AsF_5 \qquad (1.10)$$

An X-ray single crystal study has shown that the $XeN(SO_2F)_2^+Sb_3F_{16}^-$ cation[69] (Figure 1.4) is structurally similar to the neutral compound, $FXeN(SO_2F)_2$. The xenon of the $XeN(SO_2F)_2^+$ cation is weakly covalently bonded to a fluorine by means of a fluorine-bridge interaction between the cation and the anion.

The Raman spectra of the $XeN(SO_2F)_2^+AsF_6^-$ and $F[XeN(SO_2F)_2]_2^+AsF_6^-$ adducts showed an absence of an Xe-F stretching mode indicating the absence of terminal Xe-F bonds. The bridging Xe...F stretches are also observed for the two adducts at much lower

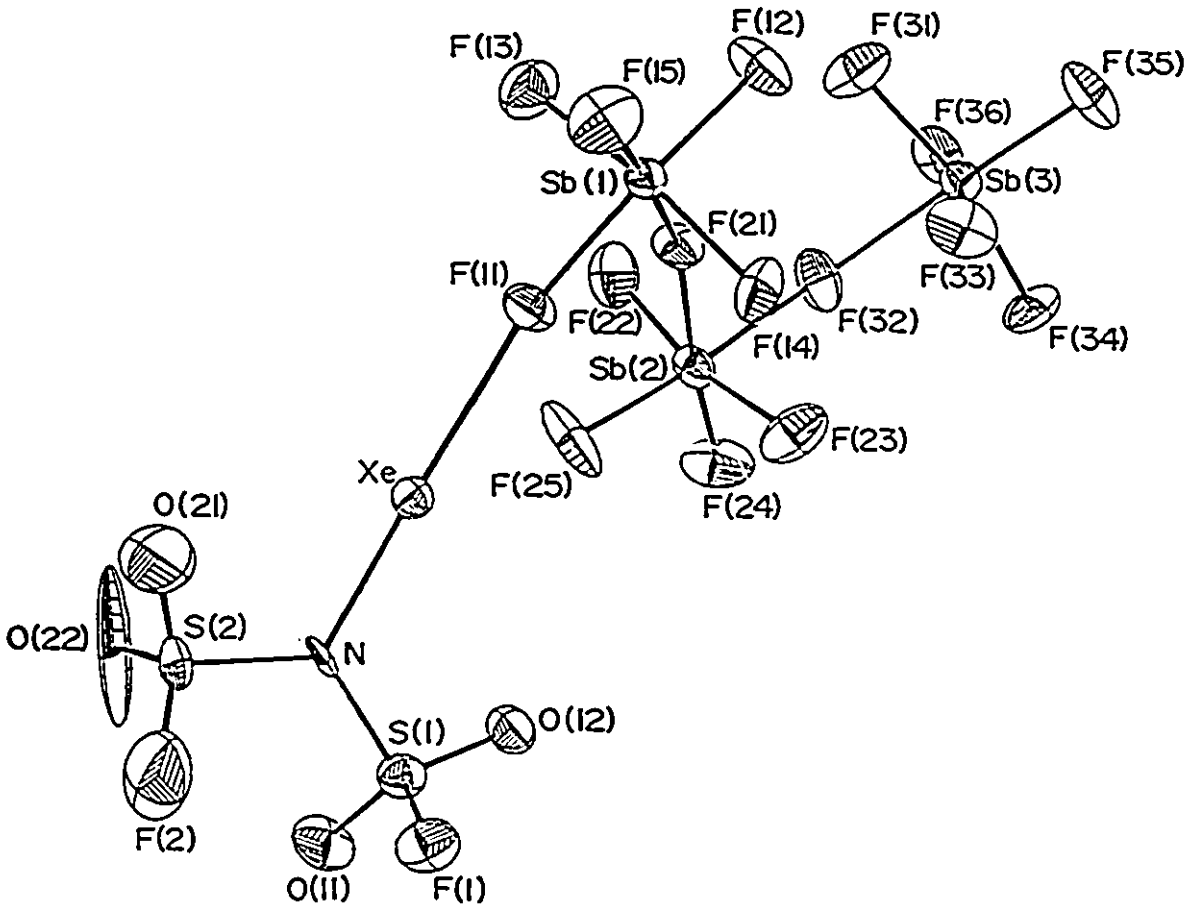

Figure 1.4 X-ray crystal structure of $XeN(SO_2F)_2^+Sb_3F_{16}^-$.[69]

lower frequencies than the stretching frequencies for the corresponding more covalent Xe-F bond in $FXeN(SO_2F)_2$ (506 cm^{-1}). The ν_{sym} (SO) and ν_{asym} (SO) stretches are shifted to 1233 and 1492 cm^{-1} in $XeN(SO_2F)_2^+AsF_6^-$, and 1228 and 1490 cm^{-1} in $F[XeN(SO_2F)_2]_2^+AsF_6^-$, respectively, and are higher than those in the neutral molecules, suggesting cation formation. No signal was obtained in the ^{19}F NMR spectra for the bridging fluorine, but this could be due to exchange broadening.

(iii) Xenon-Carbon Bonded Compounds

There are several indications that xenon-carbon bonds are strong enough so that organic xenon compounds should be detectable under normal conditions. If, for example, $CH_3{}^{131}I$ is allowed to undergo β-decay in a mass spectrometer, the resulting $CH_3{}^{131}Xe^+$ ion remains intact for about 70% of the cases, in contrast to the decay of CH_3-^3T, in which the CH_3-$^3He^+$ cation decomposes nearly 100% before detection.[71] Carlson and White[71] stated that this result must be due to the inherent greater stability of the CH_3-$^{131}Xe^+$ ion. Similar radiotracer experiments with aromatic iodine compounds indicate an even greater stability of aromatic xenon compounds.[72-74] The possibility of formation of $(Ph^{131}Xe)^+$ by reaction (1.11) was investigated; with route (a) being the most probable.

$$Ph_2{}^{131}ICl_4 \xrightarrow{-\beta^-} [Ph_2{}^{131}XeClO_4]^+ \begin{cases} \xrightarrow{(a)} Ph^{131}XeClO_4 + Ph^+ \\ \xrightarrow{(b)} Ph^{131}XeClO_4 + Ph^- \end{cases} \qquad (1.11)$$

Phenylxenonium ions were generated in C_6H_6 and $CHCl_3$ solutions of $Ph^{131}I$ and in $Ph^{131}I$ on the surfaces of crystals (80-100 mesh) of $KClO_4$, $KBPh_4$, KBF_4, K_2SO_4, KNO_3 and KCl. In the first two systems no bound xenon was observed. In the third system free xenon was released upon dissolution of the crystals in 0.1 N $HClO_4$. Addition of the reducing reagent, $Ph^{131}I$, led to the liberation of additional xenon. The fixing of xenon on the ionic crystals $KClO_4$, KBF_4, K_2SO_4, KNO_3 and KCl suggests stabilization of the $PhXe^+$ ion with a suitable anion is possible. The xenon compound in hydrochloric acid medium is stable, and only decomposes when dissolved in the more basic medium, water. Based on the yields of chemically bound xenon, the stabilizing capacity of the anions increases in the order $ClO_4^- > BPh_4^- > BF_4^- > SO_4^{2-} > NO_3^- > Cl^-$.

In addition, several research groups have reported the formation of Xe-alkyl ions in mass spectrometric experiments.[75-77] Beauchamp and Holtz[77] estimated the Xe-C bond strength in $XeCH_3^+$ from ion cyclotron resonance studies to be 43 ± 8 kcal mol^{-1} [77] according to equations (1.12) and (1.13).

$$Xe + CH_3FH^+ \longrightarrow XeCH_3^+ + HF \qquad (1.12)$$

$$Xe + CH_3ClH^+ \longrightarrow XeCH_3^+ + HCl \qquad (1.13)$$

While xenon reacts with protonated methyl fluoride, it does not react with protonated methyl chloride. Therefore, the methyl cation affinity (MCA) of xenon has to be larger than that of HF (MCA = 36 kcal) and smaller than that of HCl (MCA = 51 kcal).

The value of the xenon-carbon bond strength may be compared with the mean bond

energy for XeF_2 of 32 kcal mol^{-1},[78] while the gaseous Xe-F^+ cation has a bond energy of about 48 kcal mol^{-1}.[45]

In addition, a study has been made of the interaction of xenon and methane in the ionization chamber of a mass spectrometer[79] according to the reactions (1.14)-(1.17).

$$Xe^* + CH_4 \longrightarrow XeCH_4^+ + e^- \qquad (1.14)$$

$$Xe^+ + CH_4 \longrightarrow XeH^+ + CH_3 \qquad (1.15)$$

$$Xe^+ + CH_4 \longrightarrow XeCH_3^+ + H \qquad (1.16)$$

$$Xe^+ + CH_4 \longrightarrow XeCH_2^+ + H_2 \qquad (1.17)$$

The ions, XeC^+ and $XeCH^+$, are also formed, but by unknown reactions. In reaction (1.14), Xe^* represents a Xe atom excited to an energy of about 0.5 volt below the ionization energy of Xe. This reaction is similar to that observed for the formation of dimers of the rare gas ions, (equation (1.18)), viz

$$Xe^* + Xe \longrightarrow Xe_2^+ + e^- \qquad (1.18)$$

Ionization efficiency curves were determined for Xe_2^+ and $XeCH_4^+$ and were found to exhibit a sharp maximum about 2 volts above the onset of ionization. This is compatible with the formation of these ions from an excited neutral reactant, that is, the ionization efficiency curve is an excitation function. Rate constants were determined for the

formation of XeH^+, $XeCH_3^+$ and $XeCH_2^+$ and the values are 3.8×10^{-11}, 2.2×10^{-12} and 4.5×10^{-13} $cm^3\ mol^{-1}\ s^{-1}$, respectively. Relative rate constants for the formation of Xe_2^+ and $XeCH_4^+$ were also obtained, which leads to the conclusion that Xe^+ reacts with Xe nine times more rapidly than it does with CH_4. No net charge exchange between xenon and methane was observed, but no reason can be advanced for this somewhat unexpected behavior.

Bartlett *et al.*[46] have discussed the intermediate formation of $Xe(CF_3)_2$ during the decomposition of xenon bis-trifluoromethylsulfonate at 23 °C. Because $Xe(OSO_2CF_3)_2$ decomposes to hexafluoroethane, $FXe(OSO_2CF_3)$, and carbon tetrafluoride, it was suggested that the decomposition of $CF_3SO_3^+$ radical does not play an important role. They proposed the first reaction step could be SO_3 elimination and the formation of an unstable Xe-C bonded trifluoromethyl intermediate according to equations (1.19) and (1.20). Much the same kind of argument has been made for the decomposition of xenon trifluoroacetate at 23 °C [51,52] according to equations (1.21) - (1.24).

$$Xe(OSO_2CF_3)_2 \longrightarrow Xe(CF_3)_2 + 2\ SO_3 \longrightarrow Xe + C_2F_6 \qquad (1.19)$$

$$FXe(OSO_2CF_3) \longrightarrow FXeCF_3 + SO_3 \longrightarrow Xe + CF_4 \qquad (1.20)$$

$$Xe[OC(O)CF_3]_2 \longrightarrow Xe(CF_3)_2 + 2\ CO_2 \qquad (1.21)$$

$$Xe(CF_3)_2 \longrightarrow Xe + C_2F_6 \qquad (1.22)$$

$$2\ FXeOC(O)CF_3 \longrightarrow 2\ FXeCF_3 + 2\ CO_2 \qquad (1.23)$$

$$2\ FXeCF_3 \longrightarrow Xe + XeF_2 + C_2F_6 \qquad (1.24)$$

Lagow and co-workers[80] have obtained, from the interaction of XeF_2 with plasma generated CF_3 free radicals, a colorless waxy solid which their claim is $Xe(CF_3)_2$. The waxy material is more volatile than XeF_2 and decomposes with a half-life of 30 min at room temperature according to equation (1.25)

$$Xe(CF_3)_2 \longrightarrow XeF_2 + C_nF_m \qquad (1.25)$$

A similar plasma reaction between elemental xenon and C_2F_6 gave no indication of a xenon-carbon species.[81]

The main hindrance to a clear identification of this material is its low solubility in any of the solvents tried thus far. A Fourier transform ^{19}F NMR spectrum was obtained very rapidly during the process of decomposition in methylene chloride at -85 °C in an FEP tube.[80] The trace of this spectrum has never been published and is reported by Prof. D.D. DesMarteau of Clemson University, who has seen it, to be very unconvincing.[82] This ^{19}F NMR spectrum is reported to show a peak at δ = -9.6 ppm relative to $CFCl_3$ with two side bands indicative of ^{129}Xe-^{19}F spin-spin coupling.[80] The alleged ^{129}Xe-^{19}F two-bond coupling constant observed for this material, 1940 Hz, seems to be too large for a two-bond ^{129}Xe-^{19}F coupling. This is smaller than the one-bond coupling of 5550 Hz in

XeF_2 and is considerably larger than the three-bond coupling of 18 Hz in $FXe\text{-}N(SO_2F)_2$. The ^{13}C NMR spectrum has also been reported at a meeting by Lagow, and it is also not very convincing.[83] The infrared spectrum was also obtained which has a number of features in common with the spectrum of $Hg(CF_3)_2$. Unfortunately, the infrared spectrum is reported for the 800 - 1400 cm^{-1} range, which is far from the region expected for the Xe-C stretching vibration (300 - 400 cm^{-1}). A complete vibrational analysis has not yet been possible owing to decomposition resulting from the laser Raman excitation source.

A difluorocarbene elimination mechanism was proposed for the decomposition of $Xe(CF_3)_2$,[84] but this does not appear to be feasible on thermodynamic grounds:[84]

$$Xe(CF_3)_2 \longrightarrow Xe + 2\ CF_3 \qquad 2\ BE(Xe\text{-}CF_3) \approx 0 \tag{1.26}$$

$$2CF_3 \longrightarrow 2C + 3\ F_2 \qquad -\Delta H_f^\circ(CF_3) = +224.8\ \text{kcal mole}^{-1}\ ^{85} \tag{1.27}$$

$$2C + 2\ F_2 \longrightarrow 2\ CF_2 \qquad 2\Delta H_f^\circ(CF_2) = -87.5\ \text{kcal mole}^{-1}\ ^{85} \tag{1.28}$$

$$Xe + F_2 \longrightarrow XeF_2 \qquad \Delta H_f^\circ(XeF_2) = -28.2\ \text{kcal mole}^{-1}\ ^{86} \tag{1.29}$$

$$Xe(CF_3)_2 \longrightarrow XeF_2 + 2\ CF_2 \qquad \Delta H^\circ = +109.6\ \text{kcal mole}^{-1} \tag{1.30}$$

Even if one neglects the energy required to break the Xe-C bond, the reaction would be highly endothermic. While the existence of Xe-alkyl ions in the gas phase is well established,[73, 74, 87] no definitive Xe-C fragment has been observed in the mass spectrum of this compound.[83]

Confirmation of the synthesis of $Xe(CF_3)_2$ has not been reported and, in general,

the community of fluorine chemists does not accept the work of Lagow *et al.*[80] as having established the existence of the first Xe-C bond.

One of the most promising ligands for Xe-C formation appears to be, $-C(SO_2F)_3$ and $-C(SO_2CF_3)_3$. Thus far $HC(SO_2F)_3$ and the halogen derivatives: $FC(SO_2F)_3$, $ClC(SO_2F)_3$, $BrC(SO_2F)_3$, $IC(SO_2F)_3$ [88] and $HC(SO_2CF_3)_3$, $ClC(SO_2CF_3)_3$, $BrC(SO_2CF_3)_3$ and the anion $C(SO_2CF_3)_3^-$ [89] have been synthesized. The acid, $HC(SO_2F)_3$, is a strong monoprotic acid and its strength has been estimated by means of Raman spectroscopy to lie between those of concentrated HNO_3 and $HOSO_2F$;[88] however, the reaction between $HC(SO_2F)_3$ and XeF_2 did not yield the desired product $FXe\text{-}C(SO_2F)_3$ when attempted by Schrobilgen [90] and Seppelt,[88] yielding xenon gas and $FC(SO_2F)_3$ according to equation (1.31).

$$HC(SO_2F)_3 + XeF_2 \xrightarrow[CF_2Cl_2]{\text{-20 °C}} Xe + HF + FC(SO_2F)_3 \qquad (1.31)$$

Most recently, two independent German groups[91,92] prepared the first example of a stable compound containing a xenon-carbon bond, $C_6F_5Xe^+C_6F_5BF_3^-$, by nucleophilic displacement of fluorine from XeF_2 using $B(C_6F_5)_3$ as an aryl-transfer reagent (equation 1.32).

$$XeF_2 + B(C_6F_5)_3 \xrightarrow{CH_3C\equiv N} [C_6F_5Xe^+][B(C_6F_5)_3F^-] + BF_3X \qquad (1.32)$$

(X = $CH_3C\equiv N$, F)

It is presumed that both BF_4^- and $CH_3C\equiv N\text{-}BF_3$ are formed in a dismutation reaction of

the mixed intermediate, $B(C_6F_5)_{3-x}F_x$ according to equation (1.33).

$$3B(C_6F_5)_{3-x}F_x \longrightarrow (3-x)B(C_6F_5)_3 + xBF_3 \ (x = 1,2) \qquad (1.33)$$

The crystal structure of the $C_5F_5Xe^+$ $(C_6F_5)_2BF_3^-.CH_3C{\equiv}N$ (Figure 1.5) shows the Xe-C distance [2.092(8) Å][93] is comparable to the I-C distance in $C_6F_5I(O_2CC_6F_5)_2$ [2.072(4) Å].[94] Coordination of $CH_3C{\equiv}N$ to the $C_5F_5Xe^+$ cation serves to lower the effective positive charge at xenon by coordination of the nitrogen of $CH_3C{\equiv}N$, giving an Xe...N contact (2.681 Å) that is significantly shorter than the sum of the van der Waals radii for Xe and N (3.6 Å) and substantially longer than the Xe-N distances in $Xe\text{-}N(SO_2F)_2^+$ (2.02(1) Å)[69] and $FXe\text{-}N(SO_2F)_2$ (2.200(3) Å).[64]

(C) COVALENT DERIVATIVES OF XENON(II) BONDED TO OTHER MAIN-GROUP ELEMENTS

In addition to the well-established examples of xenon-fluorine, xenon-oxygen, xenon-nitrogen and xenon-carbon bonds, one example of a stable xenon-chlorine bond is known, namely $Cs_9(XeO_3Cl_2)_4Cl$.[95] In addition $XeCl_2$ as well as $XeBr_2$ have been detected by Mössbauer spectroscopy as products of the β-decay of their ^{129}I analogs according to equation (1.34).

$$^{129}IX_2 \longrightarrow {}^{129}XeX_2 + \beta^- \qquad (1.34)$$

where X = Cl or Br

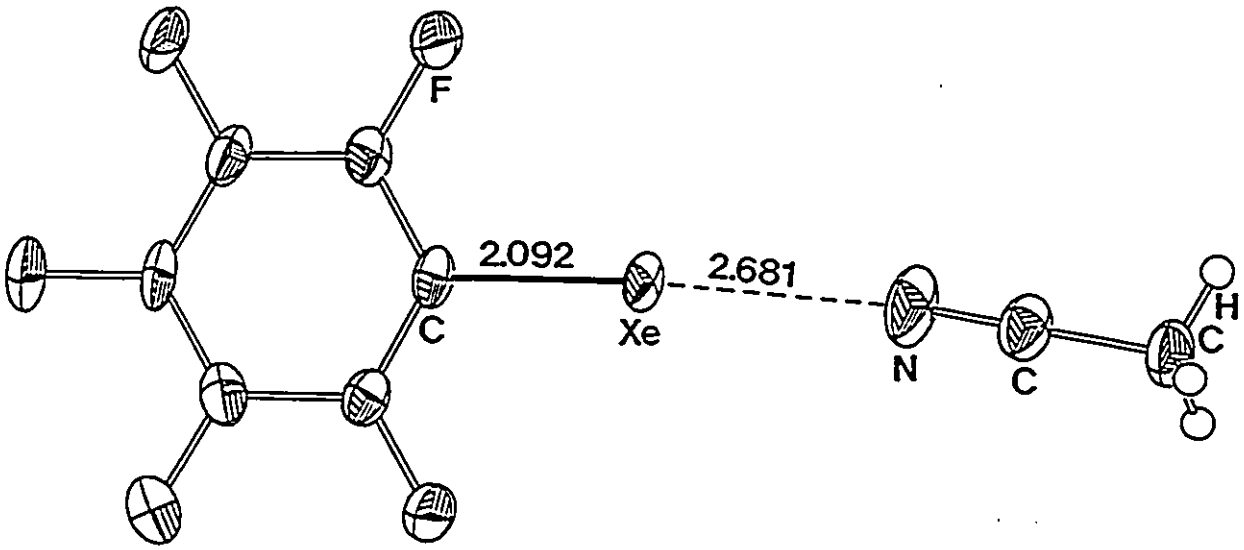

Figure 1.5 Structural unit, determined by X-ray crystallography, for the $C_6F_5Xe^+$ cation coordinated to $CH_3C{\equiv}N$.[93]

Xenon dichloride has also been trapped in a matrix of solid Xe after Xe/Cl_2 mixtures had been passed through a microwave discharge, but these halides are too unstable to be chemically characterized.[96]

The first significant evidence suggesting the existence of xenon dichloride was provided by Meinert,[97] who produced mass spectrometric data which suggested that he had isolated a xenon chloride, possibly $XeCl_2$. Using techniques similar to those of Meinert, Nelson and Pimentel[98] passed xenon/chlorine mixtures through a microwave discharge and then condensed them onto a cesium iodide optical window at 20 K. They observed an infrared spectrum which they attributed to $XeCl_2$. They confirmed their hypothesis by calculating the harmonic frequencies assuming a linear symmetric $XeCl_2$ molecule. The asymmetric stretching force constant is about half that of XeF_2 and KrF_2, which reflect the anticipated weakness of the Xe-Cl bond relative to the Xe-F bond.[98]

Andrews and Howard[99] studied the noble-gas halides using laser photolysis of matrix-isolated halogens in the inert gas matrix, and they succeeded in photoproducing $XeCl_2$ and XeClF.

There is also strong evidence to support the existence of a xenon-xenon bond in the radical cation Xe_2^+ in solution.[100] When $XeF^+Sb_2F_{11}^-$ is dissolved in excess SbF_5, it reacts and turns dark green on reduction with a large number of materials, namely, H_2O, Pb, Hg,[100] PbO, As_2O_3, SiO_2, SO_2, PF_3 and CO.[101] On the other hand, it may be generated by oxidation of xenon gas with $O_2^+Sb_2F_{11}^-$ (again dissolved in SbF_5).[100] The best mode of preparation is the reduction of $XeF^+Sb_2F_{11}^-$ (in SbF_5) with elemental xenon,[101] since this is a clean and reversible reaction. The existence of the Xe_2^+ ion in a solution of SbF_5 has

been supported by ESR, Raman, and UV-visible spectroscopic methods. The most powerful probe is the ESR spectrum of a frozen solution in SbF_5, which showed the expected hyperfine structure. Natural xenon contains 26.44% ^{129}Xe (I = ½), 21.18% ^{131}Xe (I = 3/2) and 52.38% as other isotopes with (I = 0). Since the hyperfine constants arise from ^{129}Xe and ^{131}Xe coupling, a complicated spectrum having $g_\perp$ (2.304), $g_\parallel$ (1.885), A ^{129}Xe (220 g), and A ^{131}Xe (600 g) was obtained. The experimental spectrum and the computed spectrum agreed based on the assumption of a dixenon radical cation, $Xe_2^{+\cdot}$. Furthermore, the fine structure disappeared when isotopically pure ^{136}Xe (I = 0) was used.[100] The high scattering power of the large xenon atoms results in a strong Raman band at 123 cm^{-1} which shows some resonance Raman enhancement when excited at 514.5 nm.[100] This value is close to that obtained for the isoelectronic species $I_2^{-\cdot}$.[102] Indeed, $Xe_2^{+\cdot}$ has a UV-visible absorptions at 335 and 720 nm which is quite similar to that of $I_2^{-\cdot}$;[102] both are dark green. These spectroscopic details interestingly have been predicted by *ab initio* calculations.[103,104] This species represents the only example of a xenon-xenon bond and is presumed to form in the reaction (1.35)[101]

$$3\ Xe + 3\ XeF^+Sb_2F_{11}^- + 2\ SbF_5 \longrightarrow 2\ Xe_2^{+\cdot}Sb_2F_{11}^-.XeF^+Sb_2F_{11}^- \qquad (1.35)$$

(D) XENON-BORON BONDED COMPOUNDS

The covalent xenon(II) derivative $FXeBF_2$ [105] has also been reported. A reaction between xenon and O_2BF_4 has been observed to liberate oxygen and fluorine at

an equimolar mixture of Xe and BF_3. On the basis of analytical and vibrational spectroscopic data, it was believed that the structure of the solid was $FXe\text{-}BF_2$. However, no convincing physical evidence has yet been given in support of the proposed Xe-B bonded structure. Rather, it is now known that O_2^+ salts oxidize xenon gas to XeF^+ [100] and it is possible that the white solid product was $XeF^+BF_4^-$ formed according to equation (1.36)

$$Xe + 2\ O_2^+BF_4^- \longrightarrow XeF^+BF_4^- + BF_3 + 2\ O_2 \qquad (1.36)$$

(E) COVALENT DERIVATIVES OF KRYPTON

The synthesis of krypton derivatives containing highly electronegative ligand groups is considerably more difficult than those of the analogous xenon derivatives. Krypton difluoride cannot be prepared by direct fluorination of krypton gas at high pressures and temperatures as is the case for the fluorides of xenon. The high ionization potential of krypton (322.8 kcal mol^{-1}) and anticipated thermal instability of krypton compounds, requires the use of low temperature high-energy methods.[106-108] Krypton difluoride can be prepared by electric glow discharge of Kr/F_2 mixtures at liquid oxygen temperatures (-183 °C),[109] photolysis of Kr/F_2 mixtures at liquid nitrogen temperature[110-112] or by the use of hot-wire techniques.[113]

Krypton difluoride has an estimated half-life of four hours in the vapor state at room temperature, but can be maintained indefinitely at dry-ice temperature.[114] The mean

room temperature, but can be maintained indefinitely at dry-ice temperature.[114] The mean thermochemical bond energy is approximately 14.5 kcal mol^{-1} [114] which, in fact, is the lowest bond energy of any fluoride. Krypton difluoride serves as a low-temperature source of $F^{\bullet}$ atoms. Thus, the extraordinary low temperature fluorinating ability of KrF_2 is not unexpected. For example, the krypton difluoride derivatives, $KrF^{+}AsF_6^{-}$, $Kr_2F_3^{+}AsF_6^{-}$ and $Kr_2F_3^{+}SbF_6^{-}$ are capable of oxidizing BrF_5 to BrF_6^{+},[115] a feat which the strong fluorinating agent PtF_6, is unable to achieve even in the presence of UV-light.[114] Krypton difluoride oxidizes Au metal in HF to the Au(VI) species $KrF^{+}AuF_6^{-}$ from which is derived, upon pyrolysis, AuF_5.[36]

No krypton oxides or higher oxidation state krypton fluorides are known at this time. An early report that KrF_4 was formed by electric discharge of mixtures of Kr and F_2 is erroneous[116] and was later shown to be KrF_2.[107,117]

There are several spectroscopic studies which indicate the possibility of forming krypton-carbon and krypton-nitrogen bonds. For example, $CH_3{}^{82}Br$ has been allowed to undergo β-decay, but only about 0.4% of the parent ion, CH_3Kr^{+}, was observed to remain intact by mass spectrometry,[118] as was anticipated from the rather high recoil energy. The most abundant ion observed was CH_3^{+}, 89%.[118] Hertel and Koski[119] studied the reaction of Kr^{+} with methane over an energy range 2-200 eV. An ion peak was observed at mass 98, corresponding to $KrCH_2^{+}$ (equation (1.37)), but only trace amounts of $KrCH_2^{+}$ were observed, and was similar to those seen in Xe^{+} with CH_4 reaction.[79]

$$Kr^{+} + CH_4 \longrightarrow KrCH_2^{+} + (2H, H_2) \qquad (1.37)$$

In similar mass spectrometric studies of ionic reactions in krypton-methane mixtures,[120] the ion-molecule reaction products KrH^+, KrC^+, $KrCH_2^+$ and $KrCH_3^+$ were observed. Charge exchange reactions between rare gas ions and methane were observed with Kr^+ producing CH_3^+ and CH_4^+. The ion-molecule reaction rates are of the order of 10^{-12} to 10^{-11} mL molecule^{-1}s^{-1}, while their charge exchange reaction rates are of the order of 10^{-10} to 10^{-9} mL molecule^{-1}s^{-1}. The ion peaks were observed at different masses corresponding to the krypton cations listed in Table 1.2.

In addition, mass spectrometric studies have been made for mixtures of krypton with N_2 or CO.[87c] The ions Kr_2^+, KrN_2^+, $KrCO^+$, N_4^+ and $C_2O_2^+$ were observed in these mixtures as a result of reactions with excited krypton atoms. The addition of Kr to CO promotes the formation of $C_2O_2^+$ through reactions initiated by excited states of Kr. The rate constant for reaction (1.38) was determined at a repeller field strength of 50 V/cm.

$$KrCO^+ + CO \rightleftharpoons C_2O_2^+ + Kr \qquad k = 3 \times 10^{-10} \text{ mL mol}^{-1} \text{ s}^{-1} \qquad (1.38)$$

Other combinations of krypton with N_2 and CO show no such promotional effect on the formation of N_4^+ or $C_2O_2^+$. Ratios of the rate constants for the formation of KrN_2^+ and Kr_2^+ in krypton-nitrogen mixtures and for the formation of $KrCO^+$ and Kr_2^+ in the krypton-carbon monoxide system were also determined. At high pressures of N_2 or CO alone the formation of N_4^+ or $C_2O_2^+$ is observed, and the reaction is a bimolecular chemionization involving highly excited N_2 or CO. At sufficiently high electron energies, the following ions are formed in binary mixtures of N_2 or CO with krypton: KrC^+, KrN^+,

Table 1.2

Ion Peaks Observed by Mass Spectrometery for a Mixture of Equal Parts of Krypton and Methane[a]

Mass	Ion	Relative Intensity
84	$^{84}Kr^+$, $^{83}KrH^+$	1,850
85	$^{84}KrH^+$	225
96	$^{80}KrCH_4^+$, $^{82}KrCH_2^+$, $^{83}KrCH^+$, $^{84}KrC^+$	7
97	$^{82}KrCH_3^+$, $^{83}KrCH_2^+$, $^{84}KrCH^+$	16
98	$^{82}KrCH_4^+$, $^{83}KrCH_3^+$, $^{84}KrCH_2^+$, $^{85}KrCH^+$	31
99	$^{83}KrCH_4^+$, $^{84}KrCH_3^+$, $^{86}KrCH^+$	57
100	$^{84}KrCH_4^+$, $^{86}KrCH^+$	5
101	$^{86}KrCH_3^+$	24
168	$^{84}Kr_2^+$, $^{82}Kr^{86}Kr^+$	5

a From ref. (120); ionization chamber pressure, 120 x 10^{-3} Torr; electron voltage, 70 volts and field strength of 12.5 volts/cm.

C_2O^+, CO_2^+ and N_3^+. The N_3^+ and KrN^+ ions are formed by the reaction of excited nitrogen molecule ions with Kr and/or N_2, and the relative rates of these reactions were determined.

Ion cyclotron resonance trapped ion techniques[121] have been used to examine ion-molecule reactions in CH_3F-Kr mixtures. Protonated CH_3F, formed by the reaction of CH_3F^+ with CH_3F, reacts with Kr by methyl cation transfer to yield CH_3Kr^+. Correlations of proton affinity with methyl cation affinity predict a CH_3^+-Kr bond energy of 47 kcal mol^{-1}. Methyl cation exchange equilibria involving N_2 and Kr yield a value of 47.7 ± 2.5 kcal mol^{-1} for the Kr-C bond strength. The arguments presented imply that the Kr-C bond has substantial covalent character rather than being a simple electrostatic complex.

Schrobilgen[122,123] has recently obtained the first examples of krypton bonded to nitrogen. Prior to this report only Kr-F bonded species were known, namely KrF_2, KrF^+ and $Kr_2F_3^+$. The cations $HC{\equiv}N\text{-}KrF^+$ and $R_FC{\equiv}N\text{-}KrF^+$ were prepared as their AsF_6^- salts by the low-temperature reaction of $HC{\equiv}NH^+AsF_6^-$ or $R_FC{\equiv}N\text{-}AsF_5$ with KrF_2 in HF or BrF_5 solvents and were characterized by low-temperature Raman spectroscopy and ^1H, ^{13}C, ^{15}N and ^{19}F NMR spectroscopy.

In view of the established existence of Kr-F and Kr-N bonds, a Kr-O bond should exist. It should be easier to attach an oxygen group to krypton than nitrogen because oxygen is more electronegative. The reaction of KrF_2 with $B(OTeF_5)_3$ in ClO_3F at -100 °C for 16 hours followed by a further 3 hours at -78 °C has been investigated,[52,53] but preliminary attempts failed to produce evidence for a krypton product. Similar results have been obtained in this laboratory for the reaction of KrF_2 with $B(OTeF_5)_3$ in SO_2ClF

at -78 °C for several minutes.[124] Formation of $F_5TeOOTeF_5$ and the reductive elimination of krypton gas does, however, imply the intermediacy of an $-OTeF_5$ derivative of krypton(II), namely $Kr(OTeF_5)_2$. In addition, the fact that neither TeF_6 nor O_2 was formed in this reaction (which would be expected if KrF_2 oxidatively fluorinated the $-OTeF_5$ group) supports the formation of a $Kr(OTeF_5)_2$ intermediate. The $OSeF_5$,[52,53] $-OIOF_4$ [125] and $-OSO_2F$ [126] ligands are reported to behave similarly when allowed to react with KrF_2.

More recently Schrobilgen and Sanders[127] have repeated these experiments at lower temperatures and have reported the first example of a species containing a krypton-oxygen bond, $Kr(OTeF_5)_2$, by the reaction of KrF_2 with the natural abundance and ^{17}O-enriched $B(OTeF_5)_3$ at -90 °C to -112 °C in SO_2ClF solvent.

(F) GENERAL SYNTHETIC APPROACHES TO THE FORMATION OF BONDS TO NOBLE-GAS CENTERS

One synthetic approach which has proven most useful for the preparation of xenon(II) derivatives involves the direct interaction of XeF_2 with the corresponding ligand group's protonic acid leading to HF displacement. An example of an HF displacement reaction, generalized for any ligand-group acid RH, is given by equation (1.39).

$$XeF_2 + n\ RH \rightleftharpoons F_{2-n}XeR_n + n\ HF \qquad (1.39)$$

The key factors in equation (1.39) are the volatility of HF at low temperature [v.p.

HF (-45 °C) = 40 mm Hg],[128] which is pumped off forcing the reaction to completion; the acid strength of RH and the high bond energy of HF (135.1 ± 0.3 kcal mole^{-1}). The latter method has been explored successfully in the preparation of -$OTeF_5$,[57-62] -$OSeF_5$,[56] -OSO_2F,[45,46] -$OClO_3$,[46,49] -$OPOF_2$,[51] -$OC(O)CF_3$,[50,58] -$N(SO_2F)_2$[64,69] derivatives of xenon(II).

A consideration of the preceding list of ligands, which form covalent derivatives with xenon, shows that the following set of criteria are met:

(i) The ligand forms a moderate to strong monoprotic acid.

(ii) The ligand has a high effective group electronegativity.

(iii) The least electronegative element(s) of the ligand is in its highest oxidation state, e.g., Te(VI) of the -$OTeF_5$ group.

(iv) The ligand exists as a stable anion and, as such, is capable of withstanding the high electron affinity of the noble-gas in its positive formal oxidation states.

If one considers the likelihood that a given ligand will form a stable adduct with xenon, the ligand should, in general, satisfy the above criteria. The -$OTeF_5$ group presently has the most extensive noble-gas chemistry outside of fluorine [129a] and serves to illustrate the above criteria. The boron derivative, $B(OTeF_5)_3$, was first prepared in 1973 by Sladky *et al.*[129b] according to equation (1.40).

$$BCl_3 + 3\ HOTeF_5 \longrightarrow B(OTeF_5)_3 + 3\ HCl \qquad (1.40)$$

Since then this reagent has proven to offer the most convenient route to the formation

of -$OTeF_5$ derivatives of xenon and, in fact, represents the only method for preparing xenon(IV)[51,52] and xenon(VI) -$OTeF_5$ derivatives.[52-54] When a xenon fluoride or oxide fluoride is allowed to react at low temperature with a stoichiometric amount of the ligand transfer reagent, $B(OTeF_5)_3$, in an inert solvent, the corresponding -$OTeF_5$ derivative is generated quantitatively with elimination of BF_3 gas. Equation (1.41) illustrates the general preparative method using XeF_2 as an example.[122]

$$XeF_2 + \tfrac{2}{3}\, B(OTeF_5)_3 \xrightarrow[CFCl_3]{0\ ^\circ C} Xe(OTeF_5)_2 + \tfrac{2}{3}\, BF_3 \qquad (1.41)$$

(G) PURPOSE AND GENERAL SYNTHETIC STRATEGIES UNDERPINNING THE PRESENT WORK

The overall purpose of the present work is to extend the chemistry of the noble gases and, more specifically, to form novel covalent bonds between xenon and an element other than fluorine and oxygen, namely nitrogen. In choosing a strategy for Xe-N bond formation, the investigation of the interactions of the Lewis acid cation, XeF^+, with neutral nitrogen Lewis bases was undertaken. The majority of the bases selected for the study are oxidatively resistant to the XeF^+ cation. Appropriate bases have been selected by estimating the electron affinity of the XeF^+ cation (EA ≈ 10.9 eV; Figure 1.6) and the first ionization potential of the neutral Lewis base ligands which should exceed the EA of XeF^+ and lie above 10 - 11 eV. Table 1.3 lists some possible ligands which might form Xe-N bonds and their experimentally determined first ionization potentials. In view

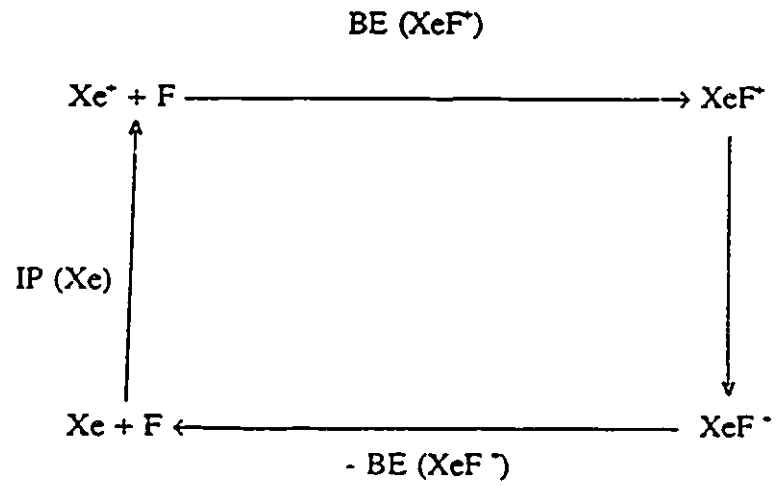

EA (XeF^+) = IP (Xe) + BE (XeF^+) - BE ($XeF^{\bullet}$)

IP (Xe) = 12.10 eV[62]

BE (XeF^+) ≈ 2.10 eV[130] = 2.03 eV[130] (gas phase)

BE ($XeF^{\bullet}$) ≈ 0.86 eV[130]

EA (XeF^+) ≈ 10.90 eV

Figure 1.6 Estimation of the electron affinity of the XeF^+ cation.

Table 1.3

Ionization Potentials of Some Organic and Inorganic Nitrogen Bases (eV)

Compound	1st Ionization Potential	Ref.
$CF_3C{\equiv}N$	13.90	(131)
$N{\equiv}C\text{-}C{\equiv}N$	13.80 ± 0.02	(132)
$HC{\equiv}N$	13.80	(133)
trans-N_2F_2	13.10 ± 0.1	(134)
$CH_2FC{\equiv}N$	13.00 ± 0.1	(135)
$CHCl_2C{\equiv}N$	12.90 ± 0.3	(135)
$CH_2ClC{\equiv}N$	12.20 ± 0.1	(135)
$CF_3N{\equiv}C$	12.60	(131)
$N{\equiv}SF_3$	12.50	(136)
$ClC{\equiv}N$	12.49 ± 0.04	(137)
$CHF_2C{\equiv}N$	12.40	(135)
$CD_3C{\equiv}N$	12.235 ± 0.005	(134)
$CH_3C{\equiv}N$	12.194 ± 0.005	(138)
N_2F_4	12.04 ± 0.1	(139)
$BrC{\equiv}N$	11.95 ± 0.08	(137)
$C_2H_5C{\equiv}N$	11.85	(132)
$N{\equiv}SF$	11.82	(136)
n-$C_3H_7C{\equiv}N$	11.67	(140)
ND_3	11.52	(141)
s-$C_3F_3N_3$	11.50	(142)
$(CH_3)_2CHC{\equiv}N$	11.49	(140)
ND_2H	11.47 ± 0.02	(141)
$N{\equiv}C\text{-}C{\equiv}C\text{-}C{\equiv}N$	11.40 ± 0.2	(143)

Continued...

Table 1.3 (continued)

Compound	1st Ionization Potential	Ref.
N≡C-C≡C-C≡C-C≡N	11.40 ± 0.2	(143)
$S(C{\equiv}N)_2$	11.32	(144)
$CH_3N{\equiv}C$	11.32	(131)
$CH_3C{\equiv}C$-H	11.24	(132)
$(CH_3)_3CC{\equiv}N$	11.11	(140)
IC≡N	10.98 ± 0.05	(137)
B-$B_3F_3N_3$	10.79	(142)
$H_2NC{\equiv}N$	10.76	(145)
NH_3	10.34 ± 0.07	(146)
C_5F_5N	10.085 ± 0.05	(142)
s-$C_3H_3N_3$	10.07 ± 0.05	(147)
C_6F_5H	10.00	(148)
CF_3·	9.25	(149)

of the aforementioned characteristics of the Lewis acid, nitriles and perfluoropyridine derivatives were also investigated as potential ligands for xenon(II).

The basicity of nitrogen bases is a function of the hybridization of the nitrogen atom, with the electronegativity of the nitrogen atom increasing as the s-character of the hybridized valence orbital increases. Hence the basicity of the lone pair decreases with increasing s-character. Table 1.4 lists the variation of electronegativity with formal hybridization for some first row elements. Figure 1.7 illustrates how the electronegativities of carbon, nitrogen and oxygen vary as a function of s-character.[150] In general, the first IP of a nitrile will be greater than that of a pyridine. From the electronegativity and ligand IP considerations alone, one predicts that a nitrogen atom having more s-character (sp-hybridization, e.g., hydrogen cyanide, HC≡N, and alkyl nitriles, RC≡N) to be more likely to form Xe-N adduct bonds that are stable to internal redox reactions. It is not necessary that the least electronegative element of the ligand be in its highest oxidation state nor that the electronegative ligating atom be bonded to a strong electron withdrawing group. In fact, the ligand may contain an electron donating group such as an alkyl group or hydrogen. In the case of perfluoropyridines (N_{sp^2}-hybridization), the formation of Xe-N bonded adducts wou ld represent the first examples in which the noble-gas element could act as an aromatic substituent.

Table 1.4

The Variation of Electronegativity *versus* Hybridization for Some Second Row Elements[a]

	sp^3	sp^2	sp
%s	25	33.3	50
oxygen	4.93	5.54	—
nitrogen	3.68	3.94	4.67
carbon	2.48	2.94	3.29

a From ref. (150).

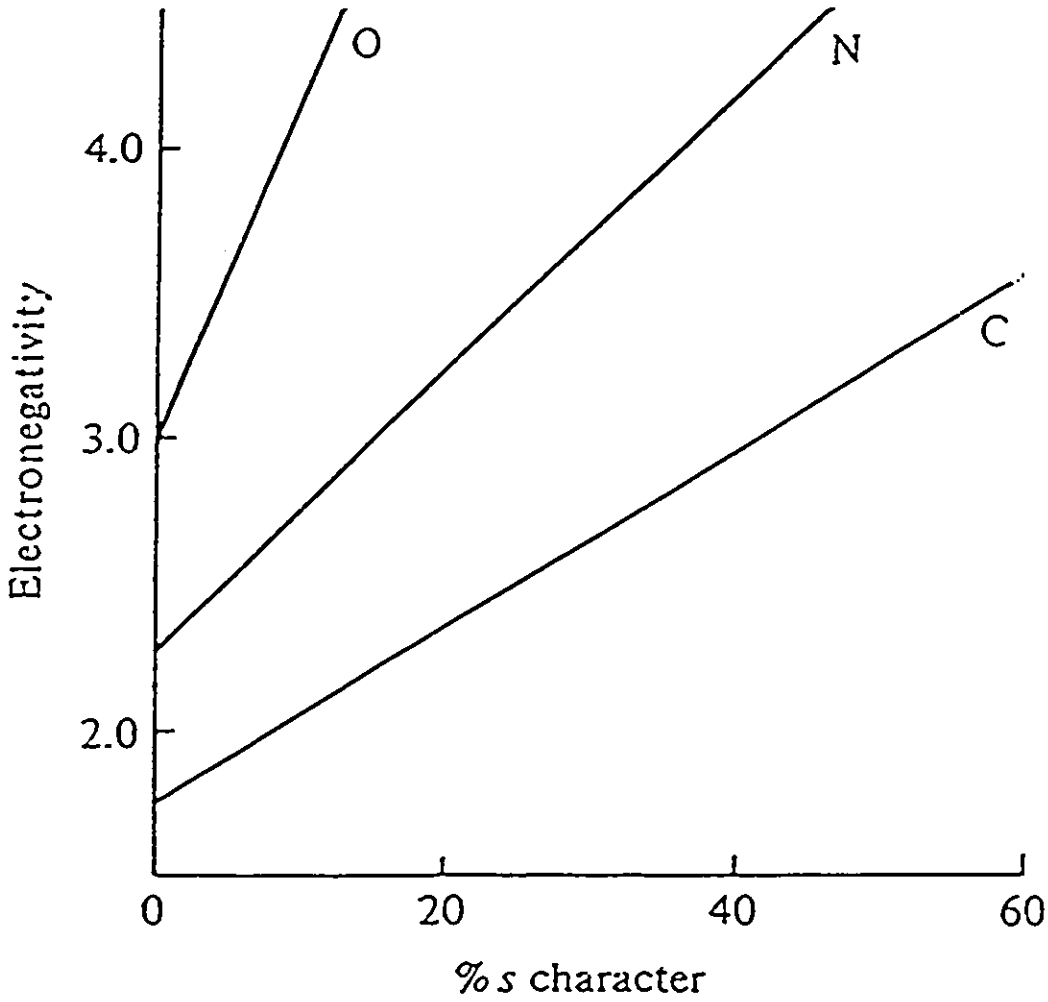

Figure 1.7 Electronegativities of carbon, nitrogen and oxygen as a function of s-character. From ref. (150).

CHAPTER 2

EXPERIMENTAL SECTION

(A) VACUUM TECHNIQUES

(i) Vacuum Systems and Inert Atmosphere Systems

Nearly all of the compounds used in the course of this work are moisture sensitive, thus requiring that they be handled under anhydrous conditions in vacuum systems or in an inert atmosphere (oxygen-free, nitrogen atmosphere) drybox. Drybox moisture levels were routinely <0.1 ppm in a Vacuum Atmospheres Model DLX drybox, which was equipped with a moisture monitor. For manipulations involving volatile reagents or products, or for the transfer of solvents, a general purpose vacuum line constructed largely from nickel and 316 stainless steel Autoclave Engineers Inc. valves and fittings (Figure 2.1) was used. Two other lines were constructed out of Pyrex; one of them incorporated grease-free 6 mm Young FEP-barrel stopcocks (Figure 2.2), and was used for drying reaction vessels and NMR tubes, and for the transfer of volatile nitriles and perfluoropyridines. The remaining glass line was outfitted with Pyrex vacuum stopcocks and a calibrated bulb (54.51 mL) and housed inside a fumehood. This line was used for preparations and reactions involving the use of anhydrous HC≡N and $H^{13}C{\equiv}N$.

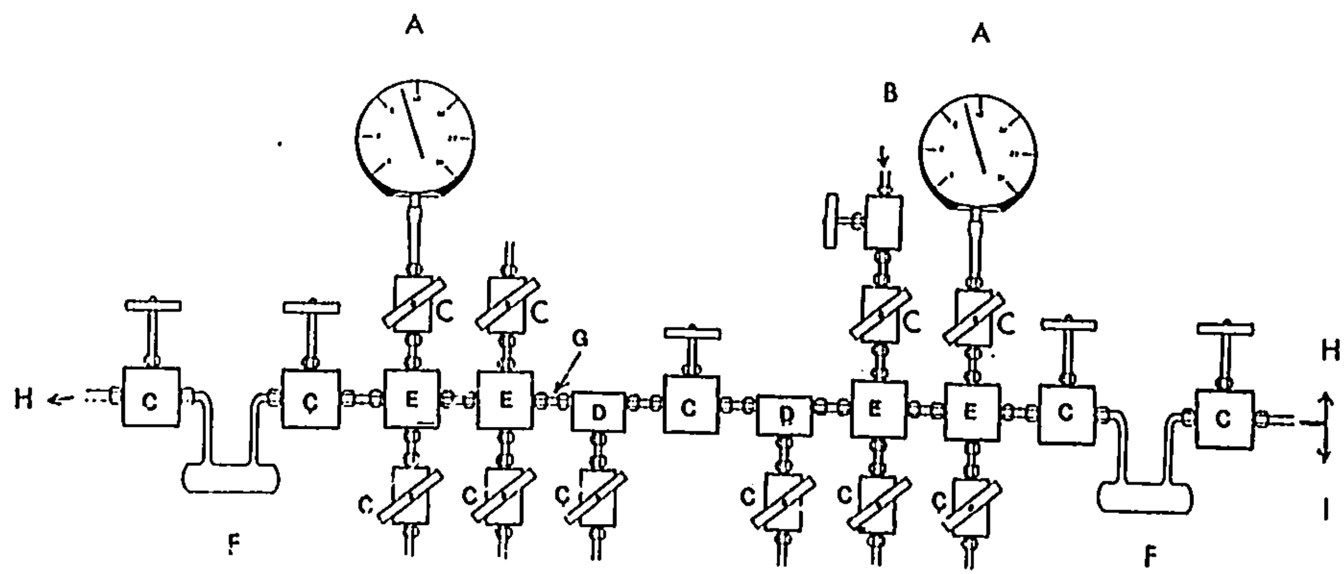

Figure 2.1 Metal vacuum line. (A) gauges reading from 0 to 30 1b. in^{-2}. absolute, (B) dry nitrogen inlet, (C) 316 stainless steel valves, (D) 316 stainless steel tees, (E) 316 stainless steel cross, (F) welded nickel cold trap, (G) nickel connectors, (H) outlet to liquid nitrogen trap followed by a two stage rotary oil vacuum pump, (I) outlet to soda lime absorbent followed by a liquid nitrogen trap and direct drive two stage vacuum pump; used to trap volatile reactive fluorides such as F_2, HF, AsF_5 etc.

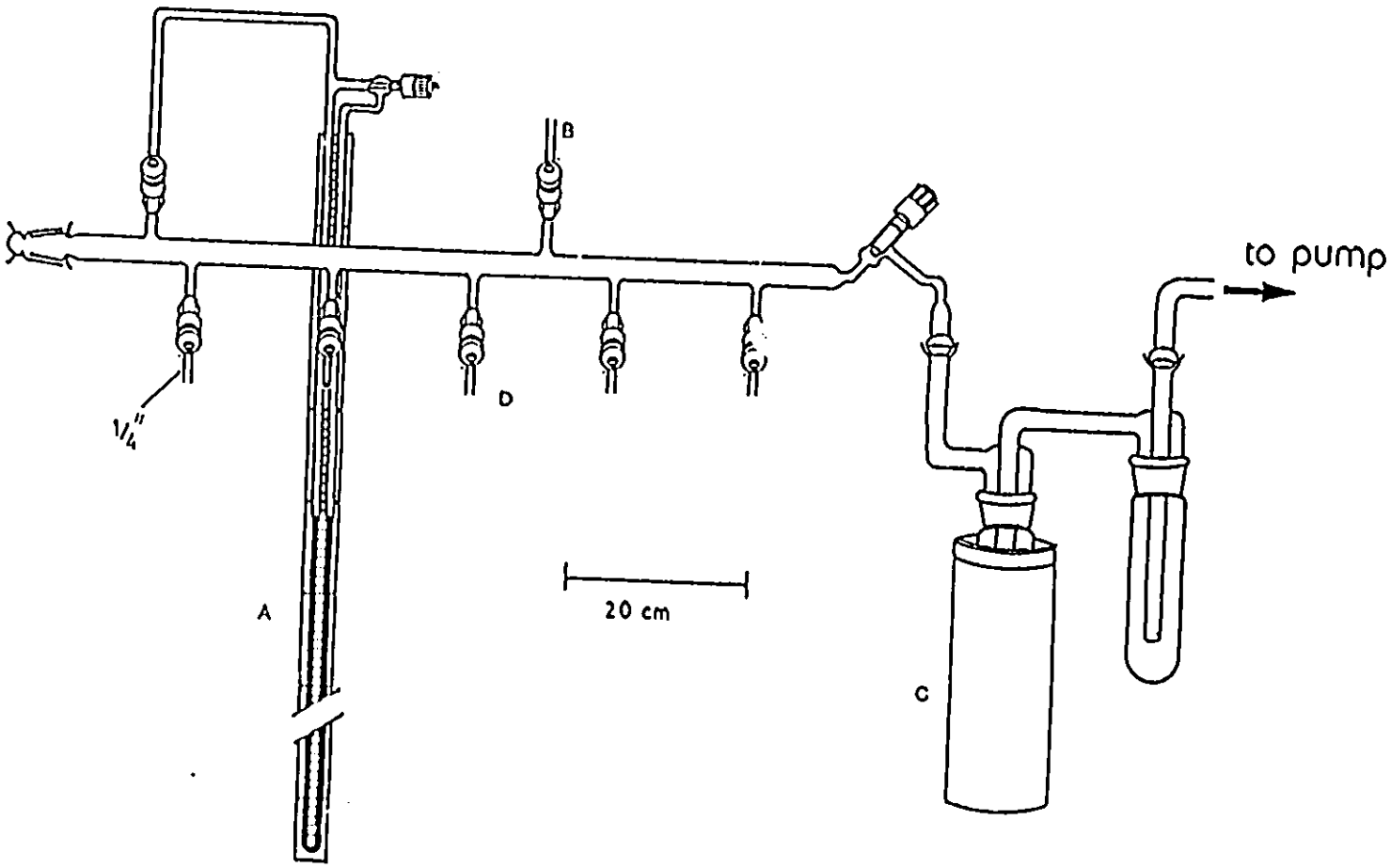

Figure 2.2 Glass vacuum line; (A) mercury manometer, (B) dry nitrogen inlet, (C) liquid nitrogen trap, (D) a grease-free 6 mm Young FEP-barrel stopcock.

Pressures in the metal vacuum lines were measured using two Aschcroft "Duraguage" model 8438 Bourdon stainless steel tube gauges reading 0 to 30 lb.in^{-2} absolute. Pressures in the glass vacuum lines were measured using mercury manometers.

Vacuum on glass lines was attained by using Edwards E2M8 direct drive vacuum pumps. Two pumps were incorporated on the metal line; one, a roughing pump (Edwards E2M8), was used for initial evacuation of the apparatus and removal of volatile fluorinated compounds by pumping through a soda lime trap. The second pump (precision Model 75 two stage rotary oil pump) provided the vacuum source (ca. $<10^{-4}$ Torr) for the manifold. In order to protect the pumps on the metal line, all volatile fluorinated compounds were disposed of by pumping, by means of the roughing pump, through a soda lime trap consisting of a copper tube (ca. 60 cm long x 15 cm dia.) packed with soda lime absorbent (Fisher Scientific, 4-8 mesh) followed by a liquid nitrogen cold trap to remove H_2O, CO_2 and other unreactive condensible volatiles.

(ii) Preparative Apparatus and Sample Vessels

All synthetic procedures were performed in apparatus constructed from either nickel, glass, Kel-F or FEP. Sample preparations were carried out in tubes fashioned from lengths of FEP tubing (Chemplast Inc. or Fluorocarbon Co.) and attached to Kel-F valves encased in aluminum housings. All vessels were seasoned with liquid HF and then pumped on the vacuum line for 1-2 days prior to use. For bulk preparations, (> 2 g), ¾" o.d. FEP tubes were used which were heat-sealed at one end and heat-flared (45° SAE)

at the other end. For small scale preparations (< 2 g), ¼" o.d. FEP tubes were used which were heat sealed at one end and flared (45° SAE) at the other end.

Nuclear magnetic resonance (NMR) spectra were recorded in FEP tubes (9 mm o.d.). The 9 mm o.d. FEP NMR tubes were fabricated from lengths of ⅜" (9.5 mm) o.d. FEP tubing by reducing their diameter to 9 mm o.d. in a heated brass cylindrical form with mechanical pressure. One end of the tube was heat-sealed by pushing it into the end of a thin-walled 10 mm o.d. glass NMR tube previously heated in a Bunsen flame. The other end was heat-flared (45° SAE) for attachment to a Kel-F valve. The 4 mm o.d. FEP tubing had one end heat-sealed by pushing the tube into the end of a heated thin walled 5 mm o.d. glass NMR tube and the other end heat-flared (45° SAE) for attachment to a Kel-F valve. The sample tubes used for recording NMR spectra were heat sealed using either an oxygen torch for the glass tubes or a small diameter nichrome wire resistance furnace for the FEP tubes. All vacuum transfers were carried out through Teflon, FEP and/or Kel-F adaptors. All tubing was connected using ¼" Teflon unions (Swagelok) and Teflon compression fittings (back and front ferrules, Hoke Controls). The fluoroplastic valves and connectors have been described in greater detail elsewhere.[125]

(B) PREPARATION AND PURIFICATION OF STARTING MATERIALS

(i) HF and BrF_5 Solvents

All solvents were transferred on a metal vacuum line through all fluoroplastic connections.

Anhydrous hydrogen fluoride, HF, (Harshaw Chemical Co.) was purified by treatment with 5 atm. of F_2 gas in a nickel can for a period of 1 month converting residual water to HF and O_2 gas. After the specified time period, anhydrous HF was vacuum distilled into a dry Kel-F storage vessel equipped with a Kel-F valve and stored at room temperature until used.

Bromine pentafluoride, BrF_5 (Ozark Mahoning) was purified as described earlier,[125] and stored over dry KF in a ¾" Kel-F storage tube equipped with a Kel-F valve.

(ii) Purification of Fluorine

Fluorine, 98% containing ca. 0.2% HF (Air Products and Chemicals, Inc.) was used during the course of this work. Hydrogen fluoride was effectively removed, prior to usage, by passing the fluorine through a Matheson model 68-1008 hydrogen fluoride trap. The trap consisted of a brass cylinder packed with porous sodium fluoride pellets and surrounded by an insulated coil of nichrome resistance wire. The activity of sodium fluoride was maintained by periodic heating at 250 to 300 °C, while purging with dry nitrogen gas.

(iii) Xenon Gas

Xenon gas, 99% (Linde) was used directly from the cylinder on a metal vacuum line.

(iv) Preparation of XeF_2

The method used for the preparation of xenon difluoride XeF_2 was similar to that used by Malm and Chernick[15] for the preparation of XeF_4. Two parts xenon and one part fluorine were allowed to react in a nickel can (249 mL) at 400 °C for 7 hours. In a typical preparation, xenon (0.354 mol) and fluorine (0.177 mol) were condensed into a nickel reaction can (826 mL; ¼" walls) at -196 °C. The can and contents were then allowed to warm to room temperature. At room temperature, the total pressure in the can was ca. 34.4 atm. An electric furnace, preheated to 400 °C, was placed around the nickel can and maintained there for 7 hours. The initial pressure in the can at 400 °C, assuming no reaction, was ca. 78.5 atm. After the specified time period, the furnace was removed and the can and the contents immediately "quenched" in cold water. The can and contents were then further cooled to -196 °C; at this temperature any unreacted fluorine was pumped off. The can and contents were then warmed to -78 °C and excess xenon was condensed into a nickel storage vessel at -196 °C. The XeF_2 was collected by pumping the contents of the nickel reaction can, warmed to 50 °C, through a ¼" o.d. FEP U-tube cooled to -78 °C. The purity of the product was checked by recording the Raman spectrum in the range 450-600 cm^{-1}. Xenon difluoride has a strong line at 496 cm^{-1}, whereas the most likely impurity, XeF_4, has two strong lines at 502 and 543 cm^{-1}. The maximum amount of XeF_4 found in any of the preparations was generally estimated to be less than 0.5%. The product was stored under an atmosphere of dry nitrogen in an FEP storage vessel at room temperature. All XeF_2 transfers were made as a solid in an inert atmosphere drybox.

(v) Preparation of Arsenic(V) Fluoride, AsF_5

Arsenic(V) fluoride was prepared according to the reactions (2.1) and (2.2)

$$As_2O_3 + 3\ CaF_2 + 3\ H_2SO_4 \longrightarrow 2\ AsF_3 + 3\ CaSO_4 + 3\ H_2O \qquad (2.1)$$

$$AsF_3 + F_2(\text{excess}) \longrightarrow AsF_5 \qquad (2.2)$$

Arsenic(III) fluoride, AsF_3, was prepared according to the method of Hoffman;[151] and purified by distillation at atmospheric pressure in an all-glass system using a column packed with glass helices. The product was stored over sodium fluoride (previously dried under low pressure and high temperature, 200 ~ 300 °C) for at least 24 hours prior to use.

Arsenic(III) fluoride (75.000 g, 568.54 mmol) and fluorine (731 mmol) were condensed into a nickel reaction can (1976 mL; ⅛" walls) at -196 °C. The can and contents were then allowed to warm to room temperature. An electric furnace, preheated to 200 °C, was placed around the nickel can and maintained there for 24 hours. After the specified time period, the furnace was removed and the can and the contents cooled to room temperature. The can and the contents were then further cooled to -196 °C; at this temperature excess fluorine was pumped off through a soda lime trap. The can and contents were then warmed to -90 °C (dry ice). Arsenic pentafluoride was collected by condensing the contents of the nickel reaction can into a nickel storage vessel at -196 °C; at this temperature no HF impurity was expected to transfer. The nickel storage can and contents were stored at room temperature until used. Arsenic pentafluoride was used without further purification.

(vi) Preparation of $Xe_2F_3^+AsF_6^-$ and $XeF^+AsF_6^-$

The salts, $Xe_2F_3^+AsF_6^-$ and $XeF^+AsF_6^-$, were prepared according to the reactions (2.3) and (2.4) in HF solvent.

$$2\ XeF_2 + AsF_5 \longrightarrow Xe_2F_3^+AsF_6^- \qquad (2.3)$$

$$XeF_2 + AsF_5 \longrightarrow XeF^+AsF_6^- \qquad (2.4)$$

In a typical preparation 0.8150 g (4.796 mmol) of AsF_5 was distilled onto 1.6267 g (9.608 mmol) XeF_2 at -196 °C in HF (10 mL) solvent. The mixture was warmed to room temperature to dissolve all the XeF_2 and then cooled to -78 °C (dry ice-acetone bath) and the HF removed under vacuum to yield $Xe_2F_3^+AsF_6^-$.

Using a method similar to that used to prepare $Xe_2F_3^+AsF_6^-$, $XeF^+AsF_6^-$ was prepared by condensing, 11.2352 g (66.123 mmol) of AsF_5 onto 11.1944 g (66.123 mmol) XeF_2 at -196 °C in HF solvent (10 mL). The procedure was then exactly the same as for the isolation of $Xe_2F_3^+AsF_6^-$.

The purities of the products were checked by recording their Raman spectra in the range 0 to 950 cm^{-1}. The products were stored under an atmosphere of dry nitrogen in FEP storage vessels at room temperature. All transfers of $XeF^+AsF_6^-$ and $Xe_2F_3^+AsF_6^-$ were made in the drybox.

(vii) Preparation of Hydrogen Cyanide, HC≡N and $H^{13}C{\equiv}N$

Hydrogen cyanide, HC≡N, was prepared according to the method of King and Nixon [152] (equation 2.5), that is to say, by dropwise addition of H_2O to an equimolar

$$3\ KCN + 3\ H_2O + P_2O_5 \longrightarrow 3\ K_3PO_4 + 3\ HC{\equiv}N \qquad (2.5)$$

mixture of KCN (Merck) or $K^{13}CN$ (Merck) and P_4O_{10} (British Drug House), vessel A (Figure 2.4). The reaction vessels for the preparation of $HC{\equiv}N$ and $H^{13}C{\equiv}N$ are depicted in Figures 2.3 and 2.4, respectively. The $HC{\equiv}N$ gas evolved was collected in a glass U-tube at -196 °C, and finally transferred to vessel B for drying over P_4O_{10}. The purity of the product was checked by recording the IR spectrum of 108 mm Hg, $HC{\equiv}N$, which gave the same frequencies as previously reported in the literature.[152] In addition, ^1H and ^{13}C NMR spectroscopy of the neat liquid confirmed that less than 1% impurities were present in the $HC{\equiv}N$.

(viii) Purification of Nitriles and Perfluoropyridines

$CH_3C{\equiv}N$ (Aldrich), $CH_2FC{\equiv}N$ (Aldrich), $CH_2ClC{\equiv}N$ (Aldrich), $C_2H_5C{\equiv}N$ (Aldrich), *n*-$C_3H_7C{\equiv}N$ (Aldrich), $(CH_3)_2CHC{\equiv}N$ (Aldrich), $(CH_3)_3CC{\equiv}N$ (Aldrich), $ClCH_2C(CH_3)HC{\equiv}N$ (Aldrich), *n*-$C_4H_9C{\equiv}N$ (Aldrich) and ^{13}C and ^{15}N enriched acetonitrile, $^{13}CH_3C{\equiv}N$, $^{13}CH_3{}^{13}C{\equiv}N$, $CH_3C{\equiv}{}^{15}N$ and $CH_3{}^{13}C{\equiv}N$ (MSD Isotopes), were dried by periodic shaking with anhydrous CaH_2 over a period of several days prior to use and were stored over anhydrous CaH_2 in 10 mL glass storage bulbs equipped with grease free 4 mm Young FEP and glass valves until used.

Pentafluoropyridine, C_5F_5N (Aldrich), and 2,3,5,6-tetrafluoro-4-trifluoromethylpyridine, 4-$CF_3C_5F_4N$ (Ishihara, Tokyo), 3,4,5,6-tetrafluoro-2-trifluoromethylpyridine, 2-$CF_3C_5F_4N$ (Ishihara, Tokyo), were dried by periodic shaking

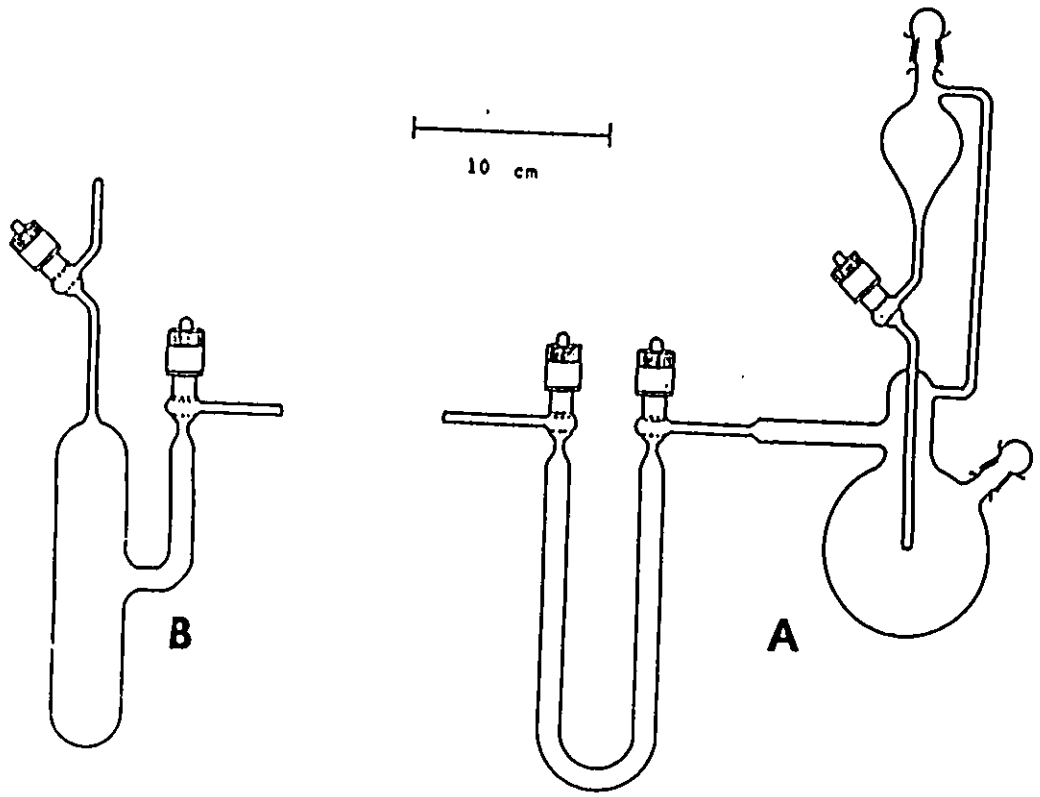

Figure 2.3 Reaction vessel for the preparation of anhydrous hydrogen cyanide HC≡N. (A) 500 mL round bottom flask and 100 mL pressure equalized dropping funnel. All stopcocks are grease-free 6 mm glass stopcocks equipped with FEP barrels (J. Young). (B) The volume of the Pyrex glass U-trap is 250 mL and serves as the HC≡N storage vessel; it is also equipped with 6 mm glass/FEP Young stopcocks.

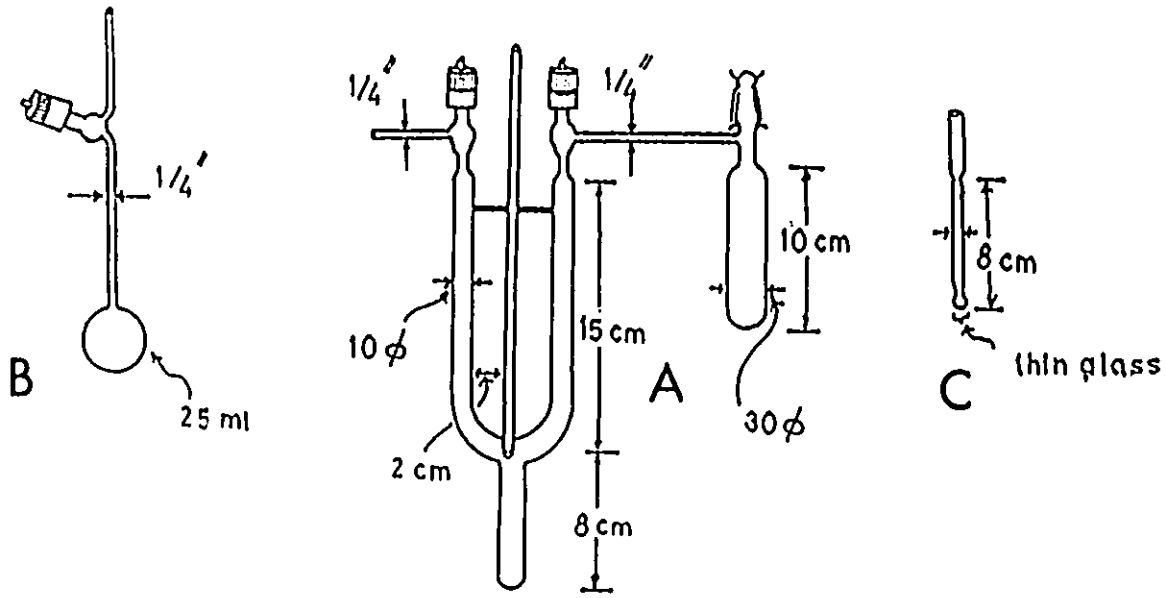

Figure 2.4 Reaction vessel for the preparation of ^{13}C-enriched hydrogen cyanide H^{13}C≡N. (A) 100 mL flask connected to a 100 mL Pyrex glass U-trap with a 35 mL finger. The stopcocks are grease-free 6 mm glass Young stopcocks equipped with FEP barrels. (C) 4 mL sealed glass ampule with a thin glass bottom used for the addition of H_2O to the reaction mixture by transfer the glass ampule to the flask A and breaking the thin glass bottom end. (B) 25 mL HC≡N storage vessel.

with CaH_2 powder over a period of several days prior to use and were stored over CaH_2 in glass storage bulbs equipped with 4 mm glass/FEP Young stopcocks (previously described) until used. The purities of these compounds were verified by ^{19}F NMR spectroscopy. In case of 2,3,5,6-tetrafluoro-4-trifluoromethylpyridine, 4-$CF_3C_5F_4N$, some minor impurities were discovered in the ^{19}F NMR spectrum, which were less than 1 mole percent, and in case of 3,4,5,6-tetrafluoro-2-trifluoromethylpyridine, 2-$CF_3C_5F_4N$, the commercial sample was found to consist of a mixture of perfluoropyridines. The ^{19}F NMR spectrum of the latter sample is given in (Figure 2.5) and shows that the fluorinated components consist of (A) 2-$CF_3C_5F_4N$, 50%; (B) C_5F_5N, 20%; (C) 3-$CF_3C_5F_4N$, 18%; (D) 4-$CF_3C_5F_4N$, 10% and 3-CF_3-4-$CF_3C_5F_3N$, 2%.

(ix) Preparation of $C_5F_4NH^+AsF_6^-$ and $R_FC_5F_4NH^+AsF_6^-$ (R_F = 2-CF_3, 3-CF_3 and 4-CF_3)

The perfluoropyridinium salts, $R_FC_5F_4NH^+AsF_6^-$ (R_F = F, 2-CF_3, 3-CF_3 and 4-CF_3), were prepared according to equations (2.6) and (2.7)

$$R_FC_5F_4N + (x + 1)\ HF \longrightarrow R_FC_5F_4NH^+F(HF)_x^- \qquad (2.6)$$

$$R_FC_5F_4NH^+F(HF)_x^- + AsF_5 \longrightarrow R_FC_5F_4NH^+AsF_6^- + x\ HF \qquad (2.7)$$

In a typical reaction, 2.8931 g (17.026 mmol) of AsF_5 was condensed in eight additions from a glass measuring bulb having a volume of 400.05 mL into an FEP vessel

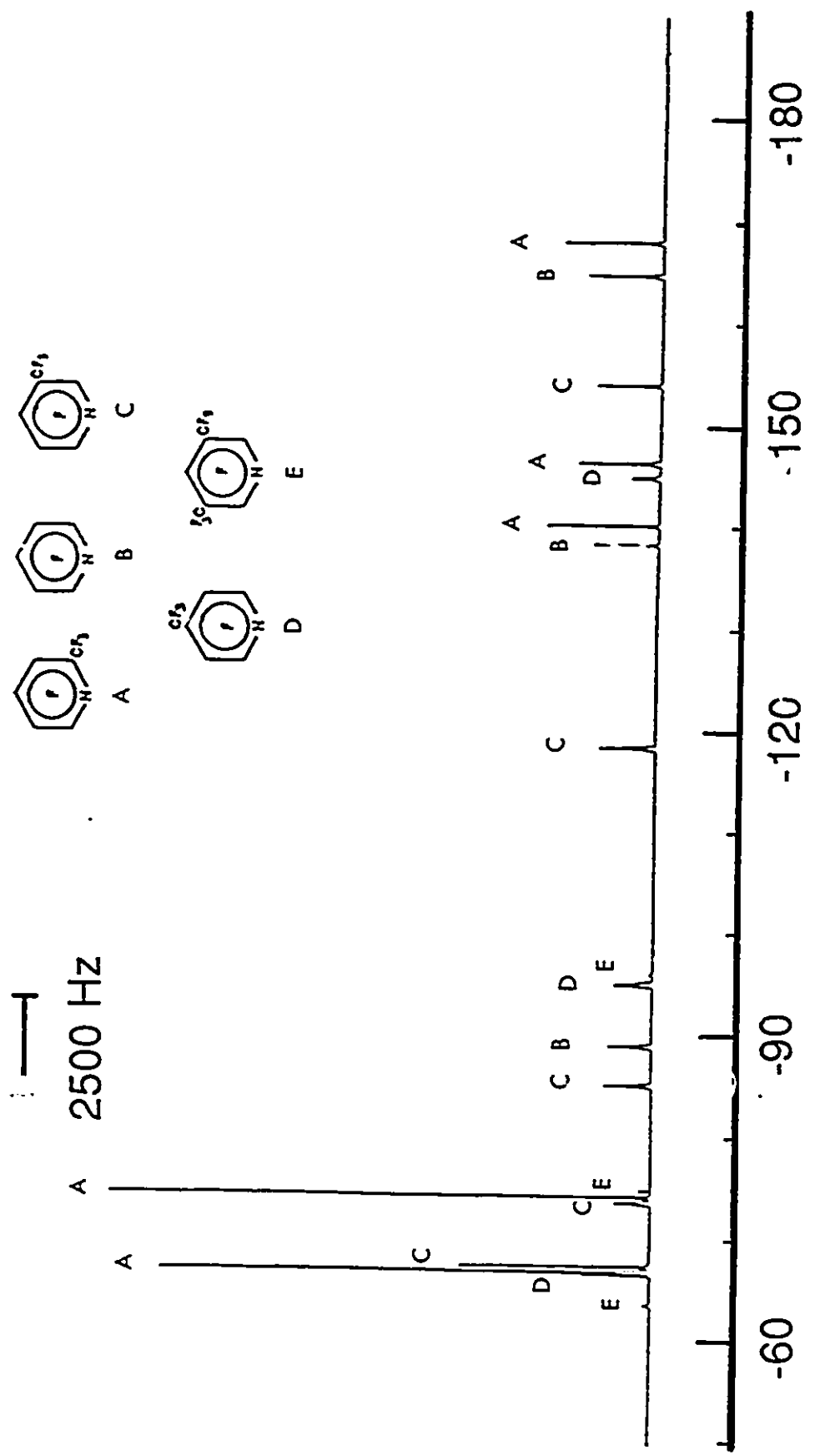

Figure 2.5 ^{19}F NMR spectrum of 2-$CF_3C_5F_4N$ (neat) at -15 °C and perfluoropyridine impurities.

containing a solution of 2.3441 g (13.866 mmol) C_5F_5N in 8 mL of anhydrous HF (cooled to -196 °C), and the sample warmed to -20 °C with mixing and then briefly to room temperature. A white precipitate formed after a few minutes upon cooling to 0 °C. The sample was then pumped on at -40 °C until all the HF and excess AsF_5 had been removed. The yield was 4.9536 g (99.98%). The ^{19}F NMR spectra confirmed the structure of $C_5F_5NH^+AsF_6^-$ in HF solvent ($\delta(^{19}F)_{ortho}$: -100.2 ppm, $\delta(^{19}F)_{meta}$: -158.6 ppm, $\delta(^{19}F)_{para}$: -108.6 ppm) and BrF_5 solvent ($\delta(^{19}F)_{ortho}$: -96.0 ppm, $\delta(^{19}F)_{meta}$: -154.1 ppm, $\delta(^{19}F)_{para}$: -102.4 ppm). The white salt was stored in a drybox at room temperature until used.

In a typical preparation, 2.3355 g (13.742 mmol) of AsF_5 was condensed in eight additions into an FEP vessel containing a solution of 2.2778 g (10.399 mmol) 4-$CF_3C_5F_4N$ in 8 mL of anhydrous HF (cooled to -196 °C), and the sample was warmed to 20 °C. Upon cooling to 0 °C, a pale yellow precipitate formed after a few minutes. The sample was then pumped on at -40 °C until all the HF and AsF_5 had been removed. The ^{19}F NMR spectrum confirmed the structure of 4-$CF_3C_5F_4NH^+AsF_6^-$ in HF solvent ($\delta(^{19}F)_{CF_3}$: -60.7 ppm, $\delta(^{19}F)_{ortho}$, -98.5 ppm, $\delta(^{19}F)_{meta}$, -136.1 ppm). The yield was 4.2530 g (100.00%). The pale yellow salt was stored in a drybox at room temperature until used.

In a typical preparation, 2.0150 g (11.801 mmol) of AsF_5 was condensed in eight additions into an FEP vessel containing a solution of 2.3134 g (11.845 mmol) 2-$CF_3C_5F_4N$ in 8 mL anhydrous HF (cooled to -196 °C). The procedure was then exactly the same as for the preparation of the $C_5F_5NH^+AsF_6^-$. The ^{19}F NMR spectrum showed the same distribution of perfluoropyridinium cations as observed for the perfluoropyridines in

Figure 2.5.

(C) PREPARATION OF XENON-NITROGEN BONDED CATIONS

Xenon-nitrogen bonded adduct cations were prepared by combining stoichiometric amounts of $XeF^+AsF_6^-$ or $Xe_2F_3^+AsF_6^-$ with hydrogen cyanide, alkylnitriles, pentafluorophenylnitrile, perfluoropyridines or by adding XeF_2 to protonated perfluoropyridine hexafluoroarsenates in HF or BrF_5 at -196 °C in the drybox and warming from -50 to -10 °C to effect reaction and dissolution in HF or BrF_5 solvents. The xenon-nitrogen cations were characterized in solution by ^{129}Xe, ^{19}F, ^{14}N, ^{15}N, ^{13}C and ^1H NMR spectroscopy and in the solid state by Raman spectroscopy at -196 °C.

(i) Preparation of $HC{\equiv}N\text{-}XeF^+AsF_6^-$, $[^{13}C]HC{\equiv}N\text{-}XeF^+AsF_6^-$ and $[^{15}N]HC{\equiv}N\text{-}XeF^+AsF_6^-$

Two additions of 0.04879 g (1.8073 mmol) of anhydrous HC≡N gas were made by condensing onto 0.4747 g (1.612 mmol) of $XeF^+AsF_6^-$ or 0.03843 g (1.038 mmol) of anhydrous HC≡N gas was distilled onto 0.4722 g (0.9286 mmol) $Xe_2F_3^+AsF_6^-$ in ca. 4 mL of HF solvent. Each addition has been done by condensing the anhydrous HC≡N gas from a 54.51 mL calibrated bulb (C) (Figure 2.6) at a known low-pressure (the total HC≡N pressure did not exceed 100 - 120 mm Hg) at 25 °C to minimize dimer formation.[152] After every addition at -196 °C, the reaction mixture was warmed to -10 °C to dissolve the starting materials, and then frozen again to -196 °C. The excess HC≡N in the main glass manifold was recovered by condensation into vessel (E) at -196 °C.

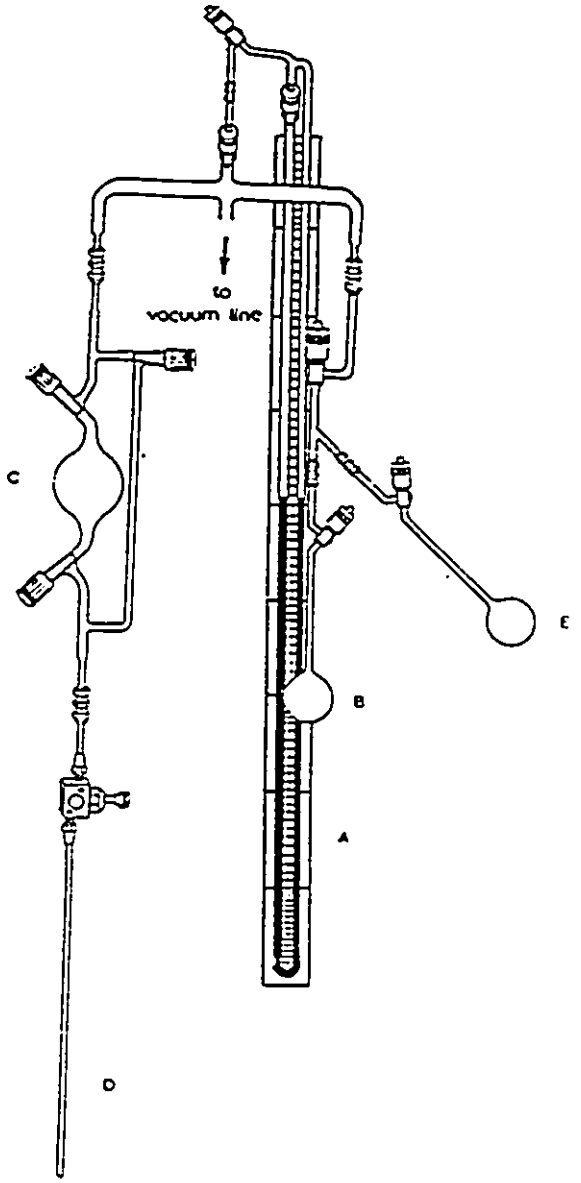

Figure 2.6 Apparatus used for the preparation of $HC{\equiv}N\text{-}XeF^{+}AsF_6^{-}$; (A) manometer, (B) liquid $HC{\equiv}N$ storage vessel, (C) calibrated bulb, 54.51 mL, (D) Kel-F valve connected to FEP reaction vessel, (E) vessel used to recover excess $HC{\equiv}N$ from main glass manifold.

After the additions were completed, the reaction mixture was warmed to -20 °C to effect dissolution and complete the reaction (equations (2 8) and (2.9). Figure 2.6 shows the

$$HC{\equiv}N + XeF^{+}AsF_6^{-} \longrightarrow HC{\equiv}N\text{-}XeF^{+}AsF_6^{-} \qquad (2.8)$$

$$HC{\equiv}N + Xe_2F_3^{+}AsF_6^{-} \longrightarrow HC{\equiv}N\text{-}XeF^{+}AsF_6^{-} \qquad (2.9)$$

apparatus used to transfer HC≡N and $H^{13}C{\equiv}N$ onto a $XeF^{+}AsF_6^{-}$/HF or $Xe_2F_3^{+}AsF_6^{-}$/HF mixture. The product, $HC{\equiv}N\text{-}XeF^{+}AsF_6^{-}$, was insoluble at -30 °C, however, by increasing the temperature gradually to -10 °C, it dissolved. Upon gradual cooling again, shiny white needle-shaped crystals were formed. The mixture was again cooled to -30 °C and HF was removed under vacuum. In the case of $Xe_2F_3^{+}AsF_6^{-}$, the product was pumped on for several additional hours at 0 °C to remove XeF_2, yielding a white product.

Another method also used for the preparation of natural abundance samples of the $HC{\equiv}N\text{-}XeF^{+}AsF_6^{-}$ salt was used for the preparation of the enriched samples, $H^{13}C{\equiv}N\text{-}XeF^{+}AsF_6^{-}$ and $HC{\equiv}^{15}N\text{-}XeF^{+}AsF_6^{-}$. This entailed dissolving dry enriched potassium cyanide in anhydrous HF and co-distilling the enriched hydrogen cyanide and the HF solvent onto $XeF^{+}AsF_6^{-}$ salt according to equations (2.10) and (2.3). In a typical preparation, 0.1498 g (2.996 mmol) of $K^{13}CN$ was dissolved in HF solvent. The resulting

$$K^{13}C{\equiv}N/KC{\equiv}^{15}N + (x+1)HF \xrightarrow{HF} KHF_2.xHF + H^{13}C{\equiv}N/HC{\equiv}^{15}N \qquad (2.10)$$

$H^{13}C{\equiv}N$ and HF solvent were then vacuum distilled into a second 9 mm FEP tube leaving behind a residue of $KHF_2{\cdot}xHF$. The $H^{13}C{\equiv}N$ and HF solvent were finally condensed into a third 9 mm FEP tube containing 0.5480 g (1.616 mmol) of $XeF^+AsF_6^-$ at -196 °C. After the addition was completed, the mixture was warmed to -20 °C to effect dissolution and complete the reaction. The product, $H^{13}C{\equiv}N\text{-}XeF^+AsF_6^-$, was completely soluble at -10 °C and by cooling gradually again, shiny needle-shaped crystals were formed. The product was isolated at -30 °C by removal of the HF under vacuum.

The ^{15}N enriched salt, $HC{\equiv}^{15}N\text{-}XeF^+AsF_6^-$, was prepared according to the reactions (2.10) and (2.8). In a typical preparation, 0.1482 g (2.242 mmol) of $KC^{15}N$ and 0.4114 g (1.213 mmol) $XeF^+AsF_6^-$ were used. The method was identical to that used for the preparation of the $H^{13}C{\equiv}NXeF^+AsF_6^-$ salt.

The Raman spectra were recorded for the isolated natural abundance and the enriched samples of $HC{\equiv}NXeF^+AsF_6^-$ salts. These samples were then transferred, at low temperature inside the dry box, into 10 mm or 5 mm thin walled glass tubes and BrF_5 solvent was vacuum distilled into each tube on the metal vacuum line. The tubes were heat sealed and used for ^{129}Xe, ^{19}F, ^{14}N, ^{15}N, ^{13}C and ^1H NMR spectroscopy.

(ii) Preparation of $RC{\equiv}N\text{-}XeF^+AsF_6^-$

The appropriate amount of each nitrile was vacuum distilled at -196 °C onto $XeF^+AsF_6^-$ or $Xe_2F_3^+AsF_6^-$ dissolved in anhydrous HF. The mixture was then warmed to -30 to -20 °C to effect dissolution and complete reaction. Figure 2.7 shows the apparatus used for the vacuum transfer of HF onto $XeF^+AsF_6^-$ or $Xe_2F_3^+AsF_6^-$ salts.

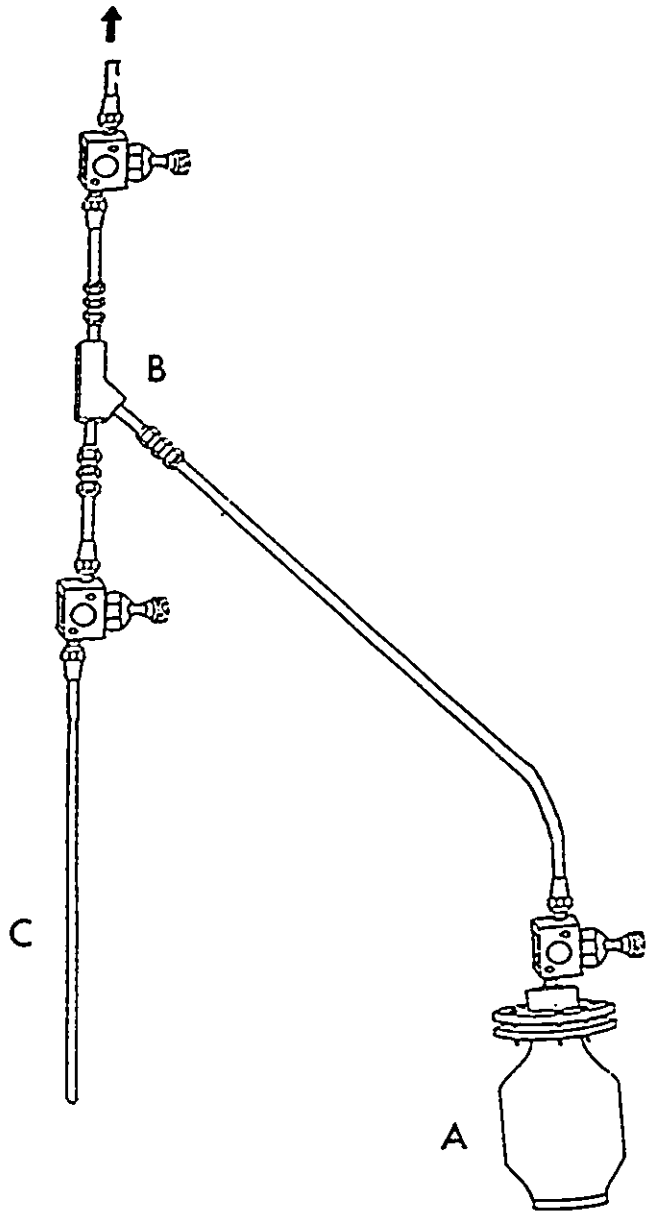

Figure 2.7 Apparatus for the vacuum transfer of anhydrous HF used in the preparation of $RC{\equiv}N\text{-}XeF^{+}AsF_6^{-}$ salts; (A) 250 mL Kel-F HF container equipped with a Kel-F valve, (B) FEP Y-connector, (C) FEP reaction tube equipped with a Kel-F valve.

Figure 2.8 shows the apparatus used to distill each nitrile onto $XeF^+AsF_6^-$ or $Xe_2F_3^+AsF_6^-$ in HF. Table 2.1 lists the amounts of $XeF^+AsF_6^-$ (or $Xe_2F_3^+AsF_6^-$) and each nitrile used in the preparation of each NMR and Raman sample. Several $RC{\equiv}N\text{-}XeF^+AsF_6^-$ (R = CH_3, CH_2F, CH_2Cl, C_2H_5, $(CH_3)_2CH$ and $(CH_3)_3C$) salts were isolated at -30 °C and the HF removed under vacuum, yielding white products.

(iii) Preparation of $C_5F_5N\text{-}XeF^+AsF_6^-$

To 0.1549 g (0.915 mmol) of XeF_2 was added 0.3221 g (0.897 mmol) of $C_5F_5NH^+AsF_6^-$ at -196 °C in a drybox. Bromine pentafluoride was then vacuum distilled onto the mixture, (ca. 3 mL) at -196 °C. The mixture was then warmed to -30 to -25 °C to effect dissolution of the reactants. The BrF_5 in the resulting yellow solution was removed under vacuum at -30 to -20 °C to give a light yellow powder which upon further pumping became white when all the solvent had been removed (Figure 2.9).

(iv) Preparation of $4\text{-}CF_3C_5F_4N\text{-}XeF^+AsF_6^-$ and $2\text{-}CF_3C_5F_4N\text{-}XeF^+AsF_6^-$

The synthetic procedures were exactly the same as for the preparation of the $C_5F_5N\text{-}XeF^+AsF_6^-$ salt. The following quantities of the reagents were used: 0.3374 g (0.825 mmol) of $4\text{-}CF_3C_5F_4NH^+AsF_6^-$ was added to 0.1397 g (0.8825 mmol) of XeF_2 and 0.3409 g (0.832 mmol) of $2\text{-}CF_3C_5F_4NH^+AsF_6^-$ was added to 0.1510 g (0.893 mmol) of XeF_2 at -196 °C. The procedure was carried out with the reaction vessel inside a cold trap precooled to -196 °C. The Raman spectrum of $4\text{-}CF_3C_5F_4N\text{-}XeF^+AsF_6^-$ showed signs of decomposition after pumping off the solvent under vacuum at -30 °C. The ^{19}F and ^{129}Xe

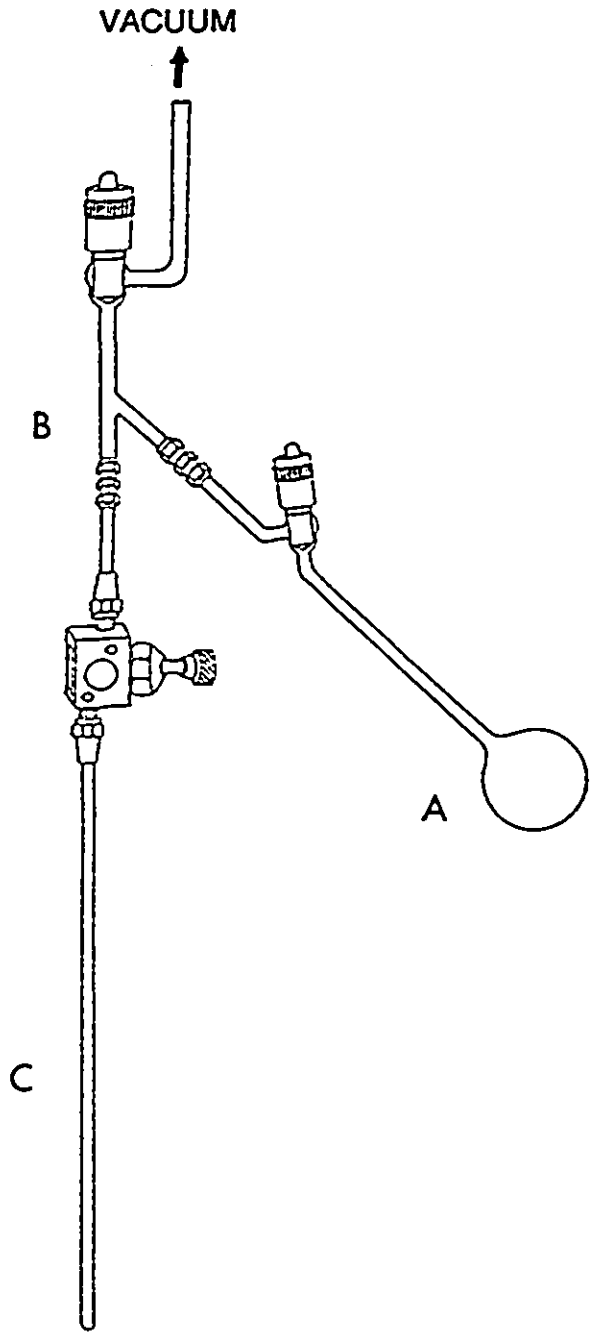

Figure 2.8 Glass vacuum distillation apparatus for the preparation of RC≡N-$XeF^+AsF_6^-$ salts; (A) nitrile storage container, (B) Y-glass connection, (C) FEP reaction tube equipped with a Kel-F valve.

Table 2.1

Quantities of Nitriles and $XeF^+AsF_6^-$ ($Xe_2F_3^+AsF_6^-$) Used to Prepare NMR and Raman Samples in Anhydrous HF solvent

Nitrile	Amount of Nitrile, g[b]	Amount $XeF^+AsF_6^-$ [$Xe_2F_3^+AsF_6^-$], g[a,b]	Conditions	$RC{\equiv}N{\rightarrow}XeF^+$
$CH_3C{\equiv}N$	0.0402(0.979)[c] 0.0109(0.267)[d] 0.0709(1.727)[e]	[0.4967](0.977) 0.0909(0.268) 0.5848(1.724)	-10 °C	$CH_3C{\equiv}N{\rightarrow}XeF^+$
$C_2H_5C{\equiv}N$	0.0588(1.068)[c] 0.0230(0.418)[d] 0.0928(1.685)[e]	[0.5424](1.067) 0.1569(0.463) 0.5700(1.680)	-10 °C	$C_2H_5C{\equiv}N{\rightarrow}XeF^+$
			25 °C, 2h	$CH_2FCH_2C{\equiv}N{\rightarrow}XeF^+$
$CH_2FC{\equiv}N$	0.0549(0.930)[c] 0.1099(1.862)[e]	[0.4715](0.927) 0.6312(1.868)	-10°C	$CH_2FC{\equiv}N{\rightarrow}XeF^+$
$CH_2ClC{\equiv}N$	0.0639(0.846)[c] 0.1057(1.400)[e]	0.2822(0.822) 0.4742(1.398)	-10°C	$CH_2ClC{\equiv}N{\rightarrow}XeF^+$
n-$C_3H_7C{\equiv}N$	0.0703(1.018)[c] 0.019(0.2735)[d]	0.3406(1.004) 0.0924(0.272)	-15 °C	$CH_3CH_2CH_2C{\equiv}N{\rightarrow}XeF^+$ $CH_2FCH_2CH_2C{\equiv}N{\rightarrow}XeF^+$ $CH_3CHFCH_2C{\equiv}N{\rightarrow}XeF^+$
			25 °C, 2h	$CHF_2CH_2CH_2C{\equiv}N{\rightarrow}XeF^+$
n-$C_4H_9C{\equiv}N$	0.0791(0.952)[c] 0.0227(0.273)[d]	0.3212(0.947) 0.0919(0.271)	-50 °C	$CH_3CH_2CH_2CH_2C{\equiv}N{\rightarrow}XeF^+$
			-25 °C	$CH_2FCH_2CH_2CH_2C{\equiv}N{\rightarrow}XeF^+$ $CH_3CHFCH_2CH_2C{\equiv}N{\rightarrow}XeF^+$
$ClCH_2C(CH_3)HC{\equiv}N$	0.0928(0.896)[c] 0.0161(0.156)[d]	0.2997(0.884) 0.0525(0.153)	-10 °C	$ClCH_2C(CH_3)HC{\equiv}N{\rightarrow}XeF^+$ $FCH_2C(CH_3)HC{\equiv}N{\rightarrow}XeF^+$
$(CH_3)_2CHC{\equiv}N$	0.0442(0.639)[c] 0.0743(1.364)[e]	0.2162(0.637) 0.4620(1.362)	-10 °C	$(CH_3)_2CHC{\equiv}N{\rightarrow}XeF^+$
$(CH_3)_3CC{\equiv}N$	0.0577(0.694)[c] 0.1170(1.409)[e]	0.2258(0.666) 0.4750(1.400)	-10 °C	$(CH_3)_3CC{\equiv}N{\rightarrow}XeF^+$
$C_6F_5C{\equiv}N$	0.1276(0.661)[c]	[0.3504](0.689)	-10 ~ -20 °C	$C_6F_5C{\equiv}N{\rightarrow}XeF^+$

Continued ...

Table 2.1 (continued)

a The amount of $Xe_2F_3^+AsF_6^-$ is given in brackets [ ].

b The amount in mmol is given in parentheses ( ).

c A 9 mm o.d. FEP tube.

d A 4 mm o.d. FEP tube.

e A ¼" o.d. FEP tube for solid Raman sample; HF solvent was removed under vacuum for 2 hours at -35 °C.

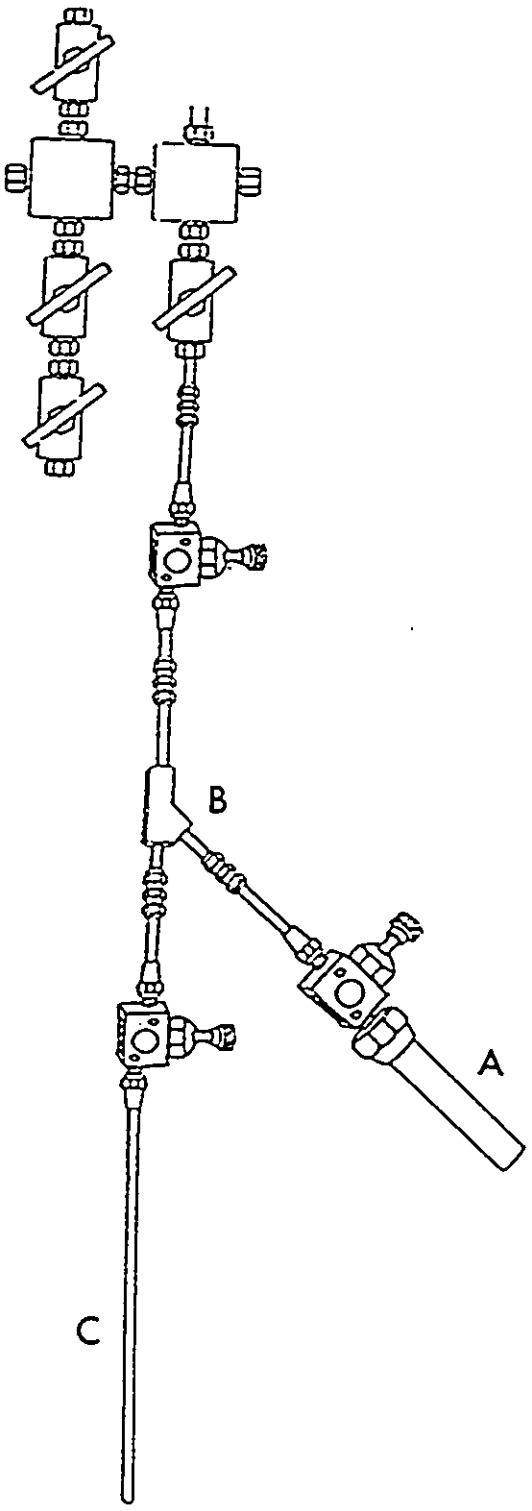

Figure 2.9 Bromine pentafluoride distillation apparatus used for the preparation of $R_FC_5F_4N$-$XeF^+AsF_6^-$ salts; (A) ¾" o.d. Kel-F storage vessel containing BrF_5 over KF, (B) Kel-F Y-connector, (C) ¼" o.d. FEP NMR tube connected to a Kel-F valve.

and ^{129}Xe NMR spectra of 2-$CF_3C_5F_4N$-$XeF^+AsF_6^-$ showed that the reaction was actually a mixture of four Xe-N bonded cations, C_5F_5N-XeF^+, 2-$CF_3C_5F_4N$-XeF^+, 3-$CF_3C_5F_4N$-XeF^+, 4-$CF_3C_5F_4N$-XeF^+ cations in the ratio 2.1 : 5.1 : 1.8 : 1.0.

(D) REACTION OF HYDROGEN CYANIDE, HC≡N, WITH ANHYDROUS HF

In a typical preparation, 0.0412 g (1.526 mmol) of HC≡N gas was distilled onto ~ 1 mL of HF solvent. The addition was accomplished by condensing anhydrous HC≡N gas from a 54.51 mL calibrated bulb at known low-pressure into the reaction vessel cooled to -196 °C. The sample was sealed and warmed to room temperature for 26 hours. The ^{19}F, ^{13}C, ^{14}N, ^1H NMR spectra showed the product of the reaction of HC≡N in HF is a single species, namely, the $CHF_2NH_3^+$ cation (equation 2.11).

$$HCN + 3\ HF \xrightarrow{x\ HF} CHF_2NH_3^+\ F(HF)_x^- \qquad (2.11)$$

(E) REACTIONS OF ALKYLNITRILES, RC≡N, WITH ANHYDROUS HF

Anhydrous HF solvent (3 mL) was vacuum distilled onto samples of the alkylnitriles, $CH_3C{\equiv}N$, 0.6450 g (15.712 mmol), $C_2H_5C{\equiv}N$, 0.3002 g (5.450 mmol), *n*-$C_3H_7C{\equiv}N$, 0.6331 g (9.161 mmol) and *n*-$C_4H_9C{\equiv}N$, 0.5543 g (6.669 mmol), in 9 mm FEP tubes and the reaction mixtures were warmed at room temperature. The mixtures were held for 7 days a. room temperature. All the samples gave yellow colored solutions

except the acetonitrile sample which remained colorless. The ^{19}F NMR spectra showed four different signals. After warming the reaction samples for 6 - 12 hours, the ^{19}F NMR spectra only showed the same signals with different intensities, indicating that the four ^{19}F signals resulted from four different fluorinated species in HF solvent. Repetition of these reactions was followed by warming 7 days at room temperature, and pumping off the HF solvent at -30 °C for 2 hours. The samples were then warmed to room temperature and pumped for a further three days. All the samples formed colorless viscous liquids. Some attempts have been made to crystallize the products as solids by redissolving the products in dimethylether, DMF, H_2O, acetone or CH_2Cl_2 without success. The viscous liquid products were very hygroscopic and formed white precipitates in H_2O. The acetonitrile sample was the only one which could be isolated as a solid product from CH_2Cl_2. The final products have been characterized by redissolving the samples in HF solvent in 9 mm or 4 mm FEP tubes and recording their ^{19}F, ^{13}C ^{14}N, ^{15}N and ^{1}H NMR spectra.

(F) NUCLEAR MAGNETIC RESONANCE SPECTROSCOPY

(i) Instrumentation

All NMR spectra were recorded unlocked (field drift < 0.1 Hz h^{-1}) with the use of Bruker AC-200 (4.6975 T), WM-250 (5.8719 T) and AM-500 (11.7440 T) spectrometers equipped with Aspect 2000 or 3000 computers.

Spectra were recorded on natural abundance, ^{13}C (99.0%, 99.2% and 99.7%) and ^{15}N (99.0% and 99.5%) enriched samples in heat sealed 9 mm o.d. or 4 mm o.d. FEP

NMR tubes (HF and BrF_5 solvents) or in 5 mm precision Pyrex tubes (BrF_5 solvent; Wilmad Glass Co.) as described below. The FEP sample tubes were placed inside precision 10 mm o.d. or 5 mm o.d. glass NMR tubes before being placed in the probe.

The ^{129}Xe, ^{14}N, ^{15}N, and ^{13}C spectra were recorded at 5.8719 T in 9 mm FEP sample tubes (HF and BrF_5 solvent) on the same 10 mm probe (broad-banded over the frequency range 23 - 103 MHz) tuned to 69.563 (^{129}Xe), 18.075 (^{14}N), 25.347 (^{15}N) or 62.915 (^{13}C) MHz, respectively. All ^{1}H and ^{13}C spectra recorded at 11.744 T in 4 mm FEP sample tubes in HF solvent were obtained using a switchable 5-mm $^{1}H/^{13}C$ probe and the standard ^{1}H and ^{13}C parameters. Proton spectra (200.133 MHz) were recorded at 4.6975 T in HF solvent in 4 mm FEP sample tubes and in BrF_5 solvent in medium or thin wall 5 mm o.d. precision glass sample tubes. Fluorine-19 spectra (235.361 MHz) were obtained on a 5 mm dual $^{1}H/^{19}F$ probe.

Xenon-129 NMR spectra of natural abundance $HC{\equiv}N\text{-}XeF^{+}AsF_6^{-}$ samples were recorded for spectral widths of 25 and 100 kHz with acquisition times of 0.164 and 0.082 s (17,000 and 150,000 scans), respectively, and a data point resolution of 6.10 Hz/pt. The ^{129}Xe NMR spectra of ^{13}C- and ^{15}N-enriched samples were recorded for spectral widths of 50 and 25 kHz (50,000 and 1200 - 2500 scans), respectively, with acquisition times of 0.328 and 0.655 s and data point resolutions of 3.05 and 1.53 Hz/pt., respectively. Fluorine-19 NMR spectra were recorded for spectral widths of 50 and 100 kHz with acquisition times of 0.082 and 0.164 s and data point resolutions of 3.05 and 6.10 Hz/pt. (4500 and 7500 scans), respectively. Nitrogen-15 and -14 relaxation times (T_1) were determined by the standard inversion-recovery method; the resulting data were

processed with standard Bruker software. The ^{1}H-2D COSY experiments were run using 521 increments in t_1 and 1024 data points in t_2. Quadrature detection was used, FIDs were multiplied by an exponential function prior to the Fourier transformations. The sweep width was 1,623 Hz in t_2 and 811 Hz in t_1 and the relaxation delay was 2 s. Eight scans were collected for each FID.

Pulse widths corresponding to bulk magnetization tip angles of ~90 ° were 22 (^{129}Xe), 2 (^{19}F), 49 (^{14}N), 35 (^{15}N), 7 (^{13}C) and 0.5 μs (^{1}H). No relaxation delays were applied except in the case of ^{15}N, where a relaxation delay of 10 or 30 s was applied. Line broadening parameters used in exponential multiplication of the free induction decays were set equal to or less than their respective data point resolutions. All line shape functions were Lorentzian with the exception of the ^{1}H and ^{13}C spectra and the ^{129}Xe NMR spectrum of [^{13}C]HC≡N-XeF$^+$AsF$_6^-$, in these cases Gaussian line shapes were applied for resolution enhancement.

The respective nuclei were referenced externally to neat samples of $XeOF_4$ (^{129}Xe), $CFCl_3$ (^{19}F), CH_3NO_2 (^{14}N and ^{15}N) and $(CH_3)_4Si$ (^{13}C and ^{1}H) at 24 °C using the WM-250 or AC-200 spectrometers and at 30 °C using the AM-500 spectrometer. Positive chemical shifts were assigned to resonances occurring to high frequency of the reference substance.[153]

For variable temperature measurements, samples were kept cold (-196 or -78 °C) until immediately prior to their placement in the probe. They were generally warmed only enough to liquify and solubilize the contents and were then quickly placed in the precooled probe. Prior to data accumulation, the tubes were allowed to equilibrate in the

probe for periods of several minutes while spinning. Temperatures were periodically checked by placing a copper constantan thermocouple into the sampling region of the probe. Temperatures were considered to be accurate to within ±1 °C.

All spectra were obtained on natural abundance compounds except ^{13}C and ^{15}N spectra; these spectra were obtained for samples prepared from 99.2% ^{13}C enriched $H^{13}C{\equiv}N$ and 99.5% ^{15}N enriched $HC{\equiv}^{15}N$, 99.7% ^{13}C enriched $^{13}CH_3C{\equiv}N$, 99.0% ^{13}C enriched $CH_3{}^{13}C{\equiv}N$, 99.7% ^{13}C enriched $^{13}CH_3{}^{13}C{\equiv}N$ and 99.0% ^{15}N enriched $CH_3C{\equiv}^{15}N$. Xenon-129 spectra were obtained in 400-1000 scans at a spectral width of 50 kHz or 100 kHz. Fluorine-19 spectra were obtained in 64-1600 scans at a spectral width of 100 kHz. Nitrogen-14 spectra were obtained in 2000-44000 scans at a spectral width of 10 kHz. Nitrogen-15 spectra were obtained in 10000-20000 scans at a spectral width of 15 kHz in HF solvent, while in BrF_5 solvent they were obtained in 20000 scans at a spectral of width 10 kHz. Carbon-13 spectra were obtained in 500-20000 scans at a spectral widths of 5, 15, 18 or 30 kHz in HF solvent, while in BrF_5 solvent they were obtained in 8 scans at a spectral width of 1 kHz. Proton spectra were obtained in 16-2000 scans at a spectral width of 4 or 7 kHz in HF solvent and 17690 scans at a spectral width of 29 kHz in BrF_5 solvent. The data point resolutions were ^{129}Xe (6.1 Hz/pt), ^{19}F (1.2, 2.2, 2.5, or 6.1 Hz/pt), ^{14}N (2.4 or 4.9 Hz/pt), ^{15}N (1.526 or 3.052 Hz/pt), ^{13}C (0.825, 1.9 or 2.4 Hz/pt) and ^{1}H (0.182, 0.368 or 0.4 Hz/pt).

(ii) NMR Sample Preparation

All sample tubes were interchangeable, and were used for either Raman or NMR

work. Tubes for use with systems that attack glass were made from 9 mm o.d., 0.9 mm wall or 4 mm o.d., 0.6 mm wall FEP tubing (Chemplast Inc. or Fluorocarbon Co.). Samples which did not attack glass surfaces were prepared in 5 mm o.d. thin wall precision polished glass NMR tubes (Wilmad) glassblown onto lengths of ¼" o.d. glass tubing.

Low volatility solids such as XeF_2, $XeF^+AsF_6^-$, $Xe_2F_3^+AsF_6^-$, $R_fC_5F_4NH^+AsF_6^-$ (R_f = F, 2-CF_3, 3-CF_3 and 4-CF_3) were conveniently transferred into preweighed sample tubes in a dry box. The solvents HF or BrF_5 were transferred under vacuum on a metal vacuum line through all fluoroplastic connections. Hydrogen cyanide was condensed from its storage vessel onto preweighed samples of solid $XeF^+AsF_6^-$ or $Xe_2F_3^+AsF_6^-$ at -196 °C in HF solvent and allowed to warm to -50 to -30 °C to effect reaction. Nitriles and perfluoropyridines were distilled directly from their storage vessels into preweighed sample tubes through a glass and fluoroplastic system.

Glass sample tubes were flame-sealed under vacuum by immersing the sample in liquid nitrogen. FEP sample tubes were sealed by immersing in liquid nitrogen, evacuating and allowing the tube to collapse by heating with a small cylindrical electrical tube furnace near the top of the sample tube. FEP tubes were inserted into thin-walled glass NMR tubes which were then placed in the NMR probe.

(G) LOW-TEMPERATURE RAMAN SPECTROSCOPY

(i) Instrumentation

A Coherent Model Innova 90 argon ion laser giving up to 3.5 W of power at 5145

Å was used to excite the Raman spectra. The spectrometer was a Spex Industries Model 1401S double monochromator equipped with 1800 grooves/mm Holographic gratings. Slit widths depended on the scattering efficiency of the sample but were typically set between 100-150 μm. The scanning rate typically used was 0.5 $cm^{-1}s^{-1}$. The typical power range used was between 0.5 and 1.5 W. All quoted Raman shifts are believed to be accurate to at least ± 2 cm^{-1}. Cylindrical FEP sample tubes (¼" o.d., 0.7 mm wall) were mounted vertically. The angle between the laser beam and sample tube was 45° and Raman scattered radiation was observed at 45° to the laser beam or 90° to the sample tubes. Low-temperature spectra were recorded by mounting the sample vertically in an unsilvered Pyrex glass Dewar filled with liquid nitrogen (Figure 2.10). All spectra were obtained directly in ¼" o.d. FEP reaction vessels.

Raman spectra were obtained exclusively in FEP sample tubes. The spectrum of the FEP sample tube was nearly always observed and in observing all the samples at -196 °C the intensities of the FEP lines relative to each other remained constant. Their prominence in the overall spectrum, however, depended on the efficiency of the sample as a Raman scatterer and where the laser beam was focused. At -196 °C, these lines and their relative intensities in the range 100-2200 cm^{-1} are: 117(2), 206(1), 295(24), 310(6), 382(19), 386(22), 579(7), 598(2), 736(100), 752(10), 1121(2), 1218(3), 1308(4) and 1383(10) cm^{-1}. Furthermore, liquid N_2 gave a strong line at 2325 cm^{-1}. In the present work, lines arising from FEP have been subtracted out of the spectra reported in the Tables but not in the Figures.

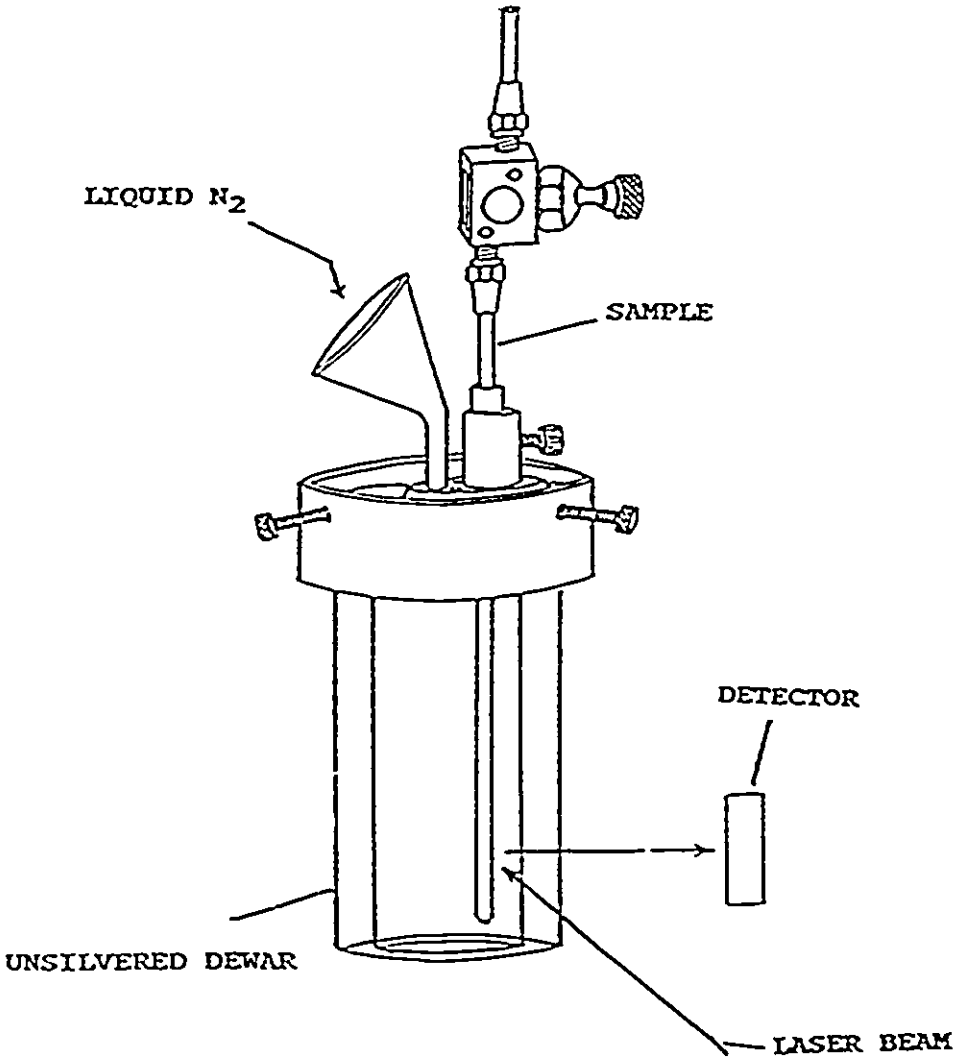

Figure 2.10 Unsilvered glass Dewar used for recording Raman spectra at low temperature.

(ii) Raman Sample Preparation

All Raman sample tubes used for Raman work were made from ¼" o.d., 0.7 mm wall FEP tubing. The ¼" o.d. FEP Raman tubing had one end that was heat sealed by pushing it into the end of a hot piece of 7 mm i.d. glass tubing that had been previously stretched to approximately 0.5 mm on one end (left open) using an oxygen torch, and the other end was heat flared (45° SAE) for attachment to a Kel-F valve. All the Raman samples were pressurized to ~2 atm. by dry N_2 gas and stored at -78 °C until used.

CHAPTER 3

FLUORO(HYDROGEN CYANIDE)XENON(II) HEXAFLUOROARSENATE

$HC{\equiv}N\text{-}XeF^{+}AsF_6^{-}$

INTRODUCTION

While many examples of xenon bonded to oxygen or fluorine and of xenon bonded to other highly electronegative inorganic ligands through oxygen were synthesized immediately following the discovery of noble-gas reactivity,[7] over a decade had elapsed before an example with a ligating atom other than oxygen and fluorine, namely nitrogen, was synthesized[66] and two decades before the Xe-N bond in $FXeN(SO_2F)_2$ was definitively characterized in the solid state by X-ray crystallography and in solution by multinuclear magnetic resonance spectroscopy.[64] Other imidodisulfurylfluoride xenon-nitrogen bonded species have since been definitively characterized using primarily NMR spectroscopy, namely, $Xe[N(SO_2F)_2]_2$,[65,67] $F[XeN(SO_2F)_2]_2^{+}$,[65,67] $XeN(SO_2F)_2^{+}AsF_6^{-}$ [69] and $XeN(SO_2F)_2^{+}Sb_3F_{16}^{-}$ [69] and the latter salt has also been characterized by single crystal X-ray diffraction. The compound, $Xe[N(SO_2CF_3)_2]_2$, [68] has also been prepared and characterized and is the most thermally stable of the imido derivatives of xenon.

Recently, a significant extension of noble-gas chemistry, and in particular compounds containing noble-gas nitrogen bonds, has been achieved by taking advantage of the Lewis acid properties of noble-gas cations.[154] In view of the propensity of the XeF^+ cation to form strong fluorine bridges to counter anions in the solid state,[3] the XeF^+ cation may be regarded as having a significant Lewis acid strength. Based on photoionization studies, HC≡N is one of the most oxidatively resistant ligands among the perfluoropyridines and nitriles that have been investigated in the course of the work described in this Thesis (first adiabatic ionization potential, 13.80 eV[134]). The estimated electron affinity of XeF^+ (10.9 eV[155]) suggested that HC≡N would be resistant to oxidative attack by the XeF^+ cation and that the HC≡N-XeF^+ cation might have sufficient thermal stability to permit its spectroscopic characterization in solution and in the solid state. The reaction of XeF^+ with HC≡N and the subsequent isolation and characterization of HC≡N-$XeF^+AsF_6^-$ have been reported in our previous communication[156] based on the present work. A subsequent report based on this Thesis reported that a large number of oxidatively resistant Lewis nitrogen bases can interact with XeF^+ to form Lewis acid-base cations with XeF^+. Included among these bases are alkyl nitriles and pentafluorophenylnitrile,[156] perfluoroalkyl nitriles,[122] perfluoropyridines[157] and *s*-trifluorotriazine.[122] This Chapter provides a detailed account of the synthesis and structural characterization of the HC≡N-XeF^+ cation by low-temperature Raman spectroscopy in the solid state and in solution by ^1H, ^{13}C, $^{14,15}N$, ^{19}F and ^{129}Xe NMR spectroscopy. More recently the krypton(II) analog, HC≡N-KrF^+ [123] and R_fC≡N-KrF^+ (R_f = CF_3, C_2F_5, *n*-C_3F_7)[122] have also been synthesized and characterized in this laboratory,

representing the first examples of krypton-nitrogen bonds.

The present Chapter outlining the synthesis of $HC{\equiv}N\text{-}XeF^{+}AsF_6^{-}$ [156] and the previously reported synthesis of $HC{\equiv}N\text{-}KrF^{+}AsF_6^{-}$ [123] have been complemented by a recent theoretical investigation of $HC{\equiv}N\text{-}NgF^{+}$ (Ng = Kr, Xe) at the SCF level by determination of the properties of the atoms and bonds in these molecules using the theory of atoms in molecules.[158]

RESULTS AND DISCUSSION

(A) PREPARATION AND ISOLATION OF $HC{\equiv}N\text{-}XeF^{+}AsF_6^{-}$

The reactions of $XeF^{+}AsF_6^{-}$ and $Xe_2F_3^{+}AsF_6^{-}$ with $HC{\equiv}N$ were carried out according to equations (3.1) and (3.2) by combining stoichiometric amounts of the reactants in anhydrous HF and warming to -20 to -10 °C to effect reaction and dissolution.

$$XeF^{+}AsF_6^{-} + HC{\equiv}N \longrightarrow HC{\equiv}N\text{-}XeF^{+}AsF_6^{-} \qquad (3.1)$$

$$Xe_2F_3^{+}AsF_6^{-} + HC{\equiv}N \longrightarrow HC{\equiv}N\text{-}XeF^{+}AsF_6^{-} + XeF_2 \qquad (3.2)$$

The compound, $HC{\equiv}N\text{-}XeF^{+}AsF_6^{-}$, was isolated as a colorless microcrystalline solid upon removal of HF solvent under vacuum at -30 °C and was stable for up to 6 hrs. at 0 °C.

After HF removal at -30 °C following reaction (3.2), XeF_2 was observed in the Raman spectrum of the solid sample prior to pumping off XeF_2 at 0 °C ($\nu_1(\Sigma_g^+)$, 495 cm^{-1}). Solutions of $HC{\equiv}N\text{-}XeF^+AsF_6^-$ in HF at ambient temperature were shown to slowly decompose over a period of 14 hours. The solvolytic behavior of $HC{\equiv}N\text{-}XeF^+AsF_6^-$ in anhydrous HF at room temperature has been compared with that of $HC{\equiv}N$ in Chapter 4. The reactions were also conducted in SO_2ClF solvent at 0 °C, but owing to the low solubility of the reactants and product in this solvent, the reactions did not go to completion.

(B) CHARACTERIZATION OF $HC{\equiv}N\text{-}XeF^+AsF_6^-$ BY ^{129}Xe, ^{19}F, ^{15}N, ^{14}N, ^{13}C AND ^1H NMR SPECTROSCOPY

Every element in the $HC{\equiv}N\text{-}XeF^+$ cation possesses at least one nuclide which is suitable for observation by NMR spectroscopy, namely, the spin-½ nuclei ^1H, ^{13}C, ^{15}N, ^{129}Xe and ^{19}F, and the spin-1 nucleus ^{14}N. Multinuclear magnetic resonance spectra were recorded for $HC{\equiv}N\text{-}XeF^+AsF_6^-$ in HF and BrF_5 solvents for all six nuclei using natural abundance and ^{13}C and ^{15}N enriched compounds. All possible nuclear spin-spin couplings have been observed (Structure 3.1 and Table 3.1), establishing the solution structure of the $HC{\equiv}N\text{-}XeF^+$ cation. In the course of the present NMR study, the couplings, $^1J(^{129}Xe\text{-}^{14}N)$, $^2J(^{129}Xe\text{-}^{13}C)$ and $^3J(^{129}Xe\text{-}^1H)$ were observed, representing the first examples of scalar couplings between these nuclides.

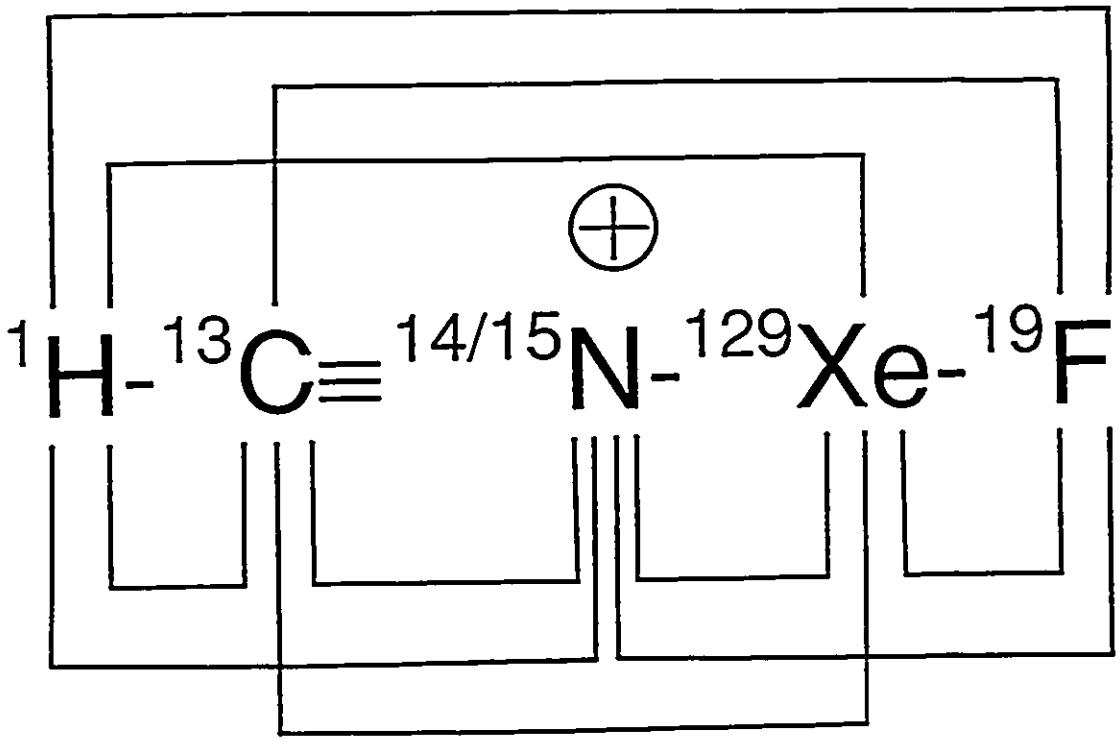

Structure 3.1

Table 3.1

NMR Chemical Shifts and Spin-Spin Coupling Constants for the $HC{\equiv}N\text{-}XeF^+$ Cation

Chemical Shifts (ppm)[a]		Coupling Constants, Hz	
$\delta(^{129}Xe)$	-1552 (-1570)	$^1J(^{129}Xe\text{-}^{19}F)$	6161 (6176)
$\delta(^{19}F)^b$	-198.7 (-193.1)	$^1J(^{129}Xe\text{-}^{14}N)$	332
$\delta(^{14}N)$	-235.1	$^1J(^{129}Xe\text{-}^{15}N)$	471 (483)
$\delta(^{15}N)^c$	-234.5 (230.2)[d]	$^1J(^{14}N\text{-}^{13}C)$	22
$\delta(^{13}C)^c$	104.1	$^1J(^{13}C\text{-}^{1}H)$	308
$\delta(^{1}H)$	4.70 (6.01)[f]	$^2J(^{129}Xe\text{-}^{13}C)$	84
		$^2J(^{15}N\text{-}^{19}F)$	23.9 (23.9)
		$^2J(^{15}N\text{-}^{1}H)$	(13.0)
		$^3J(^{19}F\text{-}^{13}C)$	18
		$^3J(^{129}Xe\text{-}^{1}H)$	24.7 (26.8)
		$^4J(^{19}F\text{-}^{1}H)$	2.6 (2.7)[f]

a Samples were referenced externally at 24 °C with respect to the neat liquid references; $XeOF_4$ (^{129}Xe), $CFCl_3$ (^{19}F), CH_3NO_2 (^{14}N and ^{15}N), $(CH_3)_4Si$ (^{13}C and ^{1}H). A positive chemical shift denotes a resonance occurring to high frequency of the reference compound. The values in parentheses have been measured in BrF_5 solvent.

b All ^{19}F spectra displayed a broad saddle-shaped feature at ca. -68 ppm arising from the partially quadrupole collapsed $^{1}J(^{75}As\text{-}^{19}F)$ of the octahedral AsF_6^- anion.

c Obtained from a 99.5% ^{15}N enriched sample of $HC{\equiv}N\text{-}XeF^+AsF_6^-$.

d The sample was prepared and run at -50 °C in BrF_5 solvent by redissolving a solid sample of 99.5% ^{15}N-enriched $HC{\equiv}N\text{-}XeF^+AsF_6^-$ that had been prepared in HF solvent.

e Obtained form a 99.2% ^{13}C enriched sample of $HC{\equiv}N\text{-}XeF^+AsF_6^-$.

f The sample was prepared and run at -50 °C in BrF_5 solvent by redissolving a solid sample of natural abundance $HC{\equiv}N\text{-}XeF^+AsF_6^-$ that had been prepared in HF solvent.

In prior studies of the imidodisulfurylfluoride derivatives of xenon(II), the low symmetry and resulting large electric field gradient (efg) at the ^{14}N nucleus in the trigonal planar $-N(SO_2F)_2$ group necessitated ^{15}N enrichment in order to observe xenon-nitrogen scalar couplings and nitrogen chemical shifts in $FXeN(SO_2F)_2$,[64] $XeN(SO_2F)_2^+$,[69] $Xe[N(SO_2F)_2]_2$ [67] and $F[XeN(SO_2F)_2]_2^+$ [69] cations in SbF_5, BrF_5 and SO_2ClF solvents. In contrast, the axial symmetry of the $HC{\equiv}N\text{-}XeF^+$ cation and resulting low efg at the ^{14}N nucleus, low viscosity of the HF solvent at -10 °C and small quadrupole moment of ^{14}N serve to minimize quadrupole relaxation of the $^{129}Xe\text{-}^{14}N$ and $^{14}N\text{-}^{13}C$ couplings (see Nature of Bonding in $HC{\equiv}N\text{-}XeF^+$), allowing ready observation of the directly bonded $^{129}Xe\text{-}^{14}N$ and $^{14}N\text{-}^{13}C$ scalar couplings. However, in the higher viscosity solvent, BrF_5 (-58 °C), the $^{129}Xe\text{-}^{14}N$ and $^{14}N\text{-}^{13}C$ couplings are quadrupole collapsed into single lines. Because they are generally obscured owing to quadrupolar relaxation caused by the ^{14}N nucleus, ^{15}N enrichment was required for the observation of scalar couplings between nitrogen and non-directly bonded nuclei when the magnitudes of the couplings were small.

The ^{129}Xe NMR spectrum of natural abundance $HC{\equiv}N\text{-}XeF^+$ consists of a doublet arising from $^1J(^{129}Xe\text{-}^{19}F)$ in the Xe(II) region of the spectrum and is centered at -1570 ppm in BrF_5 solvent at -50 °C; $^1J(^{129}Xe\text{-}^{19}F)$, 6176 Hz. The doublet ($^1J(^{129}Xe\text{-}^{19}F)$, 6161 Hz) is centered at -1552 ppm in HF at -10 °C and each doublet branch is further split into partially quadrupole collapsed 1:1:1 triplets arising from the one-bond scalar coupling $^1J(^{129}Xe\text{-}^{14}N)$, 332 Hz. The magnitude of $^1J(^{129}Xe\text{-}^{19}F)$ is comparable to directly bonded $^{129}Xe\text{-}^{19}F$ couplings of other xenon(II) compounds.[20,159,160] Failure to observe $^1J(^{129}Xe\text{-}^{14}N)$

in BrF_5 at -50 °C is attributed to the increased viscosity of BrF_5 relative to HF, leading to a longer molecular correlation time in the former solvent and quadrupole collapse of the ^{129}Xe-^{14}N scalar coupling. Carbon-13 enrichment (99.2%) led to further splitting into a doublet (84 Hz) on each peak in the ^{129}Xe NMR spectrum, and is assigned to $^2J(^{129}Xe$-$^{13}C)$, representing the first reported example of a scalar coupling between ^{13}C and ^{129}Xe (Figure 3.1).

Nitrogen-15 enrichment (99.5%) of the $HC{\equiv}N$-XeF^+ cation was necessary because $^2J(^{14}N$-$^1H)$ and $^2J(^{19}F$-$^{14}N)$ could not be observed in natural abundance $HC{\equiv}N$-$XeF^+AsF_6^-$. In addition to observing $^2J(^{15}N$-$^1H)$ and $^2J(^{19}F$-$^{15}N)$ in their respective ^{19}F, ^{15}N and ^1H NMR spectra (*vide infra*), a well resolved doublet of doublets on each doublet ($^1J(^{129}Xe$-$^{19}F)$) branch in the ^{129}Xe NMR spectrum of the ^{15}N-enriched cation was observed in both HF (-10 °C) and BrF_5 (-50 °C) solvents (Figure 3.2). The fine structure is assigned to $^1J(^{129}Xe$-$^{15}N)$ (471 Hz in HF; 483 Hz in BrF_5) and $^3J(^{129}Xe$-$^1H)$ (24.7 Hz in HF; 26.8 Hz in BrF_5); the ^{129}Xe-^1H coupling was confirmed by a ^1H broad band decoupling experiment in the ^{129}Xe spectrum (Figure 3.3). Because of the smaller size of $^3J(^{129}Xe$-$^1H)$, quadrupolar line broadening by ^{14}N precludes observation of the latter coupling in the ^{129}Xe NMR spectrum of the natural abundance cation. The magnitudes of $^1J(^{129}Xe$-$^{14}N)$ in the absence of quadrupole relaxation have been calculated for comparison with their observed values in HF solvent from the measured values of $^1J(^{129}Xe$-$^{15}N)$ using equation (3.3): 334 Hz (BrF_5 solvent at -50 °C) and 336 Hz (HF solvent at -10 °C; cf., 332 Hz, measured value) and show the effect of residual quadrupolar relaxation on the measurement of $^1J(^{129}Xe$-$^{14}N)$ is negligible.

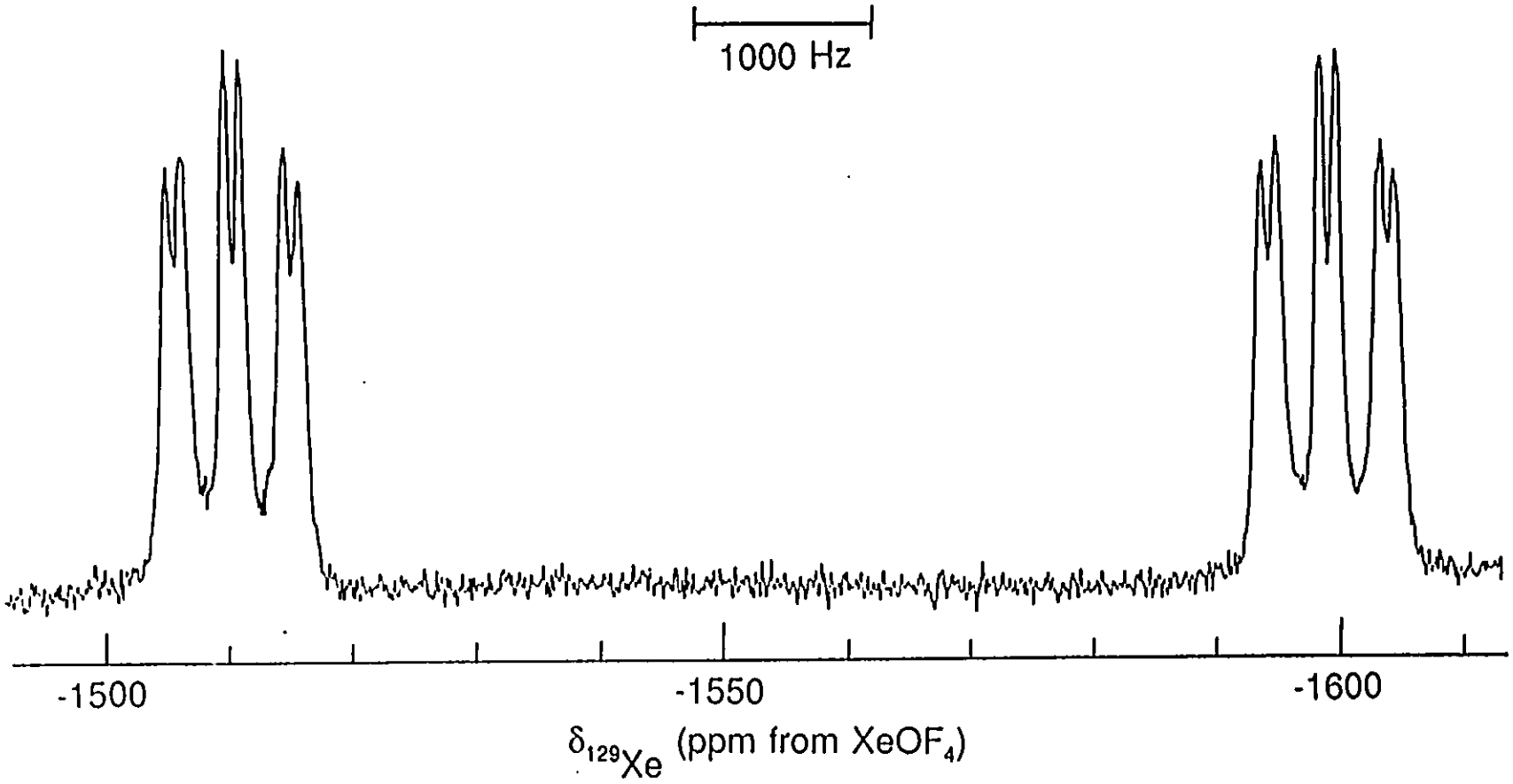

Figure 3.1 ^{129}Xe NMR spectrum (69.563 MHz) of a 99.2% ^{13}C-enriched sample of $HC{\equiv}N\text{-}XeF^{+}AsF_6^{-}$ recorded in HF solvent at -10 °C.

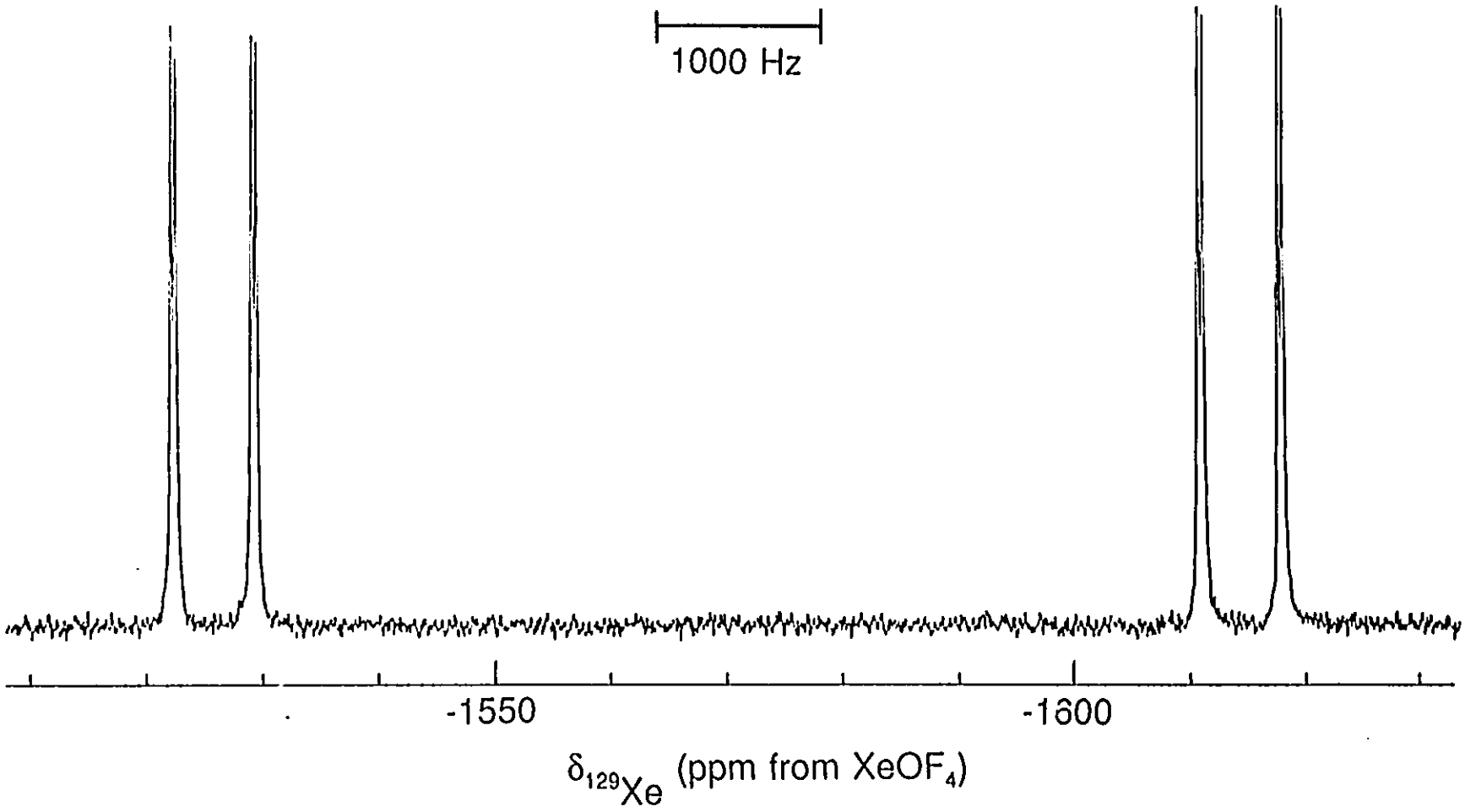

Figure 3.2 ^{129}Xe NMR spectrum (69.563 MHz) of a 99.5% ^{15}N-enriched sample of $HC{\equiv}N\text{-}Xe^{+}AsF_6^-$ recorded in BrF_5 solvent at -50 °C.

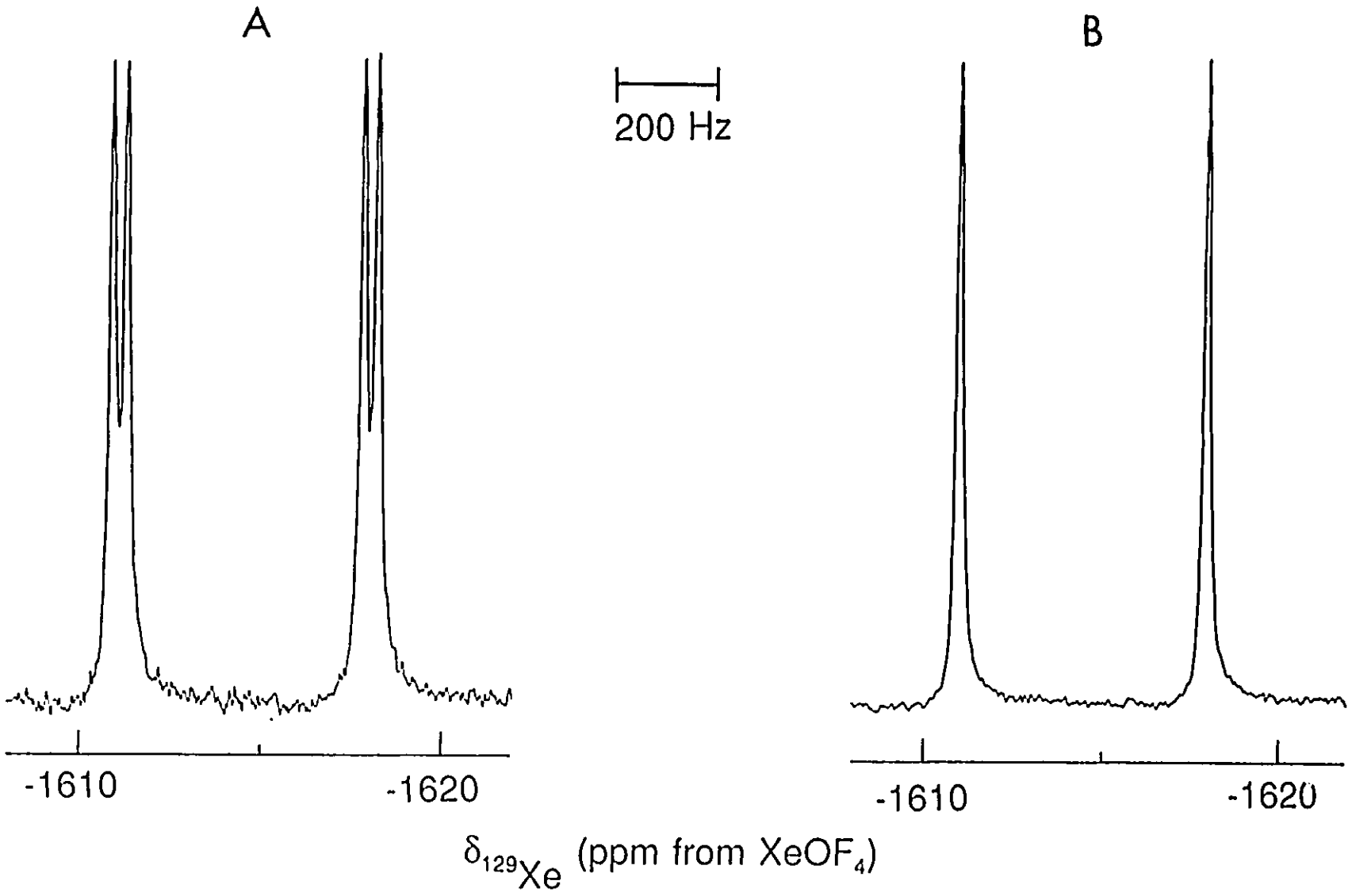

Figure 3.3 ^{129}Xe NMR spectra (69.563 MHz) of a 99.5% ^{15}N-enriched sample of $HC{\equiv}N\text{-}XeF^{+}AsF_6^{-}$ recorded in BrF_5 solvent at -50 °C; expansion (A) $\{^1H\}$-coupling and expansion (B) $\{^1H\}$-decoupled.

$$^{1}J(^{129}Xe\text{-}^{14}N) = {}^{1}J(^{129}Xe\text{-}^{15}N)\ \frac{\gamma(^{14}N)}{\gamma(^{15}N)} \qquad (3.3)$$

The ^{19}F NMR spectra for natural abundance and 99.2% ^{13}C-enriched HC≡N-$XeF^{+}AsF_6^{-}$ in HF solvent at -10 °C and for 99.5% ^{15}N-enriched HC≡N-$XeF^{+}AsF_6^{-}$ in BrF_5 solvent at -50 °C (Figure 3.4) consist of single ^{19}F environments with accompanying satellites that are attributed to $^{1}J(^{129}Xe\text{-}^{19}F)$. Under high resolution and in the absence of quadrupolar line broadening arising from ^{14}N, $^{4}J(^{19}F\text{-}^{1}H)$, 2.6 (HF), 2.7 ($BrF_5$); $^{3}J(^{19}F\text{-}^{13}C)$, 24.7 (HF), 26.8 ($BrF_5$) and $^{2}J(^{19}F\text{-}^{15}N)$, 23.9 Hz were observed in the ^{15}N enriched compounds (Table 3.1). A broad, saddle-shaped feature (3150 Hz linewidth) also occurs at -68 ppm in these spectra and arises from the partially quadrupole collapsed $^{1}J(^{75}As\text{-}^{19}F)$ coupling in the AsF_6^{-} anion.

The ^{14}N and ^{15}N NMR spectra have been recorded for natural abundance and 99.5% ^{15}N-enriched HC≡N-$XeF^{+}AsF_6^{-}$, respectively. The ^{14}N NMR spectrum recorded in HF solvent at -10 °C consisted of a single line at -235.1 ppm with ^{129}Xe satellites ($^{1}J(^{129}Xe\text{-}^{14}N)$). The ^{15}N NMR spectrum of a 99.5% enriched sample was also recorded under the same conditions in HF at -10 °C (-234.5 ppm) and in BrF_5 at -50 °C (-230.2 ppm) (Figure 3.5). The splitting pattern in the ^{15}N spectrum consisted of a doublet of doublets arising from $^{2}J(^{15}N\text{-}^{19}F)$, 23.9 (HF, BrF_5) and $^{2}J(^{15}N\text{-}^{1}H)$, 13.0 Hz ($BrF_5$) (also observed in the ^{1}H and ^{19}F NMR spectra) and were accompanied by ^{129}Xe satellites ($^{1}J(^{129}Xe\text{-}^{15}N)$).

The ^{1}H NMR resonance of natural abundance HC≡N-$XeF^{+}AsF_6^{-}$ in BrF_5 solvent at -58 °C occurred at 6.01 ppm and consisted of a doublet with ^{129}Xe satellites,

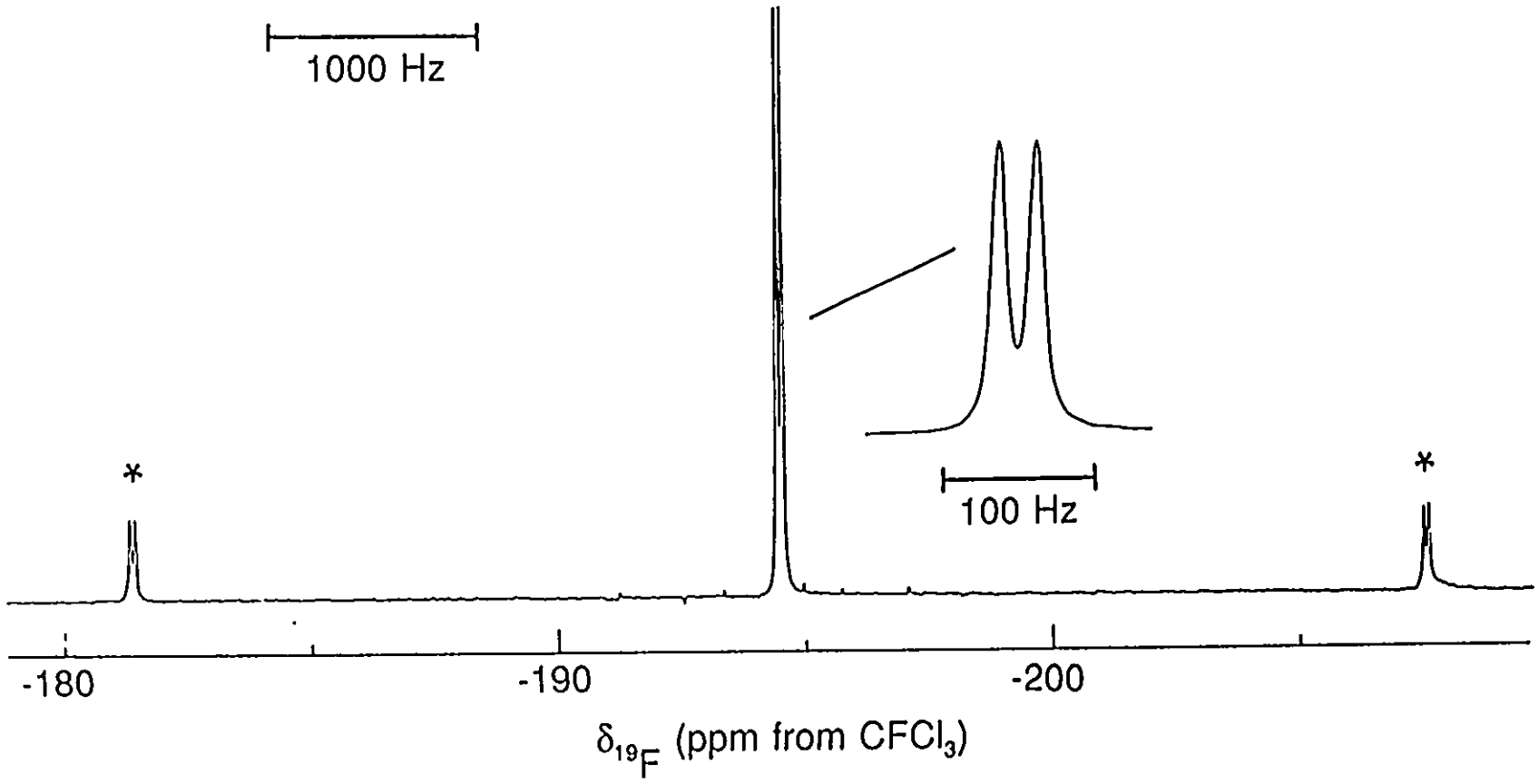

Figure 3.4 ^{19}F NMR spectrum (235.361 MHz) of 99.5% ^{15}N-enriched $HC{\equiv}N\text{-}XeF^{+}AsF_6^{-}$ recorded in BrF_5 solvent at -50 °C. Asterisks (*) denote ^{129}Xe satellites.

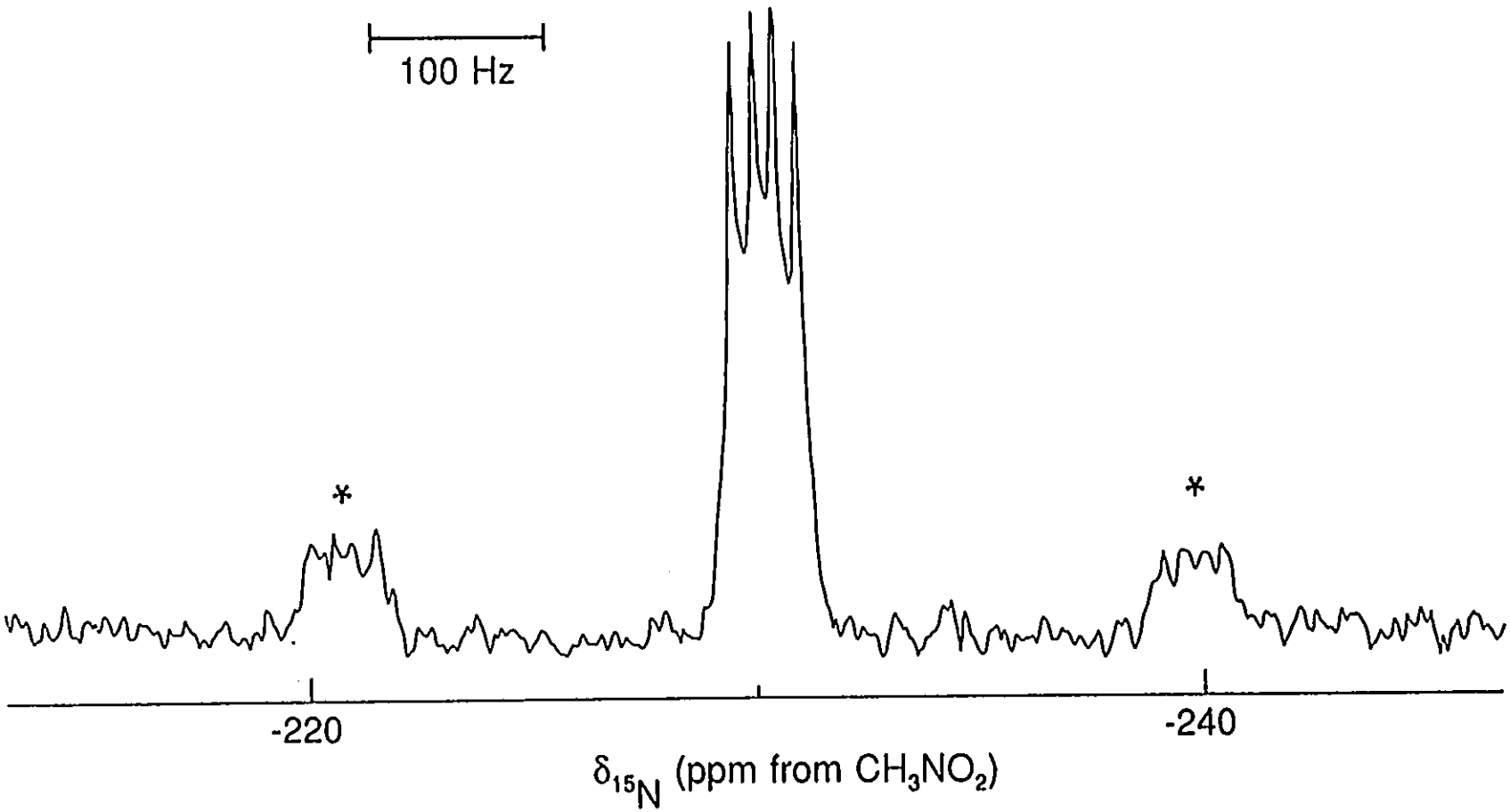

Figure 3.5 ^{15}N NMR spectrum (25.347 MHz) of a 99.5% ^{15}N-enriched $HC{\equiv}N\text{-}XeF^+AsF_6^-$ recorded in BrF_5 solvent at -50 °C. Asterisks (*) denote ^{129}Xe satellites.

$^{3}J(^{129}Xe\text{-}^{1}H)$, 2.7 Hz. The doublet is assigned to $^{4}J(^{19}F\text{-}^{1}H)$, but the two-bond $^{14}N\text{-}^{1}H$ coupling was not observed due to quadrupole relaxation by ^{14}N. However, $^{4}J(^{19}F\text{-}^{1}H)$ and $^{2}J(^{15}N\text{-}^{1}H)$ were both observed in the ^{1}H NMR spectrum for a 99.5% ^{15}N enriched sample in BrF_5 solvent at -50 °C (Figure 3.6). The ^{1}H resonance in HF at -10 °C has also been observed for a natural abundance sample and consisted of a single line at 4.70 ppm with ^{129}Xe satellites ($^{3}J(^{129}Xe\text{-}^{1}H)$).

The ^{13}C NMR resonance of $HC{\equiv}N\text{-}XeF^{+}$ (Figure 3.7) for a 99.2% ^{13}C enriched sample in HF solvent at -10 °C occurred at 104.1 ppm and consisted of a doublet ($^{1}J(^{13}C\text{-}^{1}H)$) of partially quadrupole collapsed 1:1:1 triplets ($^{1}J(^{14}N\text{-}^{13}C)$, 22 Hz) with ^{129}Xe satellites ($^{2}J(^{129}Xe\text{-}^{13}C)$) on each doublet branch.

Intense signals assigned to the $HC{\equiv}NH^{+}$ cation were also observed in the ^{1}H and ^{13}C NMR spectra and are attributed to equilibrium (3.4). The relative concentrations $[HC{\equiv}NH^{+}]/[HC{\equiv}N\text{-}XeF^{+}]$ measured in the ^{1}H NMR spectrum of an HF solution having an initial $[HC{\equiv}N\text{-}XeF^{+}AsF_6^{-}]$ of 2.18 M at -10 °C was 4 : 1. The proton chemical shift, $\delta(^{1}H)$, 7.43 ppm and $^{2}J(^{15}N\text{-}^{1}H)$, 18.6 Hz for the proton on carbon of a ^{15}N-enriched sample are in excellent agreement with the previously reported values for $HC{\equiv}NH^{+}$ in the $FSO_3H\text{-}SbF_5\text{-}SO_2$ solvent system.[161] In contrast to the previous work in $FSO_3H\text{-}SbF_5\text{-}SO_2$, the proton on nitrogen environment and $^{1}J(^{14,15}N\text{-}^{1}H)$ were not observed, and is presumably the result of proton exchange with HF solvent. Additional NMR parameters for the $HC{\equiv}NH^{+}$ cation are reported here for the first time: $\delta(^{13}C)$, 97.1 ppm; $^{1}J(^{13}C\text{-}^{1}H)$, 324.6; $^{1}J(^{13}C\text{-}^{14}N)$, 40.7 and $^{1}J(^{13}C\text{-}^{15}N)$, 59.5 Hz; however, neither the ^{14}N nor ^{15}N spectra of the $HC{\equiv}NH^{+}$ cation could be observed, even after a relaxation delay of 30 s was applied in

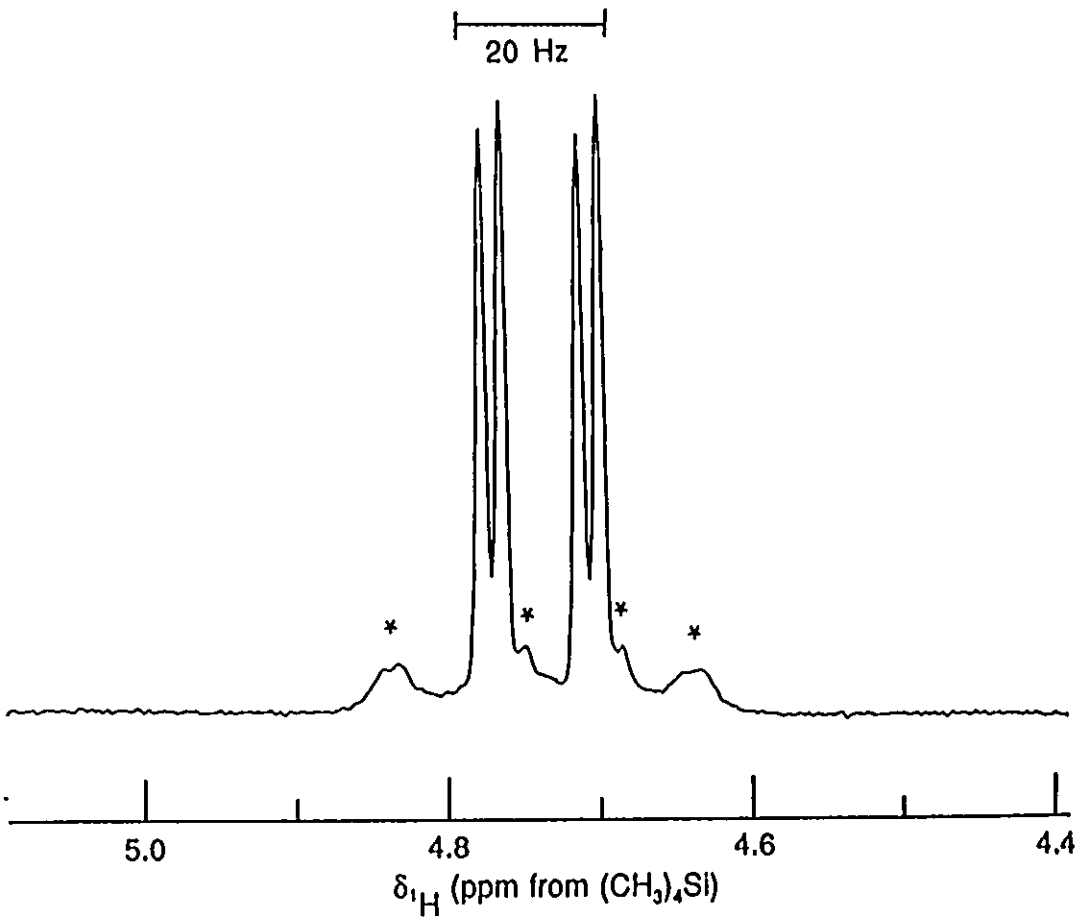

Figure 3.6 ^{1}H NMR spectrum (200.133 MHz) of a 99.5% ^{15}N-enriched $HC{\equiv}N\text{-}XeF^{+}AsF_6^{-}$ recorded in BrF_5 solvent at -50 °C. Asterisks (*) denote ^{129}Xe satellites.

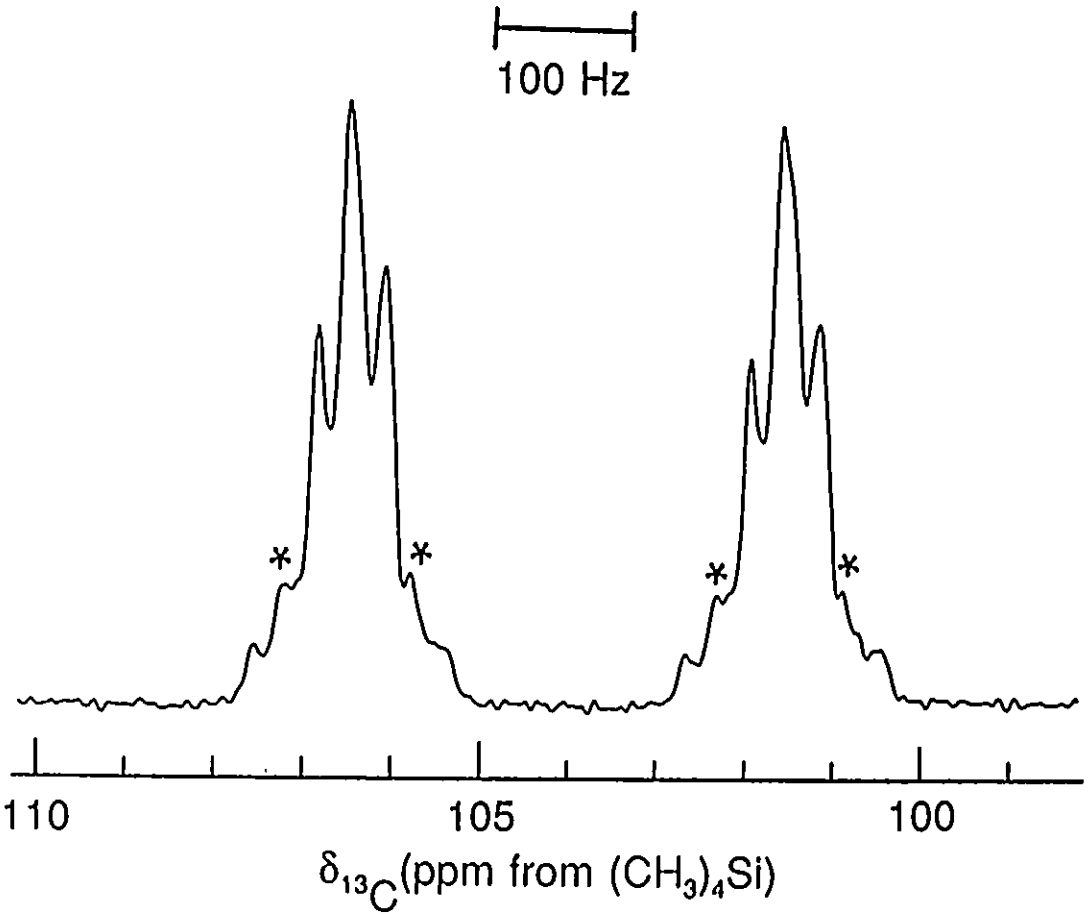

Figure 3.7 ^{13}C NMR spectrum (62.915 MHz) of a 99.2% ^{13}C-enriched $HC{\equiv}N\text{-}XeF^{+}AsF_6^{-}$ recorded in HF solvent at -10 °C. Asterisks (*) denote ^{129}Xe satellites.

the ^{15}N spectrum. A previous determination of $\delta(^{15}N)$ in FSO_3H-SbF_5-SO_2 solvent by the INDOR method gave a value of 119.4 ppm relative to external aqueous NH_4^+ [161] (chemical shift relative to neat external CH_3NO_2 is -240.3 ppm calculated from a $\delta(^{15}N)$ value of -359.7 ppm for aqueous $NH_4^+Cl^-$ relative to CH_3NO_2 [67]).

Although significant equilibrium amounts of $HC{\equiv}NH^+$ are observed in the ^{13}C and ^1H NMR spectra, XeF_2 is not observed in the ^{19}F and ^{129}Xe NMR spectra even in the presence of an equimolar amount of XeF_2 as in reaction (3.2). The apparent absence of XeF_2 in the NMR spectra is presumed to result from chemical exchange involving trace amounts of XeF^+ and $Xe_2F_3^+$ as exchange intermediates arising from equilibria (3.4) - (3.7) and XeF_2.

$$HC{\equiv}N\text{-}XeF^+ + HF \rightleftharpoons HC{\equiv}NH^+ + XeF_2 \qquad (3.4)$$

$$HC{\equiv}N\text{-}XeF^+ \rightleftharpoons HC{\equiv}N + XeF^+ \qquad (3.5)$$

$$XeF^+ + 2HF \rightleftharpoons XeF_2 + H_2F^+ \qquad (3.6)$$

$$XeF^+ + XeF_2 \rightleftharpoons Xe_2F_3^+ \qquad (3.7)$$

The ^{129}Xe NMR spectra of $HC{\equiv}N\text{-}XeF^+AsF_6^-$ and $CH_3C{\equiv}N\text{-}XeF^+AsF_6^-$ in HF at -10 °C have been reported previously[156] and clearly show that the ^{129}Xe linewidth of $HC{\equiv}N\text{-}XeF^+AsF_6^-$ (84 Hz, center line of the triplet) compared to that of $CH_3C{\equiv}N\text{-}XeF^+AsF_6^-$ (40

Hz, center line of the triplet) is significantly larger. This observation is consistent with the anticipated lower base strength of HC≡N towards XeF^+ relative to that of $CH_3C{\equiv}N$, resulting in a greater degree of dissociation for HC≡N-XeF^+ (equilibrium (3.5)) and ensuing chemical exchange by means of equilibria (3.4), (3.6) and (3.7).

In the course of this study it has also been shown that XeF_2 displaces HF in its reaction with $HC{\equiv}NH^+AsF_6^-$ in HF or BrF_5 solvents according to the reverse of equilibrium (3.4). The ^{129}Xe NMR spectrum was recorded for the molar ratio $XeF_2/HC{\equiv}NH^+AsF_6^-$ = 2.47 at -15 °C in HF solvent (initial $[XeF_2]$ = 0.230 M), and gave the relative equilibrium concentrations $[XeF_2]/[HC{\equiv}N\text{-}XeF^+]$ = 0.81. While the XeF_2 1:2:1 triplet (-1555 ppm; $^1J(^{129}Xe\text{-}^{19}F)$, 5530 Hz) could be observed under these conditions, it was significantly exchange broadened (linewidth, 2590 Hz) relative to that of HC≡N-XeF^+ (-1555 ppm; $^1J(^{129}Xe\text{-}^{19}F)$, 6156 Hz; $^1J(^{129}Xe\text{-}^{14}N)$, 330 Hz; linewidth, 110 Hz), indicating that XeF_2 was undergoing slow chemical exchange, presumably via equilibria (3.5) - (3.7). Because HC≡N-$XeF^+AsF_6^-$ has a low solubility in HF at temperatures approaching -30 °C, an equilibrium mixture of $HC{\equiv}NH^+AsF_6^-$ and XeF_2 was also studied in BrF_5 solvent at -50 °C for the molar ratio $XeF_2/HC{\equiv}NH^+AsF_6^-$ = 2.17, giving $[XeF_2]/[HC{\equiv}N\text{-}XeF^+]$ = 0.72 at equilibrium (initial $[XeF_2]$ = 0.314 M). In contrast, the XeF_2 triplet (-1666 ppm; $^1J(^{129}Xe\text{-}^{19}F)$, 5629 Hz) was significantly sharper (linewidth, 250 Hz), which is consistent with a lower degree of dissociation of HC≡N-XeF^+ according to equilibrium (3.5) (-1573 ppm; $^1J(^{129}Xe\text{-}^{14}N)$ was quadrupole collapsed at low temperatures in BrF_5; linewidth, 470 Hz).

(C) CHARACTERIZATION OF $HC{\equiv}N\text{-}XeF^{+}AsF_6^{-}$ BY LOW-TEMPERATURE RAMAN SPECTROSCOPY

The low-temperature (-196 °C) Raman spectra of the crystalline product, isolated from the reaction of natural abundance, ^{15}N- and ^{13}C-enriched $HC{\equiv}N$ with $XeF^{+}AsF_6^{-}$ in anhydrous HF solvent are shown in Figures 3.8 and 3.9 and the observed frequencies, along with their assignments, are listed in Table 3.2. The ^{13}C (99.2%) and ^{15}N (99.5%) enriched salts were prepared in order to aid in the assignments of the ν(XeN) stretching and $\delta(HC{\equiv}N)$, δ(CNXe) and δ(NXeF) bending frequencies. The isotopic shifts are given by the ratios $\Delta\lambda(^{14/15}N)/\lambda(^{14}N)$ and $\Delta\lambda(^{12/13}C)/\lambda(^{12}C)$, as described in reference (162) and are defined and listed in Table 3.2.

The Raman spectra are consistent with the formation of $HC{\equiv}N\text{-}XeF^{+}AsF_6^{-}$ in the solid state. The linear $HC{\equiv}N\text{-}XeF^{+}$ cation is expected to give rise to 3N - 5 = 10 normal modes belonging to the irreducible representations $4\,\Sigma^{+} + 3\,\Pi$ under the point symmetry $C_{\infty v}$. All ten modes are predicted to be Raman and infrared active, and consist of four stretching modes, $\nu_1(\Sigma^{+})$, ν(H-C); $\nu_2(\Sigma^{+})$, ν(C-N); $\nu_3(\Sigma^{+})$, ν(Xe-F) and $\nu_4(\Sigma^{+})$, ν(Xe-N) and three doubly degenerate bending modes $\nu_5(\Pi)$, δ(HCN); $\nu_6(\Pi)$, δ(CNXe) and $\nu_7(\Pi)$, δ(NXeF). Therefore, seven bands are expected in the Raman and infrared spectra of the $HC{\equiv}N\text{-}XeF^{+}$ cation. In addition, the octahedral AsF_6^{-} anion is expected to give rise to three Raman-active vibrational bands under O_h symmetry, $\nu_1(a_{1g})$, $\nu_2(e_g)$ and $\nu_5(t_{2g})$. However, 28 bands as opposed to the predicted 13 from a consideration of free ion symmetries are observed in the Raman spectrum of $HC{\equiv}N\text{-}XeF^{+}AsF_6^{-}$ (Table 3.2). The

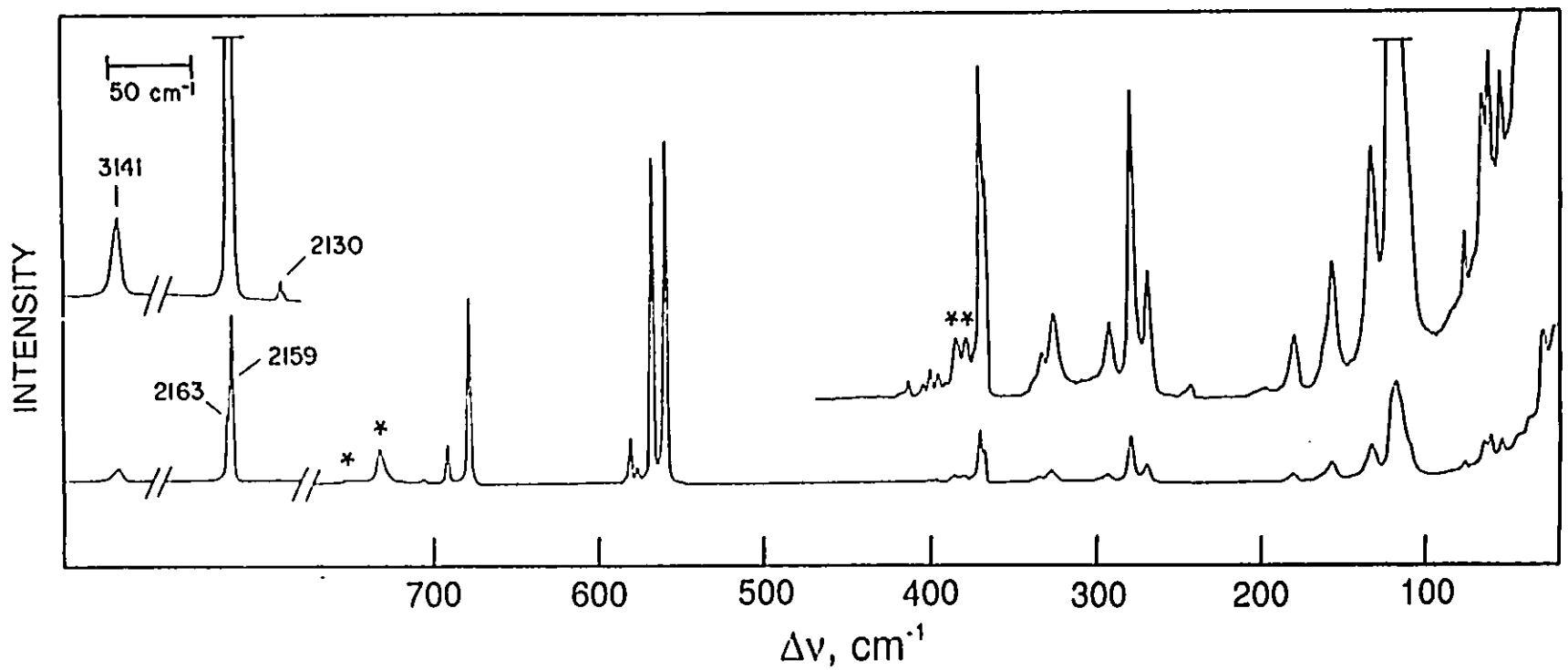

Figure 3.8 Raman spectrum of natural abundance $HC{\equiv}N\text{-}XeF^{+}AsF_6^{-}$ recorded at -196 °C. Asterisks (*) denote FEP sample tube lines.

Figure 3.9 Raman spectra of natural abundance, 99.2% ^{13}C-enriched and 99.5% ^{15}N-enriched $HC{\equiv}N\text{-}XeF^{+}AsF_6^{-}$, recorded at -196 °C; (a) 3200 - 2100 cm^{-1} region and (b) 400 - 100 cm^{-1} region. Asterisks (*) denote FEP sample tube lines.

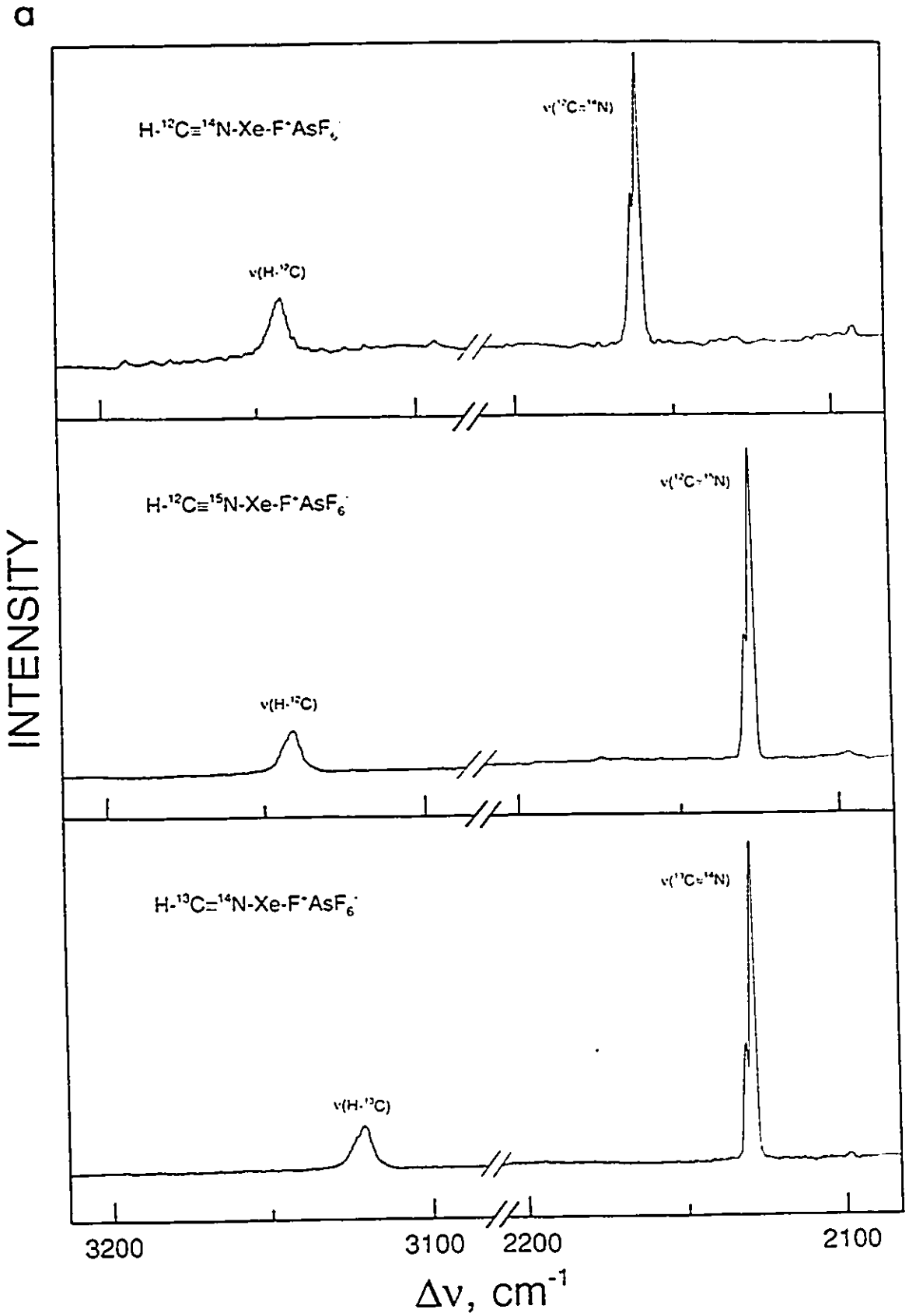
a
H-12C≡14N-Xe-F+AsF6-
ν(H-12C)
ν(12C≡14N)
H-12C≡15N-Xe-F+AsF6-
ν(H-12C)
ν(12C≡15N)
H-13C≡14N-Xe-F+AsF6-
ν(H-13C)
ν(13C≡14N)
INTENSITY
3200
3100
2200
2100
Δν, cm-1

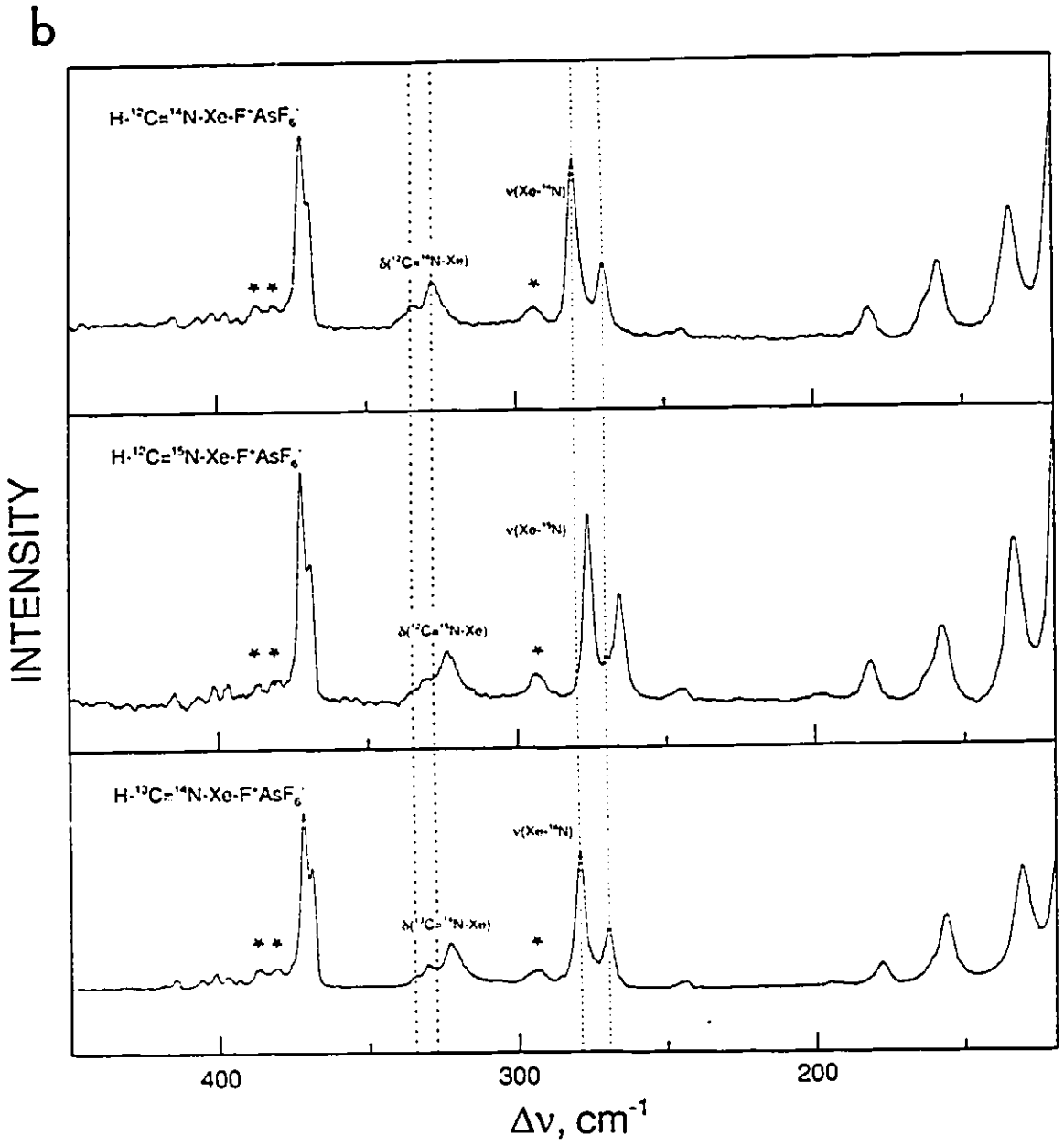
b
H-12C=14N-Xe-F+AsF6-
ν(Xe-14N)
δ(12C=14N-Xe)
H-12C=15N-Xe-F+AsF6-
ν(Xe-15N)
δ(12C=15N-Xe)
H-13C=14N-Xe-F+AsF6-
ν(Xe-14N)
δ(13C=14N-Xe)
INTENSITY
400
300
200
Δν, cm-1

Table 3.2 Raman Frequencies and Assignments for $HC\equiv N\text{-}XeF^+AsF_6^-$, $[^{15}N]HC\equiv N\text{-}XeF^+AsF_6^-$ and $[^{13}C]HC\equiv N\text{-}XeF^+AsF_6^-$ and Related Compounds

Frequency (cm^{-1})[a]									
HCN[b]	$XeF^+AsF_6^-$[c]	$HC\equiv N\text{-}XeF^+$ AsF_6^-	$[^{15}N]HC\equiv N\text{-}XeF^+$ AsF_6^-	$[^{13}C]HC\equiv N\text{-}XeF^+$ AsF_6^-	$\Delta\nu(^{14/15}N)$[d,e]	$\Delta\nu(^{12/13}C)$[d,e]	$\Delta\lambda(^{14/15}N)$[f] $\lambda(^{14}N)$	$\Delta\lambda(^{12/13}C)$[f] $\lambda(^{12}C)$	Assignment
3311		3141.9(2)	3139.3(3)	3121.0(4)	-2.6	-20.9	-0.0016	-0.0133	$\nu_1(\Sigma^+)$, ν(CH)
2097		2162.1(18) 2160.0(41)	2129.0(17) 2126.9(47)	2130.8(23) 2128.7(64)	-33.1 -33.1	-31.3 -31.3	-0.0304 -0.0304	-0.0287 -0.0288	$\nu_2(\Sigma^+)$, ν(CN)
712									ν_5(Π), δ(HCN)
	612(61) 610(80) 608(100) 602(8)	569.4(93) 561.2(100)	569.4(97) 561.2(100)	569.4(97) 561.2(100)	0.0 0.0	0.0 0.0	0.000 0.000	0.000 0.000	$\nu_3(\Sigma^+)$, ν(XeF)
	347 sh 345(58)								ν(F···XeF)
		-	-	334.3(1)					?
		334.7(2) 327.9(4)	330.6(1) 323.4(3)	330.6(3) 322.9(5)	-4.1 -5.5	-4.1 -5.0	-0.024 -0.027	-0.024 -0.030	$\nu_4(\Sigma^+)$, ν(XeN)
		280.9(14) 270.6(6)	276.3(11) 265.4(6)	279.7(14) 269.9(6)	-4.6 -5.2	-1.2 -0.7	-0.032 -0.038	-0.008 -0.005	ν_6(Π), δ(CNXe)
	167(2) 164(5) 160(7) 150(9) 147(6) 142(3)								δ(F···XeF)
		181.2(3) 163.0 sh 157.6(6) 134.6(10) 118.0(20)	181.2(2) 163 sh 156.9(5) 133.6(9) 117.1(18)	177.8(2) 163.3 sh 156.2(7) 132.1(11) 117.0(24)	0.0 0.0 -0.7 -0.8 -0.9	-3.4 -1.7 -1.4 -2.5 -1.0	0.000 0.00 -0.009 -0.015 -0.015	-0.037 -0.021 -0.018 -0.037 -0.017	ν_7(Π), δ(FXeN)

Continued...

Table 3.2 (continued)

Frequency (cm^{-1})[a]			Assignment	
AsF_6^-	$XeF^+AsF_6^-$	$HC{\equiv}N\text{-}XeF^+AsF_6^-$	O_h (AsF_6^-)	C_s (AsF_6^-)
700	735(20) 730(5)		$\nu_3(t_{1u})$	A"
	723(13)	707(2)		A'
		693(11)		A'
689	681(56)	680(49)	$\nu_1(a_{1g})$	A'
573		582(12)	$\nu_2(e_g)$	A'
		577(5)		A'
	465(3)		ν(As---F)	
384	421(11)	419(<1), 415(1)	$\nu_4(t_{1u})$	A'
		406(1)		A'
		401(2)		A"
375	386(14)	397(1), 392(<1)	$\nu_5(t_{2g})$	A'
	378(5)	372(15), 370(10)		A"
				A"
252		244(1)	$\nu_6(t_{1u})$	A'
				A"
				A"
	73(9)	111(sh), 77(2), 71(1), 65(6), 62(8), 54(5), 44(2), 43(3)	Lattice modes	

a Raman spectra of all of the $HC{\equiv}N\text{-}XeF^+AsF_6^-$ salts were recorded with FEP sample tubes at -196 °C using 514.5 nm excitation. Lines due to FEP have been deleted from the spectra. Values in parentheses denote intensities; sh denotes a shoulder. Data given are for the spectra depicted in Figures 3.8 and 3.9.

Continued...

Table 3.2 (continued)

b Reference (163).

c Recorded at -196 °C; this work.

d $\Delta\nu(^{14/15}N) = \nu(^{15}N) - \nu(^{14}N)$; $\Delta\nu(^{12/13}C) = \nu(^{13}C) - \nu(^{12}C)$.

e The estimated precision of each value is ± 0.4 cm^{-1}.

f $\Delta\lambda(^{14/15}N) = \lambda(^{15}N) - \lambda(^{14}N)$; $\Delta\lambda(^{12/13}C) = \lambda(^{13}C) - \lambda(^{12}C)$; where $\lambda = 4\pi^2c^2\nu^2$. c is the velocity of light and ν the observed frequency (in cm^{-1}).

g Reference (164).

disparity between the number of observed bands and the number predicted from a consideration of the free species is attributed to vibrational coupling within the unit cell and/or reduction of the free ion symmetries due to site symmetry effects. The removal of all degeneracies by lowering of the cation and anion site symmetries to C_{2v} or lower would result in 25 Raman-active bands, however, in the absence of a crystallographic space group for $HC{\equiv}N\text{-}XeF^{+}AsF_6^{-}$, it has not been possible in the ensuing discussion to determine their site symmetries and thereby account for the additional splittings and assign their symmetry species in a rigorous manner.

Vibrational assignments were aided by comparison with the vibrational frequencies of $HC{\equiv}N$,[163] $FXe\text{-}N(SO_2F)_2$,[64] $XeF^{+}AsF_6^{-}$,[165] $Xe_2F_3^{+}AsF_6^{-}$ [162] and $M^{+}AsF_6^{-}$,[164] where M is an alkali metal and by recent theoretical calculations of the harmonic frequencies of the $HC{\equiv}N\text{-}KrF^{+}$ cation.[158, 167-170] The three fundamental stretching modes ν(Xe-F), ν(C-N) and ν(C-H) are readily assigned by comparison with the Raman spectra of $HC{\equiv}N$ in the gas phase and $XeF^{+}AsF_6^{-}$, which are also listed in Table 3.2. As the Xe-F and C-N stretching modes belong to the totally symmetric representation, Σ^{+}, their splittings can only be attributed to coupling of vibrational modes within the unit cell. The C-H stretching mode is also presumed to be factor-group split, but owing to its broadness, the anticipated splitting could not be resolved.

The most intense bands at 561(100) and 569(93) cm^{-1} are assigned to the Xe-F stretching frequency of the $HC{\equiv}N\text{-}XeF^{+}$ cation and is characteristic of the terminal Xe-F bond in xenon(II) species of the type L-Xe-F (see Table 3.3). The Xe-F stretching frequency can be used to assess the covalent nature of the Xe-F bond. The XeF^{+} cation

Table 3.3

Comparison of Xe-F Stretching Frequencies, Chemical Shifts and Coupling Constants in F-Xe-L Derivatives

	XeF/XeL[b]	NMR Parameters[c]					
	Bond Lengths	ν(Xe-F)	$^1J(^{129}Xe-^{19}F)$[d]	$\delta(^{129}Xe)$[e,f]	$\delta(^{19}F)$[d,e]		
Species[a]	Å	cm^{-1}	Hz	ppm	ppm	T, °C	Ref.
$XeF^+...FSb_2F_{10}^-$[f]	1.82(3)/2.34(3)	619	7230	-574	-290.2	23[g]	20,27,171,172,
$XeF^+...FAsF_5^-$[f]	1.873(6)/2.212(5)	610	6892	-869		-47	122,165,166,173,174
$(FXe)_2F^+$[f]	1.90(3)/2.14(3)	593	6740	-1051	-252.0	-62	20,27,165,171
$CF_3C{\equiv}N$-XeF$^+$			6397	-1337	-210.4	-63	123
$C_2F_5C{\equiv}N$-XeF$^+$			6437	-1294	-212.9	-63	123
n-$C_3F_7C{\equiv}N$-XeF$^+$			6430	-1294	-213.2	-63	123
$HC{\equiv}N$-XeF$^+$	(1.904)/(2.421)	564	6181	-1569	-198.4[h]	-58	156
$CH_3C{\equiv}N$-XeF$^+$[i]		560	6020	-1708	-185.5	-10	156
s-$C_3F_3N_2N$-XeF$^+$		548	5932	-1862	-145.6	-50	123
			5909	-1808	-154.9	-5	
FO_2SO-XeF	1.940(8)/2.155(8)	528	5830	-1666		-40	20,27,71,175
cis/trans-							
F_4OIO-XeF		527	5803/	-1824/	-161.7[j]	0	60
			5910	-1720	-170.1[k]	0	
C_5F_4N-XeF$^+$		528	5926	-1922	-139.6	-30	157
4-$CF_3C_5F_4N$-XeF$^+$		524	5963	-1853	-144.6	-50	157
F_5TeO-XeF[b]		520		-2051	-151.0[l]	26	176,177
$(FO_2S)_2N$-XeF	1.967(3)/2.200(3)	506	5586	-1977	-126.1	-58	64,67
			5664[l]	-2009[l]	-126.0[l]	-40	
XeF_2	1.977	496	5621	-1685	-184.3	-52	65,158,178
	(1.984)						

Continued...

Table 3.3 (continued)

a Unless otherwise indicated, all cations have AsF_6^- as the counterion.

b Bond lengths obtained from theoretical calculations are indicated in parentheses.

c Spectra were obtained in BrF_5 solvent unless otherwise indicated.

d The NMR parameters of XeF group, in particular $\delta(^{129}Xe)$, are very sensitive to solvent and temperature conditions; it is therefore important to make comparisons in the same solvent medium at the same or nearly the same temperature.

e Referenced with respect to the neat liquids $XeOF_4$ (^{129}Xe) and $CFCl_3$ (^{19}F) at 24 °C: a positive sign denotes the chemical shift of the resonance in question occurs to higher frequency of (is more deshielded than) the resonance of the reference substance.

f Table entries refer to the terminal fluorine on the xenon atom.

g Recorded in SbF_5 solvent.

h $\delta(^{19}F)$ measured in anhydrous HF solvent at -10 °C.

i NMR parameters measured in HF solvent.

j $\delta(^{19}F)$ measured in SO_2ClF solvent at -40 °C.

k NMR parameters measured in SO_2ClF solvent.

l NMR parameters measured in SO_2ClF solvent at -50 °C.

has been shown to be weakly coordinated to the anion by means of a fluorine bridge, and the Xe-F stretch has been shown to correlate with the degree of covalent character in the Xe---F bridge bond, decreasing with increasing base strength of the anion.[124] Consequently, the Xe-F stretching frequency is expected to increase as the xenon-nitrogen bond becomes more ionic and the terminal Xe-F bond becomes more covalent. A comparison of the Xe-F stretching frequency of HC≡N-XeF$^+$ with other Xe-N bonded species, XeF$^+$ and $Xe_2F_3^+$ allows one to assess the relative covalency of the Xe-N bond in the HC≡N-XeF$^+$ cation. The stretching frequencies of the terminal XeF bond for F-Xe-L type derivatives are listed in Table 3.3 along with their Xe-F and Xe-L bond lengths when known. The HC≡N-XeF$^+$ cation has the most ionic xenon-nitrogen bond when compared to previously reported Xe-N bonded compounds for which vibrational data are available and is also in accord with our NMR findings (see above and Table 3.3) and theoretical calculations at the SCF level (see Nature of the Bonding in HC≡N-XeF$^+$). The latter calculations show that the reaction of the gas phase XeF$^+$ ion with F$^-$ to yield the difluoride results in an increase in the calculated Xe-F bond length of 0.1 Å, while the reaction of XeF$^+$ with HC≡N causes the same bond length (calculated) to increase on average by only 0.016 Å.[158] Similar conclusions have been reached based on the high-frequency position of the Kr-F stretching frequency of HC≡N-KrF$^+$AsF$_6^-$ [122] and theoretical calculations for the HC≡N-KrF$^+$ cation.[158,167-170]

The $\nu_1(\Sigma^+)$ C-H stretching vibration is assigned to a broad, weak band at 3142(2) cm^{-1} and occurs at a significantly lower frequency than in gaseous HC≡N, i.e., 3311 cm^{-1},[163] and is consistent with coordination of the nitrogen lone pair to an electron pair

acceptor. Two sharp lines at 2160(41) and 2162(18) cm^{-1} are assigned to the factor-group split $\nu_2(\Sigma^+)$ C≡N stretching mode and occur 63 cm^{-1} to higher frequency than the C≡N stretch of gaseous HC≡N. The shift to higher frequency upon coordination to XeF^+ is consistent with cation formation and with HC≡N acting as a σ-electron pair donor to XeF^+. The C-H and C≡N stretching frequencies also exhibit the expected sensitivities to ^{13}C and ^{15}N substitution (Table 3.2). The calculated changes in C-H and C≡N bond lengths parallel the observed shifts in the stretching frequencies in the $HC{\equiv}N\text{-}XeF^+AsF_6^-$ salt (see Nature of the Bonding in $HC{\equiv}N\text{-}XeF^+$).[158]

The assignments of the low-frequency cation bands arising from ν(Xe-N), δ(CNXe) and δ(FXeN) were aided by ^{15}N and ^{13}C isotopic enrichment. The relative order of the corresponding calculated frequencies for $HC{\equiv}N\text{-}KrF^+$,[167-170] which are uniformly lower than in the xenon analog, are consistent with the order arrived at for $HC{\equiv}N\text{-}KrF^+$, i.e., ν(Xe-N) > δ(CNXe) > δ(FXeN).

The $\nu_3(\Sigma^+)$ Xe-N stretching vibration of the $HC{\equiv}N\text{-}XeF^+$ cation is assigned to the weak, low-frequency lines 328(4) and 335(2) cm^{-1} where the splitting is again attributed to vibrational coupling within the crystallographic unit cell. The assignment of the Xe-N stretch has been confirmed using ^{15}N and ^{13}C enrichment and results in relative shifts $\Delta\lambda(^{14/15}N)/\lambda(^{14}N)$, -0.027 and -0.024, for the two bands in the spectrum of $[^{15}N]HC{\equiv}N\text{-}XeF^+AsF_6^-$, and $\Delta\lambda(^{12/13}C)/\lambda(^{12}C)$, -0.030 and -0.024 for $[^{13}C]HC{\equiv}N\text{-}XeF^+AsF_6^-$ (Figure 3.9). The similarity between the $^{14}N/^{15}N$ and $^{12}C/^{13}C$ isotopic shifts is expected from a consideration of the form of the normal coordinate corresponding to $\nu_3(\Sigma^+)$. In the case of a heavy atom like Xe, the N and C displacements are expected to essentially equal to

one another and in the same but opposite sense to the small Xe displacement (cf. the actual form of the displacements in the normal coordinate corresponding to $\nu_1(\Sigma^+)$, the C-X stretch in XC≡N, where X = Cl, Br or I [179]). The Xe-N frequency of the HC≡N-$XeF^+AsF_6^-$ salt occurs at lower frequency than those of $FXeN(SO_2F)_2$ (422 cm^{-1})[64] and $Xe[N(SO_2F)]_2$ (386 - 413 cm^{-1}).[67] This is attributed to the greater covalent character of the Xe-N bonds in the imidodisulfurylfluoride derivatives, whereas the Xe-N bond of the HC≡N-XeF^+ cation is among the most ionic Xe-N bonded species presently known (the Xe-N bonds in *n*-C_3F_7C≡N-XeF^+, C_2F_5C≡N-XeF^+ and CF_3C≡N-XeF^+ appear to be weaker based on a comparison of their ^{129}Xe and ^{19}F chemical shifts, however, the vibrational spectra of these cations have not been recorded[123]). This is corroborated by the high-frequency position of the Xe-F stretch, which is among the highest of any F-Xe-L type species known where L is not bonded to the XeF group through fluorine.

The formally doubly degenerate bending mode $\nu_5(\Pi)$, δ(HCN) was not observed; this band is very weak in the Raman spectrum of gaseous HC≡N.[163] Although the frequency of the weak band at 707(2) cm^{-1} is similar to δ(HCN) of gaseous HC≡N (712 cm^{-1}), it was found to be insensitive to either ^{13}C or ^{15}N isotopic substitution and was accordingly assigned to an anion mode (*vide infra*). The assignments of the remaining doubly degenerate bending modes have been made with the aid of their relative $^{12}C/^{13}C$ and $^{14}N/^{15}N$ isotopic shift data. The presence of more than a single band for the δ(CNXe) and δ(FXeN) bending modes is ascribed to factor-group splitting and/or removal of the degeneracy by a cation site symmetry lower than $C_{\infty v}$.

The bending mode, $\nu_6(\Pi)$, δ(CNXe) is assigned to lines at 271(6), and 281(14) cm^{-1}

and exhibits the anticipated low-frequency shifts in the Raman spectra of [^{13}C]HC≡N-XeF$^+$AsF$_6^-$ and [^{15}N]HC≡N-XeF$^+$AsF$_6^-$, i.e., $\Delta\lambda(^{14/15}N)/\lambda(^{14}N)$, -0.038 and -0.032 and $\Delta\lambda(^{12/13}C)/\lambda(^{12}C)$, -0.005 and -0.008 (Figure 3.9). The ^{14}N/^{15}N dependence is large, and is in fact similar to $\nu_1(\Sigma^-)$, the Xe-N stretching mode. The displacement of nitrogen from the molecular axis is expected to be large when bonded to a heavy atom while that of carbon is expected to be considerably less than the nitrogen displacement and in the opposite sense (cf. displacements for the normal modes in XC≡N[179]). The relatively small ^{12}C/^{13}C isotopic dependence for this mode is also supported by this qualitative description and is consistent with a smaller carbon displacement.

The bending mode $\nu_7(\Pi)$, δ(FXeN) is expected at lower frequencies than δ(CNXe), and is assigned to the moderately intense bands at 118(20) and 135(10), 158(6) and 181(3) cm^{-1} by comparison with XeF$^+$AsF$_6^-$ [165] and $Xe_2F_3^+AsF_6^-$,[166] where δ(FXe---F) are 155 (average) and 161 cm^{-1} (average), respectively, and FXe-N$(SO_2F)_2$,[64] where δ(FXeN) is 200 cm^{-1} (average). The FXeN bend of HC≡N-XeF$^+$ is expected to be significantly lower than that of FXe-N$(SO_2F)_2$. These modes also exhibit ^{14}N/^{15}N and ^{12}C/^{13}C isotopic dependences (Table 3.2 and Figure 3.9); however, no simple explanation for the relative magnitudes of each shift for each component of this doubly degenerate bend is presently available.

Although the AsF$_6^-$ anion is not expected to be fluorine bridged to the HC≡N-XeF$^+$ cation, the AsF$_6^-$ anion exhibits 14 bands compared to the three Raman-active bands that are expected under O_h symmetry. Because the totally symmetric mode of AsF$_6^-$, $\nu_1(a_{1g})$, is not split, additional Raman-active bands are largely attributed to site symmetry

lowering (15 Raman-active bands are expected for a site symmetry of C_{2v} or lower), although vibrational coupling in the unit cell may also contribute to the number of observed bands. The modes have been assigned under C_s symmetry by analogy with $XeF^+AsF_6^-$ (Table 3.2) in which the O_h symmetry of the anion is reduced to C_s or lower symmetry by formation of a fluorine bridge to the anion. The vibrational frequencies for AsF_6^- under O_h symmetry have also been listed for comparison.

Lines occurring below 112 cm^{-1} exhibit no measurable shifts upon ^{13}C or ^{15}N substitution and have been assigned to lattice modes.

(D) NATURE OF THE BONDING IN HC≡N-XeF$^+$

Previous NMR studies of xenon(II) derivatives containing XeF groups bonded to oxygen or fluorine have shown that the NMR parameters measured in the ^{19}F and ^{129}Xe spectra can generally be used to assess relative covalent characters of the Xe-O, Xe---F bridge and Xe-F terminal bonds.[20, 159, 160] In general, as the ionic character of the Xe-L (L = ligand atom) bond increases, the covalent character of the terminal Xe-F bond increases, increasing the formal charge on xenon. These trends are paralleled by decreases in $\delta(^{129}Xe)$ and increases in both $^1J(^{129}Xe\text{-}^{19}F)$ and $\delta(^{19}F)$ for the terminal XeF group. Table 3.3 provides the $\delta(^{129}Xe)$ and $\delta(^{19}F)$ chemical shifts and $^1J(^{129}Xe\text{-}^{19}F)$ for a number of xenon(II) compounds containing terminal Xe-F bonds for comparison with $HC{\equiv}N\text{-}XeF^+$, showing that the Xe-F bond of $HC{\equiv}N\text{-}XeF^+$ is second only to $R_fC{\equiv}N\text{-}XeF^+$

(R_F = CF_3, C_2F_5, n-C_3F_7), $Xe_2F_3^+$ and XeF^+ in covalent character. Excluding fluorine bridging to xenon and the $R_FC{\equiv}N\text{-}XeF^+$ cations,[123] the Xe-N bond of $HC{\equiv}N\text{-}XeF^+$ is then among the weakest xenon-ligand bonds observed thus far. The XeF^+ character of the XeF group in $HC{\equiv}N\text{-}XeF^+$ is supported by theoretical calculations of the efgs at the Xe nuclei in XeF^+ and $HC{\equiv}N\text{-}XeF^+$,[158] which are found to differ by only 7%, in agreement with the experimental observation that the quadrupolar splitting in the ^{129}Xe Mössbauer spectra of $HC{\equiv}N\text{-}XeF^+$ (40.2 ± 0.3 mm s^{-1}) is the same, within experimental error, as that obtained for the salt $XeF^+AsF_6^-$ (40.5 ± 0.1 mm s^{-1}).[180]

The observation of a well resolved $^{129}Xe\text{-}^{14}N$ coupling in HF is the combined result of the low viscosity of HF, the axial symmetry and accompanying low efg at the ^{14}N nucleus.[181] The axial symmetry of the cation results in an asymmetry parameter $\eta = 0$ so that the efg at the ^{14}N nucleus is dominated by q_{zz}, the efg component along the C_∞ axis of the cation. Consequently, the effect of the efg on quadrupolar relaxation of ^{14}N will only depend on q_{zz} and the molecular correlation time, τ_c. Coordination of XeF^+ to the nitrogen sp lone pair of $HC{\equiv}N$ is expected to reduce q_{zz} significantly in the adduct cation, leading to a longer spin lattice relaxation time relative to the free base, further enhancing the possibility of observing $^1J(^{129}Xe\text{-}^{14}N)$ in the low viscosity solvent, HF. The principal components of the efg tensor ($+z$ is in the direction H $\rightarrow$ N) at the nitrogen nuclei in $HC{\equiv}N$ and $HC{\equiv}N\text{-}XeF^+$ have been calculated and the corresponding reduction in efg in going from $HC{\equiv}N$ to $HC{\equiv}N\text{-}XeF^+$ is 48%, in accord with our observation of $^1J(^{129}Xe\text{-}^{14}N)$ and $^1J(^{14}N\text{-}^{13}C)$ for $HC{\equiv}N\text{-}XeF^+$ in HF solvent. The axial component of the efg tensor at the nitrogen nucleus is also halved upon the formation of $HC{\equiv}N\text{-}KrF^+$.

The difference in the magnitudes of the reduced coupling constants $^1K(Xe\text{-}N)$ in $HC{\equiv}N\text{-}XeF^+$ (1.389×10^{22} $NA^{-2}m^{-3}$) and $FXeN(SO_2F)_2$ (0.949×10^{22} $NA^{-2}m^{-3}$)[64,67,69] may be discussed using a previous assessment of the nature of bonding to xenon in solution for $FXeN(SO_2F)_2$. The Xe-N bond of $FXeN(SO_2F)_2$ is regarded as a σ-bond having sp^2 hybrid character. In high-resolution NMR spectroscopy spin-spin coupling involving heavy nuclides is generally dominated by the Fermi contact mechanism.[69] For Xe-N spin-spin couplings dominated by the Fermi contact mechanism, one-bond coupling constants can be discussed on the basis of the formalism developed by Pople and Santry.[182] In discussions of xenon-nitrogen scalar couplings in xenon(II) imidodisulfurylfluoride compounds,[183] the s-electron density at the xenon nucleus was assumed constant and a change in the hybridization at nitrogen accounted for changes in xenon-nitrogen spin-spin coupling. The dependence of xenon-nitrogen spin-spin coupling on nitrogen s-character in the xenon-nitrogen bond may also be invoked to account for the substantially larger $^1K(Xe\text{-}N)$ value observed for $HC{\equiv}N\text{-}XeF^+$ than for xenon bonded to the trigonal planar nitrogen in $FXeN(SO_2F)_2$. A comparison of $^1K(Xe\text{-}N)$ for $HC{\equiv}N\text{-}XeF^+$ with that of the trigonal planar sp^2 hybridized nitrogen atom in $FXeN(SO_2F)_2$ allows assessment of the relative degrees of hybridization of the nitrogen orbitals used in σ-bonding to xenon. The ratio, $[^1K(Xe\text{-}N)_{sp}]/[^1K(Xe\text{-}N)_{sp^2}] = 1.46$, for the $HC{\equiv}N\text{-}XeF^+$ cation and $FXeN(SO_2F)_2$ is in excellent agreement with the theoretical ratio, 1.50, calculated from the predicted fractional s-characters of the formally sp- and sp^2-hybridized nitrogen orbitals used in bonding to xenon in these compounds.

The Xe-N bond of the $HC{\equiv}N\text{-}XeF^+$ cation may be thought of as a classical Lewis

acid-base donor acceptor bond. Implicit in this description of the Xe-N bond is a considerable degree of ionic character, which appears to be a dominant feature of the stability of the $HC{\equiv}N\text{-}XeF^+$ cation. This premise has been supported and further illuminated by theoretical calculations on the $HC{\equiv}N\text{-}NgF^+$ cations.[158,167-170] The ability of NgF^+ (Ng = Kr, Xe) cations to act as Lewis acids was shown to be related to the presence of holes in the valence shell charge concentrations of the Ng atoms that expose their cores.[158] The mechanism of formation of the Ng-N bonds in the adducts of NgF^+ with $HC{\equiv}N$ is similar to the formation of a hydrogen bond, i.e., the mutual penetration of the outer diffuse nonbonded densities of the Ng and N atoms is facilitated by their dipolar and quadrupolar polarizations, which remove density along their axis of approach, to yield a final density in the interatomic surface that is only slightly greater than the sum of the unperturbed densities. Thus, not surprisingly, the KrF^+ and XeF^+ cations are best described as hard acids, which form weak covalent Ng-N adduct bonds as already noted in the context of the present NMR and Raman spectroscopic studies. The energies of formation of these adducts are dominated by the large stabilizations of the Ng atoms that result from the increase in the concentration of charge in their inner quantum shells. The Ng-N bonds that result from the interaction of the closed-shell reactants NgF^+ and $HC{\equiv}N$ actually lie closer to the closed shell limit than do bonds formed in the reaction of NgF^+ with F. The calculated gas phase energies of the reactions between the closed-shell species are -32.5 and -34.5 kcal mol^{-1} for Ng = Kr and Xe,[158] respectively, for

$$NgF^+ + HC{\equiv}N \longrightarrow HC{\equiv}N\text{-}NgF^+ \qquad (3.8)$$

and -209.0 and -211.9 kcal mol^{-1} for

$$NgF^{+} + F^{-} \longrightarrow F\text{-}Ng\text{-}F \qquad (3.9)$$

The reaction of the gas phase NgF^{+} ions with F^{-} to yield the difluorides results in increases in the calculated Ng-F bond lengths of 0.1 Å, while their reaction with HC≡N causes the same bond lengths (calculated) to increase on average by only 0.016 Å.[158] The C-N bond of HC≡N is calculated to shorten by –0.005 Å on forming the adduct, while the C-H bond is calculated to lengthen by 0.008 Å.[158] These predicted changes in bond length also correlate with the observed shifts in their corresponding stretching frequencies, ν(C≡N), increasing by 63 cm^{-1} and ν(C-H) decreasing by 169 cm^{-1} for HC≡N-XeF^{+}.

A simple valence bond description may also be used to satisfactorily account for qualitative trends in bond lengths and associated spectroscopic parameters. The bonding in XeF_2 and HC≡N-XeF^{+} may be represented by valence bond Structures 3.2 - 3.7, where Structures 3.4 and 3.7 are the least important contributing structures. The XeF_2 molecule has a formal bond order of ½ and the Xe-F bond of HC≡N-XeF^{+} has a formal bond order of ½ ≤ b.o. < 1; b.o. = 1 is approached only in the most weakly coordinated case of FXe^{+}---F-$Sb_2F_{10}^{-}$.

$$F\text{-}Xe^{+}\ F^{-} \longleftrightarrow F^{-}\ {}^{+}Xe\text{-}F \longleftrightarrow F^{-}\ Xe^{2+}\ F^{-}$$

3.2 3.3 3.4

$$HC{\equiv}N\text{-}Xe^{2+}\ F^- \longleftrightarrow HC{\equiv}N^{+}Xe\text{-}F \longleftrightarrow HC{\equiv}N\ Xe^{2+}\ F^-$$

3.5 3.6 3.7

Unlike valence bond Structures 3.2 and 3.3 of XeF_2 the analogous structures for $HC{\equiv}N\text{-}XeF^+$, namely, Structures 3.5 and 3.6 do not have equal weighting owing to the large build up of formal positive charge on the Xe atom of Structure 3.5, consequently, Structure 3.6 dominates, resulting in an Xe-F bond having considerable covalent (XeF^+) character and a weak covalent Xe-N bond.

CHAPTER 4

THE DECOMPOSITION AND SOLVOLYSIS OF $HC{\equiv}N\text{-}XeF^{+}AsF_6^{-}$ AND $HC{\equiv}N$ IN ANHYDROUS HF; AND THE CHARACTERIZATION OF THE $CF_3NH_3^{+}$, $FHC{=}NH_2^{+}$, $CF_2{=}NH_2^{+}$ AND $CHF_2NH_3^{+}$ CATIONS BY MULTINUCLEAR MAGNETIC RESONANCE SPECTROSCOPY

INTRODUCTION

It has been shown in Chapter 3 that the very weak monoprotic acid, $HC{\equiv}N$, forms a stable adduct with XeF^{+} in anhydrous HF by donation of the nitrogen sp lone pair to the xenon valence shell to form the linear $HC{\equiv}N\text{-}XeF^{+}$ cation. NMR and Raman spectroscopic studies and related theoretical calculations indicate that the Xe-N bond of the $HC{\equiv}N\text{-}XeF^{+}$ cation is among the weakest Xe-N bonds known.

In this Chapter the thermal stability and the solvolytic behavior of $HC{\equiv}N\text{-}XeF^{+}AsF_6^{-}$ have been studied at room temperature in anhydrous HF solvent. The decomposition rate of the $HC{\equiv}N\text{-}XeF^{+}$ cation was sufficiently slow so that NMR spectroscopy could be used to monitor the formation of decomposition products. The decomposition products of these reactions have been characterized using natural abundance, 99.2% ^{13}C- and 99.5% ^{15}N-enriched $HC{\equiv}N\text{-}XeF^{+}AsF_6^{-}$.

A parallel NMR study of the fluorination of $HC{\equiv}N$ in anhydrous HF at ambient temperature indicates that the fluorination mechanisms and products differ significantly

RESULTS AND DISCUSSION

(A) THE DECOMPOSITION OF $HC{\equiv}N\text{-}XeF^+AsF_6^-$ IN ANHYDROUS HF

The $HC{\equiv}N\text{-}XeF^+$ cation is unstable in HF solvent at room temperature, slowly decomposing with the liberation of xenon gas. The stepwise decomposition was studied in detail by ^{19}F, ^{14}N, ^{15}N, ^{13}C and ^1H NMR spectroscopy of natural abundance, 99.2% ^{13}C- and 99.5% ^{15}N-enriched $HC{\equiv}N\text{-}XeF^+AsF_6^-$; the NMR parameters of the decomposition products are given in Table 4.1. Fluorine-19 NMR spectra recorded after warming solutions of $HC{\equiv}N\text{-}XeF^+AsF_6^-$ to room temperature for varying periods of time, followed by quenching the reactions at -15 °C, are depicted in Figure 4.1. Upon warming $HC{\equiv}N$ and $XeF^+AsF_6^-/Xe_2F_3^+AsF_6^-$ in anhydrous HF to room temperature, it was found that the F-on-Xe peak assigned to the $HC{\equiv}N\text{-}XeF^+$ cation gradually decreased in intensity with time and eventually disappeared with concomitant broadening of the HF and AsF_6^- signals due to fluorine exchange.

Several new signals appeared in the high-frequency, fluorine-on-carbon region of the ^{19}F NMR spectra; no signals attributable to fluorine-on-nitrogen were observed. Initially, warming of $HC{\equiv}N\text{-}XeF^+AsF_6^-$ in HF solvent resulted in several weak signals in the ^{19}F NMR spectrum which are assigned to CF_4 (-61.6 ppm) and CF_3H (-81.5 ppm;

Table 4.1

NMR Parameters for the Products Resulting from the Decomposition of $HC{\equiv}N\text{-}XeF^{+}AsF_6^{-}$ in HF Solvent at Room Temperature.

	Cation/Compound					
Chemical Shifts (ppm)[a]	$HC{\equiv}NH^{+}$	CF_3^{+}	CF_2H^{+}	$CF_3NH_3^{+}$	$CHF{=}NH_2^{+}$	$CF_2{=}NH_2^{+}$
$\delta(^1H)$	7.43(CH)		6.45	8.60		10.51
$\delta(^{19}F)$		-61.6	-81.5	-64.9	-97.2	-30.5
$\delta(^{13}C)$	97.1	119.1	116.5	116.7	171.0	156.4
$\delta(^{14/15}N)$				-320.7		
Coupling Constants (Hz)						
$^2J(^{19}F\text{-}^1H)$					59.3	
$^3J(^{19}F\text{-}^1H)$			79.5	5.4		7.2
						9.7
$^1J(^{14}N\text{-}^1H)$				67.0		76.4
$^1J(^{15}N\text{-}^1H)$				76.4		97.5
$^2J(^{15}N\text{-}^1H)$	18.6					
$^1J(^{14}N\text{-}^{13}C)$	40.7				14.9	18.1
$^1J(^{15}N\text{-}^{13}C)$	59.5					
$^2J(^{15}N\text{-}^{19}F)$				-18.2		1.6
$^1J(^{13}C\text{-}^1H)$	325		241		249	
$^1J(^{19}F\text{-}^{13}C)$		260	274	261	336	315

a Referenced externally at 25 °C with respect to the neat liquid references $CFCl_3$ (^{19}F), CH_3NO_2(^{15}N and ^{14}N) and TMS (^{13}C and ^1H).

Figure 4.1 ^{19}F NMR spectra (235.361 MHz) of $HC{\equiv}N\text{-}XeF^{+}AsF_6^{-}$ recorded at -15 °C in HF solvent after warming to 25 °C for (a) 0 hr. (b) 2 hr. (c) 6 hr. (d) 9 hr and (e) expansion of spectrum (c). The ^{19}F resonances of the fluorinated products are denoted as (A) CF_4, (B) $CF_3NH_3^{+}$, (C) CF_3H, (E) $CHF{=}NH_2^{+}$ and (F) unassigned signal.

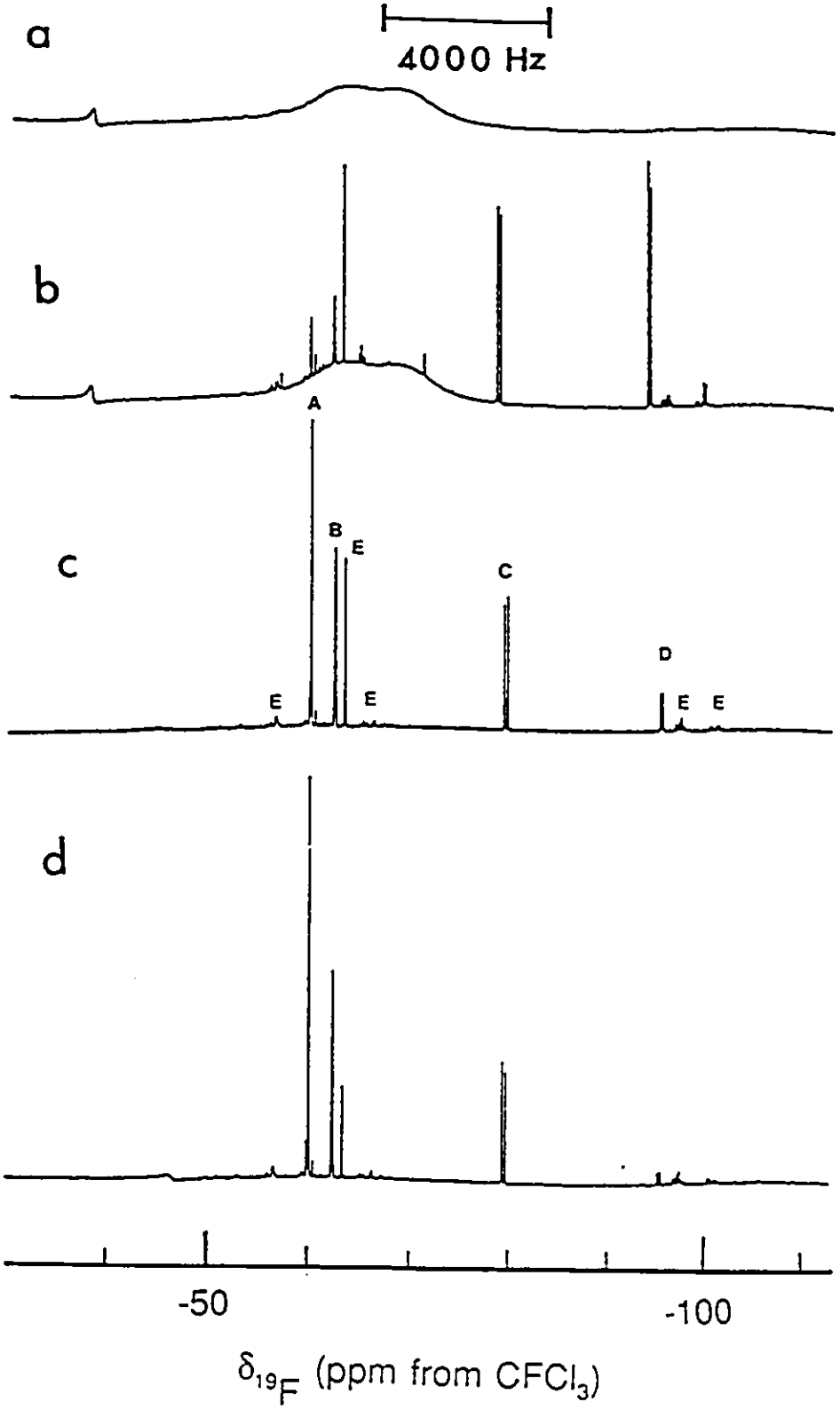
a
4000 Hz
b
A
c
B
E
C
D
E
E
E
E
d
-50
-100
δ_{19_F} (ppm from $CFCl_3$)

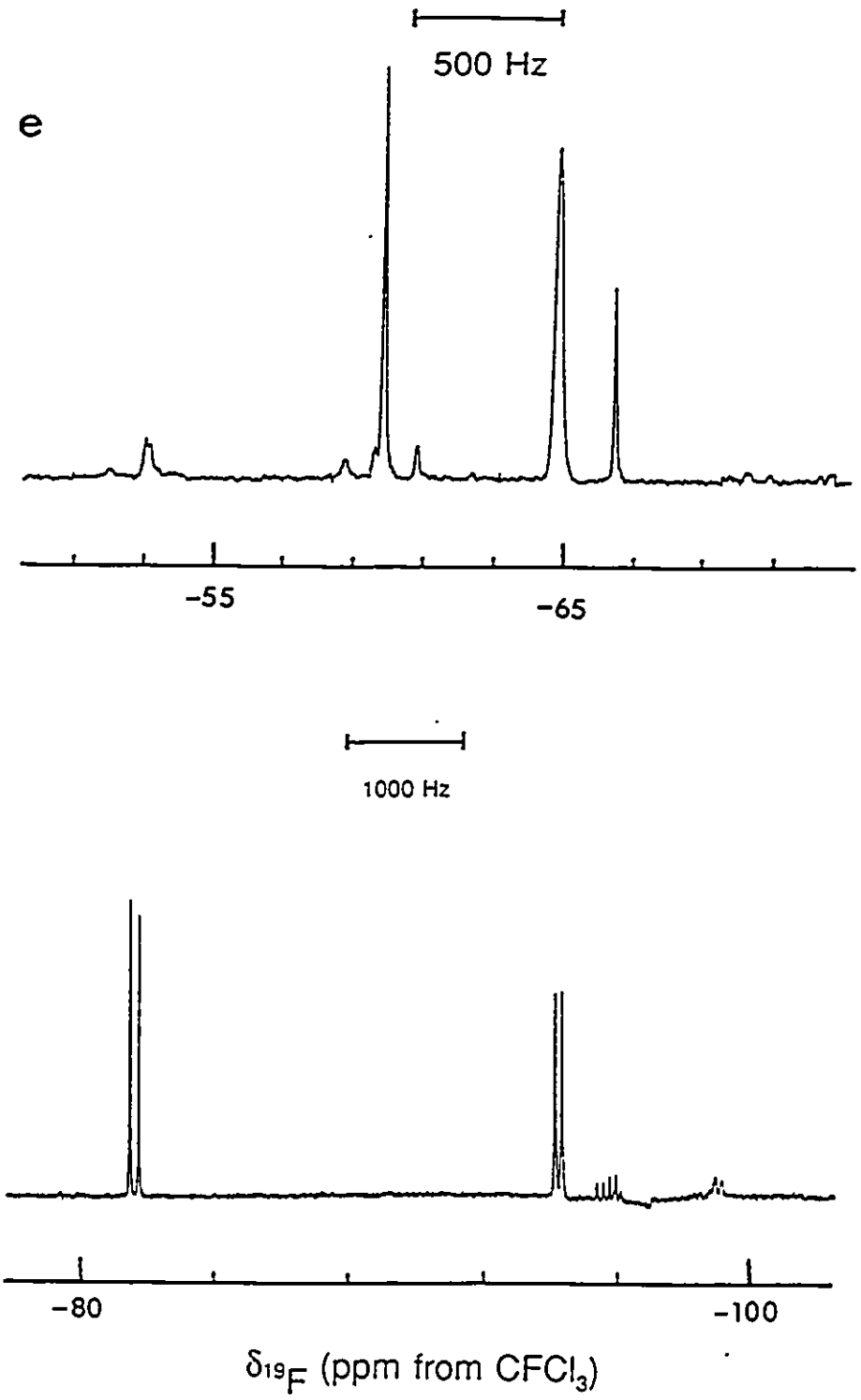
500 Hz
e
-55
-65
1000 Hz
-80
-100
$\delta_{^{19}F}$ (ppm from $CFCl_3$)

$^2J(^{19}F\text{-}^1H)$, 79.5 Hz) and strong signals at -97.2 (doublet; $J(^{19}F\text{-}^1H)$, 59.3 Hz), -64.9 (broad singlet) and -30.5 ppm (sharp singlet). Weak signals were also observed at -25.3 (quartet; J, 34 Hz), -57.9, -58.4, -61.2, -62.2, -98.7 (doublet; J, 61 Hz), -99.2 (doublet; J, 59 Hz) and -102.3 ppm (doublet; J, 60 Hz). Continued warming at room temperature showed that the two intense ^{19}F signals at -97.2 and -30.5 ppm decreased in intensity with time and disappeared after approximately 13 hours while all other signals in the ^{19}F NMR spectrum intensified.

After warming the solutions for 4 hours at room temperature, the ^1H NMR spectra of $HC{\equiv}N\text{-}XeF^+AsF_6^-$ showed a sharp quartet ($J(^{19}F\text{-}^1H)$, 79.5 Hz) at 6.45 ppm, which is in good agreement with the reported chemical shift and coupling constants of CF_3H.[184] This signal diminished in intensity in the course of warming the sample for 14 hours at room temperature along with a broad signal at 7.43 ppm, assigned to the proton on carbon of the $HC{\equiv}NH^+$ cation, and a weak signal at 5.96 ppm, assigned to the proton-on-carbon of the $HC{\equiv}N\text{-}XeF^+$ cation (cf. Chapter 3). Several proton-on-nitrogen resonances were observed in the high-frequency region of the ^1H spectrum. These consisted of a sharp singlet at 10.42 ppm, a 1:1:1 triplet at 10.51 ppm with spin-spin coupling arising from ^{14}N ($J(^{14}N\text{-}^1H)$, 67.0 Hz) which was further split into a well-resolved doublet of doublets on each branch of the 1:1:1 triplet, a broad 1:1:1 triplet, ($J(^{14}N\text{-}^1H)$ 33.4 Hz) at 10.90 ppm, a doublet (65.81 Hz) at 10.44 ppm and a broad singlet at 9.93 ppm. The ^1H NMR spectrum of the ^{15}N-enriched $HC{\equiv}N\text{-}XeF^+AsF_6^-$ at -10 °C, after warming the reaction mixture for 10 hours at room temperature, showed a sharp singlet at 10.44 ppm and further splitting in the signal at 10.51 ppm in the proton on nitrogen region with a doublet

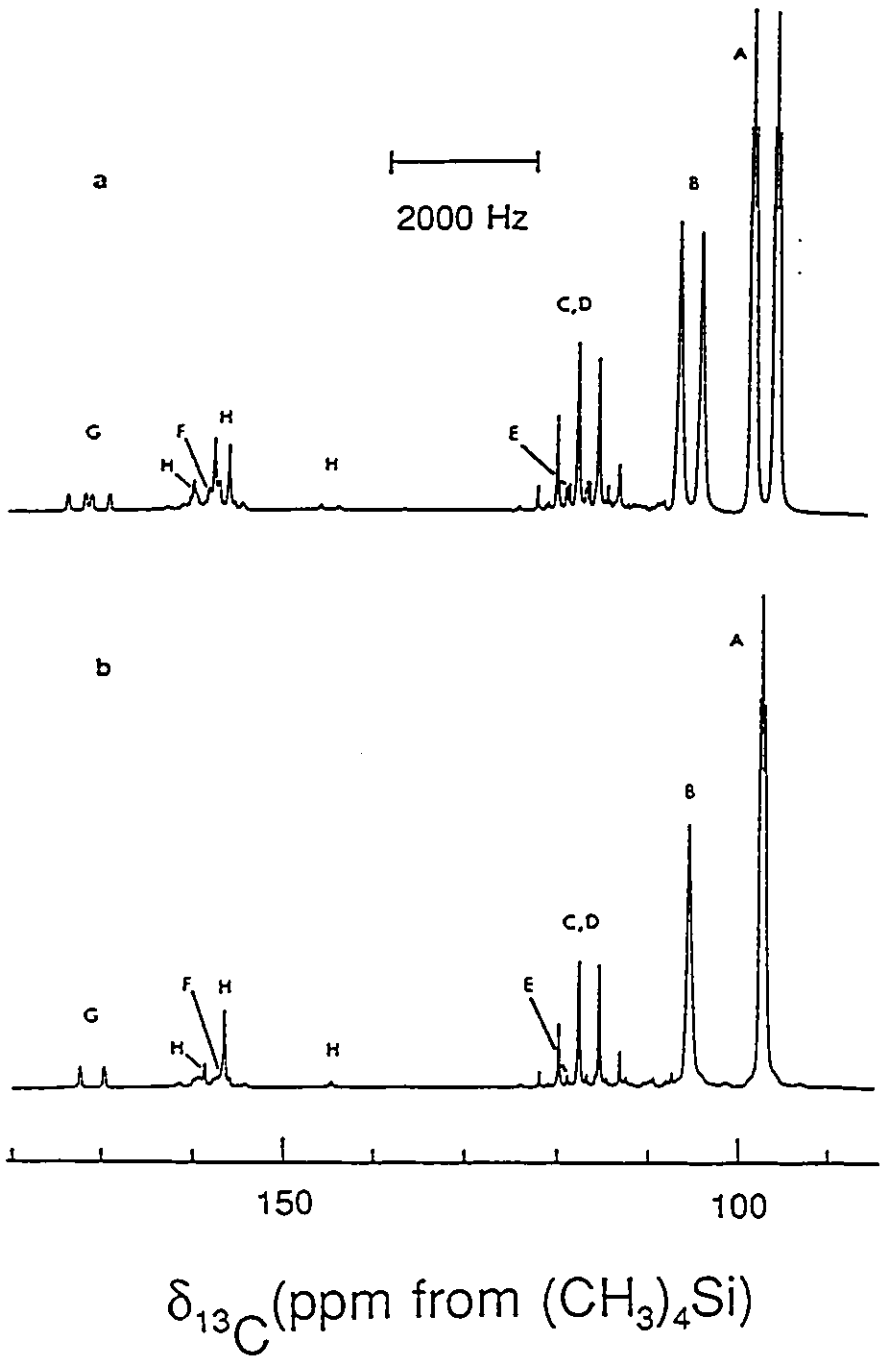

Figure 4.2 ^{13}C NMR (125.760 MHz) spectra of the decomposition products of 99.2% ^{13}C-enriched $HC{\equiv}N\text{-}XeF^{+}AsF_6^{-}$ in HF solvent at -10 °C after warming the solution for 13 hours at 25 °C; (a) $\{^1H\}$-coupled abd (b) $\{^1H\}$-decoupled. The ^{13}C resonances of the fluorinated products are denoted as: (A) $HC{\equiv}NH^{+}$, (B) $HC{\equiv}N\text{-}XeF^{+}$, (C) CF_4, (D) $CF_3NH_3^{+}$ (E) CF_3H (F) $CF_2{=}NH_2^{+}$ (G) $CHF{=}NH_2^{+}$ and (H) unassigned signals.

arising from ^{15}N ($J(^{15}N\text{-}^{1}H)$, 97.5 Hz), which was further split into a well resolved doublet of doublets, $^{3}J(^{19}F\text{-}^{1}H)$, 9.7 and 7.2 Hz) on each branch of the doublet ($J(^{15}N\text{-}^{1}H)$. This signal was assigned to $CF_2{=}NH_2^+$ cation. While the other signals in the proton on nitrogen region at 10.42 ppm and 10.90 ppm were not observed in the ^{15}N-enriched sample. The differences in the ^{1}H NMR spectra of the natural abundance and ^{15}N-enriched samples may be due to concentration effects, as the enriched samples were generally of lower concentration.

The ^{13}C NMR spectra of a 99.2% ^{13}C-enriched sample of $HC{\equiv}N\text{-}XeF^+AsF_6^-$ showed several signals in addition to $HC{\equiv}NH^+$ and $HC{\equiv}N\text{-}XeF^+$ after warming for 13 hours at room temperature (Figure 4.2). Two doublets at 104.1 ppm ($^{1}J(^{13}C\text{-}^{1}H)$, 308 Hz) and at 97.1 ppm ($^{1}J(^{13}C\text{-}^{1}H)$ 324.6 Hz) are assigned to the $HC{\equiv}N\text{-}XeF^+$ and $HC{\equiv}NH^+$ cations, respectively (cf. Chapter 3). Each branch of the $HC{\equiv}NH^+$ doublet is split into a partially quadrupole collapsed 1:1:1 triplet arising from the one-bond scalar coupling $^{1}J(^{14}N\text{-}^{13}C)$, 40.7 Hz. The doublet fine structure on each signal was shown to arise from $^{1}H\text{-}^{13}C$ coupling by a $\{^{1}H\}$-broad-band decoupling experiment (Figure 4.2 b). Three multiplets were observed at 119.1, 116.5 and 116.7 ppm and are assigned to CF_4 (quintet; $^{1}J(^{13}C\text{-}^{19}F)$, 260.5 Hz), CF_3H (doublet of quartets; $^{1}J(^{13}C\text{-}^{19}F)$, 241.4 Hz and $^{1}J(^{13}C\text{-}^{1}H)$, 273.7 Hz) and $CF_3NH_3^+$ (quartet; $^{1}J(^{13}C\text{-}^{19}F)$, 261 Hz), respectively. The signal at 171.0 ppm consisted of a doublet of doublets arising from the one-bond scalar couplings $^{1}J(^{13}C\text{-}^{1}H)$, 249 Hz and $^{1}J(^{13}C\text{-}^{19}F)$, 336 Hz and is assigned to the $CHF{=}NH_2^+$ cation. A ^{1}H broad-band decoupling experiment resulted in a doublet, and each branch of the doublet was found to be split into a partially quadrupole collapsed 1:1:1 triplet arising from $^{1}J(^{14}N\text{-}^{13}C)$, 14.9

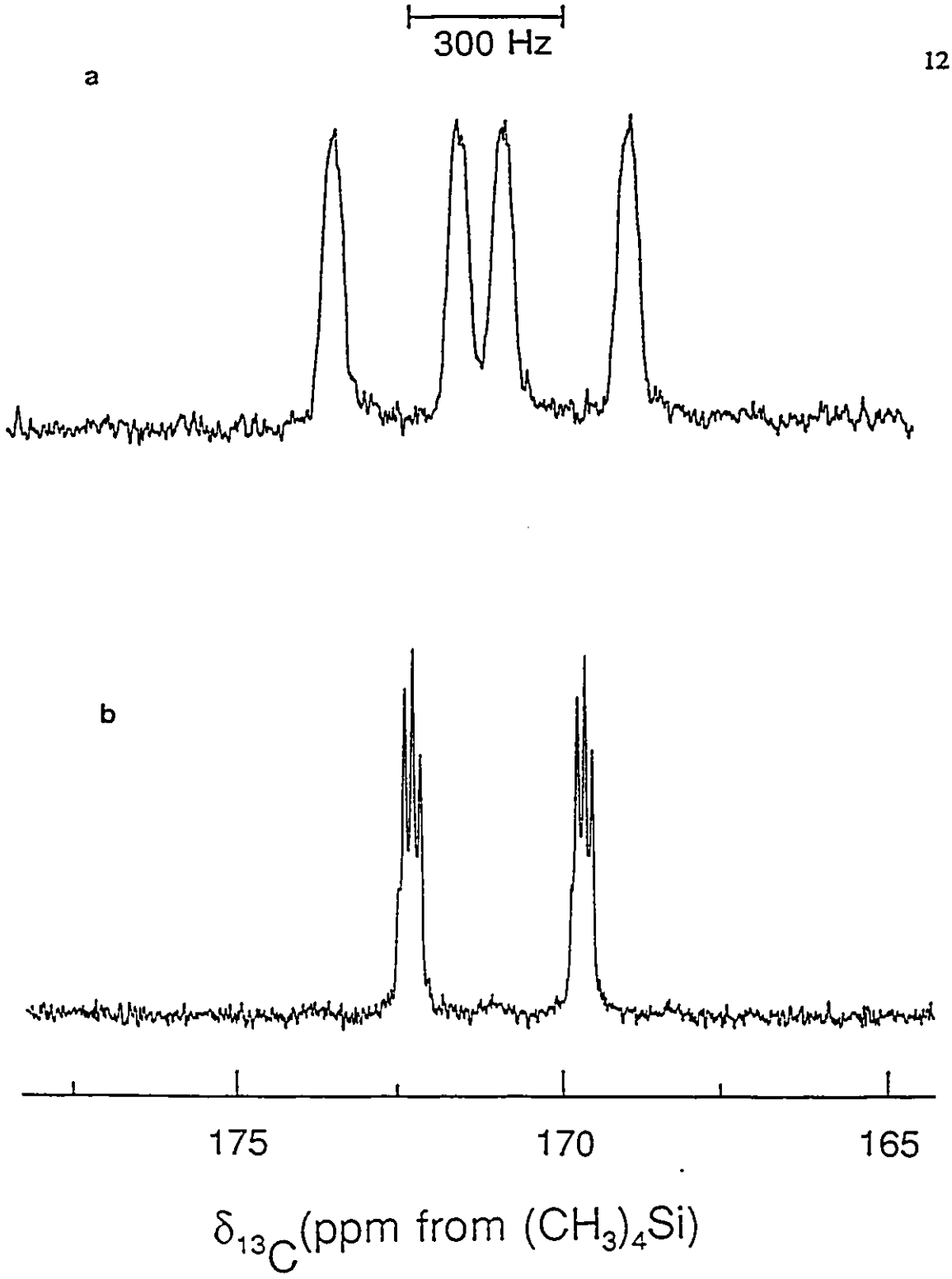

Figure 4.3 ^{13}C NMR (125.760 MHz) spectra of $CHF=NH_2^+$ (G) in HF solvent, expanded from Figure 4.2: (a) $\{^1H\}$-coupled and (b) $\{^1H\}$-decoupled.

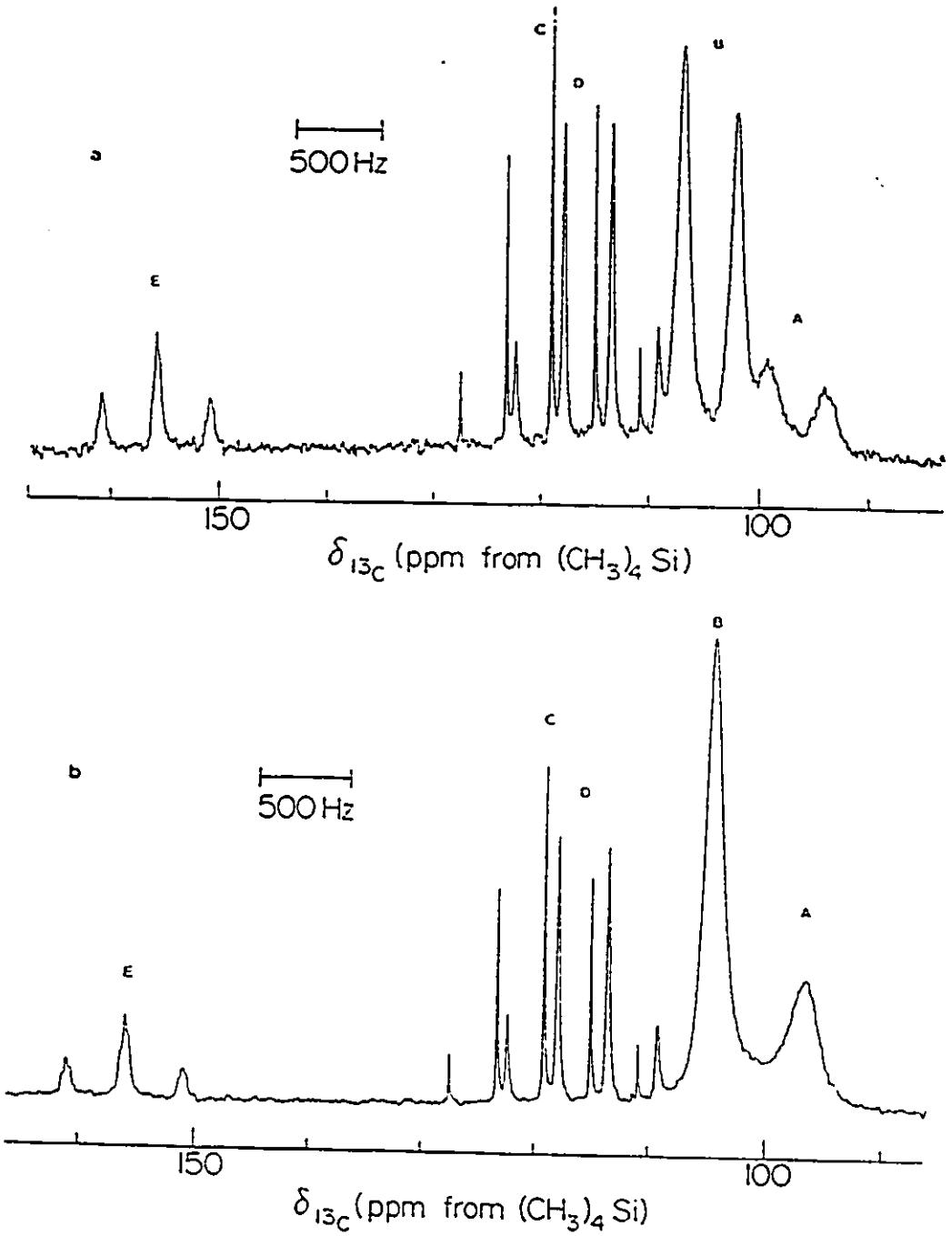

Figure 4.4 ^{13}C NMR (62.896 MHz) spectra of the decomposition products of 99.2% ^{13}C-enriched HC≡N and $Xe_2F_3^+AsF_6^-$ in HF solvent recorded at 3 °C after warming the solution for 13 hours at room temperature; (a) $\{^1H\}$-coupled and (b) $\{^1H\}$-decoupled. The ^{13}C resonances of the fluorinated products are denoted as: (A) $HC{\equiv}NH^+$, (B) $HC{\equiv}N\text{-}XeF^+$, (C) CF_4, (D) $CF_3NH_3^+$ and (E) $CF_2{=}NH_2^+$.

Hz (Figure 4.3). The enhanced resolution of $^{1}J(^{14}N\text{-}^{13}C)$ in the $\{^{1}H\}$-decoupled spectrum is due to the decoupling of the small unresolved $^{2}J(^{13}C\text{-}^{1}H)_{cis}$ and $^{2}J(^{13}C\text{-}^{1}H)_{trans}$ couplings. The ^{13}C NMR spectra also showed several unresolved signals at 156.4 (doublet), 156.5 (triplet) and 158.6 (doublet) ppm. A $\{^{1}H\}$-broad-band decoupling experiment showed the two doublets arose from $^{1}J(^{13}C\text{-}^{1}H)$ couplings of 199.3 and 252.3 Hz, respectively. The triplet was not affected by decoupling, and the magnitude of the coupling indicates that it is a one bond $^{19}F\text{-}^{13}C$ coupling ($^{1}J(^{19}F\text{-}^{13}C)$, 315 Hz). The nature of the triplet was confirmed by recording the ^{13}C NMR spectra of solutions comprised of a 1:1 mixture of HC≡N and $Xe_2F_3^+AsF_6^-$ in HF that had been warmed at room temperature for several hours (Figure 4.4). This mixture produced the same signals as in the case of HC≡N-XeF^+, i.e., $HC{\equiv}NH^+$, CF_4, $CF_3NH_3^+$, but the intensity of the triplet at 156.4 ppm was considerably greater and, again, $\{^{1}H\}$-broad-band decoupling confirmed the absence of proton $^{13}C\text{-}^{1}H$ coupling and showed additional ^{14}N coupling (partially quadrupole collapsed 1:1:1 triplet; $^{1}J(^{14}N\text{-}^{13}C)$, 18.1 Hz). The signal is attributed to the novel imido cation, $CF_2{=}NH_2^+$ (*vide infra*).

The ^{14}N and ^{15}N NMR spectra resulting from the reaction of natural abundance and 99.5% ^{15}N-enriched HC≡N and $XeF^+AsF_6^-$ have been monitored over a period of 10 hours at room temperature. Four intense signals were observed at -4.6 (singlet), -73.1 (singlet), -235.1 and -320.7 (quartet of quartets) ppm in the ^{15}N NMR spectrum. The signal at -235.1 ppm is assigned to the HC≡N-XeF^+ cation and is accompanied by ^{129}Xe satellites, while a signal corresponding to $HC{\equiv}NH^+$ was not observed. The ^{14}N spectrum of $HC{\equiv}NH^+$, however, has been measured where $\delta(^{14}N)$ is -240.3 ppm. The absence of

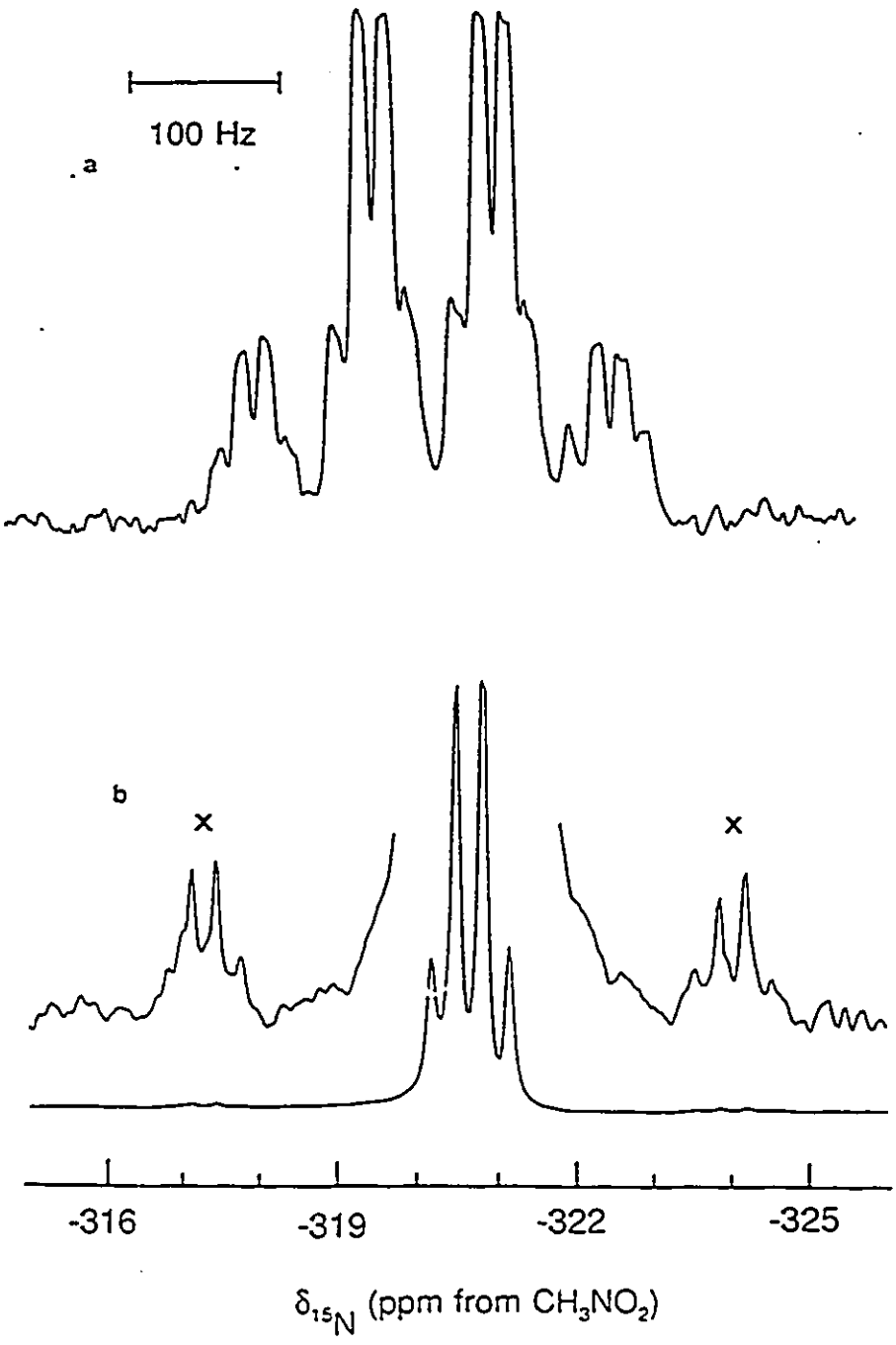

Figure 4.5 ^{15}N NMR spectra (50.698 MHz) of the $CF_3NH_3^+$ cation recorded at -15 °C in HF solvent after warming the solution for 13 hours at 25 °C; (a) $\{^1H\}$-coupled and (b) $\{^1H\}$-decoupled using a DEPT pulse sequence. (X) Unassigned signal.

a ^{15}N spectrum for $HC{\equiv}NH^+$ is possibly attributable to a long T_1 value for this species. Relaxation delays as long as 30 s failed to produce any measurable intensity for $HC{\equiv}NH^+$. The multiplet at -320.7 ppm consisted of a quartet of quartets in the ^{15}N NMR spectrum (Figure 4.5). The $\{^1H\}$-decoupled DEPT experiment showed that the large coupling arises from coupling of ^{15}N to three equivalent protons, while the smaller couplings arise from coupling of ^{15}N with three equivalent fluorines and consequently the resonance at -320.7 ppm is assigned to the $CF_3NH_3^+$ cation (*vide infra*). The ^{14}N NMR spectra gave a poorly resolved quartet of quartets at -321.8 ppm; the line broadening is attributed to partial quadrupolar relaxation of $^1J(^{14}N\text{-}^1H)$ and $^2J(^{14}N\text{-}^{19}F)$ by the ^{14}N nucleus. The complete characterizations of the $CF_3NH_3^+$, $CF_2{=}NH_2^+$ and $CHF{=}NH_2^+$ cations are discussed below.

(B) CHARACTERIZATION OF THE $CF_3NH_3^+$ CATION IN HF SOLVENT BY NMR SPECTROSCOPY

The ^{19}F NMR spectra resulting from the initial warming of $HC{\equiv}N\text{-}XeF^+AsF_6^-$ in HF showed an intense signal at -64.9 ppm that increased with time. The ^{19}F resonance at -64.9 ppm was assigned to a CF_3 group (cf. the ^{19}F resonances of CF_4; -61.4 and CF_3H; -81.5 ppm). The broadness of this signal arises from a small two-bond coupling, $^2J(^{19}F\text{-}^{14}N)$, which is partially collapsed due to quadrupole relaxation of ^{14}N, and unresolved $^3J(^{19}F\text{-}^1H)$ coupling. The corresponding ^{15}N-enriched sample was prepared and showed the anticipated doublet of quartets fine structure on the CF_3 peak (-64.9 ppm) which is attributed to $^2J(^{19}F\text{-}^{15}N)$, 18.2 Hz, and $^3J(^{19}F\text{-}^1H)$, 5.4 Hz (Figure 4.6).

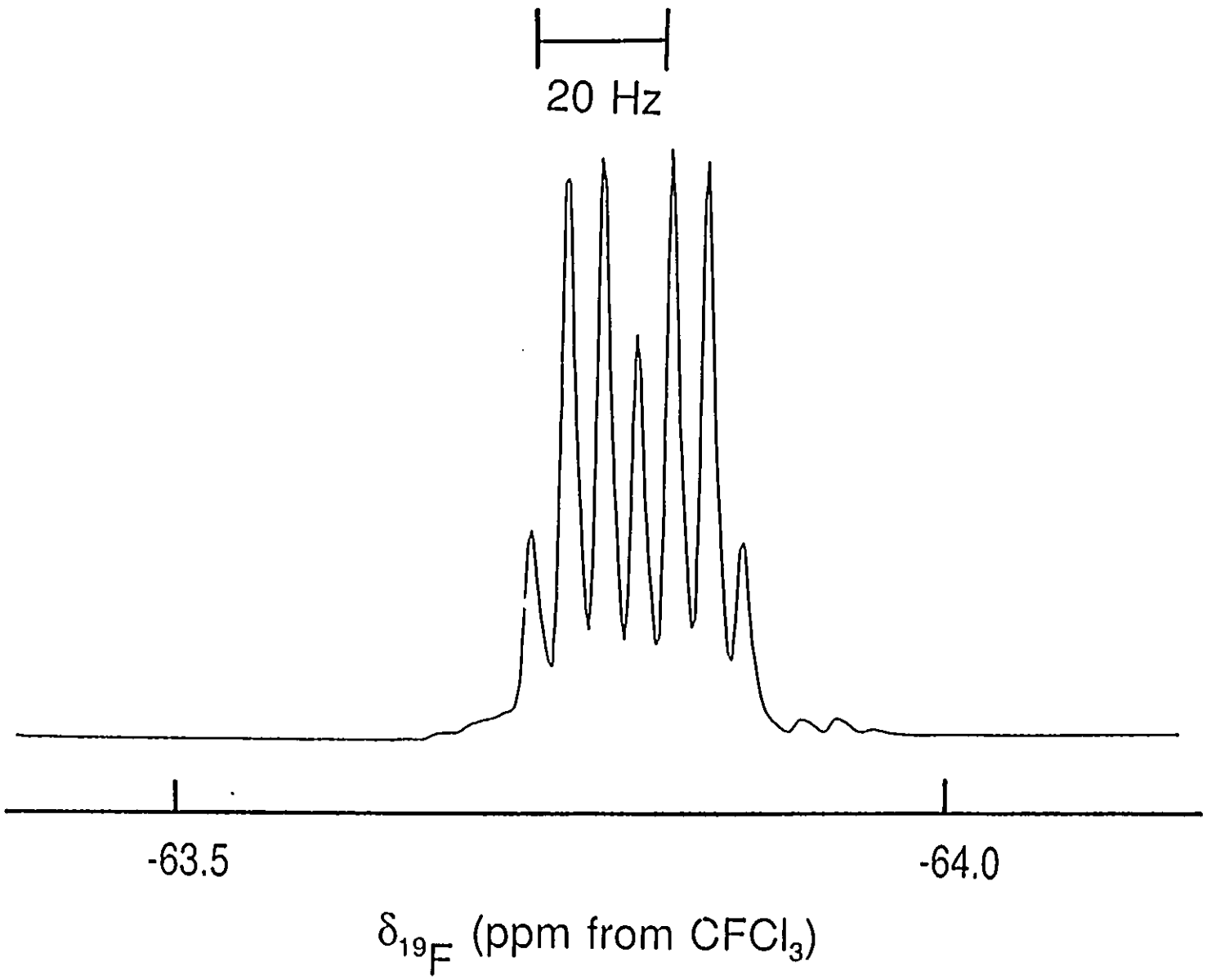

Figure 4.6 ^{19}F NMR (235.361 MHz) spectrum of the 99.5% ^{15}N-enriched $CF_3NH_3^+$ cation in HF solvent at -15 °C.

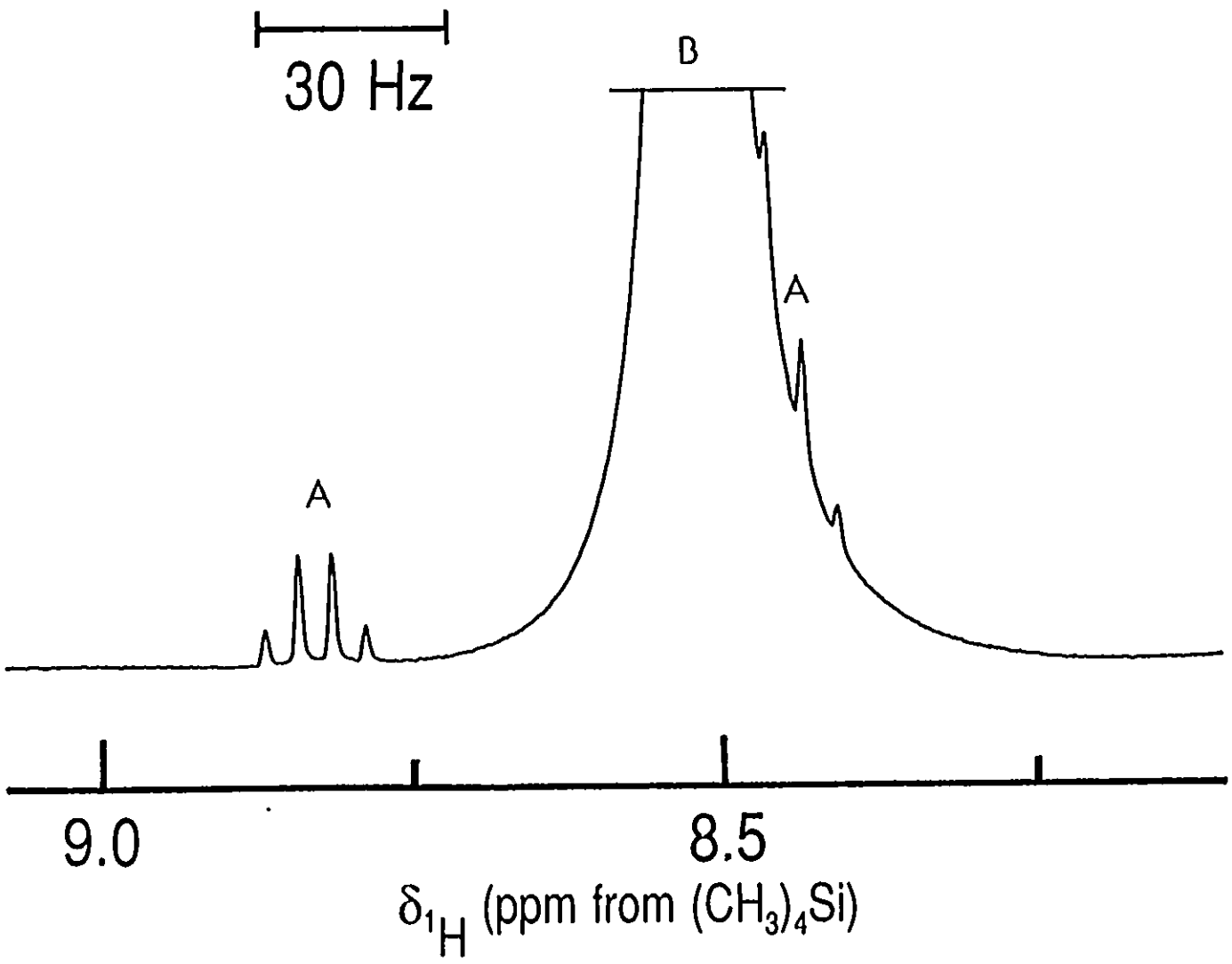

Figure 4.7 ^{1}H NMR (200.133 MHz) spectrum of the 99.5% ^{15}N-enriched $CF_3NH_3^+$ cation recorded at -15 °C in HF solvent; (A) $[^{15}N]CF_3NH_3^+$ and (B) HF solvent.

The ^1H NMR spectra of solutions of natural abundance $HC{\equiv}N\text{-}XeF^+AsF_6^-$ in HF that had been warmed for 14 hours at room temperature failed to show the ^1H resonance of $CF_3NH_3^+$, which is expected to occur at higher frequency than that of the neutral species, CF_3NH_2, ($\delta(^1H)$, 6.73 ppm) and was assumed to be coincident with the broad HF solvent peak occurring at 8.18 ppm. The ^1H NMR spectrum of a 99.5% ^{15}N-enriched $HC{\equiv}N\text{-}XeF^+AsF_6^-$ sample that had been warmed for 10 hours at room temperature was recorded at -10 °C. The spectrum is readily assigned to the $CF_3NH_3^+$ cation and showed a strong doublet of quartets centered at 8.60 ppm which straddled the HF solvent peak (Figure 4.7). The doublet arises from $^1J(^{15}N\text{-}^1H)$, 76.42 Hz and the quartet fine structure arises from $^3J(^{19}F\text{-}^1H)$, 5.4 Hz. The $^1H\text{-}^{19}F$ coupling constant observed in the ^1H NMR spectrum is in good agreement with the quartet coupling observed at -64.9 ppm in the ^{19}F NMR spectrum (5.4 Hz).

The ^{15}N NMR spectra of solutions of 99.5% ^{15}N-enriched $HC{\equiv}N\text{-}XeF^+AsF_6^-$ that had been warmed for 14 hours at room temperature showed a strong signal at -320.7 ppm which was split into a quartet of quartets due to spin-spin coupling with the three equivalent protons and the three equivalent fluorines of $CF_3NH_3^+$, $^1J(^{15}N\text{-}^1H)$, 76.42 Hz and $^2J(^{19}F\text{-}^{15}N)$, 18.2 Hz (Figure 4.5a). Proton decoupling collapsed the large quartet splitting to give a single quartet in the ^{15}N spectrum arising from $^2J(^{19}F\text{-}^{15}N)$, 18.2 Hz (Figure 4.5b).

The ^{13}C NMR spectra of $CF_3NH_3^+$ derived from natural abundance $HC{\equiv}N\text{-}XeF^+$ showed a slightly broadened quartet at 116.7 ppm (cf. $\delta(^{13}C)$ of CF_4; 119.1 ppm and CF_3H, 116.5 ppm). The line broadening relative to that of CF_4, also present in the

sample, is attributed to the quadrupole collapsed scalar coupling $^{1}J(^{14}N\text{-}^{13}C)$.

Based on the NMR findings, the $CF_3NH_3^+$ cation represents one of the major products resulting from the decomposition of $HC{\equiv}N\text{-}XeF^+AsF_6^-$ in HF solvent. Prior to this work Sundermeyer *et al.*[185] synthesized this cation as $CF_3NH_3^+Cl^-$ by two different routes, the transformation of the CF_3NCl_2 into the amine hydrochloride (equation (4.1)) and by cleavage of *t*-butyl trifluoromethylcarbamate (equation (4.2)).

$$CF_3NCl_2 + 3\ HCl \xrightarrow{-100\ ^\circ C} CF_3NH_3^+Cl^- + 2\ Cl_2 \qquad (4.1)$$

$$CF_3NH(C{=}O)\text{-}O\text{-}t\text{-}C_4H_9 + HCl \xrightarrow{-25\ ^\circ C} CF_3NH_3^+Cl^- + CO_2 + ClC(CH_3)_3 \qquad (4.2)$$

However, the characterization of the $CF_3NH_3^+$ cation was not reported, whereas the corresponding neutral trifluoromethylamine, CF_3NH_2, was prepared from $CF_3NH_3^+Cl^-$ by the action of a base (quinoline, pyridine, ethylamine or trimethylamine) and fully characterized by mass spectrometry, infrared, Raman and ^{1}H and ^{19}F NMR spectroscopy. Trifluoromethylamine, CF_3NH_2, was shown to be stable below -21 °C and was considered to be a very weak base due to the high electronegativity of the CF_3 group. Consequently, no attempt was made to isolate the neutral species, CF_3NH_2, in the present work. However, it would seem that the decomposition of $HC{\equiv}N\text{-}XeF^+AsF_6^-$ in HF could form the basis for a general synthetic route to CF_3NH_2.

(C) CHARACTERIZATION OF THE $CF_2{=}NH_2^+$ CATION IN HF SOLVENT BY NMR SPECTROSCOPY

The ^{19}F NMR spectra showed that $\delta(^{19}F)$ of the $CF_2{=}NH_2^+$ cation (-30.5 ppm) is more deshielded than the average of the ^{19}F chemical shifts reported for the neutral imine $CF_2{=}NH$ ($\delta(F)_{cis}$, -32.6 ppm; $\delta(F)_{trans}$, -59.2 ppm). The ^1H (Figure 4.8) and ^{19}F (Figure 4.9) NMR spectra of $CF_2{=}NH_2^+$ belong to an AA'XX' spin system where $^2J(^1H\text{-}^1H) \approx 0$ Hz and $^2J(^{19}F\text{-}^{19}F)$ is indeterminant. Each signal is split into a doublet of doublets arising from $^3J(^{19}F\text{-}^1H)_{cis}$ and $^3J(^{19}F\text{-}^1H)_{trans}$. The two couplings are 9.7 and 7.2 Hz, but it is not possible to definitively assign them to cis- or trans- $^3J(^{19}F\text{-}^1H)$.

The neutral imine, $CF_2{=}NH$, has recently been synthesized by Bürger and Pawelke[186] by dissolving CF_3NH_2 at -78 °C in neat $N(C_2H_5)_3$ followed by warming the solution to -20 to -10 °C in vacuo. The gaseous product, $CF_2{=}NH$, (stable below -13 °C) was identified by the ^{19}F NMR in $CFCl_3$ solution and by infrared spectroscopy in the gas phase.

(D) CHARACTERIZATION OF THE $CFH{=}NH_2^+$ CATION IN HF SOLVENT BY NMR SPECTROSCOPY

The ^{19}F NMR spectra resulting from warming $HC{\equiv}N\text{-}XeF^+AsF_6^-$ for 3 hours in HF showed a relatively intense doublet at -97.3 ppm; $^2J(^{19}F\text{-}^1H)$ 59.3 Hz. This signal diminished and disappeared within 9 hours at room temperature. The peak is assigned

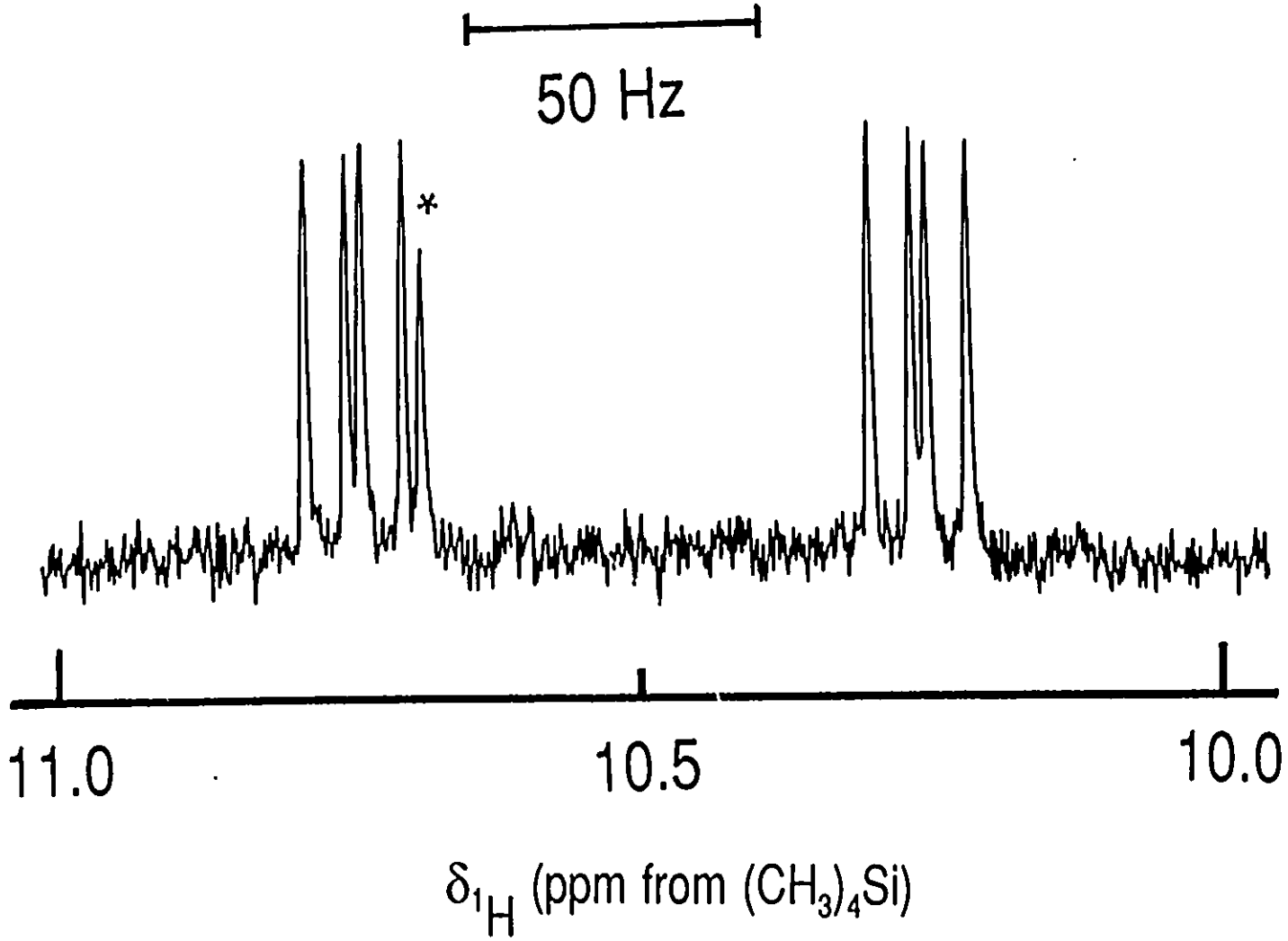

Figure 4.8 ^{1}H NMR (200.133 MHz) spectrum of the 99.5% ^{15}N-enriched $CF_2{=}NH_2^+$ at -15 °C in HF solvent. Asterisk (*) denotes a species which is unassigned.

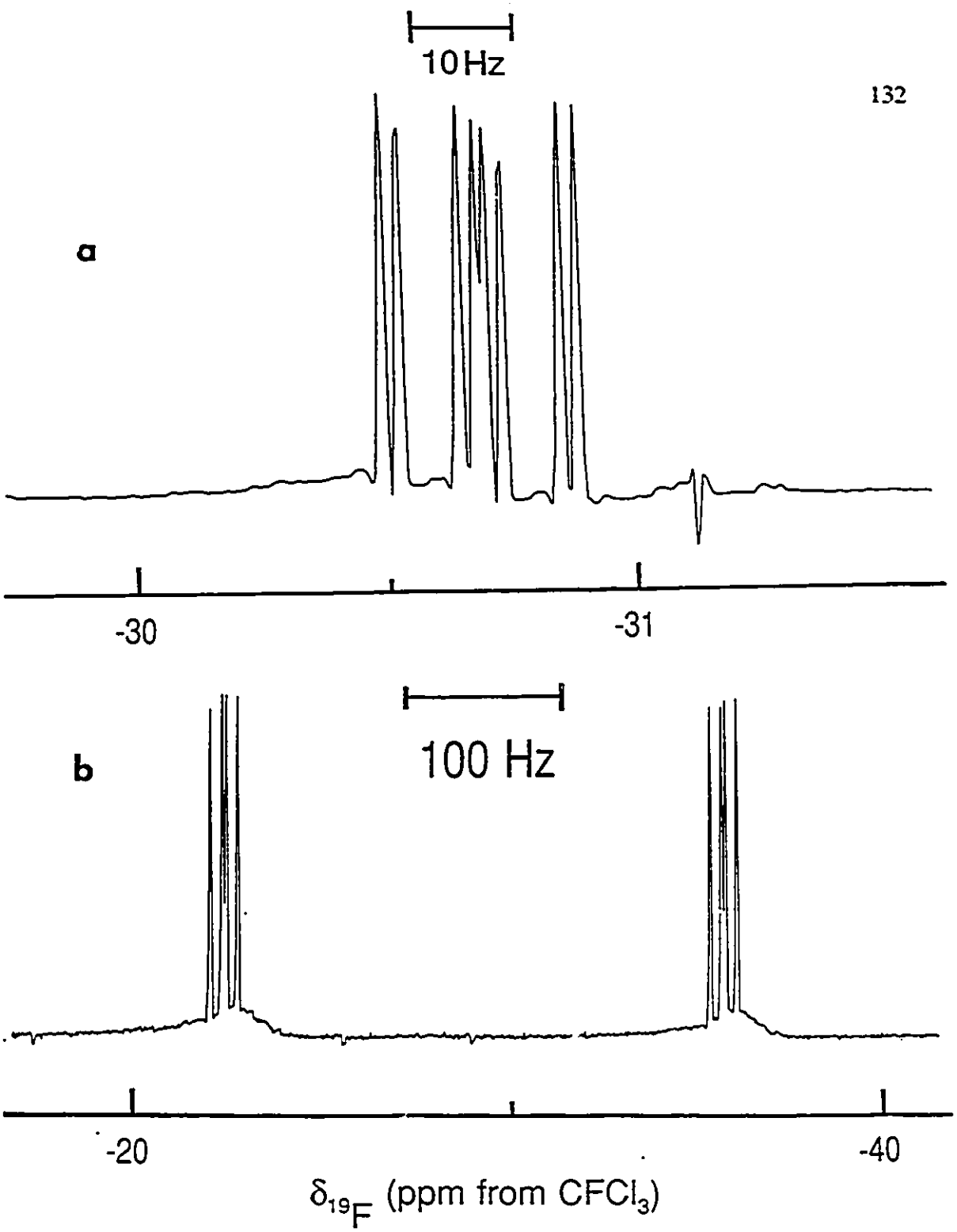

Figure 4.9 ^{19}F NMR (235.361 MHz) spectra of $CF_2{=}NH_2^+$ resulting from warming a solution of $HC{\equiv}N\text{-}XeF^+AsF_6^-$ in HF solvent for 10 hours at room temperature; (a) 99.5% ^{15}N-enriched $HC{\equiv}N\text{-}XeF^+AsF_6^-$ and (b) 99.2% ^{13}C-enriched $HC{\equiv}N\text{-}XeF^+AsF_6^-$.

to the intermediate, $CHF{=}NH_2^+$, which reacts further to form $CF_3NH_3^+$, CF_4 and CF_3H (see Table 4.1 and Scheme 4.1).

The ^{13}C resonance of $CHF{=}NH_2^+$ is assigned to a doublet of doublets occurring at 171.0 ppm. A $\{^1H\}$-broad-band decoupling experiment showed that one of these doublets is the result of the one-bond proton-carbon coupling $^1J(^{13}C\text{-}^1H)$, 249.1 Hz; while the other doublet results from the one bond fluorine-carbon coupling $^1J(^{19}F\text{-}^{13}C)$, 336 Hz. The ^1H-decoupled spectrum consisted of a partially quadrupole collapsed 1:1:1 triplet on each branch of a doublet arising from $J(^{14}N\text{-}^{13}C)$, 14.9 Hz (Figure 4.3).

The ^{15}N and ^{14}N resonance of $CHF{=}NH_2^+$ could not be observed even when a relaxation delay of 30 s was applied in ^{15}N NMR experiment. Failure to observe the ^{14}N resonance is attributed to the low symmetry about nitrogen resulting in rapid quadrupolar relaxation and severe broadening of its ^{14}N resonance.

The ^1H NMR resonance was not observed for the proton-on-carbon of $CHF{=}NH_2^+$. The CH signal of a related species, $CHF{=}N(CH_3)_2^+$, has been reported at 7.97 ppm in SO_2 solvent.[187] In the case of the $CHF{=}NH_2^+$ cation, the ^1H resonance of the CH group presumably could not be observed because it was hidden by the broad HF solvent peak at 8.18 ppm. Although, several proton on nitrogen signals were observed in the ^1H NMR spectra of the natural abundance and ^{15}N-enriched samples, it was not possible to identify the proton on nitrogen signal of $CHF{=}NH_2^+$.

(E) COMPARISON OF THE SOLVOLYTIC BEHAVIORS OF $HC{\equiv}N\text{-}XeF^+AsF_6^-$ AND $HC{\equiv}N$ IN ANHYDROUS HF

As noted in the previous discussion, $HC{\equiv}N\text{-}XeF^+$ initially undergoes solvolysis according to equilibria (4.3) - (4.6) to give equilibrium concentrations of XeF_2 and $HC{\equiv}NH^+$ (cf. Chapter 3). That XeF_2, rather than HF, is the dominant fluorinating agent

$$HC{\equiv}N\text{-}XeF^+ + HF \rightleftharpoons HC{\equiv}NH^+ + XeF_2 \qquad (4.3)$$

$$HC{\equiv}N\text{-}XeF^+ \rightleftharpoons HC{\equiv}N + XeF^+ \qquad (4.4)$$

$$XeF^+ + 2HF \rightleftharpoons XeF_2 + H_2F^+ \qquad (4.5)$$

$$XeF^+ + XeF_2 \rightleftharpoons Xe_2F_3^+ \qquad (4.6)$$

towards $HC{\equiv}NH^+$ generated in equilibrium (4.3) has been verified in a parallel study by monitoring the reaction of $HC{\equiv}N$ in HF over a period of 7 days.

Although the precise natures of the mechanistic processes leading to the observed fluorination products are not clear, a reasonable reaction sequence can be proposed (Scheme 4.1). The initial warming of HF solutions formally containing $HC{\equiv}N\text{-}XeF^+AsF_6^-$ (derived by the reaction of stoichiometric amounts of $XeF^+AsF_6^-$ and $HC{\equiv}N$) and $HC{\equiv}N\text{-}XeF^+AsF_6^-$ and XeF_2 (derived by the reaction of stoichiometric amounts of $Xe_2F_3^+AsF_6^-$ and $HC{\equiv}N$) gave rise to equilibria (4.3) - (4.6), which have been investigated

in Chapter 3 by ^{19}F, ^{13}C, ^{129}Xe and ^{1}H NMR spectroscopy. Unlike the HF solvolysis of HC≡N, there was no detectable amount of $CHF_2NH_3^+$ formed during HC≡N-XeF^+ decomposition. The absence of the $CHF_2NH_3^+$ cation is accounted for by assuming rapid electrophilic fluorination of $CHF_2NH_3^+$ by XeF_2 (see equilibria (4.4) and (4.5)) according to Scheme 4.1 to give the trifluoromethylammonium cation, $CF_3NH_3^+$, which is observed as one of the major products (Figure 4.4). In contrast, the neutral amine, CF_3NH_2, is thermally unstable, decomposing at 25 °C to form FC≡N and HF.[181] Alternatively, XeF_2 may electrophilicly fluorinate the carbon of the proposed intermediate imine cation, $HFC=NH_2^+$, in Scheme 4.1 to give $F_2C=NH_2^+$ followed by HF addition to the double bond of the later cation to form $CF_3NH_3^+$. The formation of $F_2C=NH_2^+$ was also monitored by NMR spectroscopy in HF solutions initially containing HC≡N-$XeF^+AsF_6^-$ and in systems containing an excess of XeF_2, i.e., $Xe_2F_3^+AsF_6^-$ + HC≡N (Figure 4.4 and Table 4.1). Subsequent electrophilic fluorination of $CF_3NH_3^+$ by XeF_2 at the carbon or nitrogen gave rise to CF_4. The final nitrogen-containing product(s) has not been identified, although the ^{14}N and ^{15}N NMR signals at -73.1 ppm can be assigned to N_2, and are in good agreement with the reported chemical shift of dinitrogen.[188] Interestingly, the anticipated cations, NH_4^+ and NH_3F^+ were absent in the ^{1}H, ^{14}N, ^{15}N and ^{19}F NMR spectra. As the decomposition proceeds, exchange broadening of both the HF and AsF_6^- resonances is observed in the ^{19}F NMR spectra. The exchange broadening presumably arises from AsF_5 formation which is accompanied by Xe gas evolution.

The only fluorinated product formed in the HC≡N/HF solvolysis reaction was the difluoromethylammonium cation, $CHF_2NH_3^+$, which presumably arises from the stepwise

Scheme 4.1

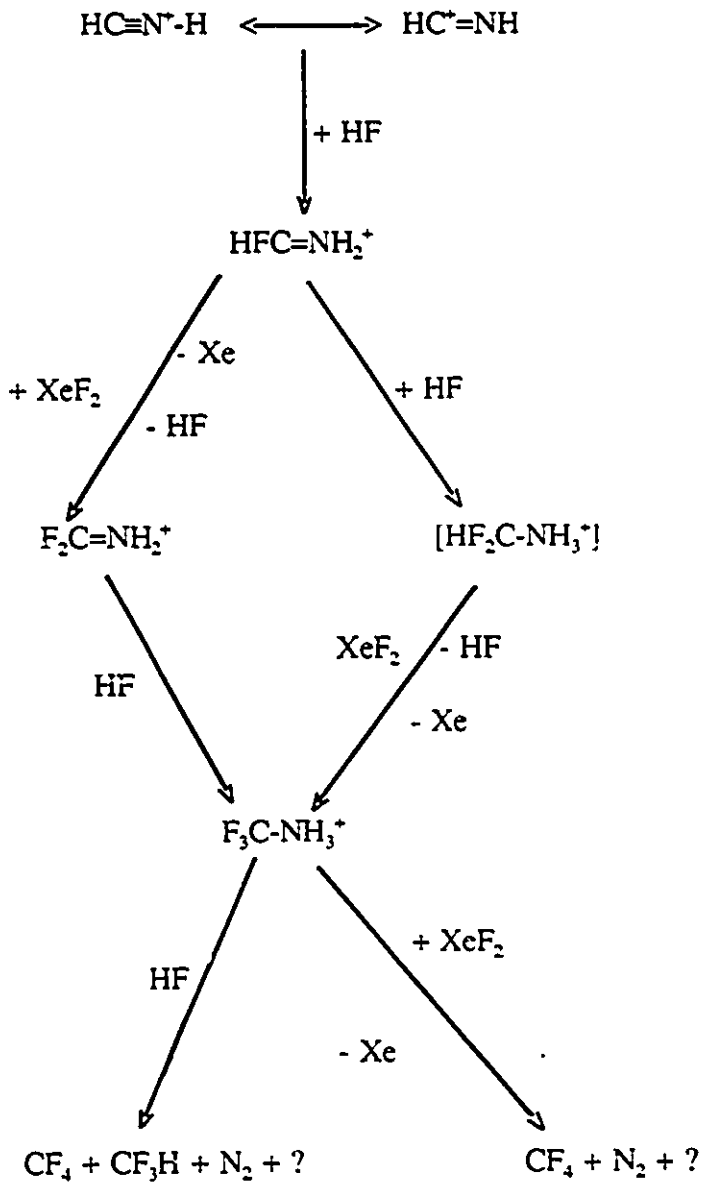
HC≡N⁺-H
HC⁺=NH
+ HF
HFC=NH2⁺
- Xe
+ XeF2
- HF
+ HF
F2C=NH2⁺
[HF2C-NH3⁺]
XeF2
- HF
HF
- Xe
F3C-NH3⁺
+ XeF2
HF
- Xe
CF4 + CF3H + N2 + ?
CF4 + N2 + ?

addition of HF according to Scheme 4.2. It is presumed that the intermediate imine cation, $HFC{=}NH_2^+$, rapidly undergoes HF addition and is not observed. The $CHF_2NH_3^+$ cation has been previously reported by Gillespie and Hulme,[189] who characterized the cation by ^{19}F and ^1H NMR spectroscopy using both natural abundance and ^{15}N-enriched $HC{\equiv}N$. The spectra reported by these workers were poorly resolved and the ^{19}F and ^1H chemical shifts were not reported. Consequently, the full set of NMR parameters for the $CHF_2NH_3^+$ cation is given in Table 4.2 and the ^1H, ^{14}N and ^{19}F NMR spectra of the cation recorded in HF solvent are depicted in Figure 4.10.

The ^{19}F NMR spectrum of $CHF_2NH_3^+$ consists of a doublet of quartets (-105.2 ppm) resulting from the spin-spin couplings $^2J(^{19}F\text{-}^1H)$, 58.4 Hz and $^3J(^{19}F\text{-}^1H)$, 9.2 Hz. At high-resolution, $^2J(^{19}F\text{-}^{14}N)$, 9.1 Hz was observed. This coupling is in excellent agreement with the value of 9.8 Hz calculated from equation (4.7) using the $^2J(^{19}F\text{-}^{15}N)$ value of 13.9 Hz reported by Gillespie and Hulme.[189]

$$^2J(^{19}F\text{-}^{14}N) = {}^2J(^{19}F\text{-}^{15}N)\ \frac{\gamma(^{14}N)}{\gamma(^{15}N)} \qquad (4.7)$$

The ^1H NMR spectrum consists of two resonances; the protons-on-nitrogen occur at 6.52 ppm and consist of a doublet of triplets of 1:1:1 triplets arising from $^1J(^{14}N\text{-}^1H)$, 54.9 Hz; $^3J(^{19}F\text{-}^1H)$, 9.2 Hz and $^3J(^1H\text{-}^1H)$, 2.9 Hz and the proton on carbon appears as a triplet of quartets at 5.75 ppm arising from $^2J(^{19}F\text{-}^1H)$, 58.4 Hz and $^3J(^1H\text{-}^1H)$, 2.9 Hz. The ^{14}N NMR spectrum consisted of a quartet at 25.7 ppm resulting from $^1J(^{14}N\text{-}^1H)$, 54.9 Hz which collapses to a single line with ^1H and $\{^1H\}$-decoupling.

Scheme 4.2

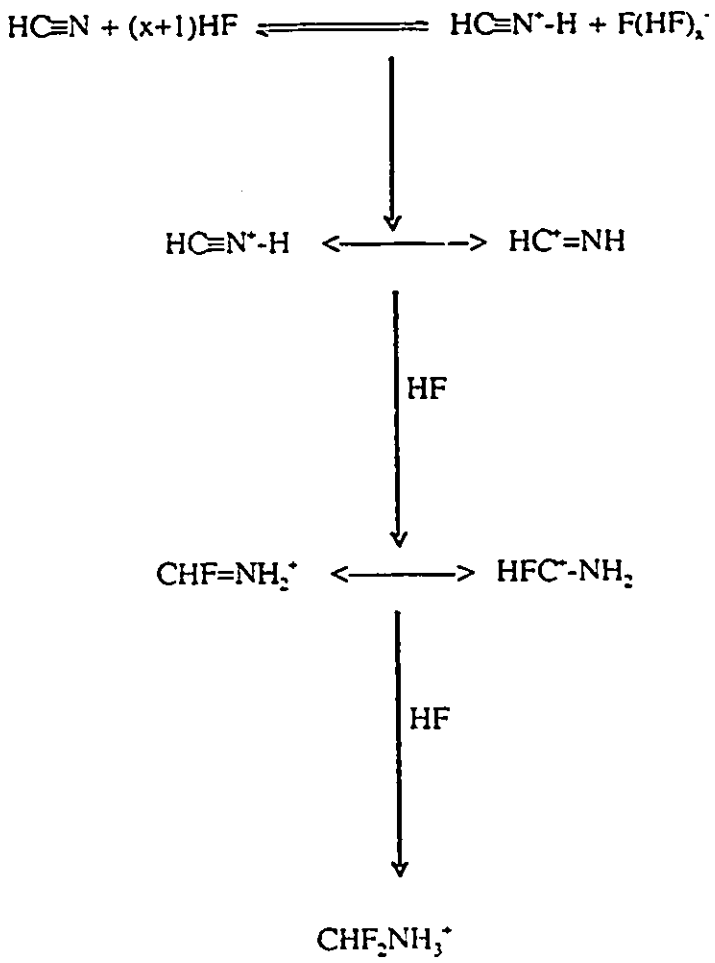

Table 4.2

NMR Parameters for the $F_2HCNH_3^+$ Cation in HF Solvent[a]

Chemical Shifts (ppm)[b]		Coupling Constants (Hz)	
$\delta(^1H)_{NH}$	6.52	$^2J(^{19}F\text{-}^1H)$	58.4
$\delta(^1H)_{CH}$	5.75	$^3J(^{19}F\text{-}^1H)$	9.2
$\delta(^{19}F)$	-105.2	$^3J(^1H\text{-}^1H)$	2.9
$\delta(^{13}C)$	108.1	$^1J(^{14}N\text{-}^1H)$	54.9
$\delta(^{14}N)$	-325.7	$^2J(^{14}N\text{-}^{19}F)$	8.5
		$^1J(^1H\text{-}^{13}C)$	226.2
		$^1J(^{19}F\text{-}^{13}C)$	263.3
		$^2J(^{19}F\text{-}^{14}N)$	9.1

[a] All spectra were recorded at -15 °C.

[b] Referenced externally at 25 °C with respect to the neat liquid references: $CFCl_3$ (^{19}F), CH_3NO_2(^{15}N and ^{14}N) and TMS (^{13}C and ^1H).

Figure 4.10 NMR spectra of $CHF_2NH_3^+$ resulting from the solvolysis of HC≡N (1.0 m) in anhydrous HF and recorded at -15 °C; (a) ^1H NMR spectrum (500.138 MHz), (b) ^{19}F NMR spectrum (235.361 MHz) and (c) ^{15}N NMR spectrum (18.076 MHz).

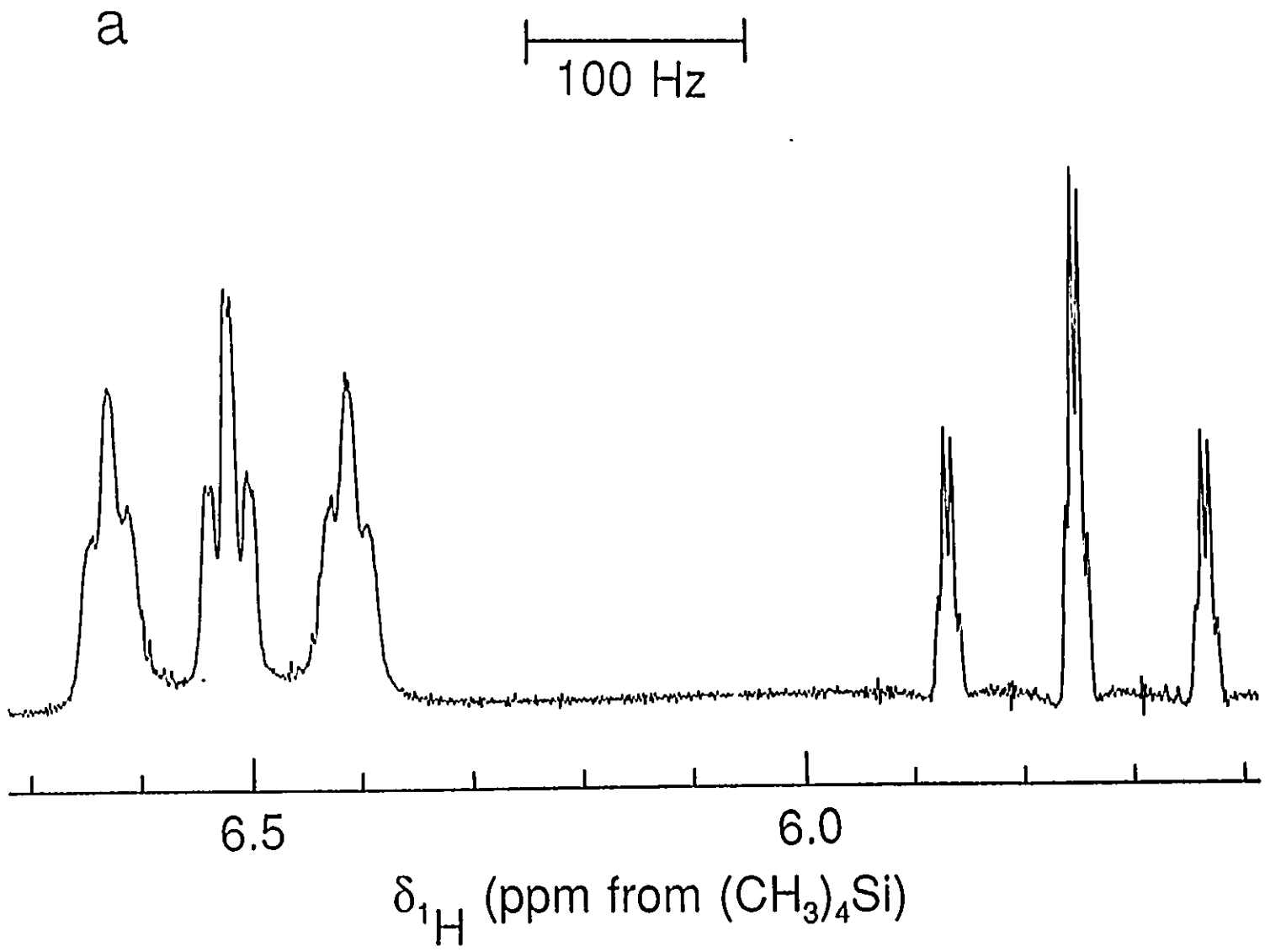
a
100 Hz
6.5
6.0
δ1H (ppm from (CH3)4Si)

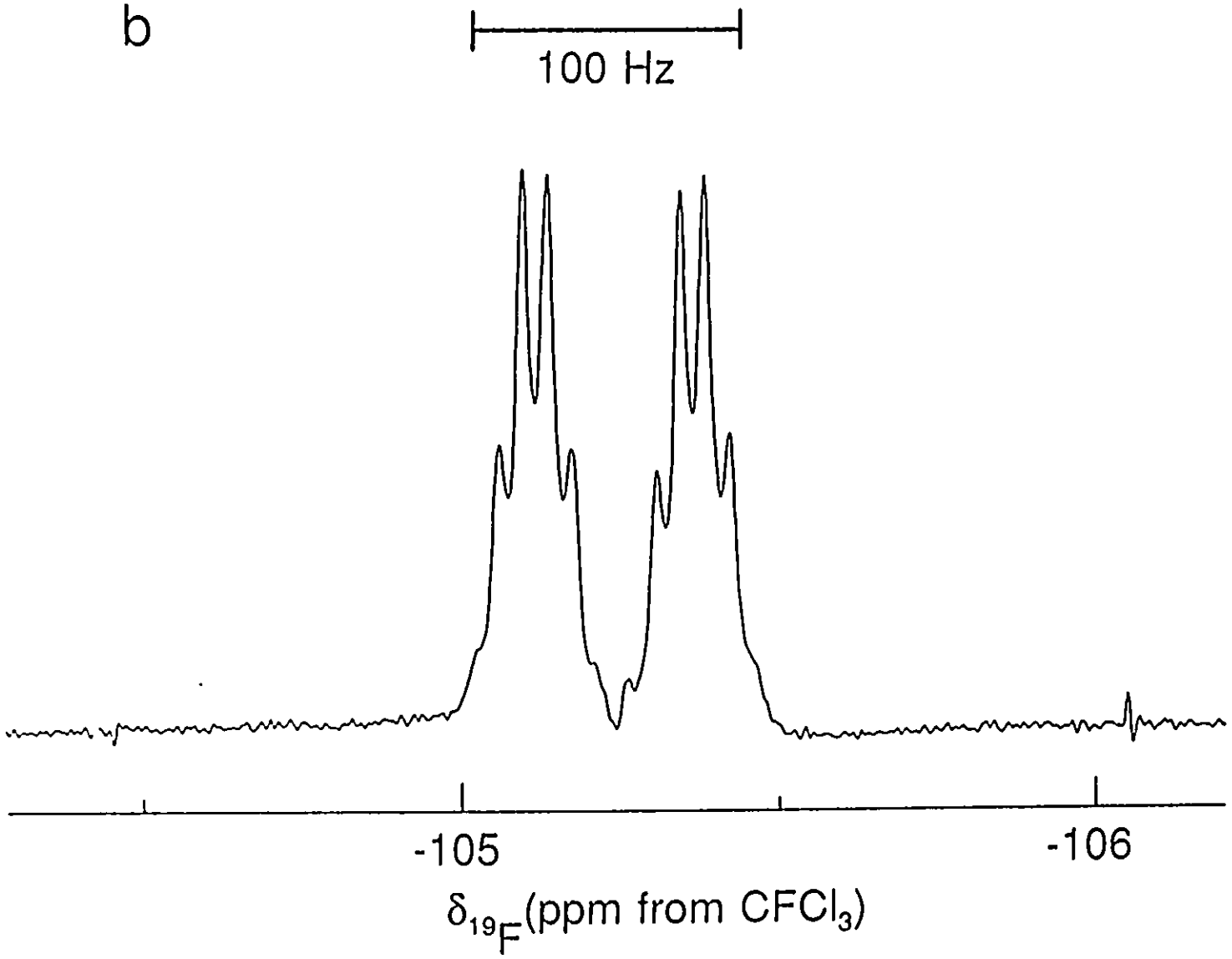
b
100 Hz
-105
-106
$\delta_{^{19}F}$(ppm from $CFCl_3$)

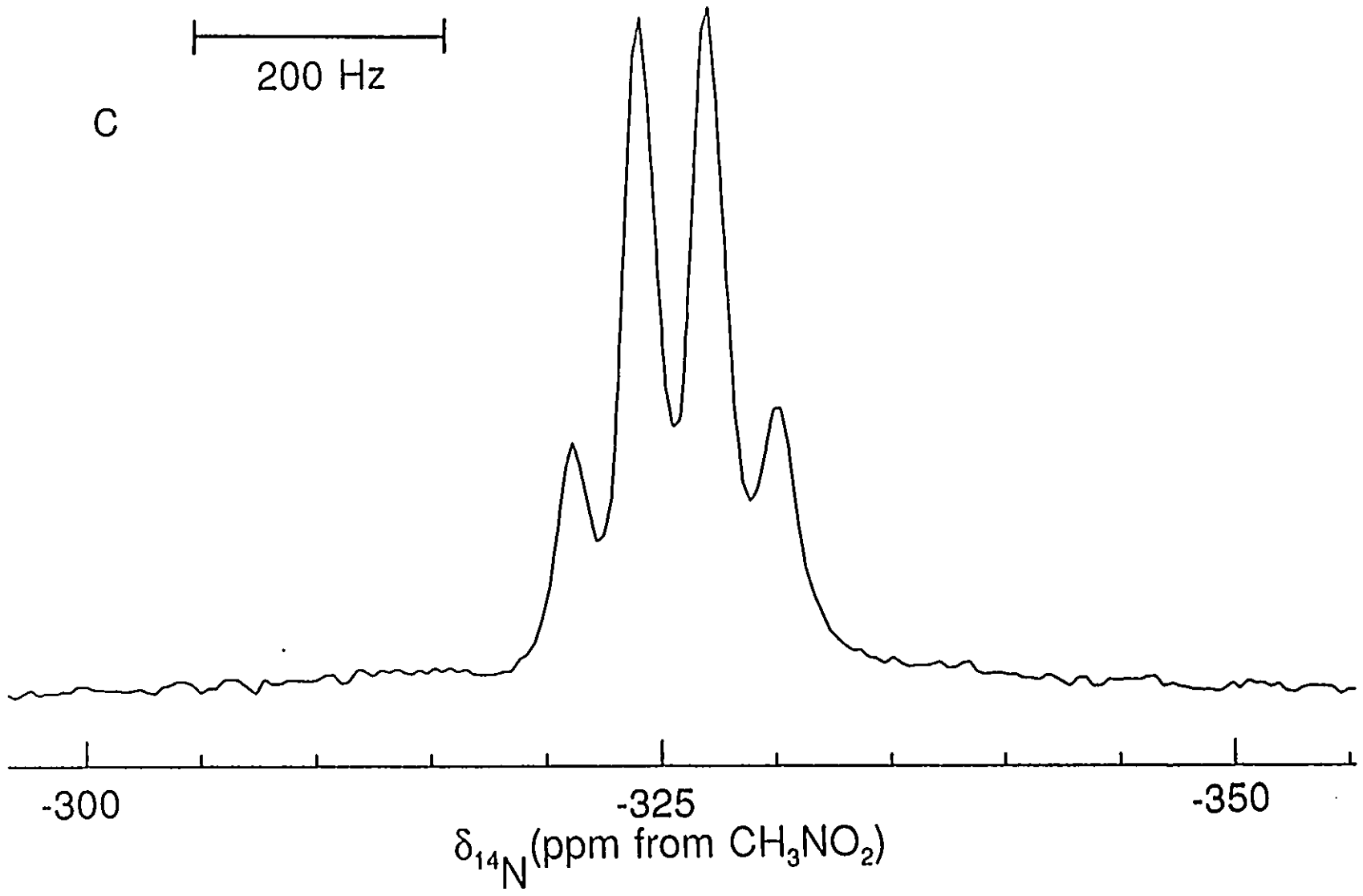
200 Hz
C
-300
-325
-350
$\delta_{^{14}N}$(ppm from CH_3NO_2)

No product other than $CHF_2NH_3^+$ was observed to form in HC≡N/HF solvolysis mixtures after 7 days at room temperature, contrasting with the earlier work, which has reported subsequent polymerization to give polymers whose structures are uncertain.[189] In contrast with the related alkyl nitrile/HF systems (see Chapter 6), the $RCF_2NH_3^+$ cations were shown to be intermediates which dimerize in HF to form the $RCF_2NHC(=NH_2)R^+$ cations.

(F) COMPARISON OF THE DECOMPOSITION OF HC≡N-XeF$^+$ AND HC≡N-KrF$^+$ IN HF SOLVENT

In previous work on the solvolysis of HC≡N-KrF$^+$ in HF,[122] the ^{19}F NMR spectrum showed an intense signal at -64.9 ppm in HF solvent. This signal was assigned to CF_4. In the present work, the ^{19}F NMR spectrum resulting from the solvolysis of HC≡N-XeF$^+$ in HF showed the same signal at -64.9 ppm, and using the ^{13}C- and ^{15}N-enriched samples as mentioned in the previous sections, this resonance could be unambiguously assigned to the $CF_3NH_3^+$ cation. Accordingly it may be concluded that the $CF_3NH_3^+$ cation is formed in both the decomposition of HC≡N-XeF$^+$ and of HC≡N-KrF$^+$. The formation of the $CF_3NH_3^+$ cation sheds some light on the mechanisms of these reactions, suggesting that the mode of the fluorination may be the same in both cases (see Scheme 4.1) and may involve a radical fluorination mechanism. However, owing to the strongly oxidizing character of KrF_2 (EA of KrF$^+$; 13.2 eV[190]) compared to that of XeF_2 (EA of XeF$^+$; 10.9 eV[155]), the initial fluorinated intermediates, $CHF{=}NH_2^+$ and $CF_2{=}NH_2^+$, have only been

observed in the case of the solvolysis/ fluorination decomposition of the $HC{\equiv}N\text{-}XeF^+$ cation in HF and could not be observed in the case of $HC{\equiv}N\text{-}KrF^+$. These intermediates are expected to be more rapidly fluorinated in the presence of the strong fluorinating agent KrF_2, which is also in equilibrium with $HC{\equiv}N\text{-}KrF^+$ and $HC{\equiv}NH^+$ (cf. equation (4.3)).

Fluorination of the $CF_3NH_3^+$ cation in both systems led to cleavage of the C-N bond. The fluorination products depend greatly upon the fluorinating ability of the difluoride, which is in equilibrium with the present cation (equilibrium (4.3)). The fluorination of the C-N linkage of the $CF_3NH_3^+$ when $HC{\equiv}N\text{-}KrF^+$ decomposes in HF leads to less complex fluorinated products that result from attack of fluorine at both carbon and nitrogen sites to give CF_3H, CF_4, NF_3 and NF_4^+. In contrast, fluorine attacks the carbon site in $HC{\equiv}N\text{-}XeF^+$, but not the nitrogen, so that only CF_3H and CF_4 have been observed. The reaction mechanisms for the decomposition of $HC{\equiv}N\text{-}XeF^+$ and $HC{\equiv}N\text{-}KrF^+$ in anhydrous HF appear to be similar and result in cleavage of the C-N bond in the $CF_3NH_3^+$ to produce $CF_3^{\bullet}$ and $NH_3^{\bullet+}$ radicals. These radicals, in the presence of the strong fluorinating agent, KrF_2, are readily fluorinated to form CF_3H, CF_4, NF_3 and NF_4^+. In contrast, XeF_2 is a relatively moderate fluorinating agent and the $NH_3^{\bullet+}$ radical cation is expected to be much less susceptable to fluorination by XeF_2. The inability to identify the unfluorinated nitrogen fragments resulting from the solvolysis of $HC{\equiv}N\text{-}XeF^+$ in HF may result from coupling reactions between nitrogen radicals, which are predominant when compared to fluorine radical reactions, and/or formation of dinitrogen.[188] However, this is very tentative since only N_2 has been identified and the

other unfluorinated nitrogen species have not been observed in their $^{14/15}N$ and ^{1}H NMR spectra.

(G) THE CORRELATION OF N-H AND C-F s-CHARACTER WITH $^{1}J(^{15}N\text{-}^{1}H)$ AND $^{1}J(^{19}F\text{-}^{13}C)$ IN THE $CF_3NH_3^+$, $CHF_2NH_3^+$, $CF_2{=}NH_2^+$ AND $CHF{=}NH_2^+$ CATIONS

The correlation of one-bond coupling constants with formal hybridization has been largely confined to $^{1}J(^{13}C\text{-}^{1}H)$[191-194] and $^{1}J(^{14/15}N\text{-}^{1}H)$.[195] Three different mechanisms have been proposed for nuclear spin-spin interactions:[196] the Fermi contact interaction, the nuclear spin-electron orbital interactions and electron-nuclear dipole-dipole interactions. Karplus and Grant[197] and others[198] have concluded that coupling of protons with other nuclei derives principally from the contact term.

An empirical relationship between the s-character of the N-H bond and $^{1}J(^{15}N\text{-}^{1}H)$ has been proposed.[195] This approach has been applied to calculate the s-characters of the N-H bonds of $HC{\equiv}NH^+$ and $CH_3C{\equiv}NH^+$ [161] and several ammonium and iminium cations.[161] The formal hybridizations of the nitrogen atoms of the $CF_3NH_3^+$, $CHF_2NH_3^+$ and $CF_2{=}NH_2^+$ cations were calculated from $^{1}J(^{15}N\text{-}^{1}H)$ using equation (4.8) and found to be sp^3 for $CF_3NH_3^+$ and $CHF_2NH_3^+$ and sp^2 for the $CF_2{=}NH_2^+$ cation, confirming their proposed structures. Table 4.3 compares $^{1}J(^{15}N\text{-}^{1}H)$ and the formal hybridizations of the nitrogen atoms.

$$\%s = 0.430\ {}^{1}J({}^{15}N\text{-}{}^{1}H) - 6.0 \qquad (4.8)$$

The one-bond scalar couplings between carbon and fluorine are also dominated by the contact interaction so that the s-character of the C-F bond should be linearly related to the ^{13}C-^{19}F coupling constants. Equation (4.9), which has been derived from only two points, namely, the $^{1}J(^{19}F\text{-}^{13}C)$ couplings of the sp^3 hybridized systems: CF_4; %s character = 25%, J = 261 Hz and the sp^2 hybridized systems $CF_2{=}N(CH_3)_2^+$, %s character = 33.3%, J = 326 Hz.[187]

$$\%s = 0.124\ {}^{1}J({}^{19}F\text{-}{}^{13}C) - 7.2 \qquad (4.9)$$

Using equation (4.9), the formal hybridizations on the carbon atoms in the $CF_3NH_3^+$, $CHF_2NH_3^+$, $CF_2{=}NH_2^+$ and $CHF{=}NH_2^+$ cations have been calculated from their $^{1}J(^{19}F\text{-}^{13}C)$ values and are consistent with sp^3 hybridization for the $CF_3NH_3^+$ and $CHF_2NH_3^+$ cations (25.1 and 25.3 %s character, respectively) and sp^2 hybridization for the $CF_2{=}NH_2^+$ and $CHF{=}NH_2^+$ cation (31.8 and 34.3 %s character, respectively). The calculated s-characters on the nitrogen and carbon atoms combined with the previously discussed NMR assignments are in agreement with the proposed cations, $CF_3NH_3^+$, $CHF_2NH_3^+$, $CF_2{=}NH_2^+$ and $CHF{=}NH_2^+$.

Table 4.3

Correlation of $^1J(^{15}N\text{-}^1H)$, $^1J(^{19}F\text{-}^{13}C)$ with %s Characters of N-H and C-F Bonds in Some Fluorocarbon and Protonated Nitrogen Species.

Cation	$^1J(^{15}N\text{-}^1H)$	$^1J(^{19}F\text{-}^{13}C)$	%s Character of N-H bond [a]	%s Character of C-F bond [b]
NH_4^+ [c]	73.2		25.5 (25)	
CF_4 [d]		261		25.1 (25)
$CH_3NH_3^+$ [c]	75.6		26.5 (25)	
$CHF_2NH_3^+$ [d]		263		25.3 (25)
$CF_3NH_3^+$ [d]	76.4	261	26.9 (25)	25.1 (25)
CF_3OF [e]		269		26.1 (25)
$(C_6H_5)_2C{=}NH_2^+$ [c]	92.6 ± 0.4		33.7 (33.3)	
CF_3NCl_2 [e]		272		26.4 (25)
CF_3H [d]		274		26.7 (25)
$CF_2{=}N(CH_3)_2^+$ [f]		326		33.1 (33.3)
$CF_2{=}NH_2^+$ [d]	97.5	315	35.9 (33.3)	31.8 (33.3)
$CHF{=}N(CH_3)_2^+$ [f]		307		30.8 (33.3)
$CHF{=}NH_2^+$ [d]		336		34.3 (33.3)
$HC{\equiv}NH^+$ [g]	134		51.6 (50)	
$CH_3C{\equiv}NH^+$ [g]	136		52.5 (50)	

a Values were determined from equation (4.8) and values in parentheses were derived from formal hybridizations.

b Values were determined from equation (4.9) and values in parentheses were derived from formal hybridizations.

c Ref. (195).

d This work; recorded at -15 °C.

e Ref. (199).

f Ref. (187).

g Ref. (161).

CHAPTER 5

FLUORO(NITRILE)XENON(II) HEXAFLUOROARSENATES, $RC{\equiv}N\text{-}XeF^{+}AsF_6^{-}$ ($R = CH_3$, CH_2F, CH_2Cl, C_2H_5, CH_2FCH_2, $(CH_3)_2CH$, $(CH_3)_3C$, *n*-C_3H_7, $CH_2FCH_2CH_2$, $CHF_2CH_2CH_2$, CH_3CHFCH_2, *n*-C_4H_9, $CH_2FCH_2CH_2CH_2$, $CH_3CHFCH_2CH_2$, $CH_2ClC(CH_3)H$, $CH_2FC(CH_3)H$ AND C_6F_5) SALTS

INTRODUCTION

The interaction of the Lewis acid XeF^{+} with the neutral nitrogen Lewis base, $HC{\equiv}N$, to form $HC{\equiv}N\text{-}XeF^{+}AsF_6^{-}$ in HF solvent suggested that the formation of XeF^{+} adducts with the alkyl nitriles ought to be a reasonable possibility. The alkyl nitriles selected for study are oxidatively resistant to XeF^{+} (EA = 10.9 eV[155]), having first ionization potentials exceeding 10 - 11 eV (see Table 1.3).

In this Chapter the reactions of several nitriles with $XeF^{+}AsF_6^{-}$ or $Xe_2F_3^{+}AsF_6^{-}$ in anhydrous HF have been studied. A novel series of $RC{\equiv}N\text{-}XeF^{+}AsF_6^{-}$ salts ($R = CH_3$, CH_2F, CH_2Cl, C_2H_5, CH_2FCH_2, *n*-C_3H_7, $CH_2FCH_2CH_2$, $CHF_2CH_2CH_2$, CH_3CHFCH_2, *n*-C_4H_9, $CH_2FCH_2CH_2CH_2$, $CH_3CHFCH_2CH_2$, $(CH_3)_2CH$, $(CH_3)_3C$, $CH_2ClC(CH_3)H$, $CH_2FC(CH_3)H$ and C_6F_5) have been characterized in anhydrous HF solution by ^{129}Xe, ^{19}F, ^{14}N, ^{15}N, ^{13}C and ^{1}H NMR spectroscopy. Several of these salts ($R = CH_3$, CH_2F, CH_2Cl, C_2H_5, $(CH_3)_2CH$ and $(CH_3)_3C$) have been isolated from anhydrous HF solvent and

characterized in the solid state by low-temperature Raman spectroscopy.

RESULTS AND DISCUSSION

(A) PREPARATION AND ISOLATION OF $RC{\equiv}N\text{-}XeF^{+}AsF_6^{-}$

The preparations of the $RC{\equiv}N\text{-}XeF^{+}AsF_6^{-}$ salts were accomplished by the reaction of $XeF^{+}AsF_6^{-}$ or $Xe_2F_3^{+}AsF_6^{-}$ with the appropriate nitrile in HF solvent according to equations (5.1) and (5.2).

$$XeF^{+}AsF_6^{-} + RC{\equiv}N \xrightarrow{HF} RC{\equiv}N\text{-}XeF^{+}AsF_6^{-} \qquad (5.1)$$

$$Xe_2F_3^{+}AsF_6^{-} + RC{\equiv}N \xrightarrow{HF} RC{\equiv}N\text{-}XeF^{+}AsF_6^{-} \qquad (5.2)$$

where R = CH_3, CH_2F, CH_2Cl, CH_3CH_2, CH_2FCH_2, $CH_3CH_2CH_2$, $CH_2FCH_2CH_2$, $CH_3CF_2CH_2$, $CHF_2CH_2CH_2$, $CH_3CH_2CH_2CH_2$, $CH_2FCH_2CH_2CH_2$, $CH_3CF_2CH_2CH_2$, $ClCH_2C(CH_3)H$, $FCH_2C(CH_3)H$, $(CH_3)_2CH$, $(CH_3)_3C$, C_6F_5.

The reactions were carried out by combining stoichiometric amounts of the reactants in anhydrous HF and warming the reaction mixtures from -50 to -10 °C to effect reaction and dissolution in the solvent. The frozen solutions were routinely stored at -196 °C in

sealed FEP NMR tubes until their NMR spectra could be run. The solid samples were isolated by pumping off the HF solvent at -35 to -30 °C and were stored under dry nitrogen at -78 °C until their Raman spectra could be run.

(B) CHARACTERIZATION OF $RC{\equiv}N\text{-}XeF^{+}AsF_6^{-}$ BY ^{129}Xe, ^{19}F, ^{15}N, ^{14}N, ^{13}C AND ^{1}H NMR SPECTROSCOPY

(i) Nitrile Adducts of $XeF^{+}AsF_6^{-}$ in Anhydrous HF Solvent

Multinuclear magnetic resonance spectra were recorded for solutions of nitriles, $RC{\equiv}N$ (R = CH_3, FCH_2, $ClCH_2$, C_2H_5, *n*-C_3H_7, $(CH_3)_2CH$, $(CH_3)_3C$, $ClCH_2C(CH_3)H$ *n*-C_4H_9 or C_6F_5), with $XeF^{+}AsF_6^{-}$ (or $Xe_2F_3^{+}AsF_6^{-}$) in anhydrous HF solvent at -50 to -10 °C. The ^{129}Xe and ^{19}F NMR studies have provided evidence for a novel series of xenon-nitrogen adduct cations analogous to $HC{\equiv}N\text{-}XeF^{+}$ which contain Xe-N bonds. The ^{129}Xe, ^{19}F, ^{14}N, ^{15}N, ^{13}C and ^{1}H NMR chemical shifts and spin-spin coupling constants for the natural abundance $RC{\equiv}N\text{-}XeF^{+}$ cations and the enriched samples of the $CH_3{}^{13}C{\equiv}N\text{-}XeF^{+}$ (99.7% ^{13}C), $^{13}CH_3C{\equiv}N\text{-}XeF^{+}$ (99.0% ^{13}C) and $CH_3C{\equiv}{}^{15}N\text{-}XeF^{+}$ (99.0% ^{15}N) cations are listed in Tables 5.1 and 5.2.

The ^{19}F NMR spectra consisted of a single line in the fluorine-on-xenon(II) region accompanied by ^{129}Xe satellites, corresponding to $^{1}J(^{129}Xe\text{-}^{19}F)$ arising from spin coupling to natural abundance ^{129}Xe (I = ½, 26.44% natural abundance), and a broad saddle-shaped feature at -64.0 ppm ($\Delta\nu_{½}$ = 1780 Hz) arising from the AsF_6^{-} anion and a strong signal from HF solvent at -198 ppm. The $^{1}J(^{129}Xe\text{-}^{19}F)$ couplings were confirmed by recording the ^{129}Xe spectra. The ^{129}Xe NMR spectra consisted of a doublet of triplets resulting from

Table 5.1

NMR Chemical Shifts for RC≡N-XeF$^+$ Cation in Anhydrous HF

Cation	Chemical shifts (ppm)[a]			
	$\delta(^{129}Xe)$	$\delta(^{19}F)$	$\delta(^{14}N)$	$\delta(^{1}H)$
$CH_3C{\equiv}N\text{-}XeF^+$ [b]	-1707	-185.5	-251.1	2.4
$CH_2ClCH_2C{\equiv}N\text{-}XeF^+$	-1718	-184.6	-251.9	1.3 (CH_3) 2.8 (CH_2)
$CH_2FCH_2C{\equiv}N\text{-}XeF^+$	-1662	-182.8 (XeF) -218.8 (CF)		—
$CH_3CH_2CH_2C{\equiv}N\text{-}XeF^+$	-1718	-189.1	-249.7	0.7 (CH_3) 1.6 (CH_2mid 2.7 ($CH_2C{\equiv}N$)
$CH_2FCH_2CH_2C{\equiv}N\text{-}XeF^+$	-1663	-184.7 (XeF) -222.7 (CF)	-233.1	4.3 (FCH_2) 1.8 (CH_2mid 3.0 ($CH_2C{\equiv}N$)
$CH_3CHFCH_2C{\equiv}N\text{-}XeF^+$	-1700	-186.1 (XeF) -172.1 (CF)	-257.8	1.1 (CH_3) 3.2 (CHF) 4.8 ($CH_2C{\equiv}N$)
$CHF_2CH_2CH_2C{\equiv}N\text{-}XeF^+$		-120.9 (CF)		—
$CH_3CH_2CH_2CH_2C{\equiv}N\text{-}XeF^+$	-1720	-183.2	-247.1	0.92 (CH_3) 1.48 (CH_2) 1.69 (CH_2) 2.66 ($CH_2C{\equiv}N$)
$CH_2FCH_2CH_2CH_2C{\equiv}N\text{-}XeF^+$	-1703	-184.6 (XeF) — (CF)	-247.1	—
$CH_3CHFCH_2CH_2C{\equiv}N\text{-}XeF^+$	-1703	-185.1 (XeF) -175.9 (CF)	-247.1	1.18 (CH_3) 1.97 (CHF) 3.09 (CH_2CHF) 4.70 ($CH_2C{\equiv}N$)
$(CH_3)_2CHC{\equiv}N\text{-}XeF^+$	-1721	-184.5	-251.4	1.4 (CH_3)
$(CH_3)_3CC{\equiv}N\text{-}XeF^+$	-1721	-184.3	-251.4	1.35
$CH_2ClC(CH_3)HC{\equiv}N\text{-}XeF^+$	-1703	-198.7	-243.8	— —
$CH_2FC(CH_3)HC{\equiv}N\text{-}XeF^+$	-1669	-187.9 (XeF) -235.3 (CF)	-231.0	— —
$CH_2ClC{\equiv}N\text{-}XeF^+$	-1583	-189.4	-236.6	5.0
$CH_2FC{\equiv}N\text{-}XeF^+$	-1541	-198.2 (XeF) -241.7 (CF)	-229.2	5.4
$C_6F_5C{\equiv}N\text{-}XeF^+$	-1424		-201.8	

a Referenced externally at 24 °C with respect to neat liquid references: $XeOF_4$ (^{129}Xe), $CFCl_3$(^{19}F), CH_3NO_2(^{14}N) and TMS(^{13}C and ^{1}H).

b $\delta(^{15}N)$ = -249.6, $\delta(^{13}C)$ = 115.3 (CN), 0.6(CH_3).

Table 5.2

NMR Coupling Constants for RC≡N-XeF$^+$ Cations in Anhydrous HF

Cation	Spin-Spin Couplings (Hz)				^1K(Xe-N)[a]
	$J(^{129}Xe\text{-}^{19}F)$	$J(^{129}Xe\text{-}^{14}N)$	$J(^1H\text{-}^1H)$	$J(^{19}F\text{-}^1H)$	NA^{2}m^{-3} x 10^{22}
$CH_3C{\equiv}N\text{-}XeF^+$ [b]	6020	313			1.296
$CH_3CH_2C{\equiv}N\text{-}XeF^+$	6016	312	7.5		1.292
$CH_2FCH_2C{\equiv}N\text{-}XeF^+$	6063	322	—	46.1 (F_1,H_1) 23.2 (F_1,H_2) 0.0 (F_1,H_3)	1.333
$CH_3CH_2CH_2C{\equiv}N\text{-}XeF^+$ [c]	6020	311	7.5 (H_1,H_2) 7.2 (H_2,H_3) 0.0 (H_1,H_3)		1.288
$CH_2FCH_2CH_2C{\equiv}N\text{-}XeF^+$ [c]	6065	321	5.3 (H_1,H_2) 6.7 (H_2,H_3) 0.0 (H_1,H_3)	46.1 (F_1,H_1) 29.3 (F_1,H_2) 0.0 (F_1,H_3)	1.329
$CH_3CHFCH_2C{\equiv}N\text{-}XeF^+$ [c]	6038	316	6.3 (H_1,H_2) 6.2 (H_2,H_3) 0.0 (H_1,H_3)	24.6 (F_2,H_1) 47.0 (F_2,H_2) — (F_2,H_3)	1.308
$CH_3CH_2CH_2CH_2C{\equiv}N\text{-}XeF^+$[d]	6023	309	7.4 (H_1,H_2) 7.4 (H_2,H_3) 7.3 (H_3,H_4)		1.279
$CH_2FCH_2CH_2CH_2C{\equiv}N\text{-}XeF^+$[d]	6026	311			1.288
$CH_3CHFCH_2CH_2C{\equiv}N\text{-}XeF^+$	6027	311	6.2 (H_1,H_2) 6.8 (H_2,H_3) 6.1 (H_3,H_4)	25.9 (F_2,H_1) 49.2 (F_2,H_2) 27.9 (F_2,H_3) 6.5 (F_2,H_4)	1.288
$(CH_3)_2CHC{\equiv}N\text{-}XeF^+$	6016	309	7.1		1.279
$(CH_3)_3CC{\equiv}N\text{-}XeF^+$	6024	309			1.279
$CH_2ClC(CH_3)HC{\equiv}N\text{-}XeF^+$	6027	314		—	1.300
$CH_2FC(CH_3)HC{\equiv}N\text{-}XeF^+$	6027	301	—	45.8 (F_1,H_1) 14.9 (F_1,H_2)	1.246
$CH_2ClC{\equiv}N\text{-}XeF^+$	6147	331			1.371
$CH_2FC{\equiv}N\text{-}XeF^+$	6164	333		44.0	1.378
$C_6F_5C{\equiv}N\text{-}XeF^+$	6610				

Continued...

Table 5.2 (continued)

a The reduced coupling constants $^{1}K(Xe\text{-}N)$ for $RC{\equiv}N\text{-}XeF^{+}$ cation were calculated as follows :

$$^{1}K(Xe\text{-}N) = \frac{4\pi^{2}}{h\,\gamma(^{14}N)\;\gamma(^{129}Xe)}\,J(^{129}Xe\text{-}^{14}N)$$

b $J(^{19}F\text{-}^{13}C)$ = 19 Hz, $J(^{129}Xe\text{-}^{13}C)$ = 79 Hz, $J(^{1}H\text{-}^{13}C)$ = 141 Hz recorded from a 99.7% ^{13}C enriched sample.

c $J(^{19}F\text{-}^{15}N)$ = 36 Hz recorded from a 99.0% ^{15}N enriched sample.

d The numbering schemes used to denote $J(^{1}H\text{-}^{1}H)$ and $J(^{19}F\text{-}^{1}H)$ are :

$\underset{1}{CH_2}\underset{2}{FCH_2}C{\equiv}N\text{-}XeF^{+}$, $\underset{1}{CH_3}\underset{2}{CH_2}\underset{3}{CH_2}C{\equiv}N\text{-}XeF^{+}$, $\underset{1}{CH_2}\underset{2}{FCH_2}\underset{3}{CH_2}C{\equiv}N\text{-}XeF^{+}$ and

$\underset{1}{CH_3}\underset{2}{CHF}\underset{3}{CH_2}C{\equiv}N\text{-}XeF^{+}$.

the spin-spin couplings $^{1}J(^{129}Xe\text{-}^{19}F)$ (doublet) and $^{1}J(^{129}Xe\text{-}^{14}N)$ (partially quadruple collapsed 1:1:1 triplet). The ^{129}Xe NMR spectra of natural abundance $CH_3C{\equiv}N\text{-}XeF^+$ and 99.7% ^{13}C enriched $CH_3{}^{13}C{\equiv}N\text{-}XeF^+$ are shown in Figure 5.1. Owing to the cylindrical symmetry of the C≡N-XeF moiety in these cations, low viscosity of HF solvent medium, and low electric field gradient at the ^{14}N nucleus, quadrupole relaxation of the $^{129}Xe\text{-}^{14}N$ coupling is found to be minimal, giving rise to a slightly quadrupole collapsed pair of 1:1:1 triplets in the ^{129}Xe NMR spectrum (Figure 5.1) and ^{129}Xe satellites in the ^{14}N spectrum. The ^{129}Xe NMR spectrum of the 99.0% ^{15}N enriched $CH_3C{\equiv}{}^{15}N\text{-}XeF^+$ cation in HF at -15 °C (Figure 5.2) showed that the ^{129}Xe signal (-1709 ppm) consisted of a doublet of doublets resulting from a large one-bond coupling with fluorine ($J(^{129}Xe\text{-}^{19}F)$, 6016 Hz) which is further split into another doublet by coupling with ^{15}N (I = ½; $J(^{129}Xe\text{-}^{15}N)$, 439.8 Hz).

The ^{14}N spectra resulting from the reaction of RC≡N and $XeF^+AsF_6^-$ in anhydrous HF solvent at -50 to -10 °C consisted of two broad single lines, one of which was accompanied by ^{129}Xe satellites. The ^{14}N resonances of both peaks were relatively narrow (see Table 5.1) and the coupling constants, $^{1}J(^{129}Xe\text{-}^{14}N)$, are very similar to those measured in the ^{129}Xe NMR spectra. The two ^{14}N NMR resonances are assigned to the $RC{\equiv}N\text{-}XeF^+$ (Table 5.1) and $RC{\equiv}NH^+$ cations which arise according to equilibria (5.3 - 5.7).

$$XeF^+AsF_6^- + HF \rightleftharpoons XeF_2 + H^+AsF_6^- \qquad (5.3)$$

$$RC{\equiv}N + (x + 1)\,HF \rightleftharpoons RC{\equiv}NH^+F(HF)_x^- \qquad (5.4)$$

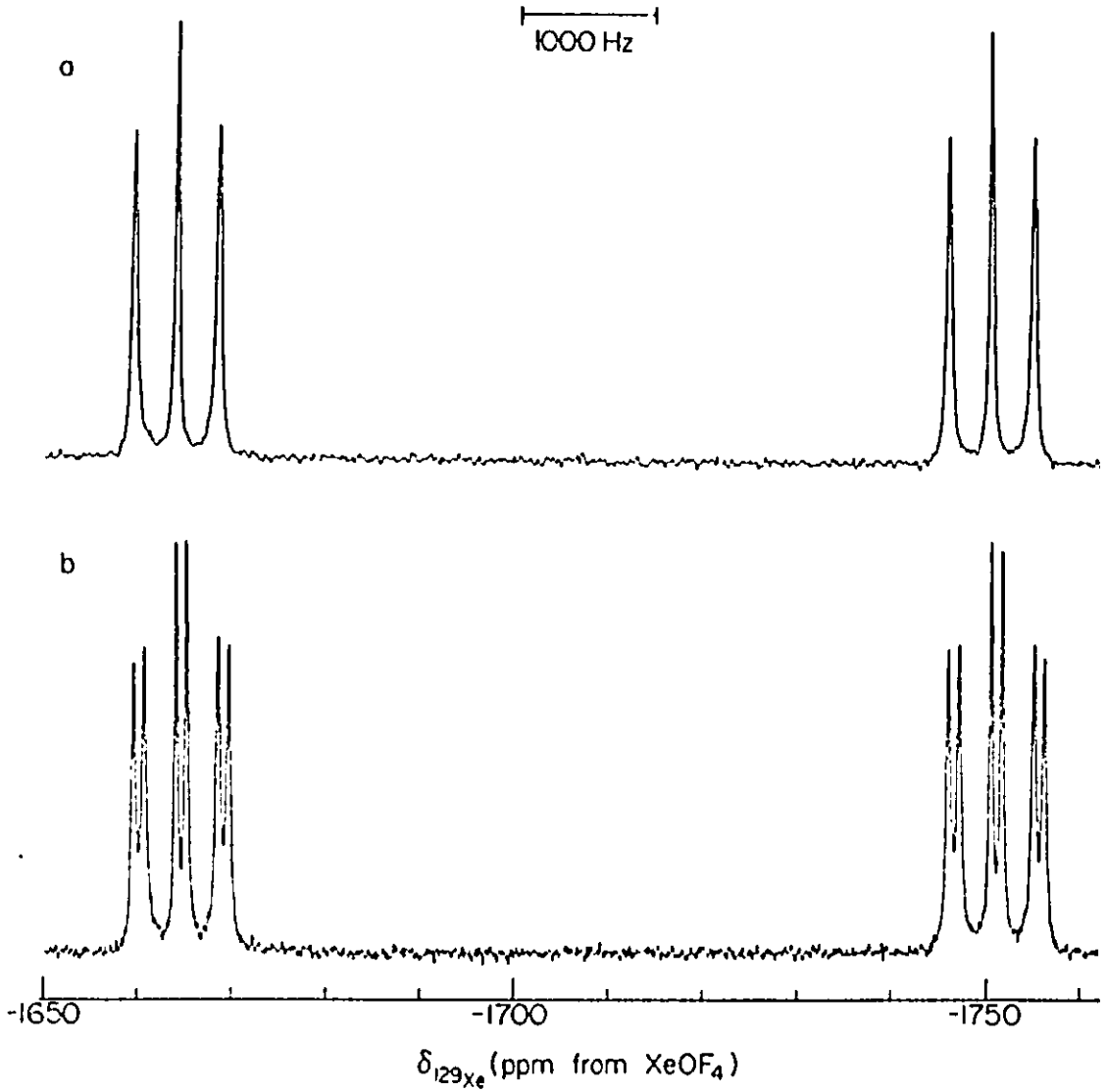

Figure 5.1 ^{129}Xe NMR spectrum (69.563 MHz) of $CH_3C{\equiv}N\text{-}XeF^+AsF_6^-$ recorded in HF solvent at -10 °C; (a) natural abundance and (b) 99.7% ^{13}C enriched at the 2-carbon.

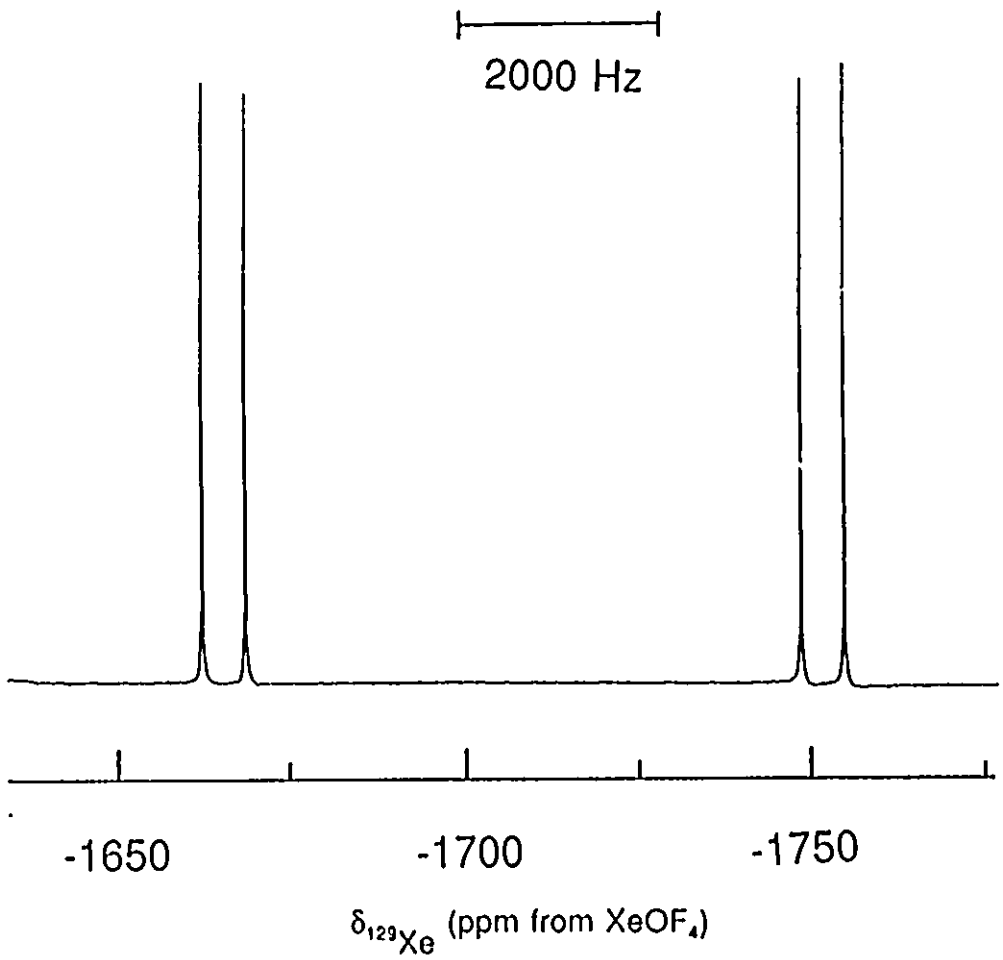

Figure 5.2 ^{129}Xe NMR spectrum (69.563 MHz) of 99.0% ^{15}N enriched $CH_3C{\equiv}N\text{-}XeF^+AsF_6^-$ recorded in HF solvent at -10 °C.

$$RC{\equiv}NH^{+}F(HF)_x^{-} + XeF_2 \rightleftharpoons RC{\equiv}N\text{-}XeF^{+}\,F(HF)_x^{-} \qquad (5.5)$$

$$RC{\equiv}N\text{-}XeF^{+}F(HF)_x^{-} + H^{+}AsF_6^{-} \rightleftharpoons RC{\equiv}N\text{-}XeF^{+}AsF_6^{-} + (1 + x)\ HF \qquad (5.6)$$

$$XeF^{+}AsF_6^{-} + XeF_2 \rightleftharpoons Xe_2F_3^{+}AsF_6^{-} \qquad (5.7)$$

The equilibrium between the $RC{\equiv}NH^{+}$ and $RC{\equiv}N\text{-}XeF^{+}$ cations (equilibrium 5.5) was also confirmed by ^{1}H, ^{13}C and ^{15}N NMR spectroscopy. In the case of a 1:1 stoichiometric ratio of $RC{\equiv}N$ and $XeF^{+}AsF_6^{-}$, ^{129}Xe and ^{19}F NMR spectra did not show evidence for XeF_2. This may be attributed to an equilibrium between XeF_2 and $XeF^{+}AsF_6^{-}$ (equilibrium (5.7)), which results in fast chemical exchange processes on the ^{129}Xe and ^{19}F NMR time scales. In the reactions of nitriles with $Xe_2F_3^{+}AsF_6^{-}$ in anhydrous HF, equilibrium (5.5) is apparently shifted to the right, corresponding to a reduction in ^{14}N signal intensity for $RC{\equiv}NH^{+}$. Resonances arising from XeF_2 could be observed in both the ^{19}F and ^{129}Xe NMR spectra. Significant broadening of the HF signal in the ^{19}F NMR spectra also occurred and is consistent with equilibria (5.3), (5.4) and (5.6). The ^{14}N NMR parameters of the $RC{\equiv}N\text{-}XeF^{+}$ cations in anhydrous HF solvent are listed in Table 5.1. Figure 5.3 shows the ^{14}N NMR spectrum of the 1:1 molar ratio of $CH_3C{\equiv}N$: $XeF^{+}AsF_6^{-}$ in anhydrous HF solvent at -10 °C. The ^{129}Xe and ^{14}N NMR spectra for the $RC{\equiv}N\text{-}XeF^{+}$ cations showed well resolved and only partially quadrupole collapsed $^{1}J(^{129}Xe\text{-}^{14}N)$ couplings. The long T_1, which is dominated by quadrupolar relaxation, is attributed to the small linewidth factor associated with the ^{14}N nucleus,[200] the reduction

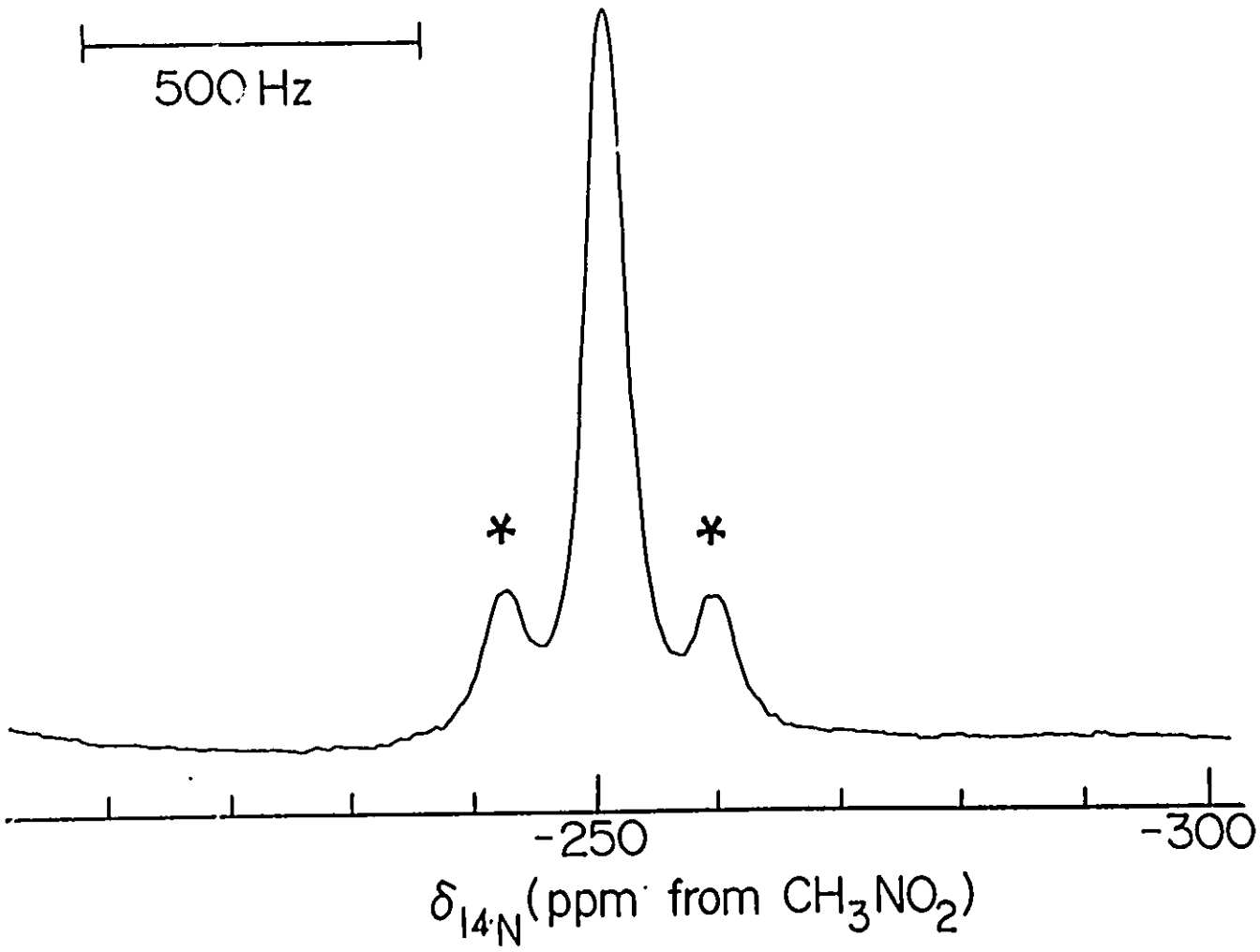

Figure 5.3 ^{14}N NMR spectrum (18.076 MHz) resulting from the reaction of $CH_3C{\equiv}N$ and $XeF^+AsF_6^-$ in anhydrous HF at -10 °C. Asterisks (*) denote ^{129}Xe satellites.

of electric field gradient at the ^{14}N nucleus upon coordination of the N_{sp} lone pair to xenon and low solvent viscosity. The anticipated lower electric field gradient in the adduct is similar to that already discussed for $HC{\equiv}N\text{-}XeF^+$ in Chapter 3.

The ^{15}N NMR spectrum resulting from the reaction of 99.0% ^{15}N enriched $CH_3C{\equiv}^{15}N$ and $XeF^+AsF_6^-$ at -15 °C resulted in a strong signal at -248.2 ppm with accompanying ^{129}Xe satellites, each split into a doublet due to coupling with fluorine. A second signal was observed at -237.8 ppm, which is due to protonated acetonitrile, $CH_3C{\equiv}NH^+$. Figure 5.4 depicts the ^{15}N NMR spectrum resulting from the reaction of 99.0% ^{15}N enriched $CH_3C{\equiv}N$ and $XeF^+AsF_6^-$ in anhydrous HF.

The ^{129}Xe and ^{14}N NMR chemical shifts of the weaker Lewis bases $CH_2FC{\equiv}N$ and $CH_2ClC{\equiv}N$ are more deshielded (Table 5.1) and the magnitudes of $^{129}Xe\text{-}^{19}F$ coupling constants are correspondingly greater for the $CH_2FC{\equiv}N\text{-}XeF^+$ (6164 Hz) and $CH_2ClC{\equiv}N\text{-}XeF^+$ (6147 Hz) cations, reflecting the weaker covalent characters of the Xe-N bonds in these cation adducts (see Chapter 8).

In the case of the perfluorophenylnitrile adduct cation, $C_6F_5C{\equiv}N\text{-}XeF^+AsF_6^-$, the ^{129}Xe chemical shift and the $^{129}Xe\text{-}^{19}F$ spin-spin coupling indicates that the Xe-N bond is one of the most ionic Xe-N bonds known in this series. Rapid decomposition occurred at -10 °C in HF solvent, preventing a full characterization of the cation by ^{19}F and ^{14}N NMR spectroscopy.

Assuming that the Xe-N spin-spin couplings in the xenon-nitrogen compounds are dominated by the Fermi contact term, a comparison of $^1K(Xe\text{-}N)$ values for the $RC{\equiv}N\text{-}XeF^+$ cations with that of the trigonal planar sp^2-hybridized nitrogen atom in

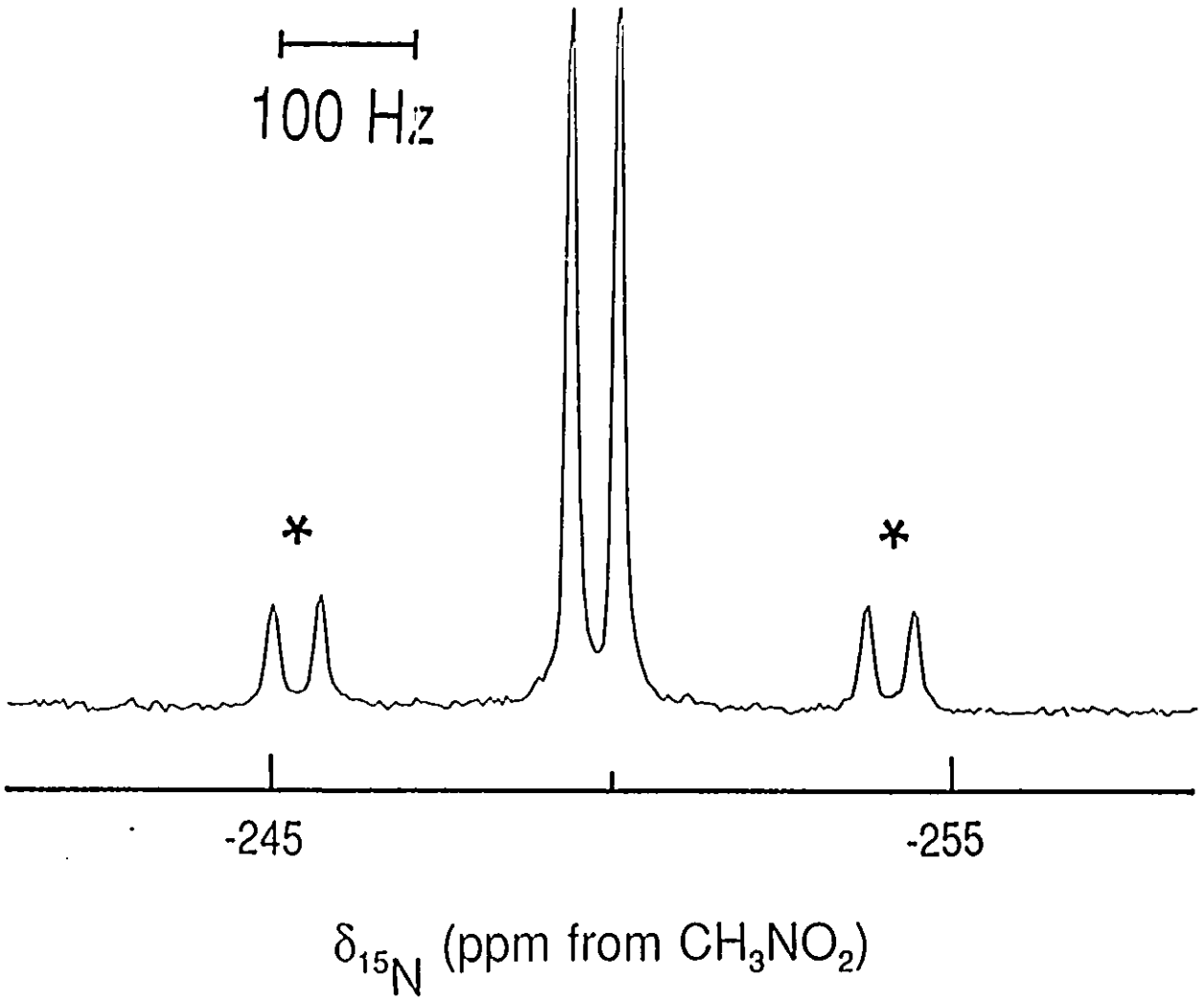

Figure 5.4 ^{15}N NMR spectrum (25.347 MHz) resulting from the reaction of 99.0% ^{15}N enriched $CH_3C{\equiv}N$ and $XeF^+AsF_6^-$ at -15 °C in anhydrous HF. Asterisks (*) denote ^{129}Xe satellites.

$FXeN(SO_2F)_2$ allows assessment of the relative degrees of hybridization for the nitrogen orbitals used in bonding to xenon. The ratios of $[^1K(Xe\text{-}N)]_{sp^2}$ / $[^1K(Xe\text{-}N)]_{sp}$, are 1.42-1.53 for the cations listed in Table 5.2, in excellent agreement with the theoretical ratio, 1.50, calculated from the predicted fractional s-characters of the nitrogen orbitals used in bonding. The reduced coupling constants $^1K(Xe\text{-}N)$ for $RC{\equiv}N\text{-}XeF^+$ cations are listed in Table 5.2.

(ii) The ^{14}N Relaxation Times of $CH_3C{\equiv}N\text{-}XeF^+$ and $CH_3C{\equiv}NH^+$ Cations

The ^{14}N relaxation times of the $CH_3C{\equiv}N\text{-}XeF^+$ and $CH_3C{\equiv}NH^+$ cations in anhydrous HF solvent at -3 °C have been measured using the inversion recovery pulse sequence $[180°\text{-}\tau\text{-}90°\ (FID)\text{-}T_d]_n$ (Figure 5.5), which resulted in the ^{14}N relaxation times $T_1 = 8 \pm 1$ ms and $T_1 = 37 \pm 6$ ms for the $CH_3C{\equiv}N\text{-}XeF^+$ and $CH_3C{\equiv}NH^+$ cations, respectively.

The ^{14}N NMR signals are sharp but the linewidth of the $CH_3C{\equiv}NH^+$ cation is smaller than that of the $CH_3C{\equiv}N\text{-}XeF^+$ cation, as would be expected based on the anticipated longer correlation time of the $CH_3C{\equiv}N\text{-}XeF^+$ cation (equation (5.8)).

$$\Delta\nu_{\frac{1}{2}} = \frac{1}{\pi T_1} = \frac{3\pi}{10}\left(\frac{2I+3}{I^2(2I-1)}\right)\left(1 + \tfrac{1}{3}\eta^2\right)\left(\frac{e^2qQ}{h}\right)^2\tau_c \qquad (5.8)$$

where $\Delta\nu_{\frac{1}{2}}$ is the linewidth of the quadrupolar nucleus (^{14}N in this case), T_1 is the spin

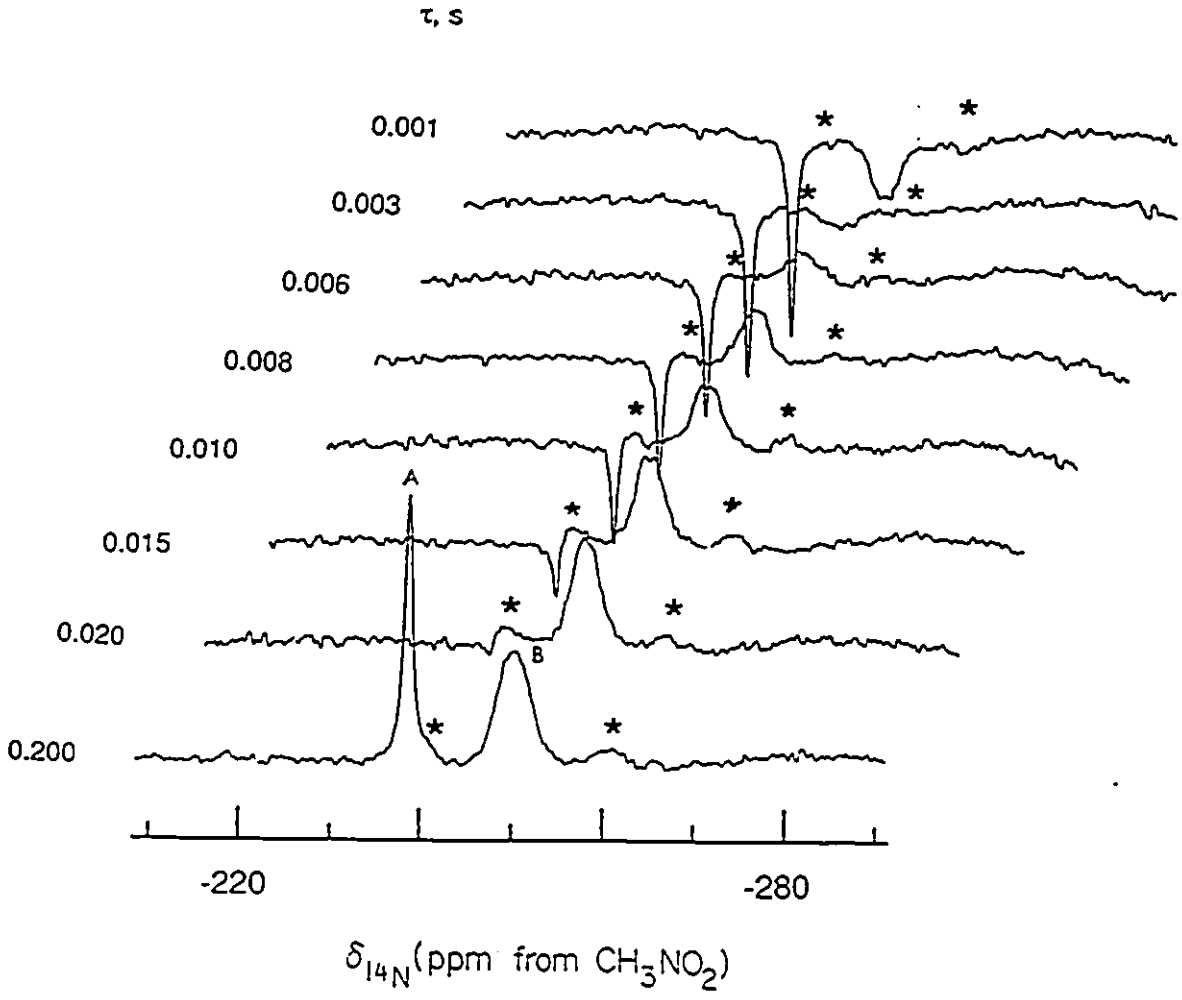

Figure 5.5 The T_1 measurements for the ^{14}N nuclei of $CH_3C{\equiv}N\text{-}XeF^+$ and $CH_3C{\equiv}NH^+$ cations obtained using the inversion recovery pulse sequence [180°-τ-90° (FID)-T_d]$_n$ at -3 °C; T_1 = 37 ± 6 ms for ^{14}N of (A) $CH_3C{\equiv}NH^+$ cation and T_1 = 8 ± 1 ms for ^{14}N of (B) $CH_3C{\equiv}N\text{-}XeF^+$ cation. Asterisks (*) denote ^{129}Xe satellites.

lattice relaxation time, I is the nuclear spin quantum number 1 in the case of ^{14}N, η is the asymmetry parameter (η ranges from 0 to 1; in the case of linear species it is unity), eq is the electric field gradient and τ_c is the molecular correlation time. Using equation (5.8), the T_1 values calculated for the linewidths ($\Delta\nu_{1/2}$) of $CH_3C{\equiv}N\text{-}XeF^+$ and $CH_3C{\equiv}NH^+$ are 41.3 and 8.6 Hz, respectively, which are in a good agreement with the experimental values of 45 Hz and 10.7 Hz, respectively, indicating that the linewidths of both cations are indeed dominated by quadrupolar relaxation of the scalar coupling.

(iii) Fluorinated Alkylnitrile Adducts Resulting From the Reaction of the Alkyl Nitrile and $XeF^+AsF_6^-$ in HF Solvent

The ^{19}F and ^{129}Xe NMR study of $ClCH_2C(CH_3)HC{\equiv}N\text{-}XeF^+$ and $RC{\equiv}N\text{-}XeF^+$ (R = C_2H_5, n-C_3H_7 and n-C_4H_9) cations indicates not only the formation of adducts with the XeF^+ cation in anhydrous HF solvent, but also replacement of the chlorine by fluorine in $ClCH_2C(CH_3)HC{\equiv}N$ and fluorination of the alkyl group in $RC{\equiv}N$ (R = C_2H_5, n-C_3H_7 and n-C_4H_9), resulting in, the formation of a new series of fluorinated nitriles and their adducts with the XeF^+ cation.

The formation of the fluorinated adduct from the reaction of $ClCH_2C(CH_3)HC{\equiv}N$ and $XeF^+AsF_6^-$ is represented by equations (5.9) - (5.12) and has been characterized by ^{129}Xe, ^{19}F and ^{14}N NMR spectroscopy (Tables 5.1 and 5.2). In addition to the $ClCH_2C(CH_3)HC{\equiv}N\text{-}XeF^+$ and $ClCH_2C(CH_3)HC{\equiv}NH^+$ cations, the ^{19}F and ^1H NMR spectra showed several decomposition products which have not been identified.

$$ClCH_2C(CH_3)HC{\equiv}N + XeF^+AsF_6^- \xrightarrow{HF} ClCH_2C(CH_3)HC{\equiv}N\text{-}XeF^+AsF_6^- \quad (5.9)$$

$$ClCH_2C(CH_3)HC{\equiv}N\text{-}XeF^+AsF_6^- \xrightarrow{HF} FCH_2C(CH_3)HC{\equiv}N\text{-}XeF^+AsF_6^- + \tfrac{1}{2}Cl_2(?) \quad (5.10)$$

$$ClCH_2C(CH_3)HC{\equiv}N\text{-}XeF^+AsF_6^- \overset{HF}{\rightleftharpoons} ClCH_2C(CH_3)HC{\equiv}NH^+AsF_6^- + XeF_2 \quad (5.11)$$

$$FCH_2C(CH_3)HC{\equiv}N\text{-}XeF^+AsF_6^- \overset{HF}{\rightleftharpoons} FCH_2C(CH_3)HC{\equiv}NH^+AsF_6^- + XeF_2 \quad (5.12)$$

The ^{129}Xe NMR study of $ClCH_2C(CH_3)HC{\equiv}N$ with $XeF^+AsF_6^-$ at -30 °C in anhydrous HF solvent reveals the presence of two signals at -1669 and -1703 ppm. Each signal consisted of a doublet of 1:1:1 (partially quadrupole collapsed) triplets resulting from the spin-spin couplings $^1J(^{129}Xe\text{-}^{19}F)$ and $^1J(^{129}Xe\text{-}^{14}N)$. The ^{19}F NMR study at -30 °C showed two fluorine-on-xenon environments corresponding to two single high-field peaks at -198.7 and -187.9 ppm with ^{129}Xe satellites. The NMR spectral findings are consistent with the replacement of chlorine by fluorine leading to the adduct cations $ClCH_2C(CH_3)HC{\equiv}N\text{-}XeF^+$ and $FCH_2C(CH_3)HC{\equiv}N\text{-}XeF^+$.

The NMR spectra of solutions of stoichiometric amounts of $CH_3CH_2CH_2C{\equiv}N$ and $XeF^+AsF_6^-$ in anhydrous HF solvent at -30 °C are consistent with the presence of three xenon-nitrogen adduct cations having the formulations $CH_3CH_2CH_2C{\equiv}N\text{-}XeF^+$, $CH_2FCH_2CH_2C{\equiv}N\text{-}XeF^+$ and $CH_3CHFCH_2C{\equiv}N\text{-}XeF^+$. The ^{129}Xe NMR study reveals the presence of three signals at -1719, -1700 and -1663 ppm, respectively, with each signal consisting of a doublet of 1:1:1 (partially quadrupole collapsed) triplets resulting from the spin-spin couplings $^1J(^{129}Xe\text{-}^{19}F)$ and $^1J(^{129}Xe\text{-}^{14}N)$. Figure 5.6 shows the ^{129}Xe spectrum

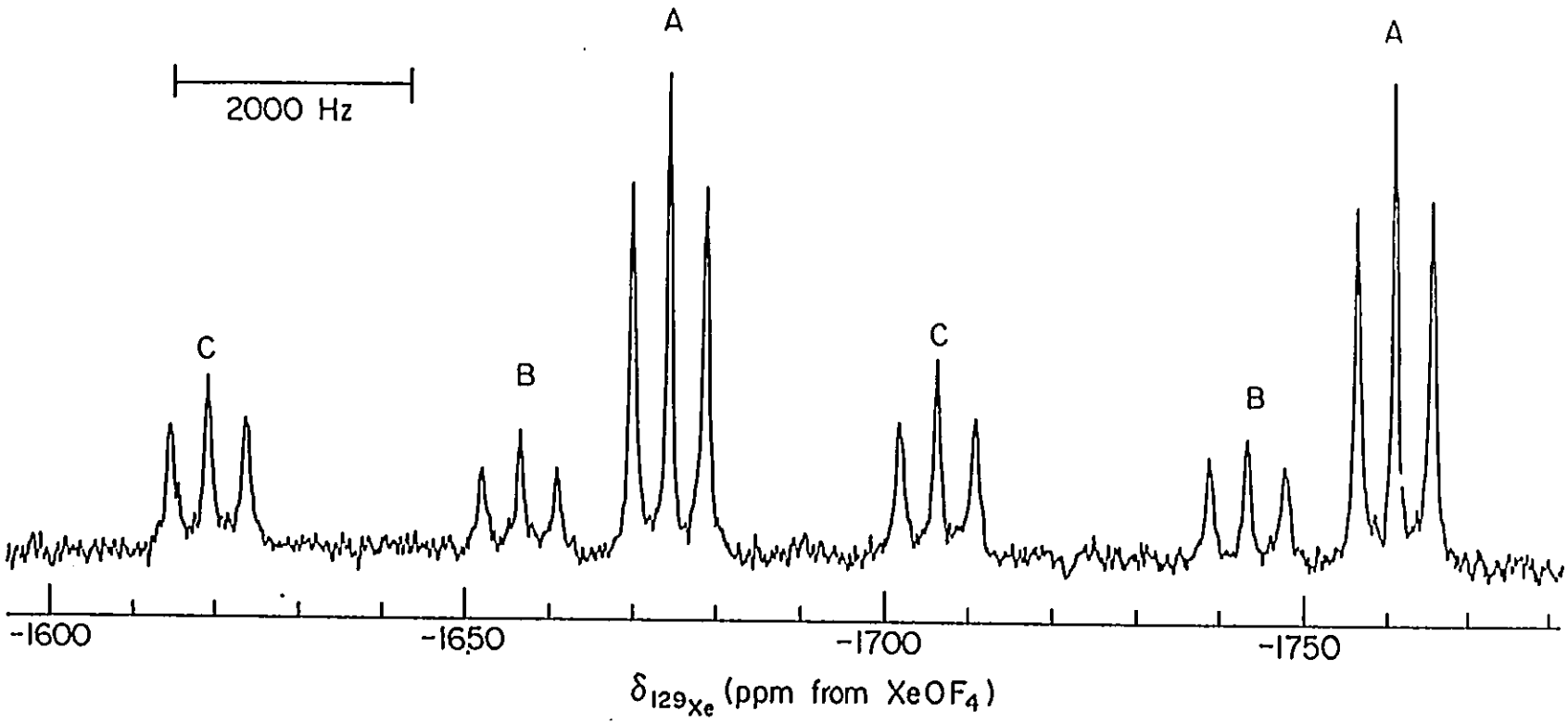

Figure 5.6 ^{129}Xe NMR spectrum (69.563 MHz), recorded in HF solvent at -30 °C, of (A) $CH_3CH_2CH_2C{\equiv}N\text{-}XeF^+AsF_6^-$ and the fluorinated products, (B) $CH_2FCH_2CH_2C{\equiv}N\text{-}XeF^+AsF_6^-$ and (C) $CH_3CHFCH_2C{\equiv}N\text{-}XeF^+AsF_6^-$.

of n-$C_3H_7C{\equiv}N$ and $XeF^+AsF_6^-$ recorded in HF solvent at -30 °C. The ^{19}F NMR spectra showed three fluorine-on-xenon(II) resonances at low frequency -189.1, -186.1 and -187.1 ppm with ^{129}Xe satellites which are assigned to the n-$C_3H_7C{\equiv}N$-XeF^+, $CH_2FCH_2CH_2C{\equiv}N$-XeF^+ and $CH_3CHFCH_2C{\equiv}N$-XeF^+ cations, respectively.

The ^{19}F NMR spectra consisted of well-defined multiplets corresponding to four fluorine-on-carbon environments with multiplets arising from ^1H-^{19}F coupling. A triplet of triplets at -221.9 ppm is assigned to the fluorine environment of the $FCH_2CH_2CH_2C{\equiv}N$-XeF^+ cation. This resonance overlaps with the multiplet resulting from the $FCH_2CH_2CH_2C{\equiv}NH^+$ cation (-223.3 ppm). A multiplet at -172.2 ppm is assigned to the fluorine environment of the $CH_3CHFCH_2C{\equiv}NH^+$ cation and overlaps with the multiplet arising from the $CH_3CHFCH_2C{\equiv}N$-XeF^+ cation. The $CH_2FCH_2CH_2C{\equiv}N$-XeF^+, $CH_2FCH_2CH_2C{\equiv}NH^+$, $CH_3CHFCH_2C{\equiv}N$-XeF^+ and $CH_3CHFCH_2C{\equiv}NH^+$ cations were confirmed by high-resolution ^1H NMR spectroscopy at -30 °C, which showed all possible ^{19}F-^1H and ^1H-^1H spin-spin couplings. Figure 5.7 shows the ^1H NMR spectrum resulting from the reaction of n-$C_3H_7C{\equiv}N$ and $XeF^+AsF_6^-$ in anhydrous HF at -30 °C. The proton environments of the $CH_3CH_2CH_2C{\equiv}N$-XeF^+, $CH_3CH_2CH_2C{\equiv}NH^+$, $CH_2FCH_2CH_2C{\equiv}N$-XeF^+, $CH_2FCH_2CH_2C{\equiv}NH^+$, $CH_3CHFCH_2C{\equiv}N$-XeF^+ and $CH_3CHFCH_2C{\equiv}NH^+$ cations can be unambiguously assigned from their connectivities using a ^1H-2D COSY NMR pulse sequence (Figure 5.8). Interestingly, fluorinations that give rise to monofluoro alkylnitriles occurred at the β- and γ-carbons, and not at the α-carbon. The reactivities of the three types of hydrogen in n-$C_3H_7C{\equiv}N$ are significantly different and showed the product distributions α : β : γ = 0 : 68 : 32. This product distribution is similar to the

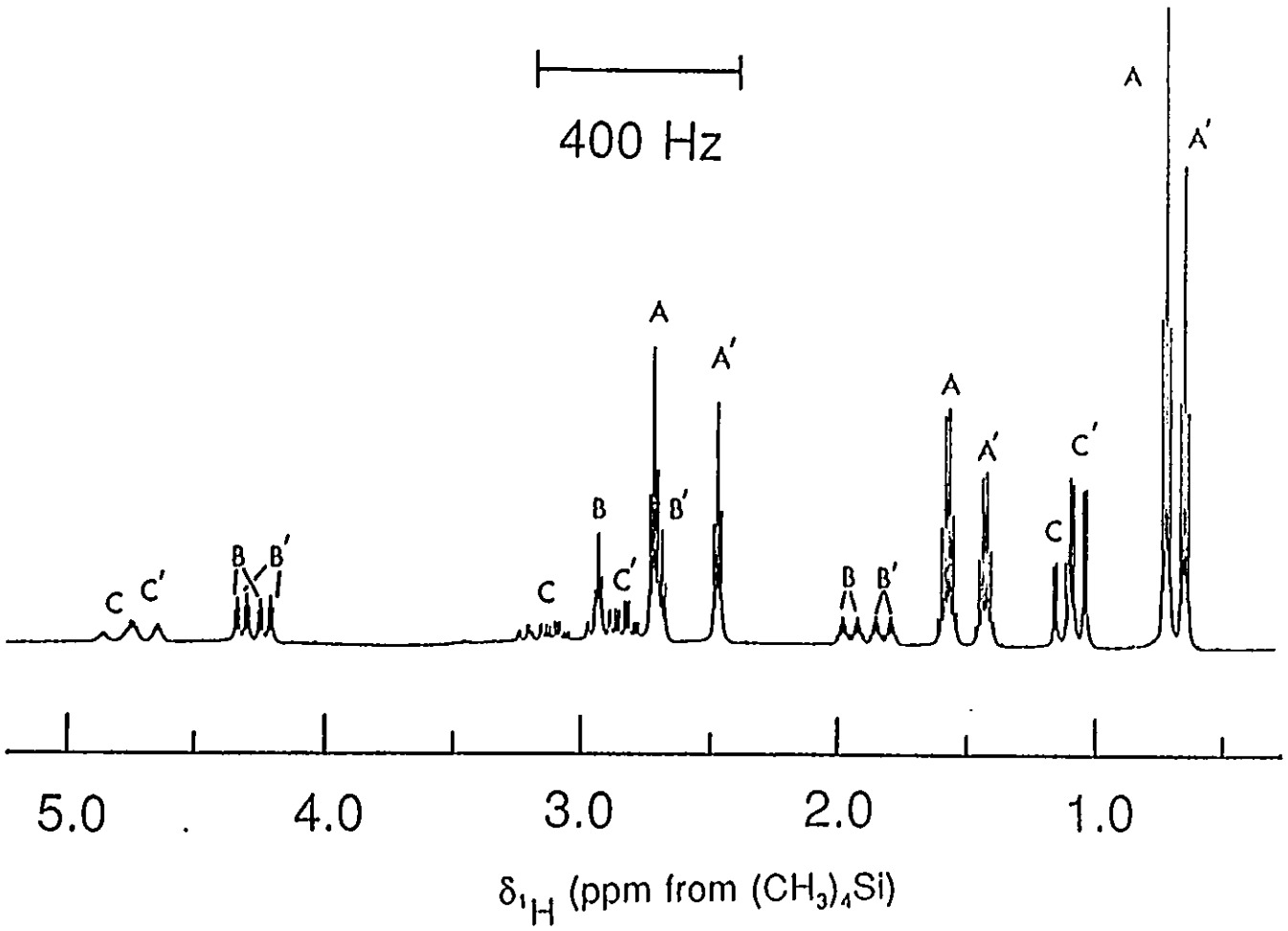

Figure 5.7 ^{1}H NMR spectrum (500.125 MHz) resulting from the reaction of n-$C_3H_7C{\equiv}N$ and $XeF^+AsF_6^-$ in anhydrous HF at -30 °C; (A) $CH_3CH_2CH_2C{\equiv}N\text{-}XeF^+$, (A′) $CH_3CH_2CH_2C{\equiv}NH^+$, (B) $CH_3CHFCH_2C{\equiv}N\text{-}XeF^+$, (B′) $CH_3CHFCH_2C{\equiv}NH^+$, (C) $CH_2FCH_2CH_2C{\equiv}N\text{-}XeF^+$ and (C′) $CH_2FCH_2CH_2C{\equiv}N\text{-}XeF^+$.

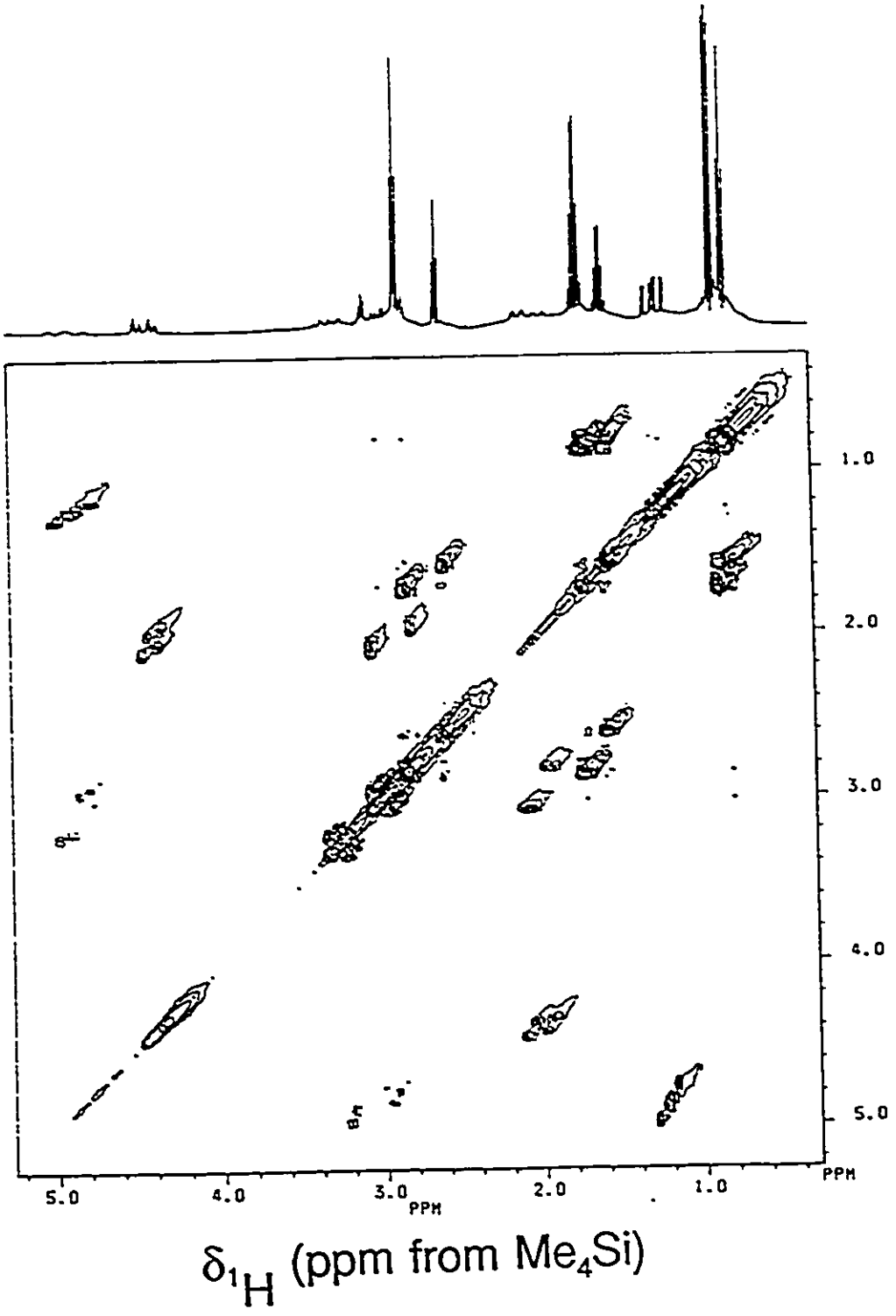

Figure 5.8 ^{1}H-2D COSY spectrum (500.125 MHz) resulting from the reaction of n-$C_3H_7C{\equiv}N$ and $XeF^+AsF_6^-$ in anhydrous HF at -30 °C.

photochlorination of n-$C_3H_7C{\equiv}N$ where the distribution ratio was 0 : 69 : 31.[201]

Subsequent warming of the aforementioned samples at room temperature followed by obtaining the ^{19}F NMR spectra in the fluorine-on-xenon region showed that these adducts decompose completely after approximately 2 hours. In addition to the aforementioned protonated nitriles and their XeF^+ adduct cations, a weak signal at -120.2 ppm, having the same pattern as the strong signal at -120.9 ppm, also grew in and the two signals are assigned to the $CHF_2CH_2CH_2C{\equiv}N\text{-}XeF^+$ and $CHF_2CH_2CH_2C{\equiv}NH^+$ cations, respectively. No fluorine-on-xenon resonance was observed for the $CHF_2CH_2CH_2C{\equiv}N\text{-}XeF^+$ cation and this is attributed to the small amount of adduct present in solution and masking of the signal by the broad HF solvent signal (see Figures 6.1 and 6.2).

During the study of the thermal stability of the $RC{\equiv}N\text{-}XeF^+$ cation in anhydrous HF it was found that, after warming solution mixtures of $C_2H_5C{\equiv}N$ and $XeF^+AsF_6^-$ in anhydrous HF for 2 hours at room temperature and recording the ^{19}F NMR spectra at -15 °C, a second fluorine-on-xenon environment accompanied by ^{129}Xe satellites grew in at -218.8 ppm. The resonance is in the monofluoroalkylnitrile region and is assigned to the $CH_2FCH_2C{\equiv}N\text{-}XeF^+$ cation. The ^{129}Xe NMR spectrum for this reaction mixture provides additional proof for the formation the $CH_2FCH_2C{\equiv}N\text{-}XeF^+$ cation, with a new doublet of partially quadrupole collapsed 1:1:1 triplets arising from coupling with the fluorine and nitrogen appearing at -1662 ppm.

Initial attempts to obtain ^{19}F and ^{129}Xe NMR spectra resulting from the reaction of n-$C_4H_9C{\equiv}N$ and $XeF^+AsF_6^-$ indicated that the xenon-nitrogen adduct was very unstable.

However, ^{19}F NMR spectra obtained at -50 °C showed a signal at -183.2 ppm and accompanying ^{129}Xe satellites ($^1J(^{129}Xe\text{-}^{19}F)$, 6023 Hz) and a signal at -199.5 ppm with ^{129}Xe satellites ($^1J(^{129}Xe\text{-}^{19}F)$, 5572 Hz) that is readily assigned to XeF_2, which arises as a result of equilibrium (5.5). Upon gradually warming the reaction mixture in the probe to -25 °C, three signals with ^{129}Xe satellites were observed at -183.2 ($^1J(^{129}Xe\text{-}^{19}F)$, 6023 Hz), -184.6 ($^1J(^{129}Xe\text{-}^{19}F)$, 6026 Hz) and -185.1 ppm ($^1J(^{129}Xe\text{-}^{19}F)$, 6027 Hz), respectively, as well as several signals in the fluorine-on-carbon region of the spectrum. The ^{129}Xe NMR spectrum prior to warming at -50 °C showed one doublet of partially quadrupole collapsed 1:1:1 triplets at -1720 ppm which is assigned to the n-$C_4H_9C{\equiv}N$-XeF^+ cation. Upon gradual warming of the reaction mixture to -25 °C, the intensity of this signal decreased and another signal grew in at -1703 ppm, which is assigned to a fluorinated nitrile-xenon fluoride cation.

In general, the ^{19}F NMR spectra of $C_2H_5C{\equiv}N$, n-$C_3H_7C{\equiv}N$ and n-$C_4H_9C{\equiv}N$ in anhydrous HF solvent at -15 °C showed no fluorinated species arising from solvolysis. In contrast, the ^{19}F and ^1H NMR spectra of $C_2H_5C{\equiv}N$, n-$C_3H_7C{\equiv}N$ and n-$C_4H_9C{\equiv}N$ with $XeF^+AsF_6^-$ in anhydrous HF solvent showed several fluorinated species. During this investigation, fluorination was found to occur at the ß-, γ- and δ-positions rather than at the α- position (from the C≡N group). The precise nature of the fluorination of $C_2H_5C{\equiv}N$, n-$C_3H_7C{\equiv}N$ or n-$C_4H_9C{\equiv}N$ by $XeF^+AsF_6^-$ is not clear, although one reasonable mechanism may be proposed. Initially, XeF_2 is formed according to equilibrium (6.3), which then undergoes thermal dissociation to form F· atoms. The F· atoms abstract hydrogen from the alkyl group of the alkylnitrile to form the stable HF molecule,

generating alkylnitrile radicals. The alkylnitrile radicals are then destroyed by reaction with $XeF^{\cdot}$ radical to form monofluoroalkylnitriles and xenon gas. The new fluorinated nitriles then form Lewis acid-base adducts with the XeF^{+} cation.

(C) CHARACTERIZATION OF $RC{\equiv}N\text{-}XeF^{+}AsF_6^{-}$ (R = CH_3, CH_2Cl, CH_2F, C_2H_5, $CH(CH_3)_2$, AND $C(CH_3)_3$) IN THE SOLID STATE BY LOW-TEMPERATURE RAMAN SPECTROSCOPY

The low-temperature Raman spectra of the solid adduct cations $RC{\equiv}N\text{-}XeF^{+}$ (R = CH_3, FCH_2, $ClCH_2$, C_2H_5, $(CH_3)_2CH$, $(CH_3)_3C$) have been recorded as their AsF_6^{-} salts in order to confirm their structures in the solid state. The spectra are shown in Figure 5.9 and the frequencies and their tentative assignments are listed in Tables 5.3 and 5.4. The assignments were made by comparison with the Raman spectra of the free nitrile ligands ($RC{\equiv}N$[202-206]), $XeF^{+}AsF_6^{-}$,[165] $HC{\equiv}N\text{-}XeF^{+}AsF_6^{-}$ and $F\text{-}Xe\text{-}N(SO_2F)_2$.[64] As can be seen from the solid state Raman spectra, the $RC{\equiv}N\text{-}XeF^{+}AsF_6^{-}$ salts are ionic and exhibit bands characteristic of AsF_6^{-}; however, site symmetry lowering and/or vibrational coupling within the unit cell result in splitting into additional bands. Owing to the absence of crystal structure data, no attempt has been made in the following discussion to account for these solid state effects. The cations are expected to possess C_{3v} (for $CH_3C{\equiv}N\text{-}XeF^{+}$ and $(CH_3)_3CC{\equiv}N\text{-}XeF^{+}$) and C_s symmetries (for $FCH_2C{\equiv}N\text{-}XeF^{+}$, $ClCH_2C{\equiv}N\text{-}XeF^{+}$, $C_2H_5C{\equiv}N\text{-}XeF^{+}$ and $(CH_3)_2CHC{\equiv}N\text{-}XeF^{+}$). The irreducible representations of the normal vibrational modes expected for the $RC{\equiv}N\text{-}XeF^{+}$ cations (choosing xy as the molecular

Figure 5.9 Raman spectra of $RC{\equiv}N\text{-}XeF^{+}AsF_6^{-}$ recorded at -196 °C using the 514.5 nm exciting line of an argon ion laser for excitation; (a) $CH_3C{\equiv}N\text{-}XeF^{+}AsF_6^{-}$, (b) $CH_3CH_2C{\equiv}N\text{-}XeF^{+}AsF_6^{-}$, (c) $(CH_3)_2CHC{\equiv}N\text{-}XeF^{+}AsF_6^{-}$, (d) $(CH_3)_3CC{\equiv}N\text{-}XeF^{+}AsF_6^{-}$, (e) $FCH_2C{\equiv}N\text{-}XeF^{+}AsF_6^{-}$, (f) $ClCH_2C{\equiv}N\text{-}XeF^{+}AsF_6^{-}$ and comparison to the Raman spectrum of $HC{\equiv}N\text{-}XeF^{+}AsF_6^{-}$. The verical solid lines denote the ν(Xe-F) and ν(C≡N) stretching frequencies of $XeF^{+}AsF_6^{-}$ and the corresponding free nitriles. Asterisks (*) denote FEP sample vessel lines.

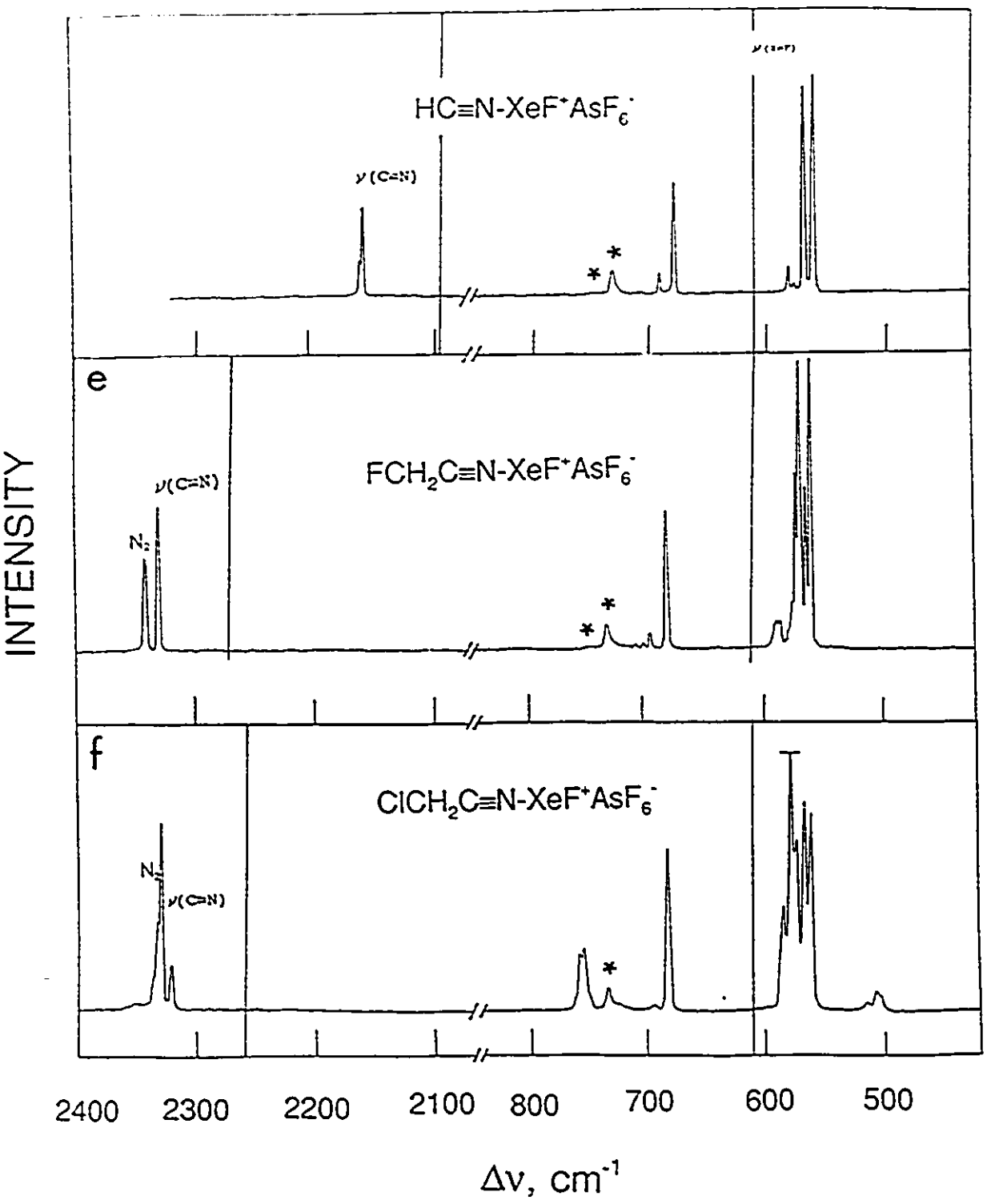
HC≡N-XeF⁺AsF₆⁻
ν(C≡N)
ν(Xe-F)
e
FCH₂C≡N-XeF⁺AsF₆⁻
ν(C≡N)
N₂
f
ClCH₂C≡N-XeF⁺AsF₆⁻
N₂
ν(C≡N)
INTENSITY
2400
2300
2200
2100
800
700
600
500
Δν, cm⁻¹

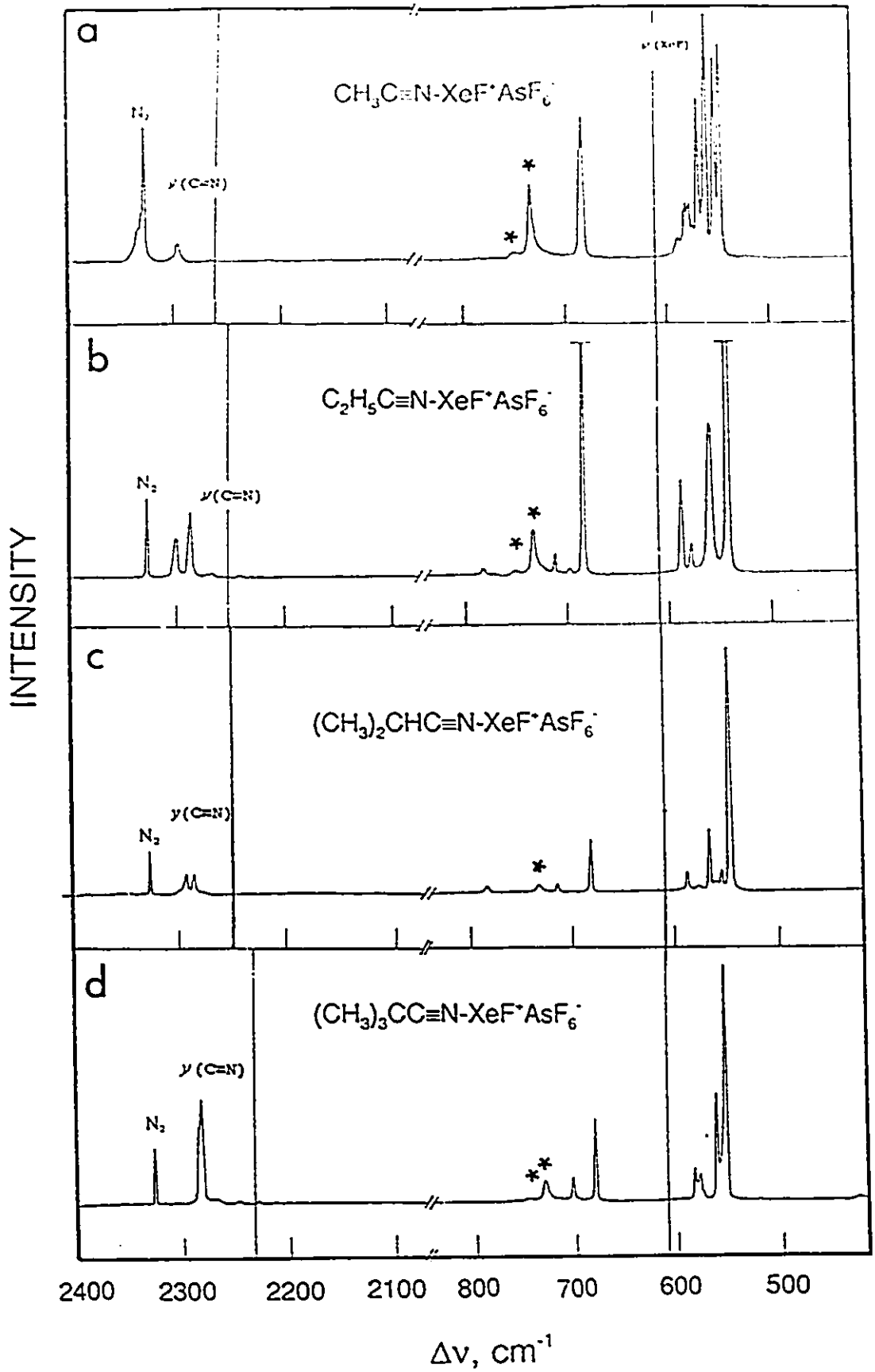
a
$CH_3C{\equiv}N\text{-}XeF^+AsF_6^-$
N_2
ν(C≡N)
b
$C_2H_5C{\equiv}N\text{-}XeF^+AsF_6^-$
N_2
ν(C≡N)
c
$(CH_3)_2CHC{\equiv}N\text{-}XeF^+AsF_6^-$
N_2
ν(C≡N)
d
$(CH_3)_3CC{\equiv}N\text{-}XeF^+AsF_6^-$
N_2
ν(C≡N)
INTENSITY
2400
2300
2200
2100
800
700
600
500
$\Delta\nu$, cm^{-1}

Table 5.3

Raman Frequencies and Assignments Under C_s Symmetry for $RC{\equiv}N\text{-}XeF^+AsF_6^-$ (R = FCH_2, $ClCH_2$, C_2H_3, $(CH_3)_2CH$)[a] and the Corresponding Free Nitriles

Frequencies (cm^{-1})								Approximate
$FCH_2C{\equiv}N\text{-}XeF^+AsF_6^-$	$FCH_2C{\equiv}N$[a]	$ClCH_2C{\equiv}N\text{-}XeF^+AsF_6^-$	$ClCH_2C{\equiv}N$[a]	$C_2H_3C{\equiv}N\text{-}XeF^+AsF_6^-$	$C_2H_3C{\equiv}N$[a]	$(CH_3)_2CHC{\equiv}N\text{-}XeF^+AsF_6^-$	$(CH_3)_2CHC{\equiv}N$[a]	Description
3045(4), 3035(2), 3027(1)	3021	3027(2), 3021(2), 3018(2),	3010					$\nu(CH_2)_{asym}$
				3020(2)	2998	3030(2), 3015(2), 3003(2), 3001(3)		$\nu(CH_2)_{asym}$
		3015(2), 3011(2)		2981(2)				$\nu(CH_3)_{asym}$
				2965(3)	2951	2993(1), 2962(2)	2992	$\nu(CH_3)_{asym}$
						2950(2), 2937(2)	2942	Combination
2991(14), 2984(10)	2983	2977(5), 2972(4),	2963	2945(6)	2941			$\nu(CH_2)_{sym}$
		2968(8), 2961(7)		2922(<1), 2899(1)	2896, 2848			
						2922(4)	2925	$\nu(CH)_{sym}$
	2895	2351(2)						$\nu(CH)_{sym}$
						2894(1)		$\nu(CH_3)_{sym}$
						2879(1)	2879	$\nu(CH_3)_{sym}$
	2299	2335 sh,		2300(4)	2750, 2628, 2528,	2784(<1), 2784(<1),	2780, 2727	Combination
					2462, 2317	2299(2)		
2341(30)	2266	2332(31)	2256	2287(6), 2267(<1)	2295	2293(9), 2286(10)	2246	$\nu(C{\equiv}N)$
		2320(16), 2290(<1)		2241(<1)	2248	2278(1), 2235(<1),		Combination
	1585					2209(<1), 2200(<1)		Combination
				1466(2)	1461			
				1460(2)	1433	1476(<1), 1469(1), 1464(2), 1459(1)		CH_3 def. as., $\omega(CH_2)$
						1454(3)	1452	CH_3 def., sym

Continued..

Table 5.3 (continued)

Frequencies (cm^{-1})								Approximate
$FCH_2C{\equiv}N{\cdot}XeF^+AsF_6^-$	$FCH_2C{\equiv}N^a$	$ClCH_2C{\equiv}N{\cdot}XeF^+AsF_6^-$	$ClCH_2C{\equiv}N^a$	$C_6H_5C{\equiv}N{\cdot}XeF^+AsF_6^-$	$C_6H_5C{\equiv}N^a$	$(CH_3)_2CHC{\equiv}N{\cdot}XeF^+AsF_6^-$	$(CH_3)_2CHC{\equiv}N^a$	Description
						1449(1)	1449	CH_3 def., as
						1445(<1)		CH_3 def.,sym.
						1393(2)		$r(CH_3)$
						1374(1), 1312(1)	1320	CH def.
				1409(3)	1386			$\delta(CH_2)$
				1301(2)	1319			$\delta(CH_2)_{ip}$ and $\omega(CH_2)$
						1279(2)	1290	$r(CH_3)$
						1270(2)		CH def.
				1257(<1)	1265			$\omega(CH_2)$, $\delta(CH_2)_{op}$, $tw(CH_2)$
1437(6), 1434(3)	1461	1404(3)	1421					$\delta(CH_3)$
1386(2), 1379(2),	1389	1267(1), 1257(1)	1270					$\omega(CH_2$
1369(1), 1362(2), 1358(1)								
1241(2)	1259	1184(1), 1181(1)	1184					$tw(CH_2)$
				1091(<1)	1173			$r(CH_3)$, $r(CH_3)$, $tw(CH_2)$
				1072(3)	1076	1174(1), 1104(5)	1174, 1105	$r(CH_3)$, $\nu(CC)$
				1000(4)	1007			$\omega(CH_3)$
						973(2)	970	$\nu(CCC)_{sym}$
				955(<1)	919			$r(CH_3)$
		1177(<1), 952(2), 947(2)						$\omega(CH_3)$
1072(3), 1066(3)	1054							$\nu(C\text{-}F)$
1047(5), 1014(3)		902(<1), 597(2)	907					$r(CH_3)$
917(<1), 913(1), 905(<1)	922	942(2)	930			950(1), 936(<1), 909(5), 900(<1)	916	$\nu(CC)$
						852(<1), 577(<1), 542(<1)		
		860(2)	837					$\nu(CC)$ and $\omega(CH_3)$
						785(1), 783(4), 719(1), 700(<1)	775, 752	$r(CH_3)$
				752(<1),712(2),	755, 755			$r(CH_2)$
				705(1), 695(<1)				

Continued ...

Table 5.3 (continued)

Frequencies (cm^{-1})								Approximate
$FCH_2C{\equiv}N{\cdot}XeF^+AsF_6^-$	$FCH_2C{\equiv}N^a$	$ClCH_2C{\equiv}N{\cdot}XeF^+AsF_6^-$	$ClCH_2C{\equiv}N^a$	$C_2H_5C{\equiv}N{\cdot}XeF^+AsF_6^-$	$C_2H_5C{\equiv}N^a$	$(CH_3)_2CHC{\equiv}N{\cdot}XeF^+AsF_6^-$	$(CH_3)_2CHC{\equiv}N^a$	Description
		760(20), 756(22), 751(3), 696(2)	746					ν(CC)
721(1), 716(1), 709(2), 703(3), 697(6)								
682(48)		682(56)		684(25)		685(22)		$\nu_4(a_{1g})$ AsF_6^-
588(10), 585(11)		584(37)		587(9)		574(4)		$\nu_2(e_g)$ AsF_6^-
				559(14)	544			δ(CCC)
580(3), 574(15)	575							δ(CCF)
571(60), 565(98), 563(55), 559(100)		577(100), 573(59), 566(72), 561(68)		541(100)		566(26), 559(5), 557(4) 554(10), 545(100)		ν(Xe-F)
409(1)	457	409(1), 404(1), 400(2)		406(3), 400(3), 397(1), 406(2),		405(2), 396(<1)		ν(Xe-N)
		516(3), 507(7), 504(5)	492					δ(HCC)
397(1), 395(1)								δ(HCF)
372(10), 368(8)		375(10), 370(14)		371(6), 360(5)		370(6), 366(3)		$\nu_3(t_{1u})$ AsF_6^-
						363(2)	358	CCC def.
						357(<1)		ω(CCC)
						325(3)	275	ω(CCC)
		362(8), 300(3), 287(4)	352					δ(CCC)
361(5), 307(7), 304(6)	357			392(4)	382	339(2), 329(6)		δ(CCN)
				282(10), 275(4)	346	270(1), 263(1)		$\tau(CH_3)$
263(7), 255(4), 247(5)		251(1), 241(1)		248(<1), 234(2)		261(1), 253(2), 245(1)		δ(XeNC)
230(2), 226(3), 188(1)	238, 191	225(2), 221(1), 214(<1)	206	204(<1), 197(<1)	220	243(1), 239(<1)	190	δ(CCN)
180(1), 171(3), 141(2), 124(5),		146(1), 140(1), 131(2), 116(6), 114(6),		181(2), 172(<1), 116(2)		184(1), 176(1), 168(<1), 159(1)		δ(FXeN)
105(12), 82(7), 62(7), 94(7), 77(4), 54(6)		116(6), 114(6), 106(4), 97(4), 84(1), 66(4), 56(7), 54(5)		116(2), 108(3), 104(7), 77(3), 66(9), 62(1), 57(1), 47(6), 40(6)		99(1), 86(2), 80(3), 77(3)		Lattice modes.

Continued..

Table 5.3 (continued)

a Raman spectra of $RC{\equiv}N\text{-}XeF^{+}AsF_6^{-}$ (R = CH_2F, CH_2Cl, C_2H_5 and $(CH_3)_2CH$) salts were recorded in FEP sample tubes at -196 °C using 514.5 nm excitation. Lines due to FEP have been deleted from this Table. Values in parentheses denote intensities, sh a shoulder, δ a bending mode, τ a torsional mode, ν a stretching mode, ω a waging mode, r a rocking mode and tw a twisting mode. Data given are for the spectra depicted in Figure 5.9.

b Ref. (202).

c Ref. (203).

d Ref. (204).

Table 5.4

Raman Frequencies and Assignments Under C_3, Symmetry for $RC{\equiv}N\text{-}XeF^{+}AsF_6^{-}$ (R = CH_3, $(CH_3)_3C$) and the Corresponding Free Nitriles

Frequency (cm^{-1})[a]				Approximate
$CH_3C{\equiv}N\text{-}XeF^{+}AsF_6^{-}$	$CH_3C{\equiv}N$[b]	$(CH_3)_3CC{\equiv}N\text{-}XeF^{+}AsF_6^{-}$	$(CH_3)_3CC{\equiv}N$[c]	Description
3028(4), 3021(7),	3009	3015(2)	2988	$\nu(CH_3)_{asymm}$
3014(4)		3007(1)	2960	$\nu(CH_3)_{asym}$
		3000(2)	2933	$\nu(CH_3)_{asym}$
		2987(2)	2912	$\nu(CH_3)_{asym}$
		2973(1)	2893	$\nu(CH_3)_{sym}$
2950(19), 2945(19)	2954	2944(2)	2878	$\nu(CH_3)_{symm}$
		2914(1)	2878	Combination
		2876(1)	2795	Combination
		2727(2)	2728	$\nu(CH_3)_{symm}$
2335(14)				Combination
2331(19)	2267	2283(28)	2240	$\nu(C{\equiv}N)$
2321(2)				
296(7)				Combination
		2285(22)		Combination
		2270(2)		Combination
		2231(1)		
1431(1), 1416(<1),	1453	1465(6), 1460(5)	1466	CH_3 def., as.
1397(2)		1448(2), 1412(2),	1455	
		1402(2)		
1356(5), 1351(4)	1385			CH_3 def., sym.
		1234(<1), 1212(7)	1245	$\nu(C\text{-}C{\equiv})$
		1203(7)	1209	$\nu(C\text{-}C)$
1035(3), 1032(2),	1041	1045(3), 1041(4),	1032	$r(CH_3)$
1025(3), 1017(3)		947(8)		
952(<1)	920			$\nu(C\text{-}C)$
		943(7), 935(1),	873	$r(CH_3)$
		862(8)		
		721(1), 716(1),	760	Combinations
		712(1), 705(11)		
685(44), 681(59)		681(34)		$\nu_1(a_{1g})\ AsF_6^{-}$

Continued ...

Table 5.4 (continued)

Frequency (cm^{-1})[a]				Approximate
$CH_3C{\equiv}N{\cdot}XeF^+AsF_6^-$	$CH_3C{\equiv}N^b$	$(CH_3)_3CC{\equiv}N{\cdot}XeF^+AsF_6^-$	$(CH_3)_3CC{\equiv}N^c$	Description
588(8), 580(23)		584(13), 574(4)		$\nu_2(e_g)AsF_6$
568(65), 560(100),		565(44), 555(100)		ν(XeF)
551(82), 546(8)				
		431(1), 422(1)	378	δCCC def., symm.
408(4)		401(2)		ν(Xe-N)
393(4)	362	264(6), 255(2)		δ(CCN)
			366	ω(CCC)
		277(4), 273(7),	195	$\tau(CH_3)$
		269(6)		
370(26)		371(8), 368(12)		$\nu_5(t_{2g})AsF_6$
364(2), 357(3)				ω(CCC)
288(10), 284(12),		245(2), 239(1),		δ(XeNC)
268(5), 235(4)		191(3), 185(5)		
230(5), 225(3),				
		169(1), 156(1),		δ(FXeN)
160(2), 127(3)		150(1)		
116(7), 97(7),		104(3), 92(3),		Lattice modes.
92(5), 75(5)		83(4), 77(4),		
		68(10), 58(3),		
		47(3), 31(3)		

a Raman spectra of $RC{\equiv}N{\cdot}XeF^+AsF_6^-$ (R = CH_3 and $(CH_3)_3C$) salts were recorded in FEP sample tubes at -196 °C using 514.5 nm excitation. FEP sample tube lines have been deleted from the spectra. Values in parentheses denote intensities; sh a shoulder; δ a bending mode; τ a torsional mode; ν a stretching mode; ω a twisting mode; r a rocking mode and tw a twisting mode. Data given are for the spectra depicted in Figure 5.9.

b Ref. (205).

c Ref. (206).

plane) are given in Table 5.5. Under C_s symmetry, all modes are Raman and infrared active. In case of the $(CH_3)_3CC{\equiv}N\text{-}XeF^+$ cation, forty-five vibrational modes are predicted ($11A_1 + 4A_2 + 15E$) of which fifteen modes are doubly degenerate. Twenty-six bands are expected in the Raman spectrum of the $(CH_3)_3CC{\equiv}N\text{-}XeF^+$ cation where $4A_2$ modes are Raman and infrared inactive. Also, all eighteen modes of the $CH_3C{\equiv}N\text{-}XeF^+$ cation ($6A_1 + 6E$) are Raman and infrared active under C_{3v} symmetry, with six doubly degenerate modes. Thus, twelve bands in all are expected in the Raman spectrum of the $CH_3C{\equiv}N\text{-}XeF^+$ cation.

The AsF_6^- anion possesses O_h symmetry and the resulting in 15 normal modes of vibration are classified belonging to the irreducible representations

$$\Gamma_{vib} = A_{1g} + E_g + 2\,T_{1u} + T_{2g} + T_{2u} \qquad (5.13)$$

Of these, the triply degenerate T_{1u} modes are infrared active and T_{2u} mode is infrared and Raman inactive, while only the A_{1g}, E_g and T_{2g} modes are Raman active, i.e, only three Raman-active bands are expected for an AsF_6^- anion having O_h symmetry.

The Raman spectra of related compounds [202-206] are also given in Tables 5.3 and 5.4 for comparison. The Raman spectra of the $RC{\equiv}N\text{-}XeF^+$ cations, the free nitriles and the other Xe-N and Xe-F stretching and F-Xe-N bending modes of known xenon-nitrogen compounds[64,67,69] have been used as guides in making spectral assignments.

The Raman spectra of the $RC{\equiv}N\text{-}XeF^+$ cations show very strong bands at 540 - 580 cm^{-1}, which can be assigned to the Xe-F stretch of $RC{\equiv}N\text{-}XeF^+$ and which is characteristic of the terminal Xe-F bond in Xe(II) compounds. The Xe-F stretching modes are readily

Table 5.5

Number of Normal Vibrational Modes Predicted for the $RC{\equiv}N\text{-}XeF^+$ Cations

Cation	Molecular Symmetry	3N - 6	Number of Fundamentals
$CH_3C{\equiv}N\text{-}XeF^+$	C_{3v}	$18 = 6A_1 + 6E$	12
$ClCH_2C{\equiv}N\text{-}XeF^+$	C_s	$18 = 12A' + 6A''$	18
$FCH_2C{\equiv}N\text{-}XeF^+$	C_s	$18 = 12A' + 6A''$	18
$C_2H_5C{\equiv}N\text{-}XeF^+$	C_s	$27 = 17A' + 10A''$	27
$(CH_3)_2CHC{\equiv}N\text{-}XeF^+$	C_s	$36 = 21A' + 15A''$	36
$(CH_3)_3CC{\equiv}N\text{-}XeF^+$	C_{3v}	$45 = 11A_1 + 4A_2 + 15E$	30

assigned by comparison with the frequencies of known LXeF species.[67,25] The splittings observed on these bands are attributed to factor-group splitting as the XeF stretching is a totally symmetric mode. The position of the Xe-F band is a strong indication of the increased covalent character of these cations when compared to $HC{\equiv}N\text{-}XeF^+$, which is expected to decrease as the xenon-nitrogen bond becomes more covalent and the terminal Xe-F bond becomes correspondingly more ionic. A comparison of the Xe-F stretching frequencies for $RC{\equiv}N\text{-}XeF^+$ cations may be used to assess the relative covalencies of the Xe-N bonds in $RC{\equiv}N\text{-}XeF^+$ cations. The stretching frequencies of the terminal Xe-F bond do indeed increase in the order C_2H_5, 541 < $(CH_3)_2CH$, 545 < $(CH_3)_3C$, 555 < FCH_2, 559 < H, 559 < CH_3, 560 < $ClCH_2$, 577 cm^{-1}, indicating that the $ClCH_2C{\equiv}N\text{-}XeF^+$ cation is the most ionic xenon-nitrogen compound studied in the above series.

The Xe-N stretching frequencies of $RC{\equiv}N\text{-}XeF^+$ cations are tentatively assigned to weak lines at the lower frequencies in the 396 - 409 cm^{-1} region, which are in agreement with the Xe-N stretching frequency of the previously reported xenon-nitrogen bonded compounds, $FXeN(SO_2F)_2$ [67] (which was observed at 422 cm^{-1} and its assignment confirmed by ^{15}N isotopic enrichment) and $Xe[N(SO_2F)_2]_2$,[65,67] which was observed at 413, 406 cm^{-1}. Table 5.6 lists tentative assignments of the Xe-N stretching frequencies of $RC{\equiv}N\text{-}XeF^+$ cations along with those of previously reported xenon-nitrogen bonded compounds. The Xe-N stretching frequencies for the $RC{\equiv}N\text{-}XeF^+AsF_6^-$ salts occur at lower frequencies than those of $FXeN(SO_2F)_2$ and $Xe[N(SO_2F)_2]_2$ and is attributed to the lower covalent characters of the Xe-N bonds in the imidodisulfurylfluoride derivatives.

The FXeN and C≡NXe bending frequencies are tentatively assigned to weak bands at 124 - 186 and 185 - 268 cm^{-1}, respectively. Each of F-Xe-N and C≡N-Xe groups are

Table 5.6

Tentative Assignments for the Xe-N Stretching and C≡N-Xe and N-Xe-F Bending Modes of the $RC{\equiv}N\text{-}XeF^+$ Cations

Cation	ν(Xe-N) cm^{-1}	δ(CNXe) cm^{-1}	δ(NXeF) cm^{-1}
$CH_3C{\equiv}N\text{-}XeF^+$	408(4)	235(4), 268(5)	127(3), 160(2)
$ClCH_2C{\equiv}N\text{-}XeF^+$	397(1), 400(3) 406(3)	241(1), 251(1)	131(2), 140(1) 146(1)
$FCH_2C{\equiv}N\text{-}XeF^+$	400(2), 404(1)	247(5), 255(4) 263(7)	124(5) 171(3), 180(1)
$C_2H_5C{\equiv}N\text{-}XeF^+$	392(4), 400(2) 406(2)	234(2), 248(<1)	172(<1), 181(2)
$(CH_3)_2CHC{\equiv}N\text{-}XeF^+$	396(<1), 405(2)	249(1), 253(2) 261(1)	159(1), 168(<1) 176(1), 184(1)
$(CH_3)_3CC{\equiv}N\text{-}XeF^+$	401(2)	185(5), 191(3) 239(1), 245(2)	150(1), 156(1) 169(1)
$C_5F_5N\text{-}XeF^+$ [a]	401(2), 419(4)	239(1), 245(2)	158(13), 154(sh)
$FXeN(SO_2F)_2$ [b]	422(4)		180(7), 186(13) 215(113), 220(113)
$F[XeN(SO_2F)_2]^+$ [c]	423(2)		
s-$C_3F_3N_2N\text{-}XeF^+$ [d]	313(1)		156(23), 159sh
$Xe[N(SO_2F)_2]_2$ [c]	406, 413		

(a) See Chapter 7.

(b) Ref. (64).

(c) Ref. (67).

(d) Ref. (123).

expected to contribute two types of bending vibrations: in-plane and out-of-plane for $RC{\equiv}N\text{-}XeF^+$ cations (except for $CH_3C{\equiv}N\text{-}XeF^+$ and $(CH_3)_3CC{\equiv}N\text{-}XeF^+$, which have cylindrical symmetry, thus rendering the in-plane and out-of-plane bends doubly degenerate). The bending modes of the FXeN group are expected at lower frequencies than those of the XeN≡C group. These bending modes are assigned to several lines in the 124 - 186 and 185 - 268 cm^{-1} regions; respectively, with the splittings most probably arising from solid state effects.

The Raman spectra of the $RC{\equiv}N\text{-}XeF^+$ cations all exhibit sharp lines at 2231 - 2341 cm^{-1} attributed to ν(C≡N). The corresponding frequencies of the free nitriles[202-206] occur at 2240 - 2295 cm^{-1} in the liquid state. Upon coordination with XeF^+, the ν(C≡N) stretching frequency shifts to higher frequency as shown in Tables 5.3 and 5.4. This is consistent with the nitrile ligands acting as σ-donors by donating their N_{sp} electron pairs to the XeF^+ cation.

Additional weak bands were also observed at 2231 - 2341 cm^{-1} in the spectra of the $RC{\equiv}N\text{-}XeF^+$ cations. These bands may arise from the formation of equilibrium amounts of $RC{\equiv}NH^+AsF_6^-$ according to equilibrium (5.5). One example has been examined, namely, the reaction of $FCH_2C{\equiv}N$ with AsF_5 in HF under the same reaction conditions, and its Raman spectrum has been compared with that of $FCH_2C{\equiv}N\text{-}XeF^+AsF_6^-$. The ν(C≡N) stretching frequency of $FCH_2C{\equiv}N\text{-}XeF^+AsF_6^-$ occurred at 2226(10), 2258(9) cm^{-1}, which is lower than ν(C≡N) (2266 cm^{-1}) in $FCH_2C{\equiv}N$. Thus, the weak bands observed at 2231 -2341 cm^{-1} in the $RC{\equiv}N\text{-}XeF^+$ cation do not appear to result from ν(C≡N) of the $RC{\equiv}NH^+$ cations. The bands observed at 2231 - 2341 cm^{-1} are ascribed to combination bands in which the combination band frequency interacts with a

fundamental vibration of the C≡N stretch by means of a Fermi resonance interaction.[207] Fermi resonance results in two bands where one fundamental ν(C≡N) stretch is ordinarily expected. The combination band, in effect, borrows intensity from the fundamental and the two bands "repel" each other, therefore, neither is found where it is expected. The relative intensities and separations of the bands depend on the separation of the two unperturbed frequencies. The line positions may be approximately calculated using equation (5.14).[207]

$$\nu_o = \tfrac{1}{2}(\nu_a + \nu_b) \pm \tfrac{1}{2}(\nu_a - \nu_b)\,[(I_a - I_b)/(I_a + I_b)] \qquad (5.14)$$

where the two values of ν_o are the unperturbed frequencies, ν_a and ν_b are the observed frequencies and I_a and I_b are their respective intensities. The unperturbed frequencies of the coupled combination and fundamental ν(C≡N) stretching frequencies of the RC≡N-XeF$^+$ cations are given in Table 5.7; the ν(C≡N) stretching frequencies of the RC≡N-XeF$^+$ cations and RC≡N are given in Table 5.8. In general ν(C≡N) is 44 - 69 cm^{-1} higher than in the free nitrile.

The Raman spectra of the RC≡N-XeF$^+$ cations show strong similarities to the free nitriles in the asymmetric and symmetric CH_3, CH_2 and CH stretching regions (2727 - 3045 cm^{-1}) and at 1301 - 1476 and 1404 - 1437 cm^{-1}, where the CH_3 and CH_2 bending frequencies occur. The assignments of the CH_3 and CH_2 stretching and deformations are, however, less certain due to the occurrence of several fundamental and overtone/combination vibrations in these regions and Fermi-resonance between them.[197-201] The assignments of the carbon-hydrogen and carbon-carbon stretching and deformation modes for individual RC≡N-XeF$^+$ cations in this series have been made as follows:

Table 5.7

The Fermi Resonance of ν(C≡N) With Combination/Overtone Bands in the 2231 - 2351 cm^{-1} Region of the Raman Spectra of the RC≡N-XeF$^+$ Cations

Cation	Observed Bands (cm^{-1})	Unperturbed Bands (cm^{-1})
HC≡N-XeF$^+$	2159(41), 2163(18)	2160.2, 2161.8
CH_3C≡N-XeF$^+$	2331(19), 2335(14)	2332.7, 2333.3
$ClCH_2C$≡N-XeF$^+$	2320(16), 2332(31)	2324.1, 2327.9
C_2H_5C≡N-XeF$^+$	2287(6), 2300(4)	2293.2, 2293.8
$(CH_3)_2CHC$≡N-XeF$^+$	2286(10), 2293(9)	2289.3, 2289.7
$(CH_3)_3CC$≡N-XeF$^+$	2283(28), 2285(22)	2283.9, 2284.1

Table 5.8

Raman Frequencies of the ν(C≡N) Stretching Mode in the RC≡N-XeF$^+$ Cations and the Corresponding Free Bases.

R	RC≡N $\nu_x(cm^{-1})$	RC≡N-XeF$^+$ $\nu_y(cm^{-1})$	$\Delta\nu = \nu_y - \nu_x$ (cm^{-1})	Ref.[a]
H	2097	2162	65	(163)
CH_3	2264	2333	69	(205)
$ClCH_2$	2256	2324	68	(202)
FCH_2	2266	2341	75	(202)
C_2H_5	2248	2294	46	(203)
$(CH_3)_2CH$	2246	2290	44	(204)
$(CH_3)_3C$	2240	2284	44	(206)

a References correspond to the published vibrational frequencies for the free bases, RC≡N.

$CH_3C{\equiv}N\text{-}XeF^+$. The assignment of CH_3 stretching and deformation, HCC deformation and CC stretching vibrations are given in Table 5.4 and have been made on the basis of the previously reported [205,208] assignments under C_{3v} point symmetry for the corresponding modes of $CH_3C{\equiv}N$. On the basis of these studies,[205,208] there are seven fundamental bands for the CH_3C unit, four of which are doubly degenerate, namely, the $\nu(CH_3)$ asymmetric stretch, $\delta(CH_3)$ deformation and the (CH_3) rocking and $\delta(C\text{-}C{\equiv}N)$ bending modes.

$XCH_2C{\equiv}N\text{-}XeF^+$, (X = F, Cl). The assignments of the ligand modes for the $XCH_2C{\equiv}N\text{-}XeF^+$ cations (X = F, Cl) are given in Table 5.3 and have been made on the basis of the previously reported[202] assignments for the corresponding modes of the free nitriles, $XCH_2C{\equiv}N$ (X = F, Cl). The normal modes of vibration for the methylene groups of the cations consist of the two stretching and the deformation (bending, wagging, twisting and rocking) modes. The $XCH_2C{\equiv}N\text{-}XeF^+$ cations are not cylindrical and it is reasonable to suppose that the in-plane and out-of-plane bending vibrations of the $CC{\equiv}N$ moiety are not degenerate. The bands at 188(2), 226(3) and 230 (2) cm^{-1} are therefore assigned to these modes in the $FCH_2C{\equiv}N\text{-}XeF^+$ cation and those at 214(<1), 221(1) and 228(2) cm^{-1} to those of the $ClCH_2C{\equiv}N\text{-}XeF^+$ cation.

$CH_3CH_2C{\equiv}N\text{-}XeF^+$. The assignments of the CH_3 and CH_2 stretching vibrations are presented in Table 5.3 and have been made on the basis of the previously reported assignments for the corresponding modes for ethylnitrile, $CH_3CH_2C{\equiv}N$.[203]

$(CH_3)_2CHC{\equiv}N\text{-}XeF^+$. Vibrational assignments for the free nitrile have not been published. The C-H stretching modes can be assigned on the basis that each of the two CH_3 groups will have one symmetric and two asymmetric stretching frequencies and the asymmetric stretches will be close in frequency, but higher than the symmetric stretch. The three

stretching modes of each CH_3 couple to yield 3A′ and 3A″ modes. The assignments of the CH_3 stretching vibrations are given in Table 5.3 and have been made on the basis of the previously reported assignments for the corresponding modes for isobutyronitrile,[208] isopropylhalides,[209] isopropylisocyanate[210] and isopropylamine.[211] On the basis of the previous assignment, the single CH stretch has been assigned to the frequency at 2922 cm^{-1}. The frequencies in the region 2879 - 3030 cm^{-1} must arise from the asymmetric and symmetric in-plane and out-of-plane stretches. The other observed frequencies 2784(<1) and 2782 (<1) cm^{-1} are assigned to the overtone and combination bands of the CH_3 deformation and rocking modes. There are fourteen carbon-hydrogen bends, excluding the two torsions, which are associated with two CH_3 groups. The four CH_3 asymmetric deformations are assigned to Raman bands at 1449(1), 1459(1), 1464(2) and 1468(1) cm^{-1}, and the two CH_3 symmetric deformations are assigned to bands at 1445(<1) and 1454(3) cm^{-1}. The two CCH bends are assigned to the Raman lines at 1312(1) and 1374(1) cm^{-1}. The 1104 - 1393 cm^{-1} region contains seven bands, two of which have already been assigned and four bands of which are expected due to the CH_3 rocking motions. The CCC stretches are also expected to occur in this region and therefore after assigning the asymmetric CCC stretch at 973(2) cm^{-1}, the remaining four lines are assigned to the four CH_3 rocking modes at 1174(1), 1270(2), 1279(2) and 1393(2) cm^{-1}. The two methyl torsions are assigned to bands at 263(1) and 270(1) cm^{-1}. The skeletal modes of the $(CH_3)_2CH$ group (deformation, twist and wag) are assigned to bands at 363(2), 357(<1) and 325(3) cm^{-1}, respectively. The Raman lines observed at 243(1) and 239(<1) cm^{-1} have been assigned to the $\delta(CC{\equiv}N)$ in-plane bending modes and those at 329(6), 339(2) cm^{-1} to the $CC{\equiv}N$ out-of-plane bend.

$(CH_3)_3CC{\equiv}N\text{-}XeF^+$. The assignments of the stretching and bending vibrations of the $(CH_3)_3C$ group are given in Table 5.4 and have been made on the basis of the previously reported assignments for the corresponding modes of *tert*-butylnitrile.[206] There are 14 active fundamental vibrational modes associated with the $(CH_3)_3CC{\equiv}N\text{-}XeF^+$ cation that arise from the three CH_3 groups present in the cation. There are several bands in the region of 2720 - 3015 cm^{-1} where the five CH stretching vibrations are expected to fall. Some of these bands may be due to overtones/combinations of the bending vibrations, hence detailed and unambiguous assignments of these fundamentals are not possible for the CH stretching modes. The frequencies in the region of 1402 - 1465 cm^{-1} must arise from the asymmetric and symmetric deformations, and, in all, five bands are expected. The observed bands 1402(2), 1412(2) and 1448(2) cm^{-1} are assigned to the CH_3 symmetric deformation and the bands at 1460(5) and 1465(6) cm^{-1} are assigned to the CH_3 asymmetric deformation. The remaining four bands are due to CH_3 rocking and torsional vibrations. The CH_3 torsional vibration has been observed at 269(6), 273(7) and 277(4) cm^{-1}, and the remaining three bands are due to CH_3 rocking modes and have been observed at 1203(7), 1212(7) and 1234(<1) cm^{-1}, respectively. The skeletal modes of the $(CH_3)_3C$ group have the CC stretching vibration at 1041(4) and 1045(3) cm^{-1} and the CC_3 stretching vibration at 935(1), 943(7) and 947(8) cm^{-1}. Two CCC bending vibrations are also expected at 357(3) cm^{-1} (wagging) and 401(2) cm^{-1} (deformation). The $CC{\equiv}N$ group has linear cylindrical symmetry so that the in-plane and out-of-plane bending modes are degenerate and are assigned to bands at 264 (6), 255 (2) cm^{-1}.

The three Raman-active modes associated with the octahedral AsF_6^- anion $\nu_1(a_{1g})$, $\nu_2(e_g)$ and $\nu_5(t_{2g})$ of the $RC{\equiv}N\text{-}XeF^+AsF_6^-$ salts are further supported by a comparison with

Table 5.9

Raman Frequencies and Assignments for the AsF_6^- Anion in the $RC{\equiv}N\text{-}XeF^+AsF_6^-$ salts and Related Salts

Salt	$\nu_1(a_{1g})$	$\nu_2(e_g)$	$\nu_5(t_{2g})$
$CH_3C{\equiv}N\text{-}XeF^+AsF_6^-$	681(59) 685(44)	580(23) 588(8)	370(26)
$ClCH_2C{\equiv}N\text{-}XeF^+AsF_6^-$	682(56)	584(37)	370(14) 375(10)
$FCH_2C{\equiv}N\text{-}XeF^+AsF_6^-$	682(48)	585(10) 588(11)	368(8) 372(10)
$CH_3CH_2C{\equiv}N\text{-}XeF^+AsF_6^-$	684(25)	585(9)	369(5) 371(6)
$(CH_3)_2CHC{\equiv}N\text{-}XeF^+AsF_6^-$	685(22)	574(4)	366(3) 370(6)
$(CH_3)_3CC{\equiv}N\text{-}XeF^+AsF_6^-$	681(34)	574(4) 584(13)	368(12) 371(8)
$C_5F_5N\text{-}XeF^+AsF_6^-$	677(24) 680(9)	577(4)	375(3)
s-$C_3F_3N_2N\text{-}XeF^+AsF_6^-$ [a]	684(19)	588sh 591(4)	370(5) 375(4)
$F[XeN(SO_2F)_2]_2^+AsF_6^-$ [b]	680(18) 682(10)	570(2) 574(20) 583(2)	374(3) 379(3)
$AsBr_2^+AsF_6^-$ [c]	671(17) 702(1)	568(5)	370(7)
$AsCl_4^+AsF_6^-$ [c]	680	570	371

a Ref. (123).

b Ref. (69).

c Ref. (212).

those previously given for $AsX_2^+AsF_6^-$ (X = Cl and Br),[212] $F[XeN(SO_2F)_2]_2^+AsF_6^-$,[69] *s*-$C_3F_3N_2N$-$XeF^+AsF_6^-$ [123] and C_5F_5N-$XeF^+AsF_6^-$,[156] which are listed in Table 5.9. This is true provided that the site symmetry for the AsF_6^- anion is O_h in what are deemed to be purely ionic RC≡N-$XeF^+AsF_6^-$ salts in the solid state.

A number of unassigned Raman lines have been observed at 2200 - 2332 and 2732 - 3030 cm^{-1}, which can be interpreted as overtones and/or combinations of fundamentals associated with the organic moiety of the RC≡N-XeF^+ cation. Lines below 116 cm^{-1} are attributed to lattice modes.

CHAPTER 6

THE DECOMPOSITION AND SOLVOLYTIC BEHAVIOR OF $RC{\equiv}N\text{-}XeF^{+}AsF_6^{-}$ AND $RC{\equiv}N$ IN ANHYDROUS HYDROGEN FLUORIDE

INTRODUCTION

The reactions of alkyl nitriles with $XeF^{+}AsF_6^{-}$ leads to the adduct cations, $RC{\equiv}N\text{-}XeF^{+}AsF_6^{-}$, which can be isolated from HF solvent at low temperature (see Chapter 5). However, some alkyl nitriles, especially, the long chain alkyl nitriles, were shown to be thermally unstable and were readily fluorinated at -30 °C to form monofluoro- and difluoro-alkyl nitriles at the β-, γ-, and δ-carbons, but not at the α-carbon. The protonated monofluoro- and difluoro-alkyl nitriles in turn react with XeF^{+} according to equilibria (5.3 - 5.7).

It has been shown in Chapter 4 that the related adduct cation, $HC{\equiv}N\text{-}XeF^{+}$, is thermally more stable than $RC{\equiv}N\text{-}XeF^{+}$ in HF solvent and slowly decomposes at room temperature.

In this Chapter, the stabilities and solvolytic behaviors of the $RC{\equiv}N\text{-}XeF^{+}AsF_6^{-}$ salts have been studied by monitoring their decompositions in anhydrous HF solvent over

a period of several hours at room temperature by NMR spectroscopy.

For a better understanding of the reaction mechanisms and to determine whether the fluorinating agent is XeF_2 or HF, a parallel study of the corresponding free nitriles, RC≡N (R = CH_3, C_2H_5, *n*-C_3H_7, *n*-C_4H_9), in anhydrous HF has been undertaken. Prior to this work, studies of the solvolysis of the alkyl nitriles in anhydrous HF was limited. Mohr *et al.*[213] showed the reaction of $CH_3C{\equiv}N$ and anhydrous HF forms the $CH_3CF_2NH_3^+$ cation. The $CH_3CF_2NH_3^+$ cation has been inferred by back titration of the unreacted HF with alkali metal carbonates. Based on their related, but inconclusive work on the HC≡N/HF system, Gillespie and Hulme[189] suggested that the solvolyses of alkyl nitriles in anhydrous HF may lead to the $RCF_2NH_3^+$ cations by addition of two molecules of HF to the C≡N bond. However, no definitive characterization of these cations has been reported.

Consequently, the room temperature solvolysis products resulting from RC≡N (R = CH_3, C_2H_5, *n*-C_3H_7 and *n*-C_4H_9) in anhydrous HF have been investigated in this Chapter using ^{19}F, ^{15}N, ^{14}N, ^{13}C and ^1H NMR spectroscopy to characterize the fluorinated products. This study indicates that the products and fluorination mechanisms of the decomposition of RC≡N/HF differ significantly from those resulting from the decomposition of RC≡N-XeF^+ cations in HF. In addition, this study also attempts to determine whether the two fluorination routes can provide useful synthetic routes to mono- and difluoro-nitriles and to study the influence of alkyl chain length on the fluorination products.

RESULTS AND DISCUSSION

(A) CHARACTERIZATION OF THE DECOMPOSITION PRODUCTS OF $RC{\equiv}N\text{-}XeF^{+}AsF_6^{-}$ IN ANHYDROUS HF BY ^{19}F AND ^{1}H NMR SPECTROSCOPY

Warming of stoichiometric mixtures of RC≡N and $XeF^{+}AsF_6^{-}$ in anhydrous HF for several hours at room temperature followed by recording the ^{19}F and ^{1}H NMR spectra at -15 °C showed that several fluorinated products were formed. It was found that nitriles having long-chain alkyl groups were fluorinated more rapidly. In order to understand the mechanism of fluorination, the decompositions were studied as a function of alkyl chain length where R = CH_3, C_2H_5, *n*-C_3H_7 and *n*-C_4H_9. It was noted that upon warming solutions of $RC{\equiv}N\text{-}XeF^{+}$ (R = CH_3, C_2H_5) to room temperature, the F-on-Xe(II) signals persisted, but in the case of $RC{\equiv}N\text{-}XeF^{+}$ (*n*-C_3H_7 and *n*-C_4H_9) the F-on-Xe(II) signal rapidly disappeared with the evolution of Xe gas. Table 6.1 lists the decomposition products of $RC{\equiv}N\text{-}XeF^{+}$ cations in HF solvent and summarizes the relative thermal stabilities of $RC{\equiv}N\text{-}XeF^{+}$ (R = H, CH_3, C_2H_5, *n*-C_3H_7 and *n*-C_4H_9) and their decomposition products in anhydrous HF solvent after warming the solutions for several hours at room temperature.

(i) $CH_3C{\equiv}N\text{-}XeF^{+}AsF_6^{-}$

The ^{19}F NMR spectra showed that a significant amount of the adduct cation, $CH_3C{\equiv}N\text{-}XeF^{+}$, exists after warming the reaction mixture for 48 hours at room temperature.

Table 6.1

Relative Stabilities of $RC{\equiv}N\text{-}XeF^{+}AsF_6^{-}$ (R = H, CH_3, C_2H_5 and n-C_3H_7 and n-C_4H_9) and Fluorinated Products Resulting From the Decomposition of $RC{\equiv}N\text{-}XeF^{+}AsF_6^{-}$ in Anhydrous HF at 25 °C

RC≡N	Reaction Conditions	Xe-N Bonded Adduct Cation	Warming Time[a] (Hours.)	Decomposition Products
HC≡N	-10 °C	$HC{\equiv}N\text{-}XeF^{+}$	14	$HC{\equiv}NH^{+}$, CF_3H, $CF_3NH_3^{+}$, $F_2C{=}NH_2^{+}$, $HFC{=}NH_2^{+}$, CF_4
$CH_3C{\equiv}N$ [b]	-10 °C	$CH_3C{\equiv}N\text{-}XeF^{+}$	48	$CH_3C{\equiv}NH^{+}$ $CF_3C{\equiv}NH^{+}$
$CH_3CH_2C{\equiv}N$ [b,c,d]	-15 °C	$C_2H_5C{\equiv}N\text{-}XeF^{+}$ $CH_2FCH_2C{\equiv}N\text{-}XeF^{+}$	15	$CH_3CH_2C{\equiv}NH^{+}$ $CH_2FCH_2C{\equiv}NH^{+}$
n-$C_3H_7C{\equiv}N$ [d,e]	-30 °C	$CH_3CH_2CH_2C{\equiv}N\text{-}XeF^{+}$ $CH_3CHFCH_2C{\equiv}N\text{-}XeF^{+}$ $CH_2FCH_2CH_2C{\equiv}N\text{-}XeF^{+}$ $CHF_2CH_2CH_2C{\equiv}N\text{-}XeF^{+}$ $CH_3CF_2CH_2C{\equiv}N\text{-}XeF^{+}$	2	$CH_3CH_2CH_2C{\equiv}NH^{+}$ $CH_3CHFCH_2C{\equiv}NH^{+}$ $CH_2FCH_2CH_2C{\equiv}NH^{+}$ $CHF_2CH_2CH_2C{\equiv}NH^{+}$ $CH_3CF_2CH_2C{\equiv}NH^{+}$
n-$C_4H_9C{\equiv}N$ [d,e]	-50 °C -25 °C	n-$C_4H_9C{\equiv}N\text{-}XeF^{+}$ $CH_3CHFCH_2CH_2C{\equiv}N\text{-}XeF^{+}$ $CH_3CF_2CH_2CH_2C{\equiv}N\text{-}XeF^{+}$	0.2	n-$C_4H_9C{\equiv}NH^{+}$ $CH_3CHFCH_2CH_2C{\equiv}NH^{+}$ $CH_3CF_2CH_2CH_2C{\equiv}NH^{+}$

Continued...

Table 6.1 (continued)

a The time required for complete decomposition of $RC{\equiv}N\text{-}XeF^+$ with the exception of $CH_3C{\equiv}N\text{-}XeF^+$, where a significant amount of the adduct cation remained with a significant amount after warming the reaction mixture for 48 hours at room temperature.

b The ^{19}F NMR spectra also showed an ABX spin-spin coupling pattern which is unassigned.

c The $CH_2FCHFC{\equiv}N\text{-}XeF^+$ cation was formed after warming a solution of $C_2H_5C{\equiv}N$ and $XeF^+AsF_6^-$ for two hours at room temperature.

d The fluorinated xenon-nitrogen adduct cations and the protonated nitriles result from the fluorination of $RC{\equiv}N\text{-}XeF^+AsF_6^-$ (R = C_2H_5, *n*-C_3H_7 or *n*-C_4H_9) in anhydrous HF.

e The ^{19}F NMR spectra showed other fluorinated species which have not been identified (e.g., see Figures 6.1 and 6.2).

In addition, several new ^{19}F signals were observed and their intensities increased with the time of warming. The most intense signal was observed at -70.9 ppm (singlet), while the low-intensity signals consisted of a quartet (-63.9 ppm; J, 11.6 Hz) and an ABX pattern ($\delta(F)_A$, -35.6 and $\delta(F)_B$, -39.4 ppm; $J(^{19}F_A\text{-}X)$, ~0 Hz and $J(^{19}F_B\text{-}X)$, 14.8 Hz). The ^{19}F NMR spectra of 99.0% ^{15}N-enriched $CH_3C{\equiv}^{15}N\text{-}XeF^+AsF_6^-$ and 99.0% ^{13}C enriched $CH_3{}^{13}C{\equiv}N\text{-}XeF^+AsF_6^-$ salts in HF solvent produced the same signals with no further splitting, while the 99.7% ^{13}C-enriched $^{13}CH_3C{\equiv}N\text{-}XeF^+AsF_6^-$ salt showed further splitting, i.e., the signal at -70.9 ppm was split into a doublet ($^1J(^{19}F\text{-}^{13}C)$, 279.7 Hz) and each line of the ABX pattern was split into doublets in both the F_A ($^1J(^{19}F\text{-}^{13}C)$, 312.8 Hz) and F_B portions ($^1J(^{19}F\text{-}^{13}C)$, 308.6 Hz) of the spectrum. Based on enrichment studies, the predominant signal at -70.9 ppm was assigned to $CF_3C{\equiv}NH^+$, whereas the minor product (ABX pattern) has not been assigned. The ^1H NMR spectra also showed two singlets at 2.54 and 2.26 ppm resulting from the $CH_3C{\equiv}NH^+$ and $CH_3C{\equiv}N\text{-}XeF^+$ cations, respectively, and an unidentified triplet at 2.95 ppm (J, 5.4 Hz). The latter is presumably associated with the ABX pattern in the ^{19}F NMR spectrum.

(ii) $C_2H_5C{\equiv}N\text{-}XeF^+AsF_6^-$

The ^{19}F NMR spectrum showed that the solvolysis of $C_2H_5C{\equiv}N\text{-}XeF^+AsF_6^-$ in HF progressed more rapidly than that of $CH_3C{\equiv}N\text{-}XeF^+$ under similar conditions. The F-on-Xe signal decreased in intensity and disappeared after warming the solution for 15 hours at room temperature. In the initial stages of warming, two F-on-Xe signals were observed, one of which was previously known and is readily assigned to the $C_2H_5C{\equiv}N$-

XeF^+ adduct cation. The other, a F-on-Xe(II) environment, is assigned to a new fluorinated nitrile adduct of XeF^+. The new adduct was identified as $CH_2FCH_2C{\equiv}N\text{-}XeF^+$ and was in equilibrium with the protonated nitrile in HF solvent. The fluorine-on-carbon region showed two overlapping, but distinct, multiplets at -219.3 and -219.1 ppm which are assigned to the CH_2FCH_2 groups of the protonated nitrile and the Xe-N bonded adduct cation, respectively. The ^{19}F chemical shifts of both cations are in good agreement with the ^{19}F chemical shifts of the related monofluoronitriles in HF solvent (Table 6.2). The ^{19}F NMR spectra also showed an intense ABX pattern at -35.8 (F_A) and -40.0 (F_B) ppm ($J(F_A\text{-}F_B)$, 141.6 Hz; $J(F_A\text{-}X)$, 18.3 Hz and $J(F_B\text{-}X)$, ~0 Hz), which overlapped with another low-intensity ABX pattern at -33.3 (F_A) and -36.8 (F_B) ppm ($J(F_A\text{-}F_B)$, 139.5 Hz; $J(F_A\text{-}X)$, 18.0 Hz and $J(F_B\text{-}X)$, ~0 Hz), and four singlets of different intensities at -68.2, -68.4, -66.2 and -66.0 ppm. Further warming of the solution for 15 hours at room temperature resulted in resonances arising from the $CH_2FCH_2C{\equiv}NH^+$ and $CH_2FCH_2C{\equiv}N\text{-}XeF^+$ cations, the two ABX patterns and an unidentified multiplet at -227.7 with approximate relative intensities 1 : 2 : 3 : 4 : 3 : 2 : 1. Throughout the warming, the two ABX patterns persisted with the most intense pattern belonging to the dominant fluorinated product in the mixture.

The ^1H NMR spectrum was recorded at -15 °C after warming the solution for 15 hours at room temperature and showed that the $CH_3CH_2C{\equiv}N\text{-}XeF^+$ and $CH_3CH_2C{\equiv}NH^+$ cations are the dominant products as well as several unidentified minor products at 4.83 ppm (J, 5.43 Hz; quartet), 4.71 ppm (J, 5.47 Hz; sextet), 4.62 ppm (J, 5.29; quartet), 3.06 ppm (J, 7.53 Hz; quartet) and 1.28 ppm (J, 7.50 Hz; triplet).

Table 6.2

NMR Parameters of the Decomposition Products of RC≡N-XeF$^+$ Cation in HF Solvent

Cation[b]	Chemical Shifts (ppm)[a] $\delta(^{19}F)$	$\delta(^1H)$	Spin-Spin Couplings (Hz) $J(^1H\text{-}^1H)$	$J(^{19}F\text{-}^1H)$
$CH_3C{=}NH^+$		2.4		
$CF_3C{=}NH^+$	-70.9			
$CH_3CH_2C{=}NH^+$		1.22 $(CH_3)_1$ 2.43 $(CH_2)_2$	7.6	
$CH_2FCH_2C{=}NH^+$	-218.8	— —	—	46.1 (F_1,H_1) 23.2 (F_1,H_2)
$CH_3CH_2CH_2C{=}NH^+$		2.09 $(CH_3)_1$ 2.76 $(CH_2)_2$ 3.52 $(CH_2)_3$	7.0 (H_1,H_2) 7.4 (H_2,H_3)	
$CH_2FCH_2CH_2C{=}NH^+$	-222.7	4.33 $(CH_2)_1$ 1.78 $(CH_2)_2$ 2.69 $(CH_2)_3$	5.3 (H_1,H_2) 6.7 (H_2,H_3)	46.1 (F_1,H_1) 9.3 (F_1,H_2)
$CH_3CHFCH_2C{=}NH^+$	-172.1	1.12 $(CH_3)_1$ 2.91 $(CHF)_2$ 4.70 $(CH_2)_3$	6.3 (H_1,H_2) 6.2 (H_2,H_3)	24.6 (F_2,H_1) 47.0 (F_2,H_2) — (F_2,H_3)
$CHF_2CH_2CH_2C{=}NH^+$	-120.9	— —	— —	54.9 (F_1,H_1) 17.9 (F_1,H_1)
$CH_3CF_2CH_2C{=}NH^+$	-87.7	1.72 $(CH_3)_1$ 3.80 $(CH_2)_3$	— —	18.3 (F_2,H_1) 14.2 (F_2,H_1)
$CH_3CH_2CH_2CH_2C{=}NH^+$		0.89 $(CH_3)_1$ 1.40 $(CH_2)_2$ 1.61 $(CH_2)_3$ 2.47 $(CH_2)_4$	7.4 (H_1,H_2) 7.8 (H_2,H_3) 7.2 (H_3,H_4)	
$CH_3CHFCH_2CH_2C{=}NH^+$	-175.9	1.18 $(CH_3)_1$ 1.97 $(CHF)_2$ 3.09 $(CH_2)_3$ 4.70 $(CH_2)_4$	6.2 (H_1,H_2) 6.8 (H_2,H_3) 6.1 (H_3,H_4)	25.9 (F_2,H_1) 49.2 (F_2,H_2) 27.9 (F_3,H_3) 6.5 (F_2,H_4)
$CH_3CF_2CH_2CH_2C{=}NH^+$	-97.1	1.44 $(CH_3)_1$ 1.82 $(CH_2)_3$ 2.66 $(CH_2)_4$	7.6 (H_3,H_4)	19.1 (F_2,H_1) 18.5 (F_2,H_3)

Continued...

Table 6.2 (continued)

a Referenced externally at 24 °C with respect to the neat liquid references $CFCl_3$(^{19}F) and TMS (^{1}H).

b The numbering scheme used to denote δ(^{19}F), δ(^{1}H), J(^{1}H-^{1}H) and J(^{19}F-^{1}H) is:

$\underset{1}{CH_2F}\underset{2}{CH_2}C{\equiv}NH^+$, $\underset{1}{CH_3}\underset{2}{CH_2}\underset{3}{CH_2}C{\equiv}NH^+$, $\underset{1}{CH_2F}\underset{2}{CH_2}\underset{3}{CH_2}C{\equiv}NH^+$,

$\underset{1}{CH_3}\underset{2}{CHF}\underset{3}{CH_2}C{\equiv}NH^+$ $\underset{1}{CHF_2}\underset{2}{CH_2}\underset{3}{CH_2}C{\equiv}NH^+$, $\underset{1}{CH_3}\underset{2}{CF_2}\underset{3}{CH_2}C{\equiv}NH^+$

$\underset{1}{CH_3}\underset{2}{CH_2}\underset{3}{CH_2}\underset{4}{CH_2}C{\equiv}NH^+$, $\underset{1}{CH_3}\underset{2}{CHF}\underset{3}{CH_2}\underset{4}{CH_2}C{\equiv}NH^+$, $\underset{1}{CH_3}\underset{2}{CHF}\underset{3}{CH_2}\underset{4}{CH_2}C{\equiv}NH^+$

(iii) n-$C_3H_7C{\equiv}N$-$XeF^+AsF_6^-$

The decomposition of n-$C_3H_7C{\equiv}N$-$XeF^+AsF_6^-$ has been monitored in HF solution by ^{19}F and ^1H NMR spectroscopy. Fluorination occurs at the alkyl carbons, but not on the carbon α- to the C≡N bond. The ^{19}F and ^1H NMR spectra are consistent with the fluorinated nitrile cations $CH_3CH_2CH_2C{\equiv}NH^+$, $CH_2FCH_2CH_2C{\equiv}NH^+$, $CH_3CHFCH_2C{\equiv}NH^+$, $CHF_2CH_2CH_2C{\equiv}NH^+$ and $CH_3CF_2CH_2C{\equiv}NH^+$. Figures 6.1 and 6.2 depict the ^{19}F NMR spectrum of n-$C_3H_7C{\equiv}N$-$XeF^+AsF_6^-$ in HF after warming for two hours at 24 °C and Figure 6.3 depicts the ^1H NMR spectrum of n-$C_3H_7C{\equiv}N$-$XeF^+AsF_6^-$ in HF after warming for two hours at 24 °C. Table 6.2 lists the NMR parameters of the fluorinated alkyl nitrile cations in HF solvent.

(iv) n-$C_4H_9C{\equiv}N$-$XeF^+AsF_6^-$

This cation is very unstable and forms several fluorinated products at low temperature, which have been characterized by ^{19}F, ^1H and ^1H-2D COSY NMR spectroscopy. The main decomposition products are $CH_3CHFCH_2CH_2C{\equiv}NH^+$, $CH_3CF_2CH_2CH_2C{\equiv}NH^+$ and $CH_3CH_2CH_2CH_2C{\equiv}NH^+$ (Table 6.2).

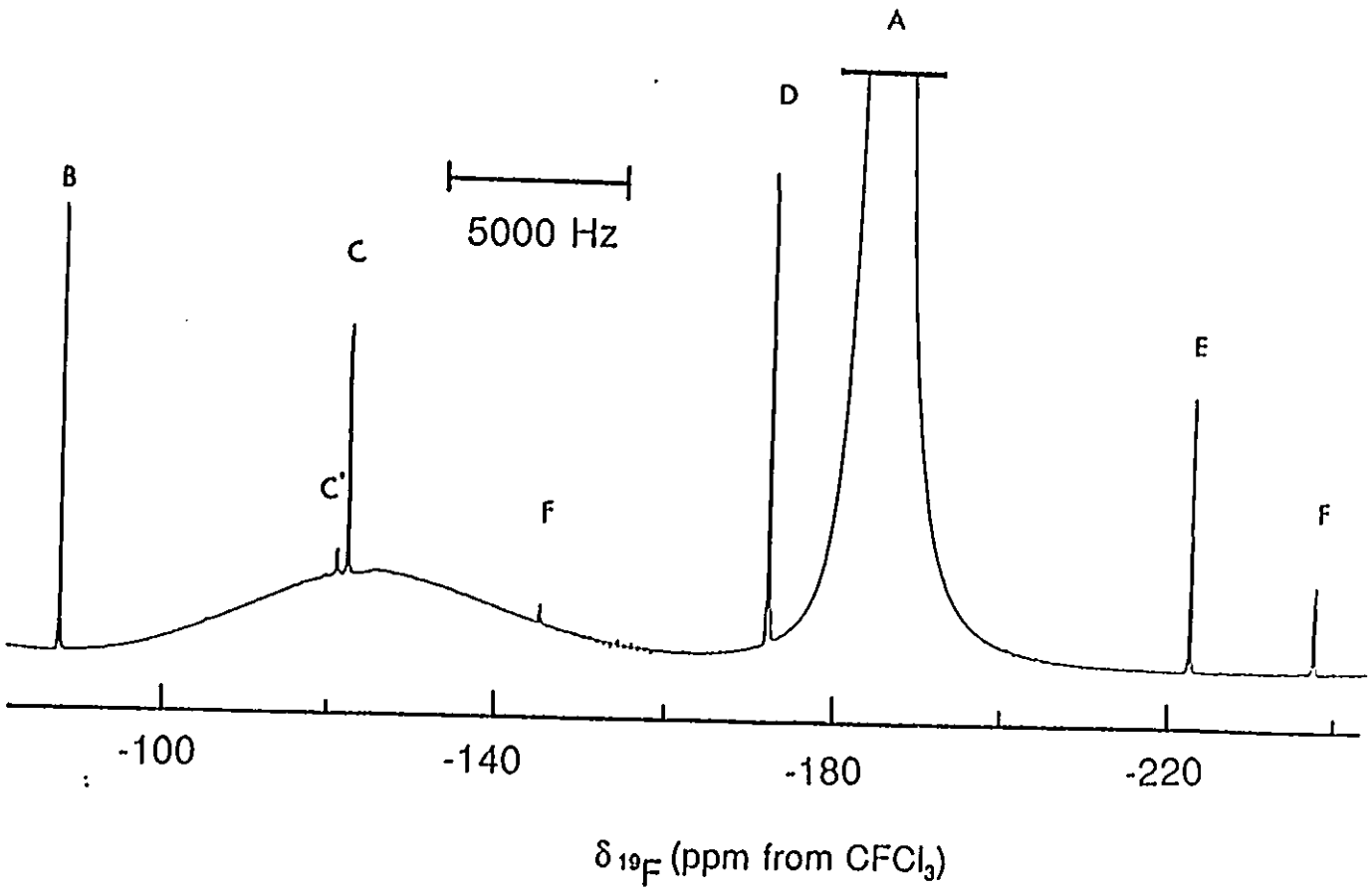

Figure 6.1 ^{19}F NMR spectrum (235.361 MHz) resulting from the reaction of a 1 : 1 stoichiometric mixture of *n*-$C_3H_7C{\equiv}N$ and $XeF^+AsF_6^-$ in HF after warming the solution for 2 hours at room temperature; (A) HF, (B) $CH_3CF_2CH_2C{\equiv}NH^+$, (C) $CHF_2CH_2CH_2C{\equiv}NH^+$, (C') $CHF_2CH_2CH_2C{\equiv}N\text{-}XeF^+$, (D) $CH_3CHFCH_2C{\equiv}NH^+$, (E) $CH_2FCH_2CH_2C{\equiv}NH^+$ and (F) unidentified resonance. Also see Figure 6.2 for multiplet expansions.

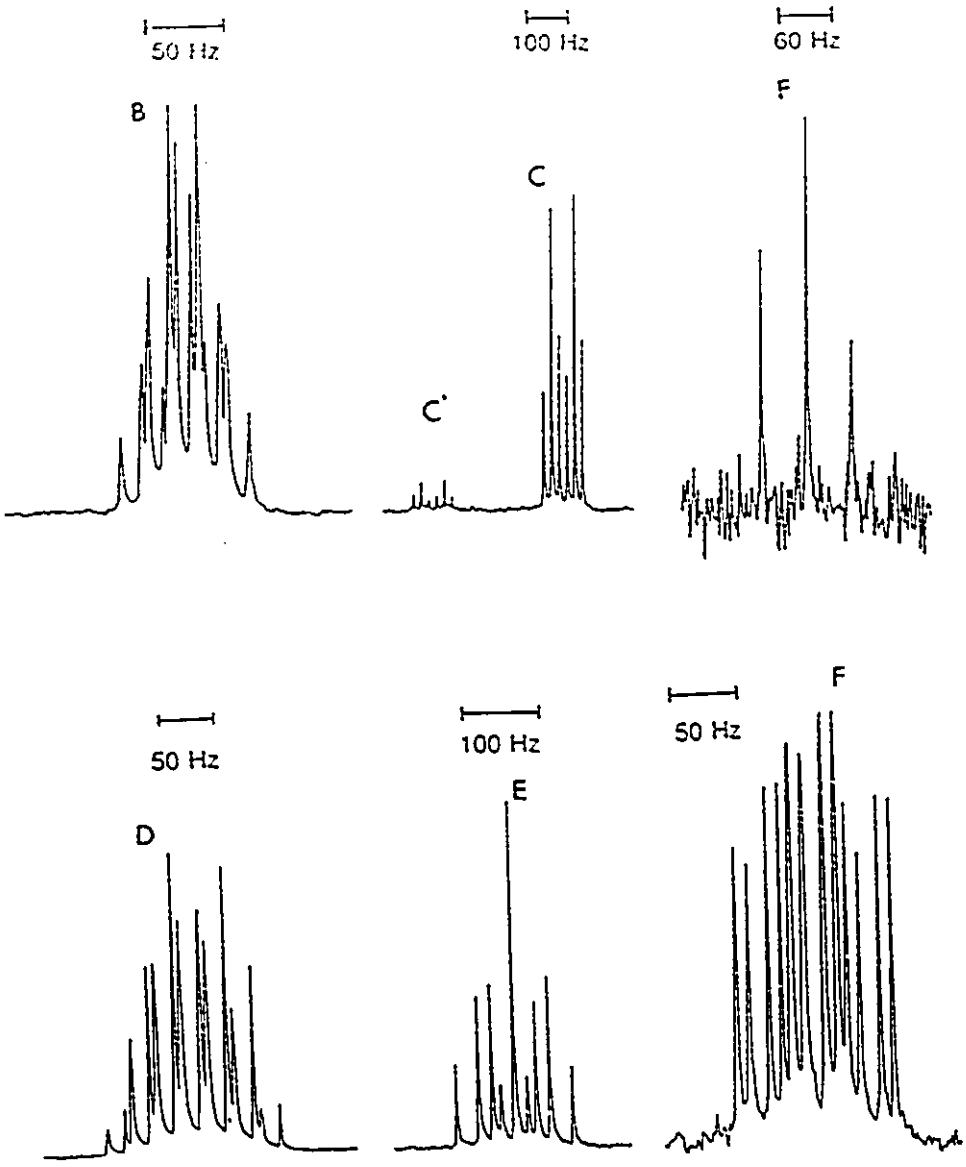

Figure 6.2 ^{19}F NMR spectra (235.361 MHz) resulting from the reaction of a 1:1 stoichiometric mixture of n-$C_3H_7C{\equiv}N$ and $XeF^+AsF_6^-$ in HF after warming the solution for 2 hours at room temperature. Spectra have been expanded from Figure 6.1; (B) $CH_3CF_2CH_2C{\equiv}NH^+$, (C) $CHF_2CH_2CH_2C{\equiv}NH^+$, (C') $CHF_2CH_2CH_2C{\equiv}NXeF^+$, (D) $CH_3CHFCH_2C{\equiv}NH^+$, (E) $CH_2FCH_2CH_2C{\equiv}NH^+$ and (F) unidentified resonance.

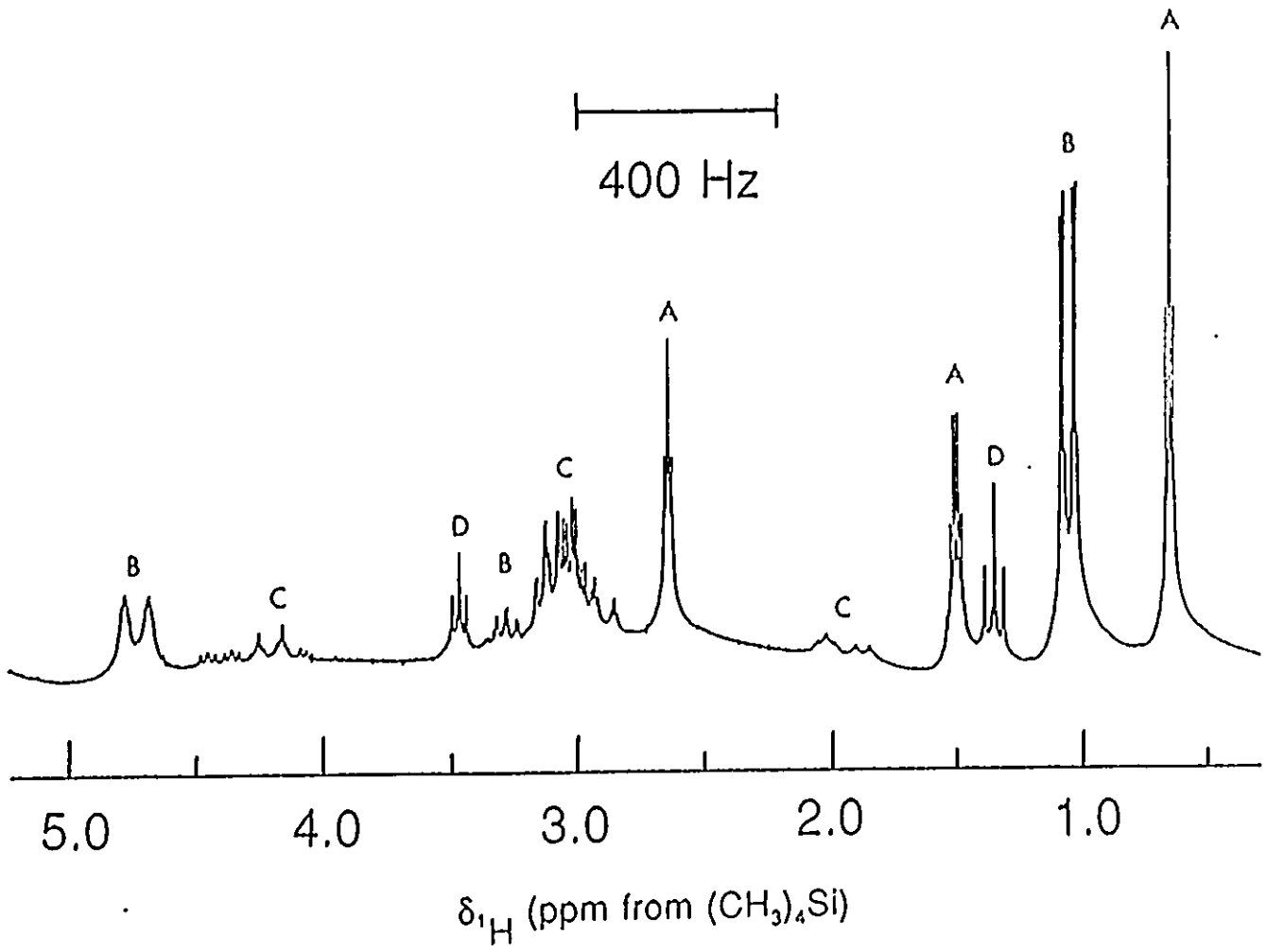

Figure 6.3 ^1H NMR spectrum (500.123 MHz) resulting from the reaction of n-$C_3H_7C{\equiv}N$ and $XeF^+AsF_6^-$ in HF solvent after warming the reaction mixture for 2 hours at room temperature; (A) $CH_3CH_2CH_2C{\equiv}NH^+$, (B) $CH_3CHFCH_2C{\equiv}NH^+$, (C) $CH_2FCH_2CH_2C{\equiv}NH^+$ and (D) $CH_3CF_2CH_2C{\equiv}NH^+$.

(B) CHARACTERIZATION OF THE FLUORINATED PRODUCTS RESULTING FROM THE SOLVOLYSIS OF ALKYL NITRILES IN ANHYDROUS HF BY ^{19}F, ^{15}N, ^{14}N, ^{13}C AND ^{1}H NMR SPECTROSCOPY

Warming solutions of the $RC{\equiv}N\text{-}XeF^+$ adduct cations in anhydrous HF solvent results in fluorination of the alkyl group. The resulting fluorinated nitriles have been characterized by multi-NMR spectroscopy in solution. The reactions of alkyl nitriles with anhydrous HF have also been investigated in a parallel study in order to better define, as in the case of $HC{\equiv}N\text{-}XeF^+$ (see Chapter 4), the fluorination routes in both systems.

The alkyl nitriles, $RC{\equiv}N$ (R = CH_3, C_2H_5, n-C_3H_7, n-C_4H_9), were dissolved in anhydrous HF at room temperature and allowed to react for 7 days at room temperature. All the reactions gave yellow colored solutions except the acetonitrile solution which remained colorless. The ^{19}F NMR spectra of these solutions showed three intense signals and a low-intensity signal in each spectrum (Figure 6.4) and their ^{19}F chemical shifts indicate that they result from related species. After 6 - 12 hours, the same signals were observed but with different relative intensities, indicating that the four ^{19}F signals in each spectrum resulted from different fluorinated species. High-frequency resonances were observed at -7.7 (doublet of quartets of doublets), -14.8 (doublet of triplets of doublets), -13.7 (doublet of triplets of doublets) and -13.6 ppm (doublet of triplets of doublets), which are assigned to $RCF{=}NH_2^+$ (R = CH_3, C_2H_5, n-C_3H_7 and n-C_4H_9), respectively. Three sets of low-frequency resonances were also observed in each spectrum (see Figures 6.4 and 6.5). One set was broad and observed at -79.0, -88.2, -85.8 and -85.7 ppm, and

Figure 6.4 ^{19}F NMR spectra (235.361 MHz) resulting from the solvolysis of (a) $CH_3C{\equiv}N$, (b) $C_2H_5C{\equiv}N$, (c) n-$C_3H_7C{\equiv}N$ and (d) n-$C_4H_9C{\equiv}N$ in HF solvent at -15 °C after warming the reaction mixtures for 7 days at room temperature; (A) $RCF{=}NH_2^+$, (B) $RCF_2NH_3^+$, (C) *Z*-$RCF_2N(H)C(NH_2)R^+$ (Structure 6.2) cations and (D) *E*-$RCF_2N(H)C(NH_2)R^+$ (Structure 6.1) cations.

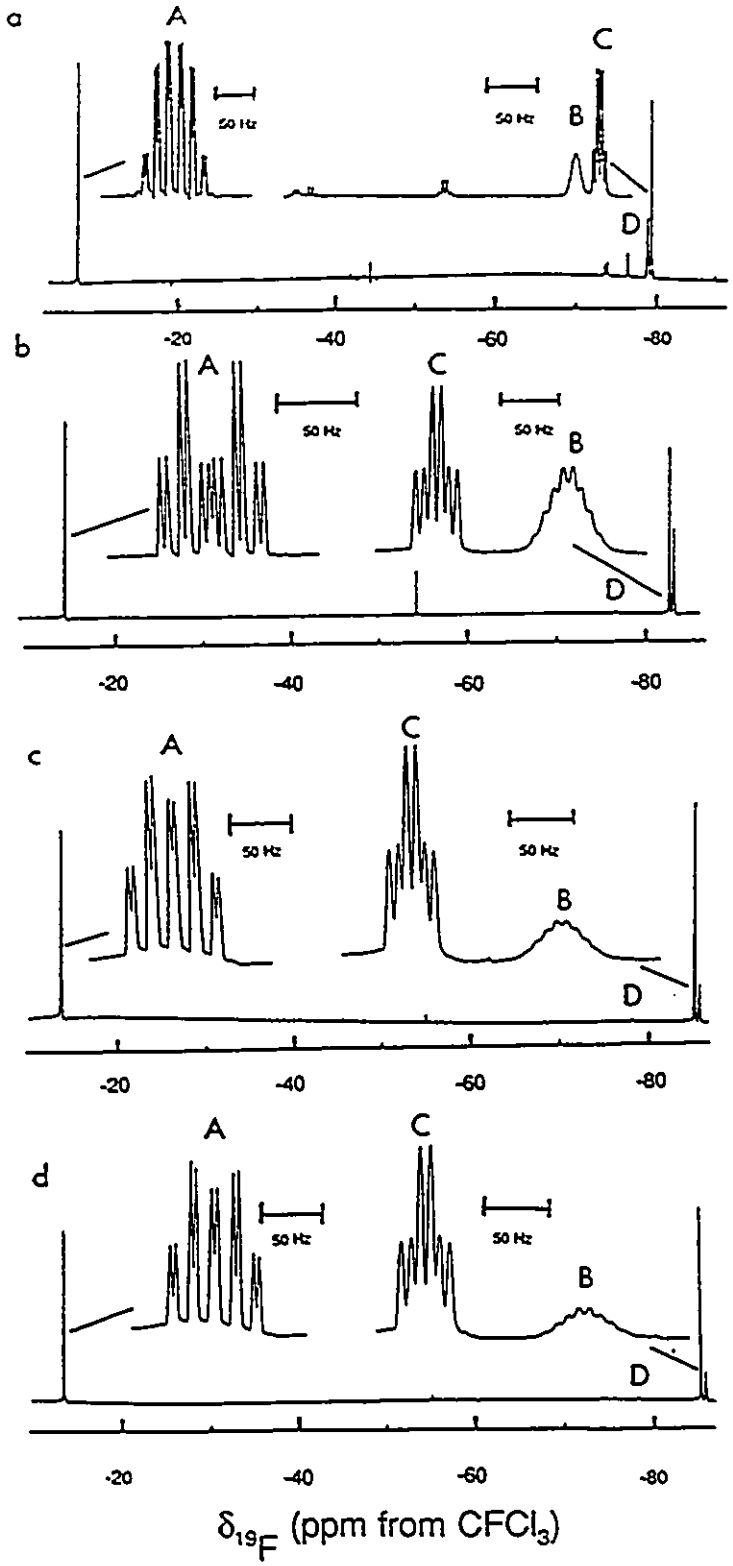
a
A
C
B
D
50 Hz
50 Hz
-20
-40
-60
-80
b
A
C
B
D
50 Hz
50 Hz
-20
-40
-60
-80
c
A
C
B
D
50 Hz
50 Hz
-20
-40
-60
-80
d
A
C
B
D
50 Hz
50 Hz
-20
-40
-60
-80
δ_{19_F} (ppm from $CFCl_3$)

is assigned to the $RCF_2NH_3^+$ (R = CH_3, C_2H_5, n-C_3H_7 and n-C_4H_9) cations, respectively. A second broadened set (C) was observed at -79.7 (doublet of quartets), -85.5 (doublet of triplets), -85.5 (doublet of triplets) and -85.5 (doublet of triplets). Set (D) displayed the same multiplicity pattern as set (C), but was less intense, occurring at -76.5, -79.3, -81.2 and -81.1 ppm. Resonances (C) and (D) are assigned to Structures 6.1 and 6.2

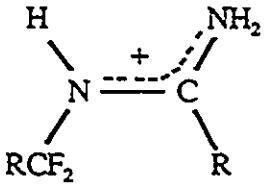

E-isomer

Structure 6.1

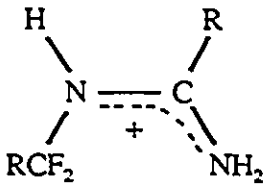

Z-isomer

Structure 6.2

R = CH_3, C_2H_5, n-C_3H_7 and n-C_4H_9.

It was not possible to distinguish between the *E*- and *Z*-isomer cations in the ^{19}F NMR spectra, but based on steric effects and the intramolecular interactions between the hydrogens of the NH_2 group and the fluorines of the CF_2 group, it is expected that the *Z*-isomer is the favored isomer.

The ^1H, ^{14}N and ^{13}C NMR spectra showed several signals which have not been assigned. The ^{19}F NMR spectra of 99.0% ^{13}C-enriched $CH_3{}^{13}C{\equiv}N$ and 99.7% ^{13}C-enriched $^{13}CH_3C{\equiv}N$ in anhydrous HF showed that HF was added to the C≡N bond in all four fluorinated species (Figure 6.5) with fluorination occurring on carbon. These reactions

Figure 6.5 ^{19}F NMR spectra (235.361 MHz) of (a) 99.7% ^{13}C enriched $^{13}CH_3C{\equiv}N$, (b) 99.0% ^{13}C enriched $CH_3{}^{13}C{\equiv}N$ and (c) natural abundance $CH_3C{\equiv}N$, in HF solvent after warming the solutions for 7 days at room temperature; (A) $RCF{=}NH_2^+$, (B) Z-isomer cation (Structure 6.1) and (C) $RCF_2NH_3^+$ cations.

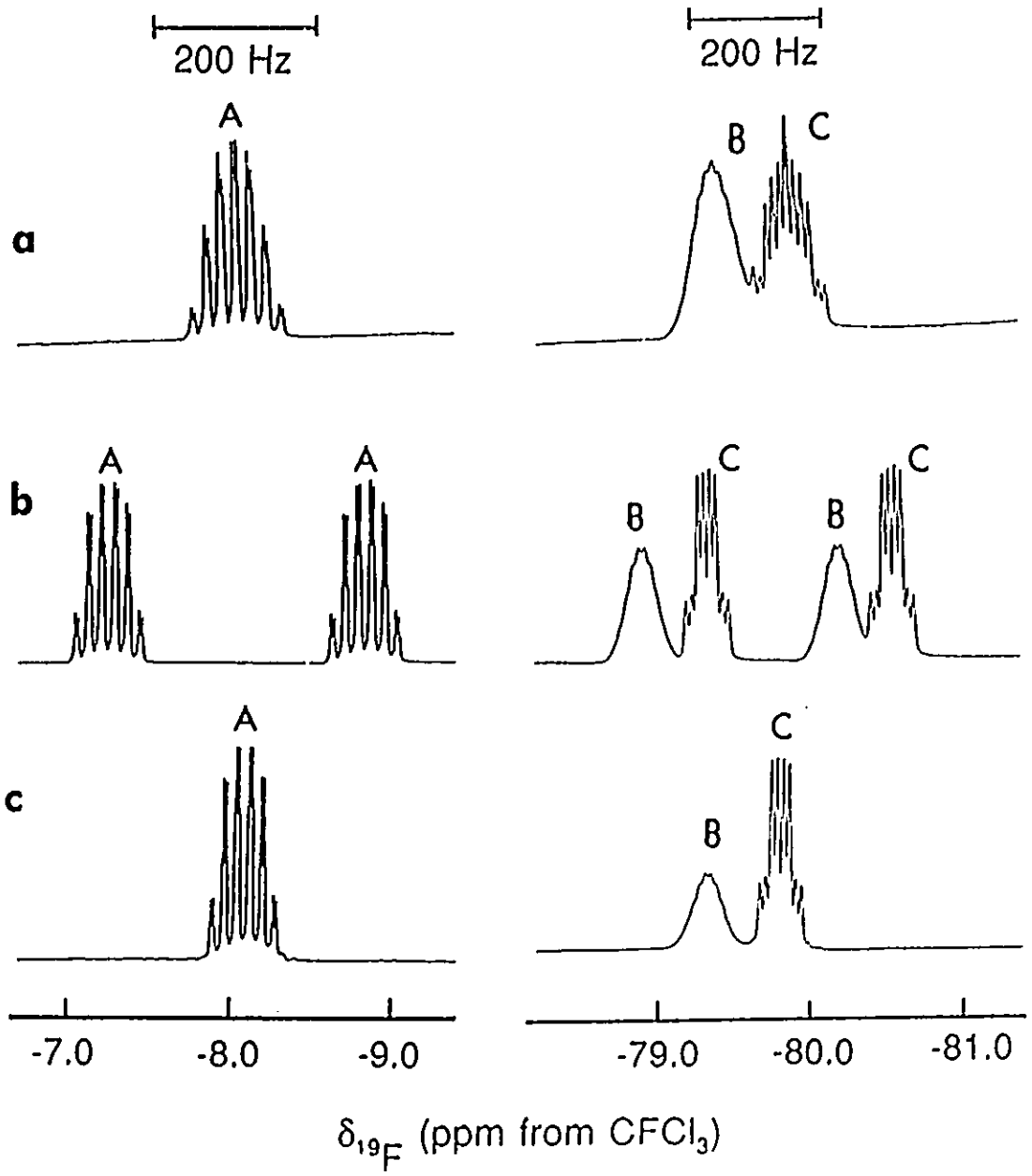
200 Hz
200 Hz
a
b
c
A
B
C
-7.0
-8.0
-9.0
-79.0
-80.0
-81.0
$\delta_{^{19}F}$ (ppm from $CFCl_3$)

were repeated by warming the HF solutions for 7 days at room temperature followed by pumping off the HF solvent at -30 °C for 2 hours. The reaction mixtures were then warmed to room temperature and pumped on for a further 3 days, resulting in colorless viscous liquids. Each sample was redissolved in dry CH_2Cl_2 and evaporated in the hope of obtaining crystalline material. Only in the case of the acetonitrile sample was a solid product isolated when CH_2Cl_2 was evaporated. The final products were redissolved in HF solvent after isolation from CH_2Cl_2 solution and the ^{19}F, ^{15}N, ^{14}N, ^{13}C and ^{1}H NMR spectra recorded. The volatile materials, which had been collected in a -196 °C cold trap, were also studied by multi-NMR spectroscopy. The ^{19}F NMR spectra of the involatile products showed signals arising from two species in the spectrum of each system, which are readily assigned to the *Z*- and *E*-isomers given by Structures 6.1 and 6.2. The ^{19}F NMR spectra of the volatile materials resulting from the reaction of RC≡N in HF at room temperature only showed a single broad signal resulting from HF solvent (-198 ppm); no volatile fluorinated compounds appear to result from these reactions.

In order to more fully characterize the isolated fluorinated products, the reactions of natural abundance $CH_3C{\equiv}N$, 99.7% ^{13}C-enriched $^{13}CH_3C{\equiv}N$ and 99.0% ^{13}C-enriched $CH_3{}^{13}C{\equiv}N$ in anhydrous HF solvent were monitored by ^{1}H and ^{13}C NMR spectroscopy. The most intense resonances in the ^{1}H NMR spectrum of natural abundance $CH_3C{\equiv}N$ in HF, recorded at -15 °C, consisted of a triplet at 1.86 ppm ($^{3}J(^{19}F\text{-}^{1}H)$, 16.4 Hz), assigned to a CH_3CF_2 group, a singlet at 2.26 ppm, assigned to a CH_3 group, a 1:1:1 triplet at 7.49 ppm (57.0 Hz) and a 1:2:1 triplet (14.3 Hz) of 1:1:1 triplets (47.7 Hz) at 7.16 ppm; the latter multiplet results from $J(^{14}N\text{-}^{1}H)$ (Figure 6.6). Carbon-13 enrichment further split

Figure 6.6 ^{1}H NMR spectra (500.125 MHz) of (a) natural abundance $CH_3C{\equiv}N$ in HF solvent at -15 °C; after warming the solution for 7 days at room temperature and (b) natural abundance $Z\text{-}CH_3CF_2N(H)C(NH_2)CH_3^+$ in HF solvent at -15 °C; : (A) $CH_3C{\equiv}NH^+$; (B) $Z\text{-}CH_3CF_2N(H)C(NH_2)CH_3^+$ cation (Structure 6.1), where (B_1) is the ^{1}H resonance of the CH_3CF_2 group and (B_2) is the ^{1}H-on-carbon resonance of the $CH_3C(NH_2)NH$ group; (C) ^{1}H resonance of the $CH_3CF_2NH_3^+$ cation; (D) ^{1}H resonance of the $CH_3CF{=}NH_2^+$ cation; (E) ^{1}H resonances showing $J(^{14}N\text{-}^{1}H)$; (F) unassigned resonances and (G) supressed HF solvent signal.

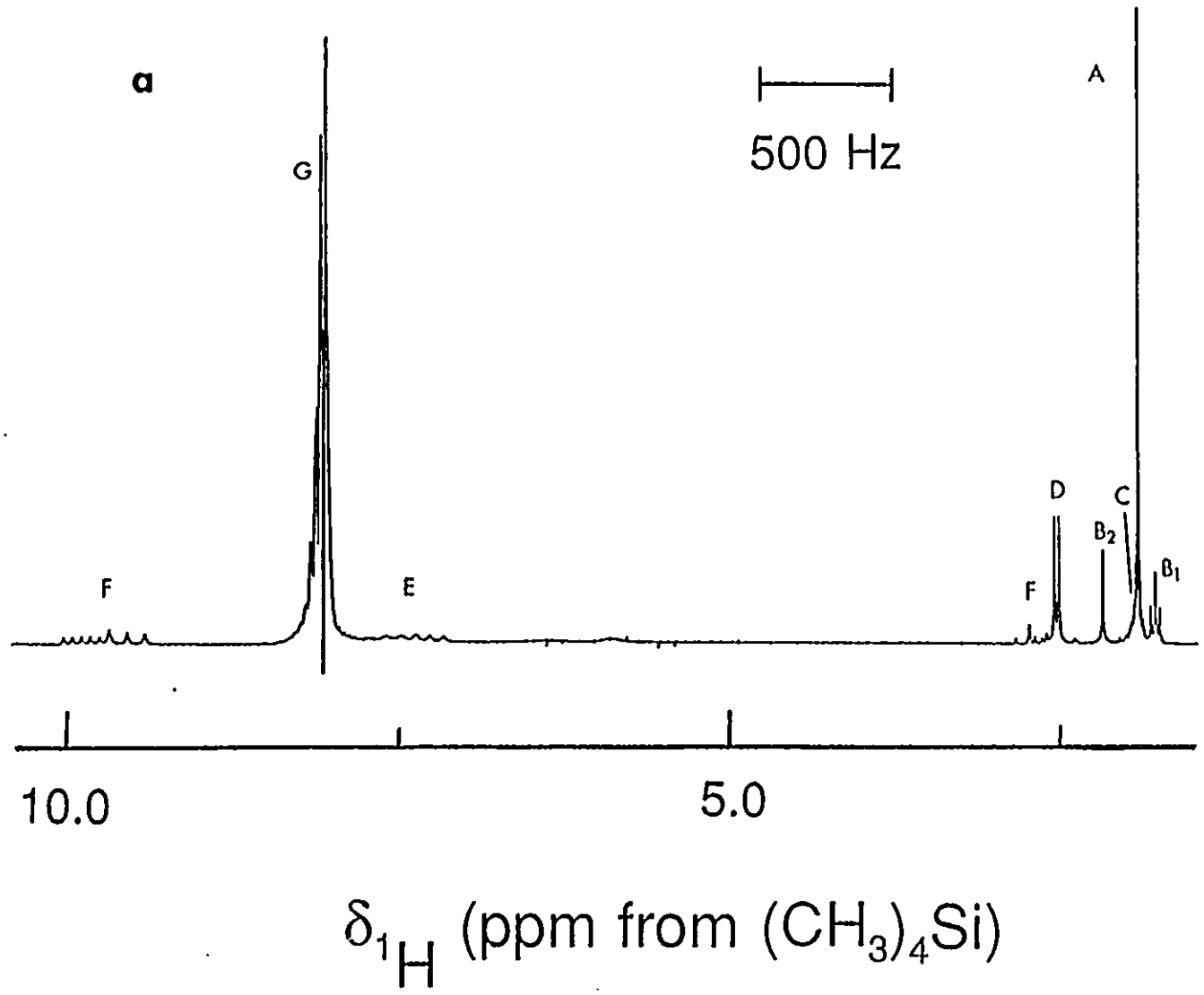
a
500 Hz
A
G
F
E
F
D
C
B2
B1
10.0
5.0
δ1H (ppm from (CH3)4Si)

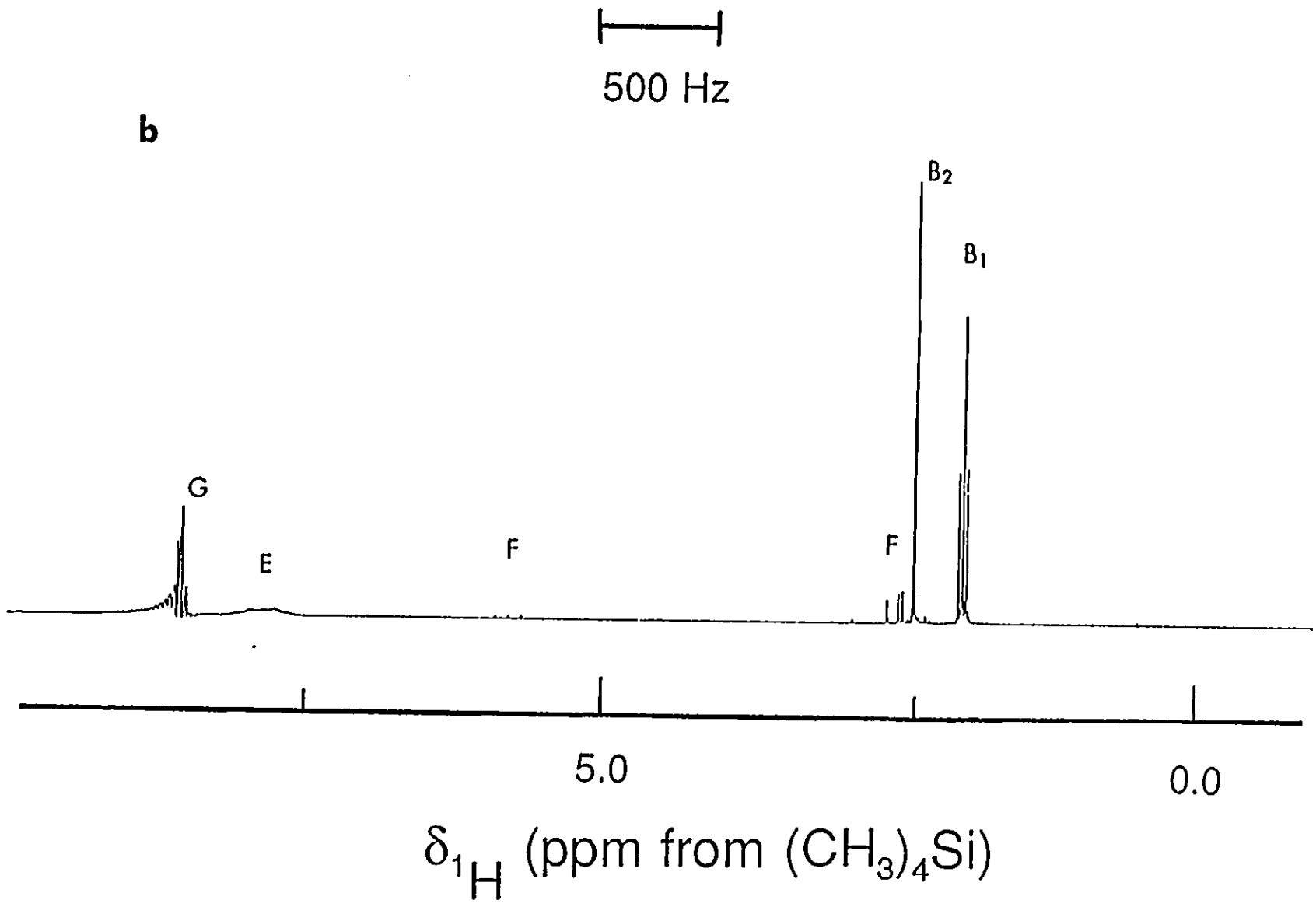
500 Hz
b
B2
B1
G
E
F
F
5.0
0.0
δ1H (ppm from (CH3)4Si)

the latter two signals into a doublet (99.7% ^{13}C-enriched $^{13}CH_3C{\equiv}N$ in HF; $^1J(^{13}C\text{-}^1H)$, 128.9 and 130.8 Hz, respectively, and 99.0% ^{13}C-enriched $CH_3{}^{13}C{\equiv}N$ in HF; $^2J(^{13}C\text{-}^1H)$, 4.7 and 4.9 Hz, respectively). The coupling constant $^3J(^{19}F\text{-}^1H)$, 16.4 Hz, is in good agreement with that observed in the ^{19}F NMR spectrum (a quartet at -79.7 ppm). The further doublet splitting on the quartet is attributed to the proton of an NH group bonded to a CH_3CF_2 group. Presumably addition of two HF molecules to the C≡N bond initially occurs, resulting in $CH_3CF_2NH_3^+$, which then undergoes further reaction to form a compound containing the CH_3CF_2NH- moiety. The ^{1}H NMR spectrum also showed another signal at 2.26 ppm (singlet) which is assigned to a second CH_3 group. The product appears to result from fluorination and dimerization of $CH_3C{\equiv}N$, where the CH_3 signal can be assigned to a $-C(NH_2)CH_3$ moiety and the major fluorinated product is $Z\text{-}CH_3CF_2N(H)C(NH_2)CH_3^+$ (Structure 6.2). The ^{1}H NMR spectra also showed weak signals consisting of a triplet at 1.96 ppm, ($^3J(^{19}F\text{-}^1H)$, 17.1 Hz assigned to a CH_3CF_2 group and a singlet at 2.48 ppm, assigned to a CH_3 group. These two signals are identified as the *E*-isomer (Structure 6.1) and had integrated relative areas *E*-isomer : *Z*-isomer = 4 : 96.

Further evidence for the fluorinated dimer cations was obtained from ^{13}C NMR spectroscopy. The {^{1}H}-decoupled ^{13}C spectrum of the solvolysis products of $CH_3C{\equiv}N$ in anhydrous HF (Figure 6.7a) showed four intense signals corresponding to *Z*-$CH_3CF_2N(H)C(NH_2)CH_3^+$ (Structure 6.2): 4.0 ppm (singlet), CH_3 group of $CH_3C\text{-}NH_2$; 8.8 ppm (triplet; $^3J(^{19}F\text{-}^{13}C)$, 26.5 Hz), CH_3 group of CH_3CF_2; 118.8 ppm (triplet; $^1J(^{19}F\text{-}^{13}C)$, 247.9 Hz), CF_2 group and 167.9 ppm (singlet), $C{=}NH_2$ group. The ^{13}C NMR spectra of

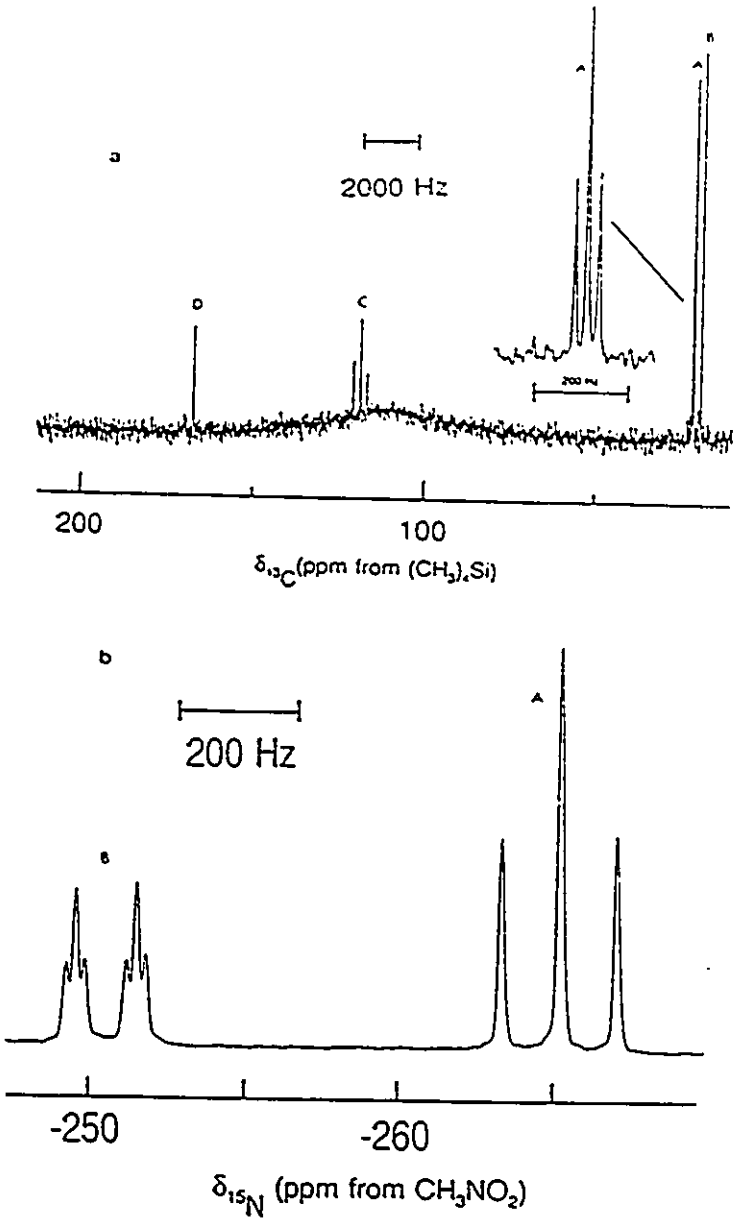

Figure 6.7 (a) Natural abundance ^{13}C NMR spectrum (125.760 MHz) of *Z*-$CH_3CF_2N(H)C(NH_2)CH_3^+$ (Structure 6.2) in HF solvent at -15 °C; (A) CH_3 group bonded to CF_2, (B) CH_3 bonded to C-NH_2, (C) CF_2 and (D) C-NH_2. (b) ^{15}N NMR spectrum (50.698 MHz) of the 99.0% ^{15}N-enriched *Z*-$CH_3CF_2N(H)C(NH_2)CH_3^+$ (Structure 6.2) in HF solvent at -15 °C; (A) NH_2 group and (B) NH group.

99.0% ^{13}C-enriched $CH_3{}^{13}C{\equiv}N$ in HF provided further evidence for dimerization and *Z*-$CH_3CF_2N(H)C(NH_2)CH_3^+$ cation and showed $^2J(^{13}C\text{-}^{13}C)$, 2 Hz (Figure 6.12). The ^{15}N NMR spectrum of 99.0% enriched $CH_3C{\equiv}^{15}N$ in anhydrous HF recorded at -15 °C (Figure 6.7b) showed two signals, one at -265.2 ppm (triplet; $^1J(^{15}N\text{-}^1H)$, 95.6 Hz) resulting from the NH_2 group and the other at -250.5 ppm (doublet of triplets; $^1J(^{15}N\text{-}^1H)$, 98.0 Hz and $^3J(^{19}F\text{-}^{15}N)$, 15.3 Hz) resulting from the CF_2NH- group of *Z*-$CH_3CF_2N(H)C(NH_2)CH_3^+$.

The NMR findings conclusively demonstrate that the dominant product from the solvolysis of $CH_3C{\equiv}N$ in HF is *Z*-$CH_3CF_2N(H)C(NH_2)CH_3^+$. It has also been possible to characterize two other intermediates which form prior to *E*- and *Z*-$CH_3CF_2N(H)C(NH_2)CH_3^+$ which have been characterized in HF solvent at -15 °C as the $CH_3CF{=}NH_2^+$ and $CH_3CF_2NH_3^+$ cations.

The $RC{\equiv}NH^+$ (R = CH_3, C_2H_5, *n*-C_3H_7 and *n*-C_4H_9) cations have also been identified by dissolving the alkyl nitriles in HF solvent and recording their ^{13}C and ^{1}H NMR spectra at -15 °C prior to warming their HF solutions to room temperature; their NMR parameters are listed in Table 6.3. The full NMR characterizations of the *E*- and *Z*-$RCF_2N(H)C(NH_2)R^+$, $RCF{=}NH_2^+$ and $RCF_2NH_3^+$ (R = CH_3, C_2H_5, *n*-C_3H_7 and *n*-C_4H_9) cations by multi-NMR spectroscopy are discussed below:

(i) <u>Characterization of the *E*- and *Z*-$RCF_2N(H)C(NH_2)R^+$ (R = CH_3, C_2H_5, *n*-C_3H_7 and *n*-C_4H_9) Cations in HF Solvent</u>

It has been found in previous studies[214] that the reactions of the alkyl nitriles, $RC{\equiv}N$ (R = CH_3, C_2H_5, *n*-C_3H_7 and *n*-C_4H_9), with anhydrous HCl form dimeric

Table 6.3

NMR Parameters for RC≡N in Anhydrous HF Solvent at -15 °C

	Chemical Shifts (ppm)[a]		Coupling Constants (Hz)	
Nitriles	$\delta(^1H)$	$\delta(^{13}C)$	$^3J(^1H\text{-}^1H)$	$^1J(^{13}C\text{-}^1H)$
$CH_3C{\equiv}NH^+$	2.17 (CH_3)	-1.3 (CH_3) 114.3 (C≡N)		
$CH_3CH_2C{\equiv}NH^+$	1.22 (CH_3) 2.43 (CH_2)	8.2 (CH_3) 9.2 (CH_2) 118.0 (C≡N)	7.6	131.8 (CH_3) 137.5 (CH_2)
$CH_3CH_2CH_2C{\equiv}NH^+$ 1 2 3	2.09 (CH_3)$_1$ 2.76 (CH_2)$_2$ 3.52 (CH_2)$_3$	11.5 (CH_3)$_1$ 17.5 (CH_2)$_2$ 18.3 (CH_2)$_3$ 116.7 (C≡N)	7.0 (CH_3CH_2) 7.4 (CH_2CH_2)	126.5 (CH_3)$_1$ 136.4 (CH_2)$_2$ 132.4 (CH_2)$_3$
$CH_3CH_2CH_2CH_2C{\equiv}NH^+$ 1 2 3 4	0.89 (CH_3)$_1$ 1.40 (CH_2)$_2$ 1.61 (CH_2)$_3$ 2.47 (CH_2)$_4$	11.6 (CH_3)$_1$ 15.4 (CH_2)$_2$ 21.7 (CH_2)$_3$ 26.5 (CH_2)$_4$ 116.6 (C≡N)	7.4 (CH_2)$_1$(CH_2)$_2$ 7.8 (CH_2)$_2$(CH_2)$_3$ 7.2 (CH_2)$_3$(CH_2)$_4$	124.5 (CH_3)$_1$ 136.8 (CH_2)$_2$ 126.4 (CH_2)$_3$ 130.4 (CH_2)$_4$

a Referenced externally at 30 °C with respect to neat TMS (^{13}C and ^1H).

hydrochlorides in which the dimer cations have Structure 6.3

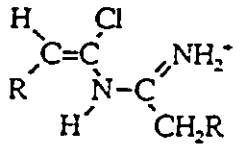

R = H, CH_3, C_2H_5 or n-C_3H_7

Structure 6.3

As mentioned previously, the dominant product resulting from the solvolysis of $CH_3C{\equiv}N$ in HF is Z-$CH_3CF_2N(H)C(NH_2)CH_3^+$. A full investigation of the dimer products resulting from the solvolysis of the longer chain alkyl nitriles has been undertaken and the NMR findings are shown to be consistent with E- and Z-$RCF_2N(H)C(NH_2)R^+$ cation structures where the Z-isomer dominates.

The ^{19}F NMR spectra of the Z-isomer (R = C_2H_5, n-C_3H_7 and n-C_4H_9) cations show multiplets consisting of a triplet of doublets having essentially the same chemical shift (-85.5 ppm). The multiplets result from $^3J(^{19}F\text{-}^1H)_{CH_2}$ (14.8 Hz) and $^3J(^{19}F\text{-}^1H)_{NH}$ (7.8 Hz). The coupling constants, $^3J(^{19}F\text{-}^1H)_{CH_2}$, agree with those measured in the ^1H NMR spectra. The ^1H NMR spectra for the Z-isomer cations in HF solvent were more complex and required the use of ^1H 2D NMR experiments to identify all the ^1H resonances in these cations and their connectivities. Table 6.4 lists the chemical shifts and coupling constants for the Z-isomer cations in HF solvent.

The $\{^1H\}$-decoupled ^{13}C NMR spectra of natural abundance Z-$CH_3CF_2N(H)C(NH_2)CH_3^+$ (Structure 6.2) in anhydrous HF (Figure 6.7a) showed two separate resonances for the two CH_3 groups; the assignments of both resonances were based on the expected higher-frequency shift for the CH_3 group in the CH_3CF_2 moiety

Table 6.4

NMR Chemical Shifts and Coupling Constants of *Z*-$RCF_2N(H)C(NH_2)R^+$ (R = CH_3, C_2H_5, *n*-C_3H_7 and *n*-C_4H_9) Cations in Anhydrous HF Solvent

	Z-$RCF_2N(H)C(NH_2)R^+$ [a]			
	(1)	(2)	(3)	(4)
Chemical Shifts (ppm)				
$\delta(^{19}F)$[b]	-79.7	-85.5	-85.5	-85.5
$\delta(^{1}H)$[c]	2.03 $(CH_3)_1$	2.01 $(CH_3)_1$	1.16 $(CH_3)_1$	0.91 $(CH_3)_1$
	2.41 $(CH_3)_2$	2.15 $(CH_3)_2$	1.17 $(CH_3)_2$	0.93 $(CH_3)_2$
		3.46 $(CH_2)_3$	1.67 $(CH_2)_3$	1.53 $(CH_2)_3$
		3.03 $(CH_2)_4$	1.78 $(CH_2)_4$	1.68 $(CH_2)_4$
			2.22 $(CH_2)_5$	1.39 $(CH_2)_5$
			2.56 $(CH_2)_6$	1.42 $(CH_2)_6$
				2.17 $(CH_2)_7$
				2.53 $(CH_2)_8$
$\delta(^{13}C)$[c]	23.3 $(CH_3)_1$	4.0 $(CH_3)_1$	11.4 $(CH_3)_1$	11.7 $(CH_3)_1$
	18.5 $(CH_3)_2$	8.8 $(CH_3)_2$	11.6 $(CH_3)_2$	12.0 $(CH_3)_2$
		28.6 $(CH_2)_3$		21.8 $(CH_2)_3$
		27.6 $(CH_2)_4$	20.5 $(CH_2)_3$	21.8 $(CH_2)_4$
			14.9 $(CH_2)_4$	23.3 $(CH_2)_5$
			37.2 $(CH_2)_5$	29.0 $(CH_2)_6$
			35.9 $(CH_2)_6$	34.0 $(CH_2)_7$
		120.4 (CF_2)		35.1 $(CH_2)_8$
	118.8 (CF_2)	172.3 (C=N)		120.3 (CF_2)
	167.9 (C=N)			171.6 (C=N)
			120.2 (CF_2)	
			171.5 (C=N)	
$\delta(^{14/15}N)$[b,c]	-250.5 (NH)	d	d	d
	-265.2(NH_2)	-271.0 (NH_2)	-271.3 (NH_2)	-268.4 (NH_2)

Continued...

Table 6.4 (continued)

	$Z\text{-}RCF_2N(H)C(NH_2)R^+$ [a]			
	(1)	(2)	(3)	(4)
Coupling Constants (Hz)				
$^3J(^{19}F\text{-}^1H)$	16.4 (CF_2CH_3) 8.7 (CF_2NH)	14.8 (CF_2)(CH_2)$_3$ 7.8 (CF_2NH)	14.8 (CF_2)(CH_2) 7.8 (CF_2NH)	14.8 (CF_2)(CH_2) 7.8 (CF_2NH)
$^1J(^{19}F\text{-}^{13}C)$	247.9 (CF_2)	250.2 (CF_2)	250.0 (CF_2)	247.7 (CF_2)
$^2J(^{19}F\text{-}^{13}C)$	26.5 (CF_2CH_3)	24.9 (CF_2CH_2)	25.2 (CF_2CH_2)	23.3 (CF_2CH_2)
$^3J(^1H\text{-}^1H)$		7.5 (CH_3)$_1$(CH_2)$_3$ 7.7 (CH_3)$_2$(CH_2)$_4$	7.8 (CH_3)$_1$(CH_2)$_3$ 8.0 (CH_3)$_2$(CH_2)$_4$ 6.6 (CH_2)$_3$(CH_2)$_5$ 7.4 (CH_2)$_4$(CH_2)$_6$	8.4 (CH_3)$_1$(CH_2)$_3$ 7.3 (CH_3)$_2$(CH_2)$_4$ 7.7 (CH_2)$_3$(CH_2)$_5$ 6.8 (CH_2)$_4$(CH_2)$_6$ 6.6 (CH_2)$_5$(CH_2)$_7$ 8.3 (CH_2)$_6$(CH_2)$_8$
$^1J(^{13}C\text{-}^1H)$	128.9 (CH_3)$_1$ 130.8 (CH_3)$_2$	129.4 (CH_3)$_1$ 130.4 (CH_3)$_2$ 130.5 (CH_2)$_3$ 130.2 (CH_2)$_4$	129.7 (CH_3)$_1$ 126.0 (CH_3)$_2$ 127.2 (CH_2)$_3$ 128.4 (CH_2)$_4$ 129.1 (CH_2)$_5$ 134.1 (CH_2)$_6$	125.6 (CH_3)$_1$ 125.7 (CH_3)$_2$ 125.2 (CH_2)$_3$ 125.2 (CH_2)$_4$ 124.1 (CH_2)$_5$ 132.8 (CH_2)$_6$ 126.4 (CH_2)$_7$ 132.7 (CH_2)$_8$
$^2J(^{13}C\text{-}^1H)$	4.7 (CH_3)$_1$ 4.9 (CH_3)$_2$	4.8 (CH_2)$_1$(CH_3)$_3$ 4.5 (CH_2)$_2$(CH_3)$_4$ 6.5 (CF_2)(CH_2)$_3$		
$^2J(^{19}F\text{-}^{15}N)$	15.3 (CF_2NH)			
$^2J(^{13}C\text{-}^{13}C)$	2.0 ($CF_2NHC\text{-}NH_2^+$)			
$^1J(^{15}N\text{-}^1H)$	95.6 (NH_2) 98.0 (NH)			

Continued...

Table 6.4 (continued)

a The numbering scheme used to denote the NMR parameters for the *Z*-$RCF_2N(H)C(NH_2)CR^+$ cations is:

(1)

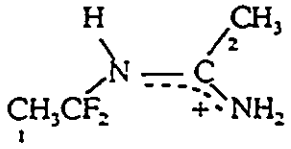

(2)

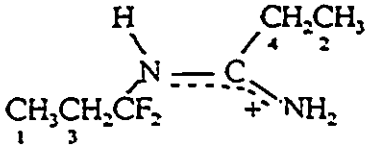

(3)

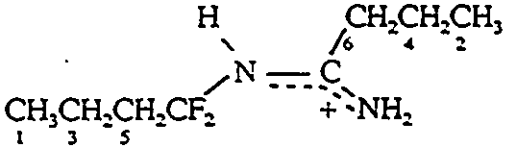

(4)

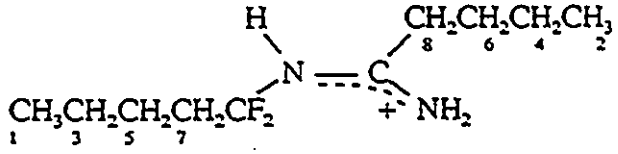

b Samples were referenced externally at 24 °C with respect to the neat liquid references $CFCl_3$ (^{19}F) and CH_3NO_2 (^{14}N).

c Samples were referenced externally at 30 °C with respect to the neat liquid reference TMS (^{13}C and ^{1}H) and CH_3NO_2 (^{15}N).

d The $\delta(^{14}N)$ chemical shifts of the NH group showed broad peaks overlapped with the more intense signals of the NH_2 groups and could not be resolved.

than in the CH_3C-NH_2 moiety. The high-frequency shift for the CH_3 group in the CH_3CF_2 moiety arises because the CH_3 group is bonded to the strongly electron withdrawing CF_2 group. The {^{1}H}-decoupled ^{13}C resonance of the CH_3 group in the CH_3CF_2 moiety of Z-$CH_3CF_2N(H)C(NH_2)CH_3^+$ was a triplet resulting from $^3J(^{19}F$-$^{13}C)$ (26.5 Hz) and was shifted to higher frequency than the ^{13}C resonance of the CH_3 group (singlet) in the CH_3C-NH_2 moiety ($\Delta\ \delta$ = 4.8 ppm, Figure 6.7a).

The ^{13}C NMR spectra of the Z-$C_2H_5CF_2N(H)C(NH_2)C_2H_5^+$ (Structure 6.2) showed six resolved resonances corresponding to two CH_3, two CH_2, a CF_2 and a C=N carbon. The chemical shifts and splitting patterns for the CH_2 groups are in agreement with the proposed cation structure. The {^{1}H}-coupled ^{13}C NMR spectrum showed that the ^{13}C resonance of the CH_2 group at 28.6 ppm in the $CH_3CH_2CF_2$ moiety was split into a triplet of triplets of quartets resulting from $^1J(^{13}C$-$^1H)$, 130.5 Hz; $^2J(^{19}F$-$^{13}C)$, 24.9 Hz and $^2J(^{13}C$-$^1H)$, 4.8 Hz, respectively, while the ^{13}C resonance of the CH_2 group in the CH_3CH_2C-NH_2 moiety at 27.6 ppm showed a triplet of poorly resolved quartets, resulting from $^1J(^{13}C$-$^1H)$, 130.2 Hz and $^2J(^{13}C$-$^1H)$, 4.5 Hz, respectively. The poor resolution on the quartet is attributed to residual scalar couplings to ^{14}N. The ^{13}C NMR spectrum also showed the ^{13}C resonances of the C=N and CF_2 groups at 172.3 (singlet) and 120.4 (triplet of triplets; $^1J(^{19}F$-$^{13}C)$, 250.2 Hz and $^2J(^{13}C$-$^1H)$, 6.5 Hz) ppm, respectively (Figure 6.8).

The ^{13}C resonances of the Z-$RCF_2N(H)C(NH_2)R^+$ (R = *n*-C_3H_7 and *n*-C_4H_9) cations have been assigned using ^{13}C-DEPT, ^{13}C-^{1}H spin-sort and ^{13}C {^{1}H}-broad-band decoupling experiments. The ^{13}C-DEPT experiments were carried out in order to distinguish between the resonances of the CH_3 groups (negative phasing) and CH_2 groups (positive phasing).

Figure 6.8 ^{13}C NMR spectra (125.760 MHz), at -15 °C of a sample of Z-$C_2H_5CF_2N(H)C(NH_2)C_2H_5^+$ (Structure 6.2) that had been isolated from the reaction of the natural abundance $C_2H_5C{\equiv}N$ in HF after warming the reaction mixture for 7 days at room temperature and redissolved in HF solvent; (a) $\{^1H\}$-coupled, (b) $\{^1H\}$-decoupled and (c) expansions of the $\{^1H\}$-coupled spectrum (a).

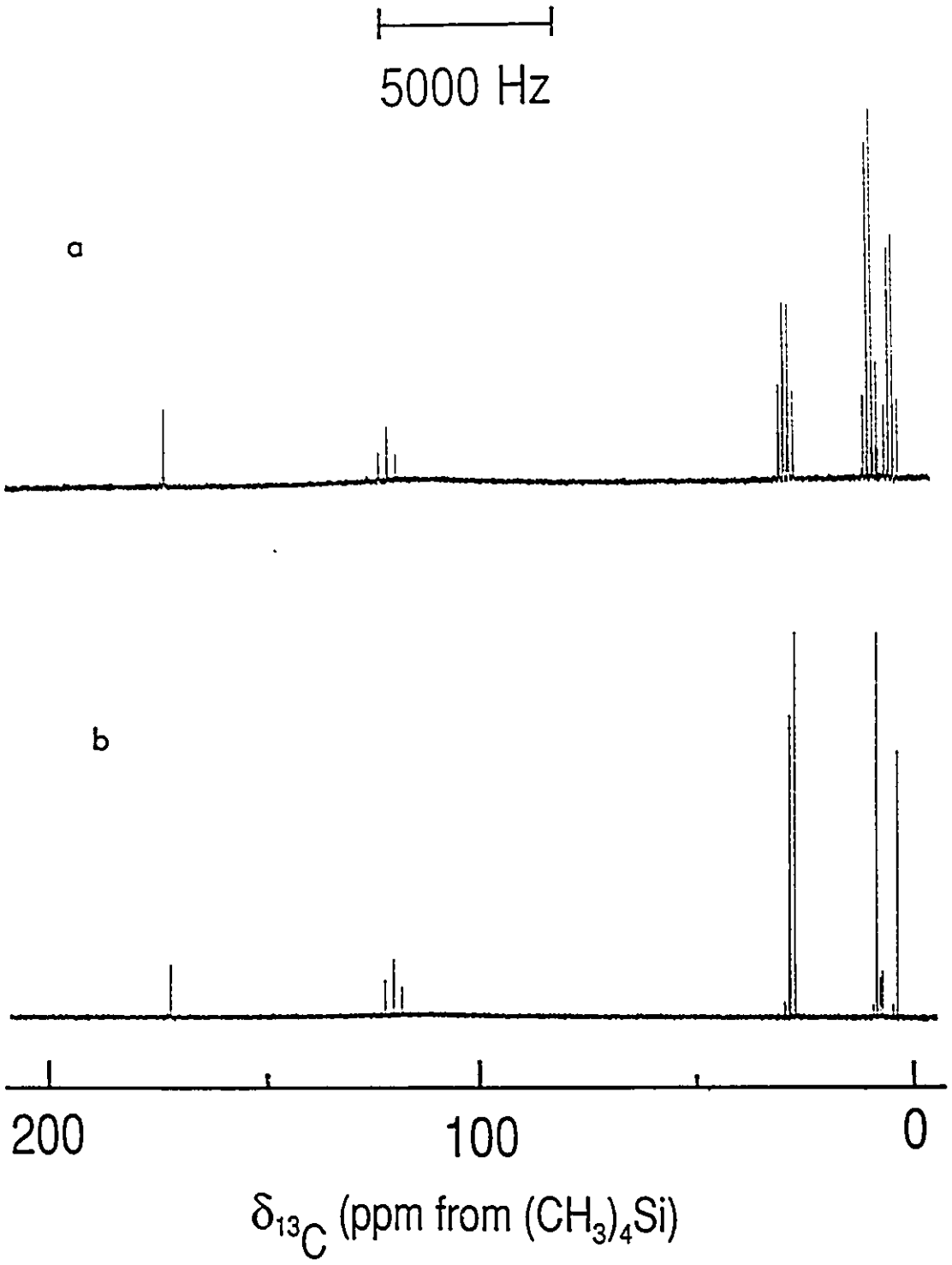
5000 Hz
a
b
200
100
0
δ13C (ppm from (CH3)4Si)

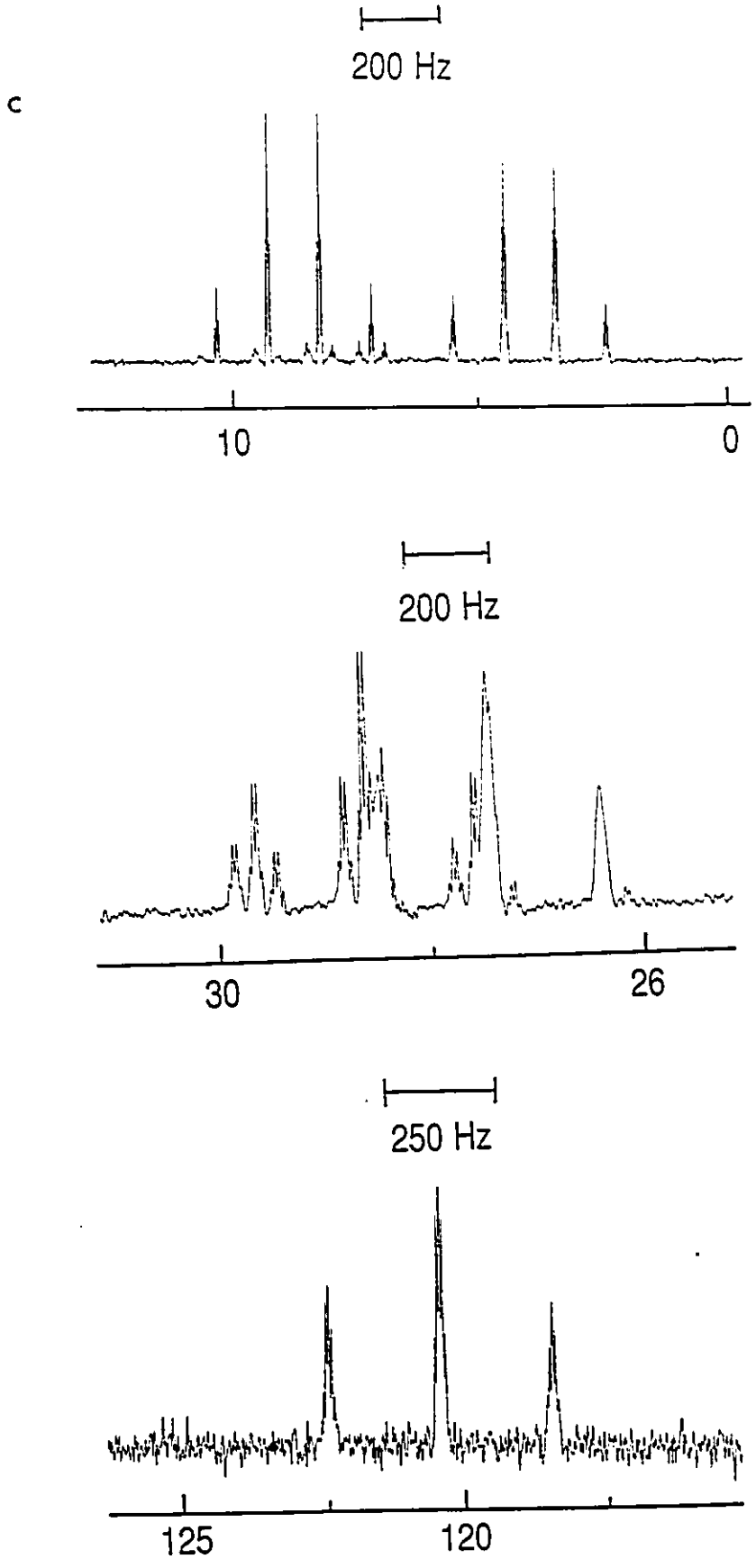
200 Hz
c
10
0
200 Hz
30
26
250 Hz
125
120
$\delta_{^{13}C}$ (ppm from $(CH_3)_4Si$)

The ^{13}C-^{1}H spin-sort experiments have been used to distinguish between the two different CH_3 groups and two sets of $(CH_2)_n$ (n = 2 or 3) chains. The ^{13}C $\{^{1}H\}$-broad band decoupled experiments were used to differentiate between the $J(^{19}F$-$^{13}C)$ and $J(^{13}C$-$^{1}H)$ coupling constants.

The formal hybridizations of the nitrogen atoms of the -NH and NH_2 groups in the *E*- and *Z*-$CH_3CF_2N(H)C(NH_2)CH_3^+$ cations (Structures 6.1 and 6.2) can be correlated with $^{1}J(^{15}N$-$^{1}H)$ using equation (4.8), which has been discussed in detail in Chapter 4. The %s characters of the N atoms are equal to 35.1% and 35.4% (*E*-isomer) and 32.2% and 36.1% (*Z*-isomer) for the NH_2 and NH groups, respectively, and are consistent with the sp^2 hybridization of the nitrogens in these cations. These findings establish that the positive charge is distributed over two nitrogen centers, forming partial double bonds between each nitrogen and the attached carbon, giving rise to planar cations (Structures 6.1 and 6.2).

Due to the weak nature of the double bond in the -NH=C-NH_2(R) moiety, hindered rotation about the double bond results in the formation of both the *E*- and *Z*-isomers. It has not been possible to differentiate between the *E*- and *Z*-isomers using NMR spectroscopy. However, the possibility of intramolecular interactions between the NH_2 and CF_2 groups in the form of hydrogen bonding and steric interactions between the two alkyl groups are expected to favor the *Z*-isomer over the *E*-isomer. These assignments are supported by observation that the ratio [*Z*-isomer] : [*E*-isomer] increases with increasing alkyl chain length.

Although the ^{15}N NMR spectrum of the products resulting from the reaction of

99.0% ^{15}N enriched $CH_3C{\equiv}^{15}N$ in HF was well resolved for the *Z*-isomer, the ^{14}N NMR spectra of *Z*-$RCF_2N(H)C(NH_2)R^+$ (R = CH_3, C_2H_5, *n*-C_3H_7 and *n*-C_4H_9) in HF solvent showed poorly resolved, broad signals which are attributed to partially quadrupole collapsed scalar couplings to ^{14}N. It was possible to assign the ^{14}N resonances of the NH_2 groups, but not those of the NH groups. Table 6.4 lists the chemical shifts and coupling constants of the *Z*-isomer cations in HF solvent at -15 °C.

The mass spectrum of the isolated product mixture resulting from the solvolysis of $C_2H_5C{\equiv}N$ in HF showed that the parent ion was triethyltriazine, m^+/e 165. Trimerization presumably occurs in the gas phase with the loss of fluoride ion and is favored at high temperature by the aromatic character of the ring.

The ^1H, ^{19}F and ^{13}C NMR spectra also showed other minor fluorinated products which have been identified as *E*-$RCF_2N(H)C(NH_2)R^+$ and which have intensity ratios of 4 : 96, 3 : 97, 2 : 98 and 2 : 98 relative to their *Z*-isomers (R = CH_3, C_2H_5, *n*-C_3H_7 and *n*-C_4H_9). All have the ^{19}F NMR signals at -76.5 (doublet of triplets). The NMR parameters of the natural abundance, 99.0%, 99.7% ^{13}C-enriched and 99.0% ^{15}N-enriched *E*-isomer cations are listed in Table 6.5.

It is clear from the resulting dimer cation series that the solvolyses of the RC≡N in anhydrous HF solvent differ significantly from those in anhydrous HCl. Moreover, the fluorinations of RC≡N in HF solvent also differ dramatically from the solvolyses of RC≡N-XeF^+ cations in HF solvent.

Table 6.5

NMR Parameters of the *E*-$CH_3CF_2N(H)C(NH_2)CH_3^+$ Cations in HF Solvent at -15 °C[a]

Chemical Shifts (ppm)[b]		Coupling Constants (Hz)	
$\delta(^{19}F)$	-76.5	$^3J(^{19}F\text{-}^1H)$	17.1 $(CH_3)_1$
$\delta(^1H)$	1.96 $(CH_3)_1$ 2.48 $(CH_3)_2$	$^3J(^{19}F\text{-}^1H)$	7.3 (NH)
$\delta(^{13}C)$[c]	21.7 $(CH_3)_1$ 19.2 $(CH_3)_2$ 119.2 (CF_2) 170.5 $(C{=}NH_2)$	$^1J(^{13}C\text{-}^{19}F)$ $^1J(^{13}C\text{-}^1H)$ $^1J(^{13}C\text{-}^1H)$ $^2J(^{13}C\text{-}^{13}C)$ $^2J(^{19}F\text{-}^{13}C)$	257.6 128.9 $(CH_3)_1$ 130.8 $(CH_3)_2$ 2.4 27.0
$\delta(^{15}N)$[d]	-232.8 (NH) -244.6 (NH_2)	$^1J(^{15}N\text{-}^1H)$ $^1J(^{15}N\text{-}^1H)$	96.3 (NH) 95.5 (NH_2)

a Unless otherwise indicated, NMR parameters are reported for the natural abundance samples. The numbering scheme used to denote the NMR parameters is:

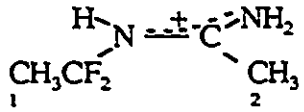

b The sample was referenced externally at 24 °C with respect to the neat liquid reference $CFCl_3$ (^{19}F) and at 30 °C with respect to the neat liquid references TMS (^{13}C and ^1H) and CH_3NO_2 (^{15}N).

c NMR parameters for 99.0% ^{13}C-enriched 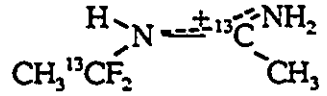 and 99.7% ^{13}C-enriched 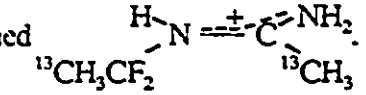 .

d NMR parameters for 99.0% ^{15}N-enriched 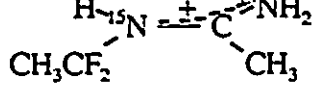 .

(ii) Characterization of $RCF{=}NH_2^+$ and $RCF_2NH_2^+$ Cations in HF Solvent

In the previous sections, it has been possible to show by ^1H and ^{13}C NMR spectroscopy that the alkyl nitriles are protonated and the resulting $RC{\equiv}NH^+$ cations are stable in anhydrous HF solvent at -15 °C (Table 6.3). Warming these solutions for several hours at room temperature led to solvolysis reactions which have been monitored by NMR spectroscopy. The ^{19}F, ^{14}N, ^{13}C and ^1H NMR spectra showed that several fluorinated products were formed. The ^{19}F NMR spectra in HF solution showed that there are three dominant resonances and one weak resonance in each system and that they result from four different fluorinated products. In addition, $RC{\equiv}NH^+$ cations have also been identified in the reaction mixture by ^1H and ^{13}C NMR spectroscopy. Isolation of the fluorination products from HF solvent by cold trapping of the HF solvent and volatile products from each reaction yielded viscous liquid residues. These liquids have been identified as the fluorinated dimer cations, *E*- and *Z*-$RCF_2N(H)C(NH_2)R^+$, which give rise to two ^{19}F resonances in each spectrum. These resonances have also been observed in the ^{19}F NMR spectra of the original reaction mixtures. The ^{19}F and ^1H NMR spectra of HF and volatile products trapped at -196 °C from the reaction mixture only showed HF signals ($\delta(^{19}F)$, -198.2 and $\delta(^1H)$, 8.28 ppm) with no other volatile products.

From these findings, it may be concluded that the reaction of $RC{\equiv}N$ in HF results in two other fluorinated products and $RC{\equiv}NH^+$; the former are present as intermediates and are in equilibrium with the fluorinated dimer cations *E*- and *Z*-$RCF_2N(H)C(NH_2)R^+$. The intermediates are presumably responsible for the yellow colors which have been observed during the reactions of the nitriles in HF at room temperature. It was not

possible to identify the two fluorinated intermediates in the initial NMR spectra of warmed solutions of RC≡N in HF solvent, but after isolation and characterization of the final fluorinated dimeric cations, it became easier to characterize these intermediates in the reaction mixture. The ^{19}F, ^{13}C, ^{14}N and ^{1}H NMR spectra showed that these intermediates are the $RCF{=}NH_2^+$ and $RCF_2NH_3^+$ cations.

It was possible to identify the fluorinated intermediates by ^{19}F NMR spectroscopy because the ^{19}F resonances are well separated with the chemical shifts of $RCF{=}NH_2^+$ lying at higher frequency (-7.7 to -13.7 ppm) and the chemical shifts of $RCF_2NH_3^+$ lying at lower frequency (-79.0 to -85.5 ppm). In the most cases it was not possible to fully assign the ^{1}H and ^{13}C NMR spectra because some of the ^{1}H and ^{13}C resonances of the methyl and methylene groups have very similar chemical shifts.

In the case of $CH_3C{\equiv}N$, it was much easier to completely characterize both intermediates. Samples of 99.7% ^{13}C-enriched $^{13}CH_3C{\equiv}N$ and 99.0% ^{13}C-enriched $CH_3{}^{13}C{\equiv}N$ provided further information which permitted fuller characterization of the structures of these fluorinated cations in HF solvent. The characterizations of the $CH_3CF{=}NH_2^+$ and $CH_3CF_2NH_3^+$ cations are discussed in detail in the following section.

(1) Characterization of the $RCF{=}NH_2^+$ Cations

The ^{19}F NMR spectrum resulting from the reaction of natural abundance and ^{13}C-enriched $CH_3C{\equiv}N$ with HF consisted of a "sextet" (doublet of quartets) at -7.7 ppm having relative intensities 1 : 3 : 4 : 4 : 3 : 1 which, in turn, showed a doublet splitting on each line. This splitting pattern arises from coupling between ^{19}F and two

magnetically nonequivalent protons on nitrogen ($^3J(^{19}F\text{-}^1H)_{NH}$, 33.4 and 4.1 Hz) and three magnetically equivalent protons on carbon ($^3J(^{19}F\text{-}^1H)_{CH}$, 16.1 Hz). The ^{19}F NMR spectra resulting from the solvolysis of $CH_3{}^{13}C{\equiv}N$ and $^{13}CH_3C{\equiv}N$ in anhydrous HF showed additional splitting arising from $^1J(^{19}F\text{-}^{13}C)$, 324.6 and $^3J(^{19}F\text{-}^{13}C)$, 16.0 Hz (Figure 6.5).

The ^1H NMR spectra, after subtracting the ^1H resonances of the *E*- and *Z*-$CH_3CF_2N(H)C(NH_2)CH_3^+$ and $CH_3C{\equiv}NH^+$ cations, showed a doublet at 1.98 ppm ($^1J(^{19}F\text{-}^1H)_{CH}$, 16.1 Hz). The ^1H 2D NMR spectrum of $CH_3C{\equiv}N$ in HF did not show any connectivity to other ^1H signals in the spectrum. The ^1H NMR spectra of the products of the reaction of $^{13}CH_3C{\equiv}N$ and $CH_3{}^{13}C{\equiv}N$ in HF solvent showed these signals were split into additional doublets assigned to $^1J(^{13}C\text{-}^1H)_{CH}$, 152.0 Hz and $^3J(^{13}C\text{-}^1H)$, 6.2 Hz. The coupling, $^3J(^{19}F\text{-}^1H)$, is in agreement with that observed in the ^{19}F NMR spectrum.

The ^{13}C resonance of the enriched carbon of the $CH_3{}^{13}CF{=}NH_2^+$ cation occurred at 184.3 ppm and consisted of a doublet arising from $^1J(^{19}F\text{-}^{13}C)$, 324.6 which was further split into poorly resolved quartets arising from $^2J(^{13}C\text{-}^1H)$, 6.2 Hz. The quartet on each doublet branch was poorly resolved and broadening may arise from residual scalar coupling to the quadrupolar ^{14}N nucleus. The $\{^1H\}$-broad band decoupled ^{13}C NMR spectrum showed this signal was a doublet with a well resolved 1:1:1 triplet (partially quadrupole collapsed) arising from $^1J(^{14}N\text{-}^{13}C)$, 14.6 Hz (Figure 6.9). The corresponding $^1J(^{14}N\text{-}^{13}C)$ coupling of the $CHF{=}NH_2^+$ cation (cf. Chapter 4) is in good agreement and it appears that the low viscosity of HF solvent greatly assists the observation of $^1J(^{14}N\text{-}^{13}C)$.

The ^{14}N NMR spectra of the reaction mixture (natural abundance) showed a sharp

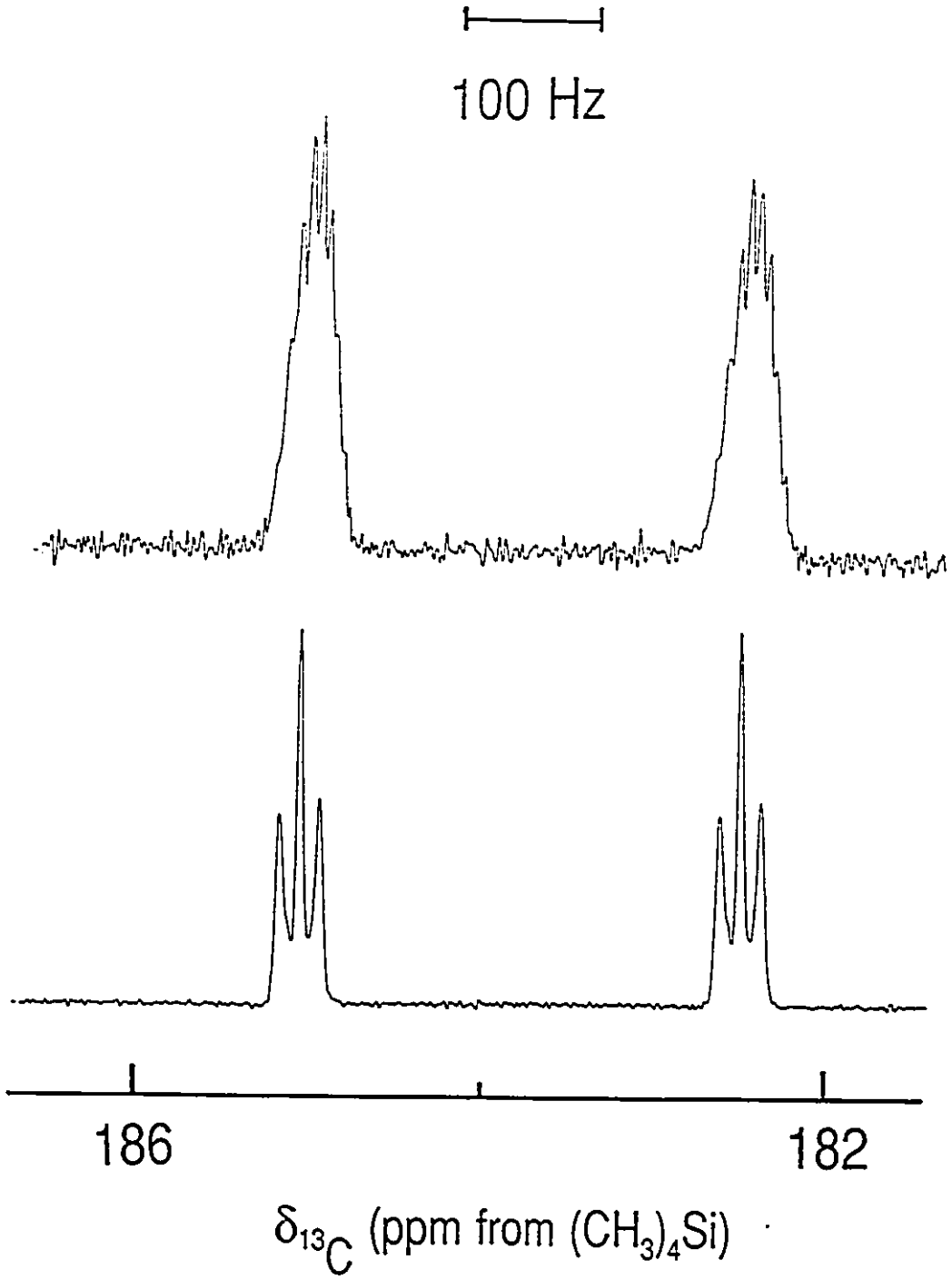

Figure 6.9 ^{13}C NMR spectra (125.760 MHz) of the 99.0% ^{13}C-enriched $CH_3{}^{13}CF{=}NH_2^+$ cation, recorded at -15 °C in HF solvent; (a) $\{^1H\}$-coupled and (b) $\{^1H\}$-decoupled.

triplet at -323.3 ppm ($^1J(^{14}N\text{-}^1H)$, 65.4 Hz), whereas the $\{^1H\}$-decoupled spectrum gave a singlet. The triplet was further split into a doublet in the case of $CH_3{}^{13}C{\equiv}N$ in HF, ($J(^{14}N\text{-}^{13}C)$, 14.6 Hz), which is in good agreement with the $^1J(^{14}N\text{-}^{13}C)$ coupling constant measured in the ^{13}C NMR spectrum of the $CH_3CF{=}NH_2^+$ cation. Further splitting in the case of $^{13}CH_3C{\equiv}N$ in HF solvent (Figure 6.10) was not observed. Table 6.6 lists the NMR parameters of the $CH_3CF{=}NH_2^+$ cation in HF solvent at -15 °C.

The formal hybridization of the nitrogen and carbon atoms of the C=N bond in the $CH_3CF{=}NH_2^+$ cation can be correlated with $^1J(^{15}N\text{-}^1H)$ and $^1J(^{19}F\text{-}^{13}C)$ using equations (4.8) and (4.9), which are discussed in detail in Chapter 4. The %s characte on the N atom was calculated from equation (4.8) after calculating $^1J(^{15}N\text{-}^1H)$ from $^1J(^{14}N\text{-}^1H)$ using equation (6.1).

$$^1J(^{15}N\text{-}^1H) = \frac{\gamma\,(^{15}N)}{\gamma(^{14}N)}\ ^1J(^{14}N\text{-}^1H) \qquad (6.1)$$

The coupling constant, $^1J(^{15}N\text{-}^1H)$, was found to be 93.1 Hz and the %s character was calculated and is equal to 33.1%, which is consistent with sp^2 hybridization for the nitrogen of the $CH_3CF{=}NH_2^+$ cation. The %s character of the carbon in the C=N bond in the $CH_3CF{=}NH_2^+$ cation was likewise calculated from equation (4.9) and is equal to 34.0%, and is also consistent with the anticipated sp^2 hybridization of carbon.

In the case of the solvolysis of $RC{\equiv}N$ (R = C_2H_5, *n*-C_3H_7 and *n*-C_4H_9) in HF, the ^{19}F NMR spectra showed sharp multiplets in each spectrum (doublet of doublets of

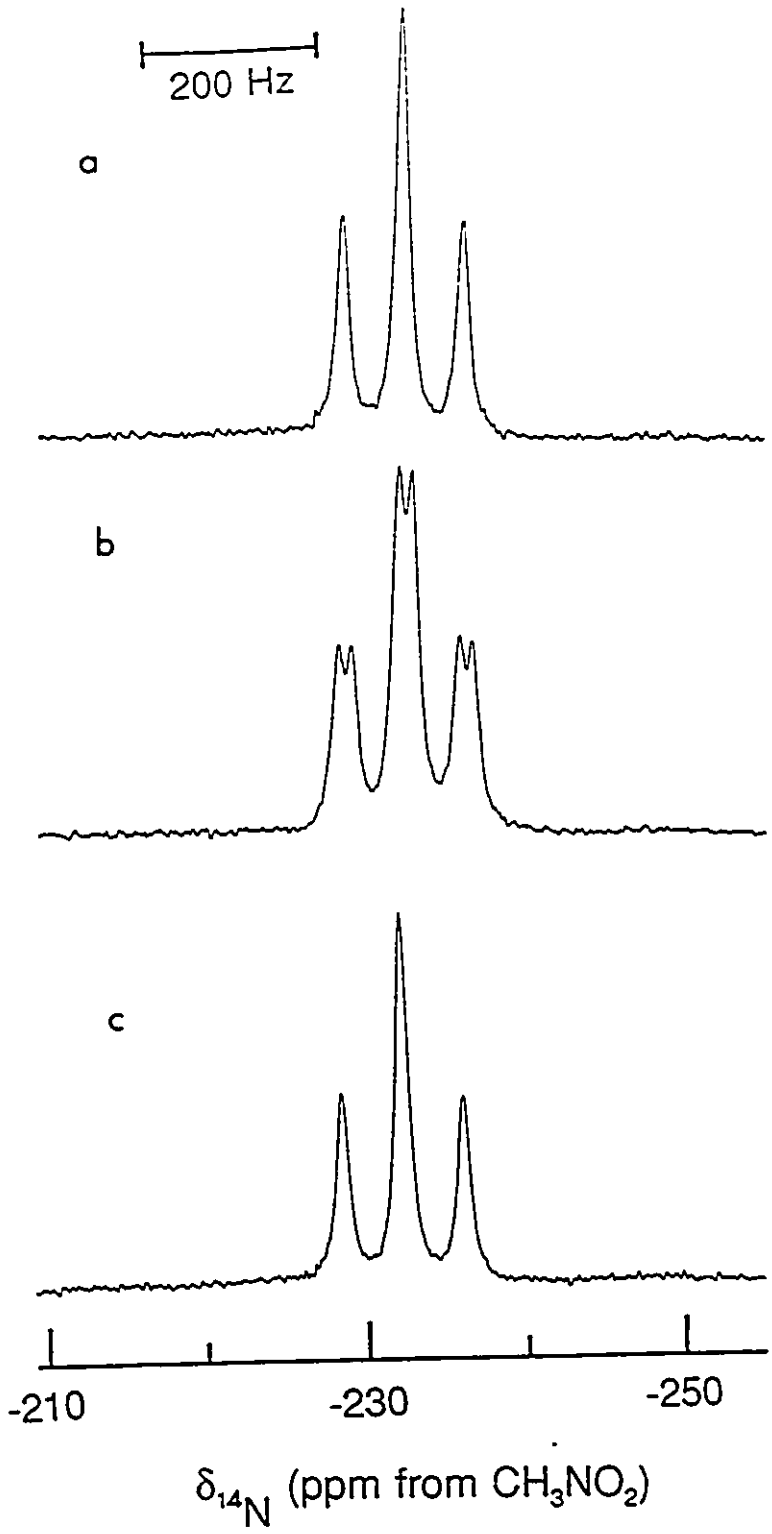

Figure 6.10 ^{14}N NMR spectra (18.076 MHz) of $CH_3CF{=}NH_2^+$ recorded at -15 °C in HF solvent: (a) natural abundance, (b) 99.0% ^{13}C enriched sample of $CH_3{}^{13}CF{=}NH_2^+$ and (c) 99.7% ^{13}C enriched sample of $^{13}CH_3CF{=}NH_2^+$.

Table 6.6

NMR Parameters of the $CH_3CF_2NH_3^+$ and $CH_3CF{=}NH_2^+$ Cations in HF Solvent at -15 °C

Cation	$CH_3CF{=}NH_2^+$	$CH_3CF_2NH_3^+$
Chemical Shifts (ppm)		
$\delta(^{19}F)^a$	-7.7	-79.0
$\delta(^{1}H)^b$	1.98	2.71
$\delta(^{13}C)^b$	184.3	118.6
$\delta(^{14}N)^a$	-323.3	-318.4
Coupling Constants (Hz)		
$^3J(^{19}F\text{-}^{1}H)_{CH}$	16.1	16.8
$^3J(^{19}F\text{-}^{1}H)_{NH}$	33.4 (*trans*) 4.1 (*cis*)	4.6
$^1J(^{14}N\text{-}^{1}H)$	68.4	75.3
$^1J(^{19}F\text{-}^{13}C)$	324.6	272.1
$^1J(^{14}N\text{-}^{13}C)$	14.6	
$^1J(^{13}C\text{-}^{1}H)$	152.0	135.1
$^2J(^{13}C\text{-}^{1}H)$	6.2	6.5
$^1J(^{14}N\text{-}^{1}H)$	65.4	56.2
$^2J(^{19}F\text{-}^{13}C)$	16.0	16.5

a Samples were referenced externally at 24 °C with respect to the neat liquid references $CFCl_3$ (^{19}F) and CH_3NO_2 (^{14}N).

b Samples were referenced externally at 30 °C with respect to the neat liquid reference TMS (^{13}C and ^{1}H).

triplets) at -14.8, -13.7 and -13.6 ppm, which are assigned to the $RCF{=}NH_2^+$ cations. Each of these signals displayed couplings with the proton on carbon, $^3J(^{19}F\text{-}^1H)_{CH}$ (13.1 to 16.5 Hz) which was split into a doublet of doublets resulting from coupling with two magnetically non-equivalent protons on nitrogen, $^3J(^{19}F\text{-}^1H)_{NH}$ (*trans*, 33.4 to 34.2 Hz and *cis*, 4.3 to 4.6 Hz). Table 6.7 lists the ^{19}F NMR parameters of the $RCF{=}NH_2^+$ (R = C_2H_5, *n*-C_3H_7 and *n*-C_4H_9) cations in HF solvent. Although the ^1H, ^{13}C and ^{14}N NMR spectra of the $RCF{=}NH_2^+$ cations were also recorded in HF solvent, it was not possible to assign the NMR parameters of these species. This is due to extensive overlap among several NMR signals of the $RC{\equiv}NH^+$, *E*- and *Z*-$RCF_2N(H)C(NH_2)R^+$ and $RCF_2NH_3^+$ cations. Figure 6.11 depicts the ^1H-2D COSY spectrum resulting from the reaction of *n*-$C_3H_7C{\equiv}N$ in HF solvent showing the overlapping ^1H NMR signals.

As far as can be determined, this is the first time examples of the intermediate cations, $RC(X){=}NH_2^+$, resulting from the reaction of the alkyl nitriles in an anhydrous hydrogen halide have been characterized. Prior to this work, this intermediate had only been proposed in reaction mechanisms leading to the formation of dimer cations (Structure 6.3) from alkylnitriles in the presence of HCl.[214]

(2) Characterization of the $RCF_2NH_3^+$ Cations

The ^{19}F NMR spectrum of $CH_3C{\equiv}N$ recorded at -15 °C in HF solvent showed a broad multiplet at -79.0 ppm which is assigned to the $CH_3CF_2NH_3^+$ cation. The ^{19}F resonance of $CH_3CF_2NH_3^+$ consists of a quartet of quartets arising from ^{19}F coupling with the protons on carbon and nitrogen, $^3J(^{19}F\text{-}^1H)$. The ^{19}F NMR spectra of ^{13}C-enriched

Table 6.7

^{19}F NMR Parameters for the $RCF_2NH_3^+$ and $RCF{=}NH_2^+$ Cations (R = C_2H_5, *n*-C_3H_7 and *n*-C_4H_9) in Anhydrous HF Solvent at -15 °C

Cation	$\delta(^{19}F)$	$^3J(^{19}F\text{-}^1H)_{NH}$	$^3J(^{19}F\text{-}^1H)_{CH}$
$CH_3CH_2CF_2NH_3^+$	-88.2	8.0	16.4
$CH_3CH_2CH_2CF_2NH_3^+$	-85.8	6.9	15.3
$CH_3CH_2CH_2CH_2CF_2NH_3^+$	-85.7	8.4	16.0
$CH_3CH_2CF{=}NH_2^+$	-14.8	33.4 (*trans*) 4.6 (*cis*)	13.1
$CH_3CH_2CH_2CF{=}NH_2^+$	-13.7	34.2 (*trans*) 4.4 (*cis*)	16.4
$CH_3CH_2CH_2CH_2CF{=}NH_2^+$	-13.6	34.1 (*trans*) 4.3 (*cis*)	16.5

a Samples were referenced externally at 24 °C with respect to the neat liquid references $CFCl_3$ (^{19}F).

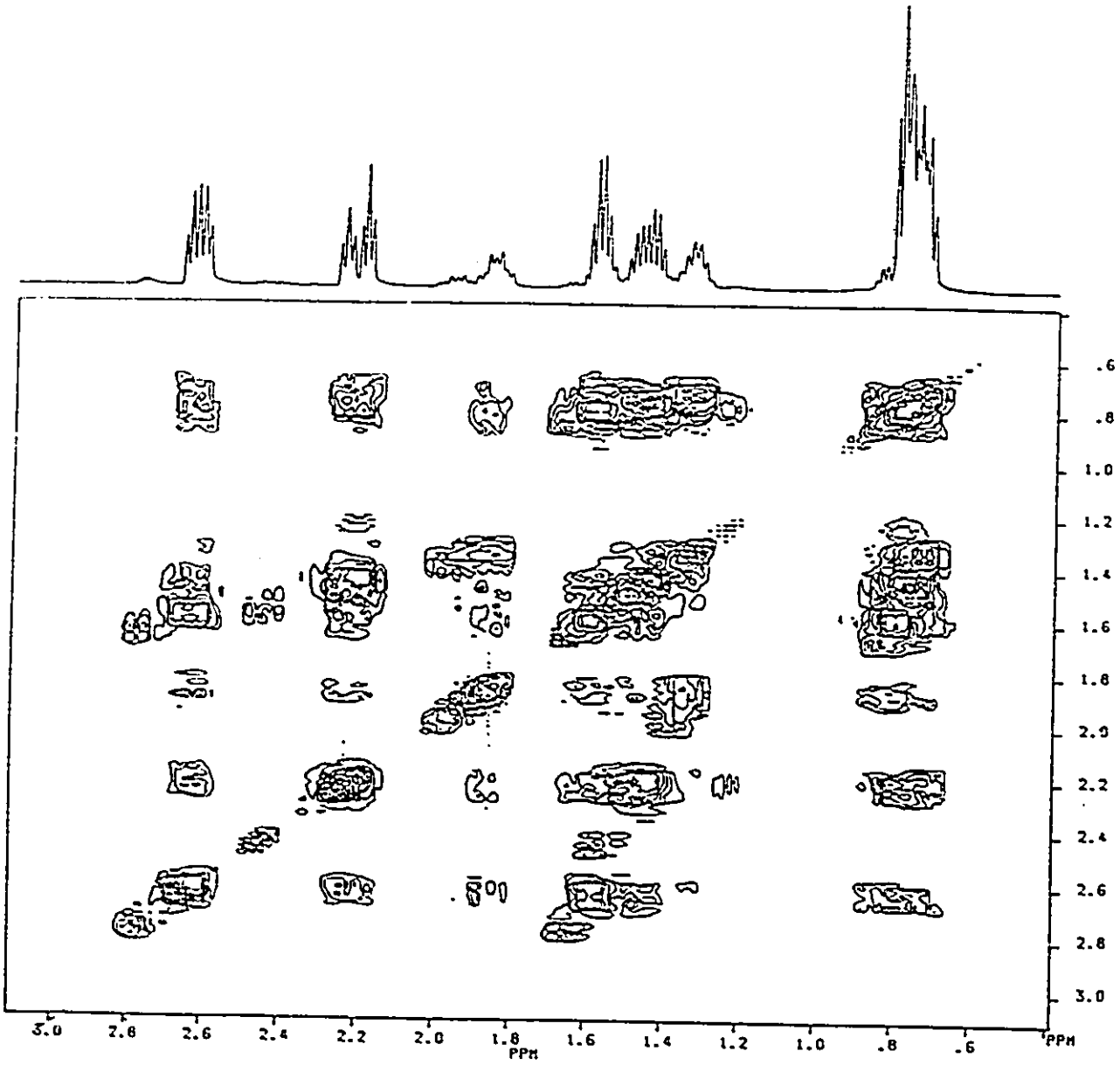

Figure 6.11 ^{1}H-2D COSY spectrum (500.125 MHz), at -15 °C, resulting from the reaction of *n*-$C_3H_7C{\equiv}N$ in HF solvent after warming the mixture for 7 days at room temperature.

$CH_3C{\equiv}N$ in HF provide further support for the structural assignments. The ^{19}F NMR spectra of 99.0% enriched $CH_3{}^{13}CF_2NH_3^+$ and 99.7% enriched $^{13}CH_3CF_2NH_3^+$ display the couplings $^1J(^{19}F\text{-}^{13}C)$, 271.1 Hz and $^2J(^{19}F\text{-}^{13}C)$, 16.5 Hz, respectively (Figure 6.5).

The ^1H NMR spectrum of the products resulting from the solvolysis of $CH_3C{\equiv}N$ in HF showed a triplet at 2.71 ppm corresponding to $^3J(^9F\text{-}^1H)$, 16.8 Hz (Figure 6.6). The ^1H 2D NMR spectrum for this signal did not show a connectivity to other proton signals. The triplet was further split into doublets when ^{13}C-enriched $^{13}CH_3C{\equiv}N$ (99.7%) and $CH_3{}^{13}C{\equiv}N$ (99.0%) were used. The doublet splittings were $^1J(^{13}C\text{-}^1H)$, 135.1 and $^2J(^{13}C\text{-}^1H)$, 6.2 Hz, respectively.

The $\{^1H\}$-decoupled ^{13}C NMR spectrum of a 99.0% ^{13}C-enriched $CH_3{}^{13}C{\equiv}N$ sample in HF showed a triplet at 118.6 ppm ($^1J(^{19}F\text{-}^{13}C)$, 272.1 Hz). Figure 6.12 depicts the ^{13}C NMR spectrum of the reaction mixture in the CF_2 region. The ^{14}N NMR spectra showed a quartet at -318.4 ppm, ($^1J(^{14}N\text{-}^1H)$, 56.2 Hz). Broad-band $\{^1H\}$-decoupling resulted in a sharp single line for the ^{14}N resonance. The NMR parameters of the $CH_3CF_2NH_3^+$ cation are listed in Table 6.6.

In the case of the solvolysis of $RC{\equiv}N$ (R = C_2H_5, n-C_3H_7 and n-C_4H_9) in HF, the ^{19}F NMR spectra showed broad multiplets consisting of a triplet of triplets at -88.2, -85.8 and -85.7 ppm, respectively that are assigned to the respective $RCF_2NH_3^+$ cations. Each of these signals displayed coupling constants arising from the proton on carbon, $^3J(^{19}F\text{-}^1H)_{CH}$ (15.3 to 16.4 Hz), which was further split into quartets arising from coupling with the proton on nitrogen, $^3J(^{19}F\text{-}^1H)_{NH}$ (6.9 to 8.4 Hz). Table 6.7 lists the ^{19}F NMR parameters of the $RCF_2NH_3^+$ cations in HF solvent. Although the ^1H, ^{13}C and ^{14}N NMR

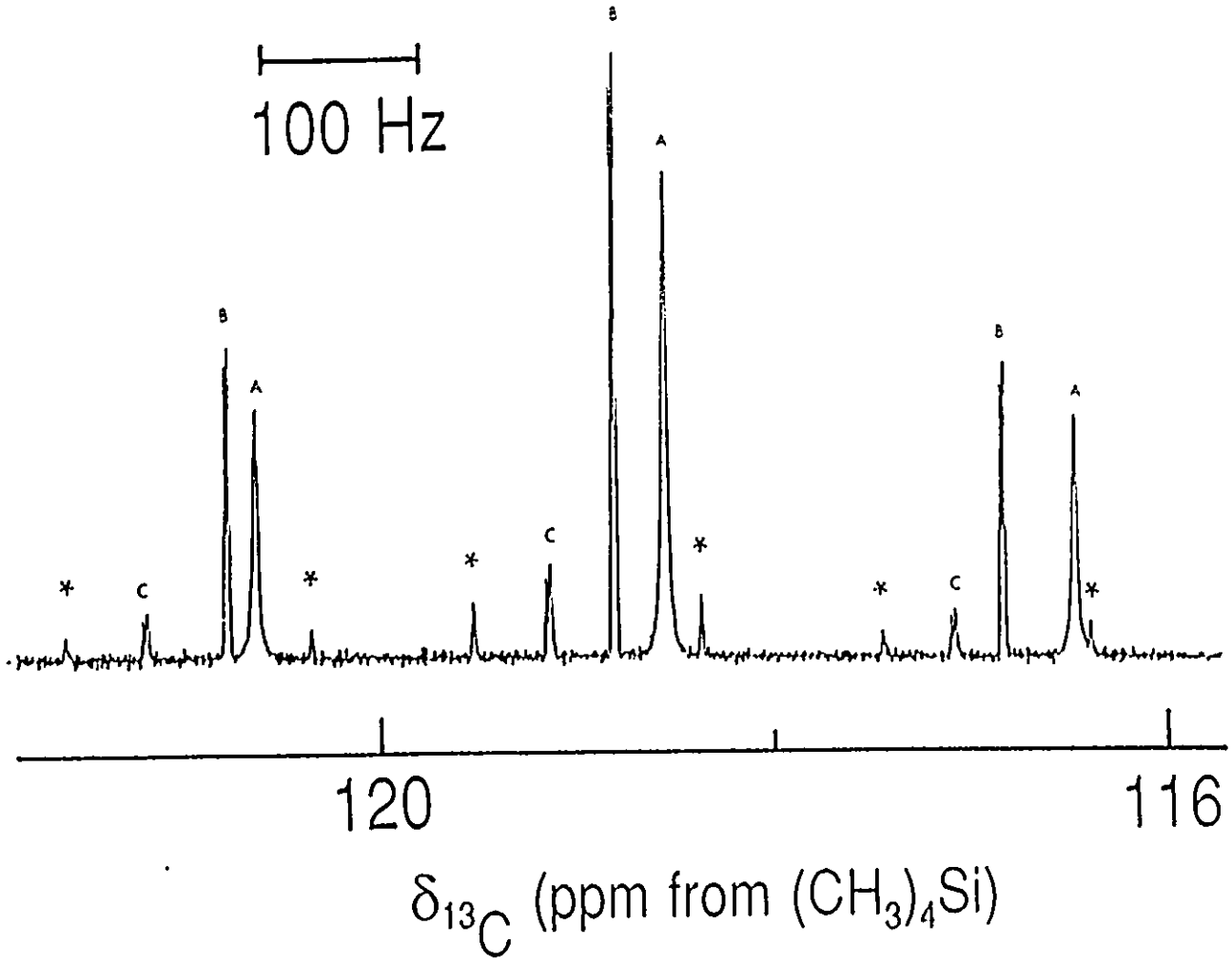

Figure 6.12 ^{13}C NMR spectrum of the $CH_3CF_2NH_3^+$ cation in the CF_2 region recorded in HF solvent at -15 °C; (A) $CH_3CF_2NH_3^+$, (B) Z-$CH_3CF_2N(H)C(NH_2)CH_3^+$ (Structure 6.2) and (C) *E*-$CH_3CF_2N(H)C(NH_2)CH_3^+$ (Structure 6.1). Asterisks (*) denote unassigned resonances.

spectra of the $RCF_2NH_3^+$ cations were recorded in HF solvent, it was not possible to identify the NMR resonances of these species. This is due to their overlap with the NMR signals of the $RC{\equiv}NH^+$, *E*- and Z-$RCF_2N(H)C(NH_2)R^+$ and $RCF{=}NH_2^+$ cations in HF solvent (Figure 6.11).

(C) COMPARISON OF THE SOLVOLYTIC BEHAVIORS OF $RC{\equiv}N\text{-}XeF^+AsF_6^-$ AND $RC{\equiv}N$ IN ANHYDROUS HF

The $RC{\equiv}N\text{-}XeF^+AsF_6^-$ salts are not stable in anhydrous HF and decompose by selectively fluorinating the alkyl chain to form mono- and difluoro-alkylnitriles. Fluorination occurs exclusively on the alkyl carbons, but not on the alkyl carbon α to the C≡N group. Comparison of the fluorination products of these reactions with the reactions of the alkyl nitriles in HF showed that the reaction mechanisms are significantly different, with the neutral alkyl nitriles invariably adding HF to the C≡N bond and dimerizing to form predominantly the *E*- and Z-$RCF_2N(H)C(NH_2)R^+$ cations (Structures 6.1 and 6.2). These reactions appear to involve the $RCF{=}NH_2^+$ and $RCF_2NH_3^+$ cations as intermediates.

It is believed that the reactions of $RC{\equiv}N\text{-}XeF^+AsF_6^-$ in anhydrous HF, where there is no attack on the C≡N triple bond, are radical reactions, consequently these reactions may be described as fluorination-substitution and not addition reactions. The major products resulting from $n\text{-}C_3H_7C{\equiv}N\text{-}XeF^+AsF_6^-$ in HF were $CH_2FCH_2CH_2C{\equiv}NH^+$, $CH_3CHFCH_2C{\equiv}NH^+$, $CF_2HCH_2CH_2C{\equiv}NH^+$ and $CH_3CF_2CH_2C{\equiv}NH^+$. There were no detectable amounts of N-F compounds. It appears from the product distributions that

replacement of a β-hydrogen by fluorine clearly predominates replacement of the a γ-hydrogen, while the replacement of an α-hydrogen is the least favorable process and could not be detected. The ^{129}Xe, ^{19}F and ^{1}H NMR spectral results are consistent with reactions (6.2) - (6.8) in the case of *n*-$C_3H_7C{\equiv}N$, and the formation of the three Xe-N bonded nitrile adducts and the corresponding protonated nitriles. The reaction of *n*-$C_3H_7C{\equiv}N$ and $XeF^+AsF_6^-$ in HF at -30 °C, prior to warming the reaction mixture to room temperature (cf. Chapter 5), showed only the protonated (*n*-$C_3H_7C{\equiv}NH^+$) and protonated monofluoro alkyl nitriles ($CH_2FCH_2CH_2C{\equiv}NH^+$, $CH_3CHFCH_2C{\equiv}NH^+$) and the Xe-N bonded cations (*n*-$C_3H_7C{\equiv}N$-XeF^+, $CH_2FCH_2CH_2C{\equiv}N$-XeF^+, $CH_3CHFCH_2C{\equiv}N$-XeF^+). The reactivities of the three types of hydrogen in *n*-$C_3H_7C{\equiv}N$ are significantly different and show the product distributions α : β : γ = 0 : 68 : 32. This behavior is similar to the photochlorination of *n*-$C_3H_7C{\equiv}N$ where the distribution ratio was 0 : 69 : 31 and deactivation by the cyano group is greater for hydrogen abstraction by the chlorine atom.[201] It seems likely that the alkyl nitriles are mainly fluorinated by a similar route, with equilibrium amounts of XeF_2 serving as the fluorinating agent (Scheme 6.1). These reactions may not proceed via simple oxidation to a radical cation, $[RC{\equiv}N]^{+\cdot}$, because the first ionization potentials of nitriles are too high (see Table 1.3). The deactivation of the α-hydrogen may be due to resonance with the ketene radical cation, which is unfavorable in acid medium. This makes the α-hydrogen the least favorable hydrogen

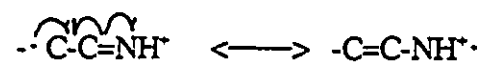

to be abstracted in these radical reactions. The fluorination mechanism presumably involves the radical reaction given in Scheme 6.1 and is initiated by thermal dissociation of XeF_2 in HF solvent.

The fluorine radical undergoes a transfer reaction to abstract a hydrogen atom from the alkyl nitrile to form HF (bond energy 153 kcal mol^{-1}), generating alkyl nitrile radicals. In this process, the fluorine radical is selective by abstracting the 2° hydrogen faster than the 1° hydrogen. This is also true in the case of aliphatic radicals where the stability increases in the order 1° < 2° < 3° and α-hydrogen abstraction is the least favored in the alkyl nitriles. The alkyl nitrile radicals can be destroyed by reaction of XeF· radical (C-F bond energy 107 kcal mol^{-1} [62]) to form monofluoroalkyl nitriles and Xe gas. The difluoroalkylnitriles thus formed can then undergo fluorination to a limited extent at the β- and γ-positions in the usual way.

A comparison between the fluorinated nitriles before and after warming the reaction mixture using ^1H NMR shows that the relative amount of $CH_2FCH_2CH_2C{\equiv}NH^+$ cation decreases, due to formation of the difluoroalkylnitrile $CHF_2CH_2CH_2C{\equiv}NH^+$ cation, which dominates in solution (Figure 6.3).

Similar reaction mechanisms can be applied in the case of the fluorination reactions arising from the decomposition of $C_2H_5C{\equiv}N\text{-}XeF^+$ and $n\text{-}C_4H_9C{\equiv}N\text{-}XeF^+$ in anhydrous HF solvent.

A parallel study of the fluorination of the corresponding alkyl nitriles in anhydrous HF indicates that the fluorination mechanisms differ significantly from those of the $RC{\equiv}N\text{-}XeF^+$ cations in HF solvent. The reactions of the alkyl nitriles with HCl and their

Scheme 6.1

$$n\text{-}C_3H_7C{\equiv}N + XeF^+AsF_6^- \overset{HF}{\rightleftharpoons} n\text{-}C_3H_7C{\equiv}N\text{-}XeF^+AsF_6^- \quad (6.2)$$

$$XeF^+AsF_6^- + HF \rightleftharpoons XeF_2 + \text{"}HAsF_6\text{"} \quad (6.3)$$

$$XeF_2 \rightleftharpoons F^\cdot + XeF^\cdot \quad (6.4)$$

$$CH_3CH_2CH_2C{\equiv}NH^+ + F^\cdot \longrightarrow \begin{matrix} CH_3{}^\cdot CHCH_2C{\equiv}NH^+ \\ \text{and} \\ {}^\cdot CH_2CH_2CH_2C{\equiv}NH^+ \end{matrix} + HF \quad (6.5)$$

$$\left\{\begin{matrix} CH_3{}^\cdot CHCH_2C{\equiv}NH^+ \\ \text{and} \\ {}^\cdot CH_2CH_2CH_2C{\equiv}NH^+ \end{matrix}\right\} + XeF^\cdot \longrightarrow \left\{\begin{matrix} CH_3CHFCH_2C{\equiv}NH^+ \\ \text{and} \\ CH_2FCH_2CH_2C{\equiv}NH^+ \end{matrix}\right\} + Xe \quad (6.6)$$

$$CH_2FCH_2CH_2C{\equiv}NH^+AsF_6^- + XeF_2 \rightleftharpoons CH_2FCH_2CH_2C{\equiv}N\text{-}XeF^+AsF_6^- \quad (6.7)$$

$$CH_3CHFCH_2C{\equiv}NH^+AsF_6^- + XeF_2 \rightleftharpoons CH_3CHFCH_2C{\equiv}N\text{-}XeF^+AsF_6^- \quad (6.8)$$

role in various reactions have been discussed in several reviews.[215, 216] Reactions of alkyl nitriles with COF_2 to form α,α-difluoroalkyl isocyanates, RCF_2NCO, were found to proceed only when anhydrous HF was present. The presence of the anhydrous HF, implies slow addition of F^- to the cyano carbon, forming $RCF{=}N^-$. [217] The $RCF{=}N^-$ anion presumably attacks the electropositive carbon of the carbonyl fluoride eliminating a fluoride ion. Alternately, attack may be by a carbonium ion (formed from carbonyl fluoride), eliminating hydrogen fluoride. In general, the reactivities of nitriles are fundamentally due to polarization of the C≡N triple bond, which arises from the greater electronegativity of nitrogen compared to that of carbon atom

$$RC{\equiv}N \longleftrightarrow RC^{+}{=}N^{-} \qquad (6.9)$$

Fluoride ions will attack at the electrophilic carbon atom while the nitrogen atom is a weakly basic site. Interaction of the nitrogen with a Lewis acid or a proton further enhances polarization and gives rise to a species that is more susceptible to the fluoride attack

$$RC{\equiv}NA^{+} \longleftrightarrow RC^{+}{\equiv}NA \qquad (6.10)$$

The special nature of the reactivity of alkyl nitrile-hydrogen fluoride compounds stems from the high nucleophilicity of the fluoride ion compared to the anions of oxo-acids. Hydrogen cyanide and $CH_3C{\equiv}N$ and other alkyl nitriles have been examined in

FSO_3H-SbF_5 solution at low temperature.[161] Under these conditions protonation occurred to form $RC{\equiv}NH^+$ cations and from the $^1J(^{14}N\text{-}^1H)$ coupling constants in the protonated nitriles, the nitrile nitrogen is shown to still be sp hybridized so that the protonated nitrile is therefore a linear species. In anhydrous HF, addition of a proton to the weakly basic nitrogen atom is followed, or perhaps accompanied, by coordination of a fluorine ion at the electrophilic carbon. The imidylfluoride which is formed, $RCF{=}NH_2^+\ F(HF)_x^-$, is usually sufficiently basic to accept a second proton to form a salt (Scheme 6.2). While the existence of imidyl halide salts is now firmly established,[216,218] it is important to note that in the reversible reaction (Scheme 6.2), the formation of $RCF{=}NH_2^+\ F(HF)_x^-$ (Structure 6.4) is frequently slow and is favored by high HF concentration.

The alkyl imidyl fluoride cations are, however, unstable at room temperature and undergo further reaction by addition of hydrogen fluoride to the nitrile to give the $RCF_2NH_3^+$ cations (Structure 6.5) followed by dimerization to give *E*- and *Z*-$RCF_2N(H)C(NH_2)R^+$ (Structures 6.6 and 6.7), which are in the ratios of 96 : 4, 97 : 3, 98 : 2 and 98 : 2 for R = CH_3, C_2H_5, *n*-C_3H_7 and *n*-C_4H_9, respectively. These reactions are predominantly addition reactions of HF to the C≡N triple bond, which differs from the radical fluorination of $RC{\equiv}N\text{-}XeF^+$ in HF.

Scheme 6.2

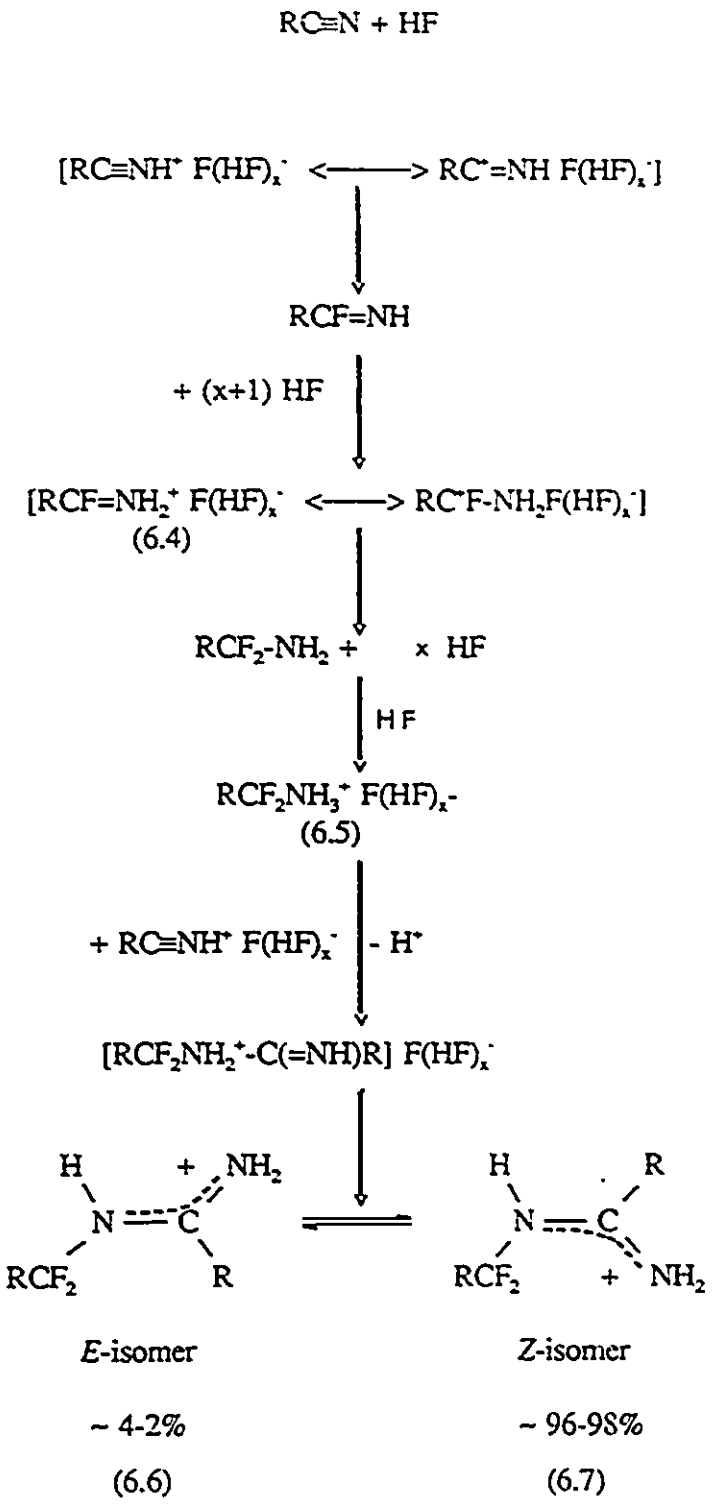
RC≡N + HF
[RC≡NH⁺ F(HF)ₓ⁻ <——> RC⁻=NH F(HF)ₓ⁻]
RCF=NH
+ (x+1) HF
[RCF=NH₂⁺ F(HF)ₓ⁻ <——> RC⁻F-NH₂F(HF)ₓ⁻]
(6.4)
RCF₂-NH₂ + x HF
HF
RCF₂NH₃⁺ F(HF)ₓ-
(6.5)
+ RC≡NH⁺ F(HF)ₓ⁻ - H⁺
[RCF₂NH₂⁺-C(=NH)R] F(HF)ₓ⁻
H
+ NH₂
N
C
RCF₂
R
H
R
N
C
RCF₂
+ NH₂
E-isomer
~ 4-2%
(6.6)
Z-isomer
~ 96-98%
(6.7)

CHAPTER 7

FLUORO(PERFLUOROPYRIDINE)XENON(II) HEXAFLUOROARSENATES: $R_fC_5F_4N\text{-}XeF^+AsF_6^-$ (R_f = F, 2-CF_3, 3-CF_3 AND 4-CF_3)

INTRODUCTION

In the previous Chapters it has been shown that hydrogen cyanide, alkylnitriles and perfluoroarylnitriles coordinate to the XeF^+ cation through the N_{sp} lone pair. All of these adduct cations are stable at low-temperature. Their stabilities are attributed to the ability of the nitrogen base donor molecule to withstand the high electron affinity of the XeF^+ cation, a functional criterion which enables one to predict, with a high degree of success, the ability of a nitrogen base to withstand the electron affinity of the XeF^+ cation (10.9 eV). The relatively high ionization potential of pentafluoropyridine, C_5F_5N (IP_1 = 10.08 eV), is similar to EA (XeF^+) and consequently might be expected to form a stable adduct cation with XeF^+.

In this work, the objective has been to extend xenon-nitrogen chemistry and the coordination of XeF^+ to aromatic nitrogen bases to provide the first examples where XeF^+ serves as an aromatic substituent. Consequently, the oxidatively resistant Lewis bases, the perfluoropyridines, have been chosen for these studies and have been shown to interact with the Lewis acid, XeF^+, to form xenon-nitrogen bonded adduct cations.

RESULTS AND DISCUSSION

(A) PREPARATION AND ISOLATION OF $R_FC_5F_4N$-$XeF^+AsF_6^-$ (R = F, 2-CF_3, 3-CF_3, 4-CF_3) SALTS

Equimolar amounts of $XeF^+AsF_6^-$ and the perfluoropyridines, $R_FC_5F_4N$ (R_F = F, 2-CF_3, 3-CF_3 and 4-CF_3), react in anhydrous HF at -30 to -20 °C according to equation (7.1) and equilibria (7.2) and (7.3) to give the novel Xe-N bonded cations, $R_FC_5F_4N$-XeF^+, as the AsF_6^- salts in solution.

$$R_FC_5F_4N + (x + 1)\ HF \longrightarrow R_FC_5F_4NH^+(HF)_xF^- \qquad (7.1)$$

$$R_FC_5F_4NH^+(HF)_xF^- + XeF^+AsF_6^- \rightleftharpoons R_FC_5F_4NH^+AsF_6^- + XeF_2 + x\ HF \qquad (7.2)$$

$$R_FC_5F_4NH^+AsF_6^- + XeF_2 \rightleftharpoons R_FC_5F_4N\text{-}XeF^+AsF_6^- + HF \qquad (7.3)$$

At -30 °C these solutions consisted of equilibrium mixtures of XeF_2, $R_FC_5F_4NH^+AsF_6^-$ and $R_FC_5F_4N$-$XeF^+AsF_6^-$ as determined by NMR spectroscopy. Removal of HF solvent by pumping at -50 °C resulted in white solids, which were shown by low-temperature (-196 °C) Raman spectroscopy to be mixtures of $R_FC_5F_4NH^+AsF_6^-$, XeF_2 and $R_FC_5F_4N$-$XeF^+AsF_6^-$.

An alternative approach, which led to the isolation of the Xe-N bonded cations, was to allow stoichiometric amounts of XeF_2 and the perfluoropyridinium cations, as their AsF_6^- salts, to react in HF and BrF_5 solvents at -30 °C according to equilibrium (7.3). The equilibria in both solvents were again monitored by ^{129}Xe, ^{19}F and ^{14}N NMR spectroscopy. In the case of BrF_5, formation of $R_FC_5F_4N\text{-}XeF^+AsF_6^-$ was strongly favored over that in HF solvent. The equlibrium ratios $K_F = [C_5F_5N\text{-}XeF^+]/[C_5F_5NH^+]$ were 0.25 and 2.1 in HF and BrF_5 solvents, respectively, at -30 °C and $K_{4\text{-}CF_3} = [4\text{-}CF_3C_5F_4N\text{-}XeF^+]/[4\text{-}CF_3C_5F_4NH^+]$ was 3.7 in BrF_5 at -50 °C (K_F = 4.5 at -50 °C and $K_{4\text{-}CF_3}$ = 13.6 at -50 °C in BrF_5). Thus, it is conculded that the formation of fluoro(perfluoropyridine)xenon(II) cations from the reaction of XeF_2 and perfluoropyridinium cations is more favorable in BrF_5 than in HF solvent.

Raman spectra of the solids, $R_FC_5F_4N\text{-}XeF^+AsF_6^-$, have been recorded at -196 °C. Only 4-$CF_3C_5F_4N\text{-}XeF^+AsF_6^-$ showed some signs of decomposition (deep blue color on the walls of the sample tube) when isolated from BrF_5 solvent and stored for two weeks at -90 °C. Decomposition occurred in the 4-$CF_3C_5F_4N\text{-}XeF^+AsF_6^-$ sample during exposure of the solid sample (at -196 °C) to the laser beam when the laser power levels were too high. The other fluoro(perfluoropyridine)xenon(II) cations, 2-$CF_3C_5F_4N\text{-}XeF^+AsF_6^-$ and 3-$CF_3C_5F_4N\text{-}XeF^+AsF_6^-$, were prepared as a mixture from a mixed sample of the perfluoropyridines and the Raman spectrum of the mixture in the region of the F-Xe(II) stretching frequency was examined as well as the ^{19}F and ^{129}Xe NMR spectra.

(B) CHARACTERIZATION OF $R_fC_5F_4N$-$XeF^+AsF_6^-$ (R_f = F, 2-CF_3, 3-CF_3 AND 4-CF_3) BY ^{129}Xe, ^{19}F and ^{14}N NMR SPECTROSCOPY

Multinuclear magnetic resonance spectra were recorded for $R_fC_5F_4N$-$XeF^+AsF_6^-$ (R_f = F, 2-CF_3, 3-CF_3 and 4-CF_3) in HF and BrF_5 solvents. The ^{129}Xe, ^{19}F and ^{14}N chemical shifts and nuclear spin-spin couplings $^1J(^{129}Xe\text{-}^{19}F)$ (doublet), $^1J(^{129}Xe\text{-}^{14}N)$ (partially quadrupole collapsed 1:1:1 triplet), and $^4J(^{19}F_1\text{-}^{19}F_4)$(1:2:1 triplet) support the proposed cation structures in solution. Figure 7.1 depicts the ^{19}F NMR spectrum resulting from the reaction of $C_5F_5NH^+AsF_6^-$ and XeF_2 in anhydrous HF solvent, showing the ^{19}F signals of C_5F_5N-XeF^+ (Structure 7.1) and $C_5F_5NH^+$ (Structure 7.2)

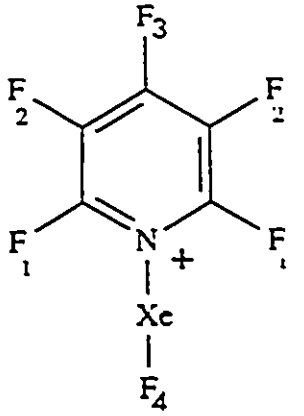

7.1

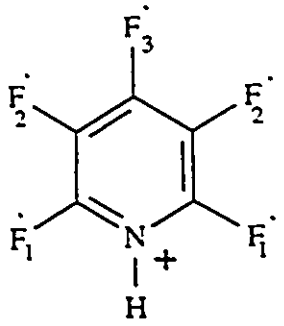

7.2

cations and the AsF_6^- anion. Figure 7.2 depicts the ^{19}F NMR spectrum of C_5F_5N-$XeF^+AsF_6^-$ in BrF_5 solvent showing the fluorine-on-xenon(II) region of the spectrum and ^{129}Xe satellites arising from spin-spin coupling of the terminal fluorine-on-xenon (F_4) to natural abundance ^{129}Xe in C_5F_5N-$XeF^+AsF_6^-$, where the 1:2:1 triplet fine structure on the central line is assigned to $^4J(^{19}F_1\text{-}^{19}F_4)$. Figure 7.3 shows the ^{129}Xe NMR spectrum of

Figure 7.1 ^{19}F NMR (235.361 MHz) spectrum resulting from the reaction of $C_5F_5NH^+AsF_6^-$ and XeF_2 in anhydrous HF; (A) C_5F_5N-XeF^+ cation (Structure 7.1) where F_1, F_2 and F_3 denote the ortho-, meta- and para-fluorine resonances of the pyridine ring, F_x denotes the fluorine-on-xenon resonance and asterisks (*) denote ^{129}Xe satellites (B) $C_5F_5NH^+$ cation (Structure 7.2) where F_1', F_2' and F_3' denote the ^{19}F resonances corresponding to ortho-, meta- and para- fluorines of the perfluoropyridine ring (C) the AsF_6^- anion.

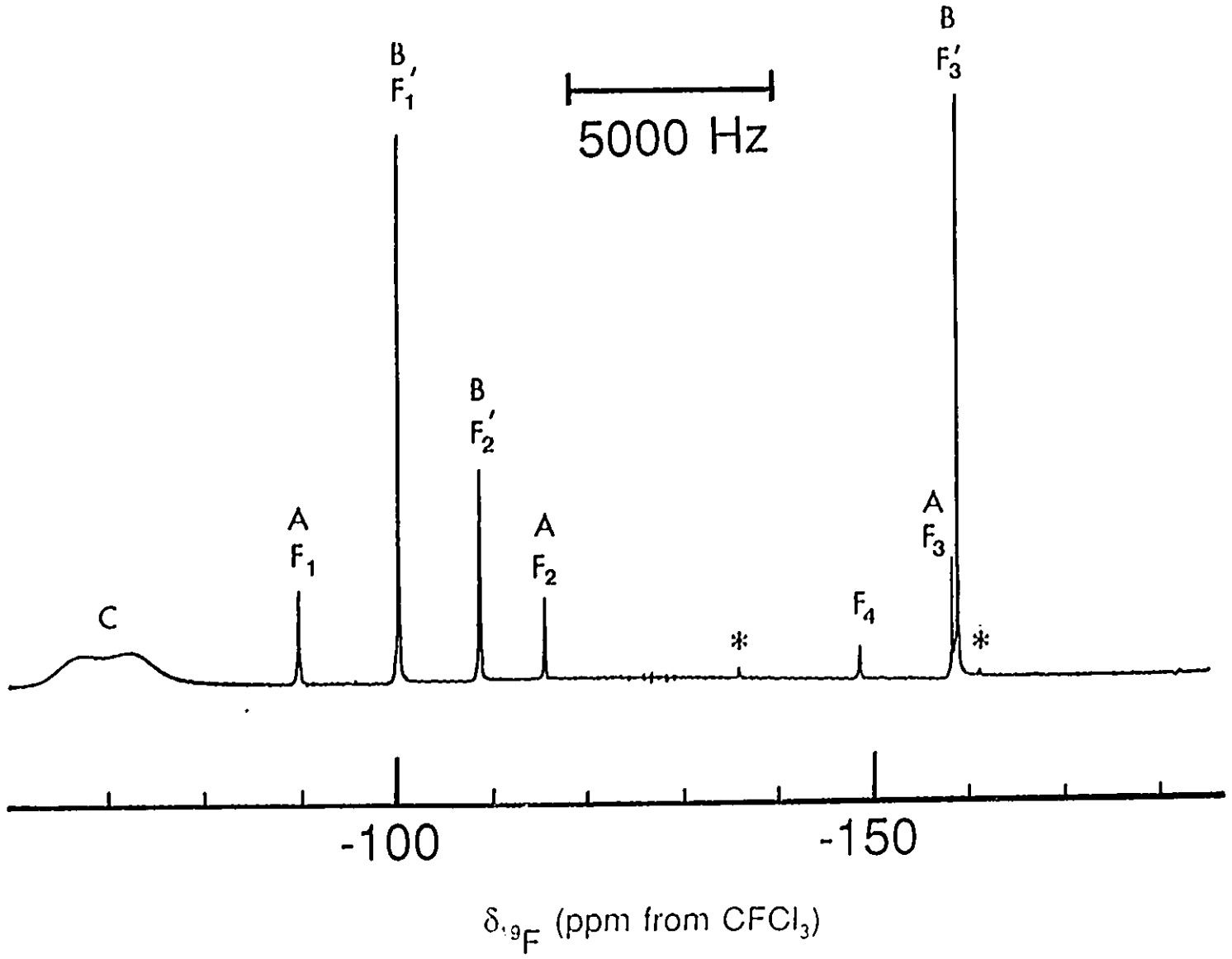
B
F1'
5000 Hz
B
F3'
B
F2'
A
F1
A
F2
A
F3
C
F4
*
*
-100
-150
δ19F (ppm from CFCl3)

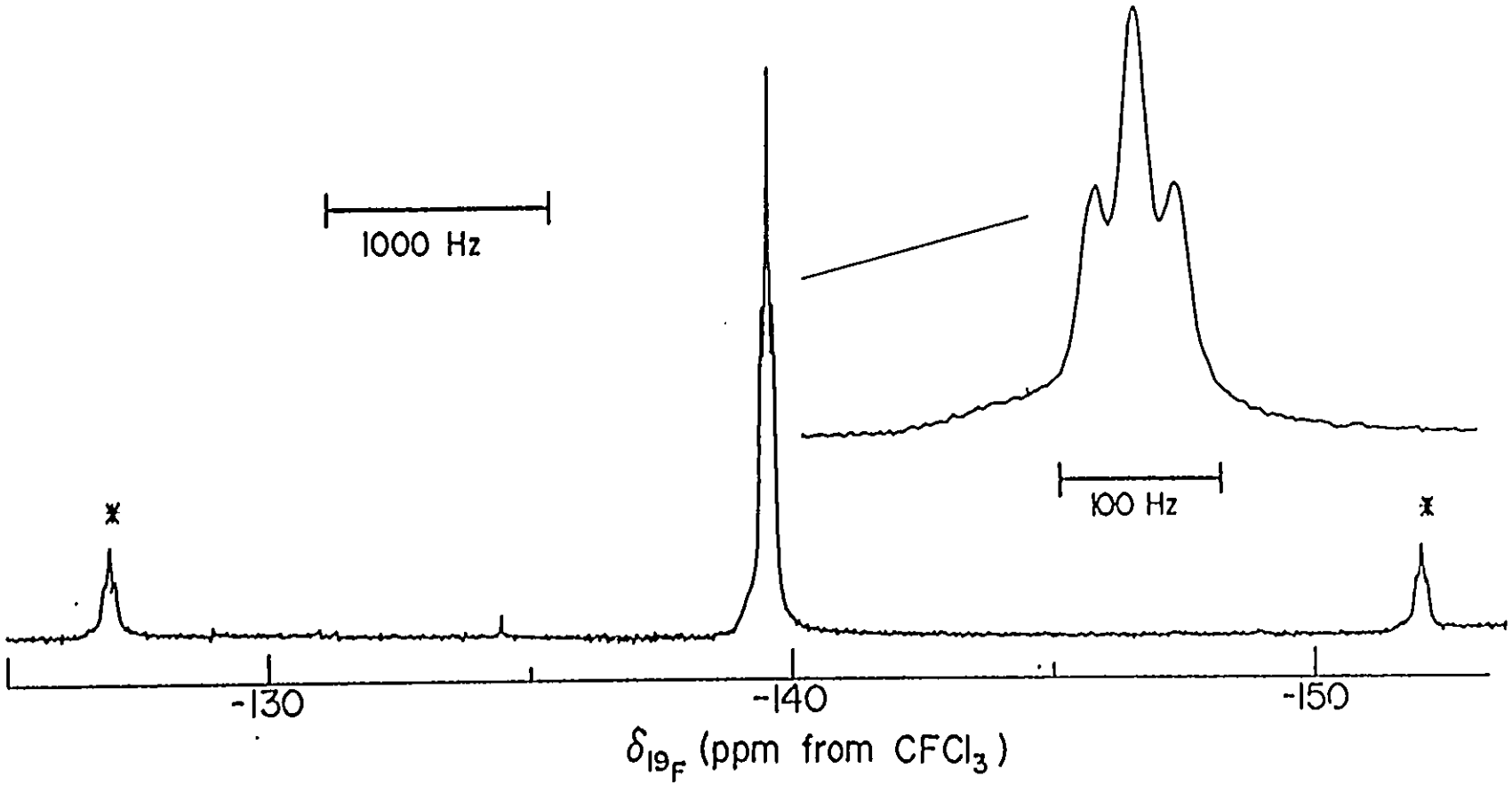

Figure 7.2 ^{19}F NMR spectrum (235.361 MHz) of C_5F_5N-$XeF^+AsF_6^-$ recorded in BrF_5 solvent for the fluorine-on-xenon(II) region (F_4) showing ^{129}Xe satellites, denoted by asterisks (*), arising from spin-spin coupling of the terminal fluorine-on-xenon to natural abundance ^{129}Xe, $^1J(^{129}Xe\text{-}^{19}F)$ and the 1:2:1 triplet on the central line arising from $^4J(F_1\text{-}F_4)$.

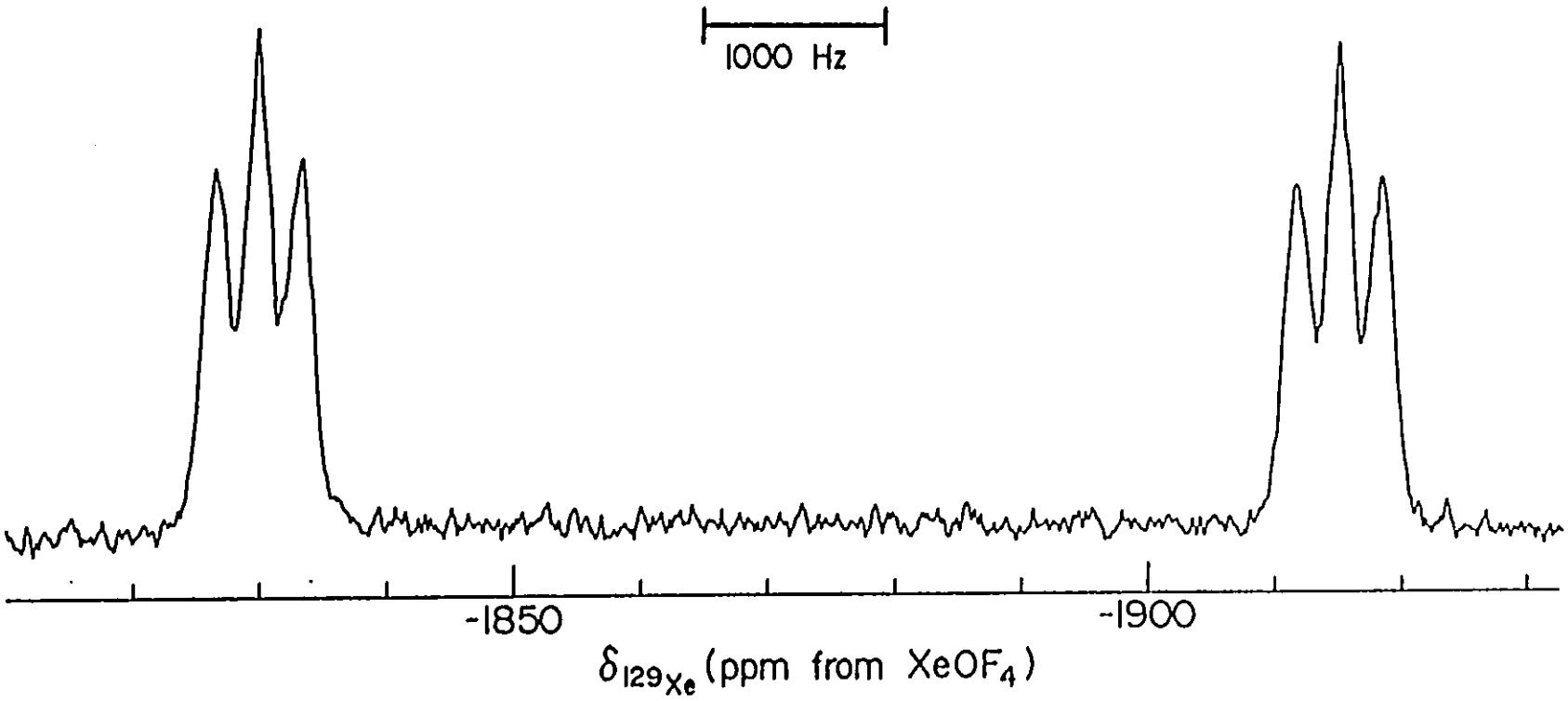

Figure 7.3 ^{129}Xe NMR spectrum (69.915 MHz) of the C_5F_5N-XeF^+ cation in HF solvent depicting the doublet arising from $^1J(^{129}Xe\text{-}^{19}F)$ and the partially quadrupole collapsed 1:1:1 triplets arising from $^1J(^{129}Xe\text{-}^{14}N)$.

C_5F_5N-$XeF^+AsF_6^-$ in HF solvent at -30 °C. The doublet arises from the one-bond coupling $^1J(^{129}Xe$-$^{19}F_2)$ of the Xe-F group and the partially quadruple collapsed 1:1:1 triplets arise from $^1J(^{129}Xe$-$^{14}N)$ for xenon directly bonded to the nitrogen of the pyridine ring. This signal in BrF_5 solvent showed a broad doublet which is $^1J(^{129}Xe$-$^{14}N)$ was not observed due to quadrupolar relaxation of the $^1J(^{129}Xe$-$^{14}N)$ by ^{14}N in the more viscous solvent, BrF_5 (i.e., the τ_c in BrF_5 is substantially larger in BrF_5 than in HF solvent).

The ^{19}F NMR spectra of the 4-$CF_3C_5F_4N$-XeF^+ cation showed well-resolved ^{19}F-^{19}F couplings at -50 °C in BrF_5, which were poorly resolved in HF solvent at -15 °C. The opposite was true for the C_5F_5N-XeF^+ cation in these solvents. The ^{19}F NMR spectra of the C_5F_5N-XeF^+ cation in HF solvent and the 4-$CF_3C_5F_4N$-XeF^+ cation in BrF_5 solvent were fitted using the spectral simulation program PANIC and the ^{19}F-^{19}F coupling constants for both cations are listed in Table 7.1. Figure 7.4 shows the ^{19}F NMR spectrum of the ortho-, meta- and para- fluorines in the perfluoropyridine ring of the C_5F_5N-XeF^+ cation and the simulated spectra. The ^{19}F NMR spectrum of "2-$CF_3C_5F_4N$-XeF^+" showed signals in addition to 2-$CF_3C_5F_4N$-XeF^+ arising from three other fluoro(perfluoropyridine)xenon(II) adduct cations; these arose because the starting material was actually a mixture of substituted pyridines and could not be fully assigned in the ^{19}F NMR spectra (see Figure 2.5). However, it was possible to assign the fluoro (perfluoropyridines)xenon(II) adduct cations from their ^{129}Xe NMR spectra in BrF_5 solvent: two of which were characterized before, namely, C_5F_5N-XeF^+ and 4-$CF_3C_5F_4N$-XeF^+. The 3-$CF_3C_5F_4N$-XeF^+ cation, was only present as a minor product (Figure 7.5).

On the assumption that the Fermi contact term is dominant for $^1J(^{129}Xe$-$^{14}N)$,

Table 7.1

NMR Parameters for the $R_FC_5F_4N$-XeF^+ (R = F, 2-CF_3, 3-CF_3 and 4-CF_3) Cations[a]

Cation	HF Solvent[b]			BrF_5[c]		Coupling Constants (Hz)				
	Chemical Shifts (ppm)			Chemical Shifts (ppm)						
	$\delta(^{129}Xe)$	$\delta(^{14}N)$	$\delta(^{19}F)$	$\delta(^{129}Xe)$	$\delta(^{19}F)$	$J(^{129}Xe\text{-}^{19}F)$	$\delta(^{19}F\text{-}^{19}F)^d$	$\delta(^{12}$	$\delta(^{129}Xe\text{-}^{14}N)^e$	$^1K(Xe\text{-}N) \times 10^{22}$ $NA^{-2}m^{-3}$
C_5F_5N-XeF^+	-1871.9	-208	-148.3 F(4)	-1922.5	-139.6 F(4)	5936	24.6 (25.3) F(1)F(4)		236	0.983
			-89.7 F(1)		-88.0 F(1)		-21.2 F(1)F(1')			
			-158.0 F(2)		-153.9 F(2)		17.6 F(1)F(2)			
			-115.4 F(3)		-110.1 F(3)		-14.4 F(1')F(2')			
							2.0 F(2)F(2')			
							-19.5 F(2)F(3)			
2-$CF_3C_5F_4N$-XeF^+	-1874.8			-1899.2		5947 (5947)			223	0.929
3-$CF_3C_5F_4N$-XeF^+	-1856.6			-1877.1		6010 (5934)			244	1.016
4-$CF_3C_5F_4N$-XeF^+	-1802.6		-153.8 F(3)	-1853.4	-144.6 F(3)	5977	25.8 (25.8) F(1)F(3)		238	0.991
			-88.7 F(1)		-86.8 F(1)		(-19.9) F(1)F(1')			
			-136.2 F(2)		-132.6 F(2)		(12.5) F(1)F(2)			
			-60.9 (CF_3)		-59.7 (CF_3)		(-19.3) F(1')F(2')			
							(-2.7) F(2)F(2')			
							(-20.4) F(2)F(CF_3)		Continued ...	

Table 7.1 (continued)

a Referenced externally at 24 °C with respect to the neat liquid references $XeOF_4$(^{129}Xe), $CFCl_3$(^{19}F) and CH_3NO_2(^{14}N).

b Recorded at -30 °C.

c Recorded at -50 °C.

d Calculated using the program PANIC on a Bruker ASPECT 2000 computer; root mean square-error 1.778 and 2.157 for the C_5F_5N-XeF^+ and 4-$CF_3C_5F_4N$-XeF^+ cations, respectively.

e ^1J(^{129}Xe-^{14}N) is quadrupole-collapsed in BrF_5 at -30 °C.

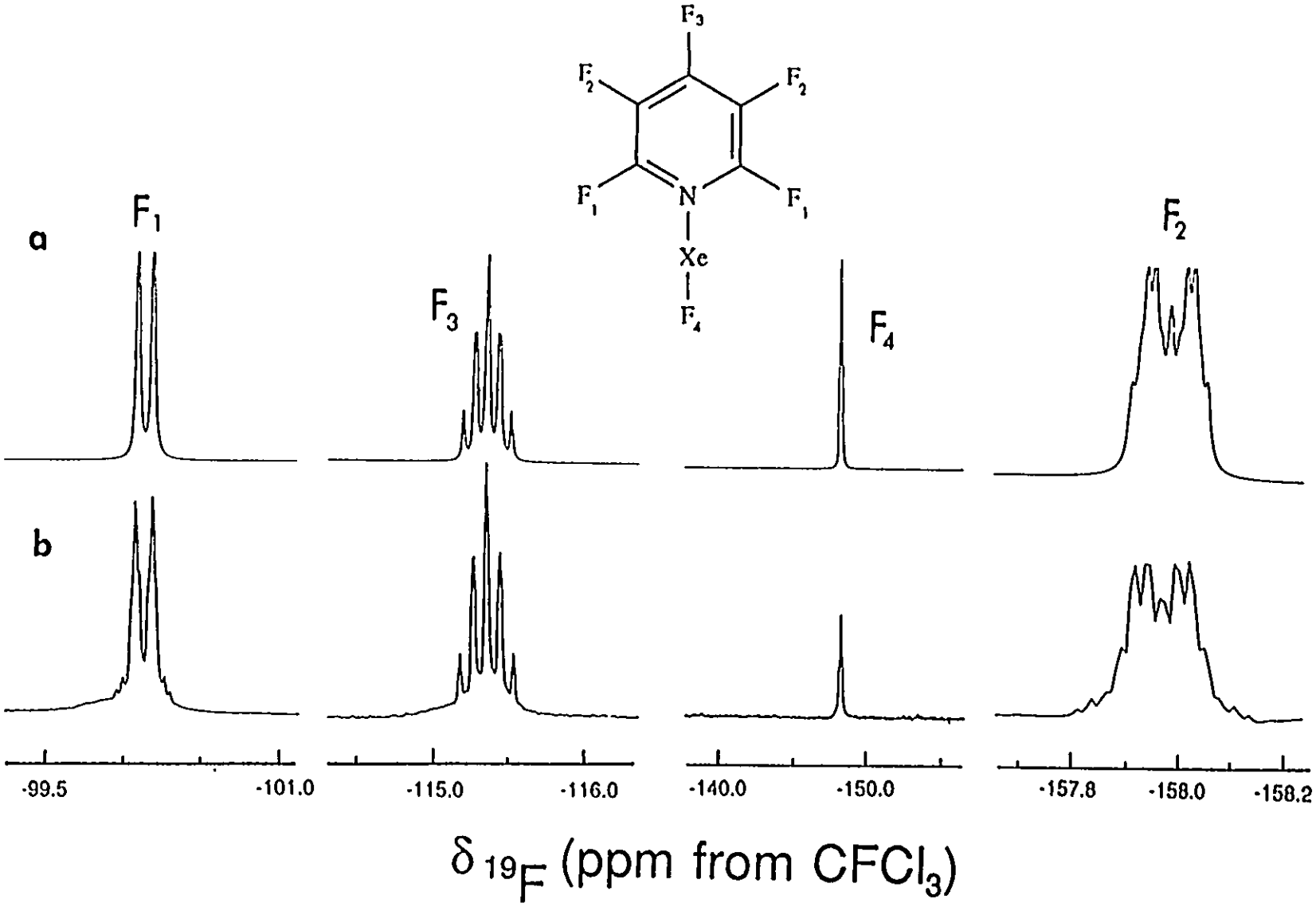

Figure 7.4 ^{19}F NMR spectra (235.361 MHz) of the ortho- (F_1), para- (F_2) and meta- (F_3) fluorines of the pentafluoropyridine ring of the C_5F_5N-XeF^+ cation in HF solvent at -30 °C; (a) the simulated spectrum using the personal computer program LAOCOON[219] and the program PANIC and (b) the experimental spectrum.

Figure 7.5 ^{129}Xe NMR spectrum (69.915 MHz) of a mixture of fluoro(perfluoropyridines)xenon(II) cations in BrF_5 at -50 °C: (A) 2-$CF_3C_5F_4N$-XeF^+, (B) C_5F_5N-XeF^+, (C) 4-$CF_3C_5F_4N$-XeF^+ and (D) 3-$CF_3C_5F_4N$-XeF^+. The ^{129}Xe signal for each cation is a doublet arising from spin coupling to the fluorine directly bonded to the xenon atom. The line broadening arises from residual scalar coupling to the quadrupolar ^{14}N nucleus.

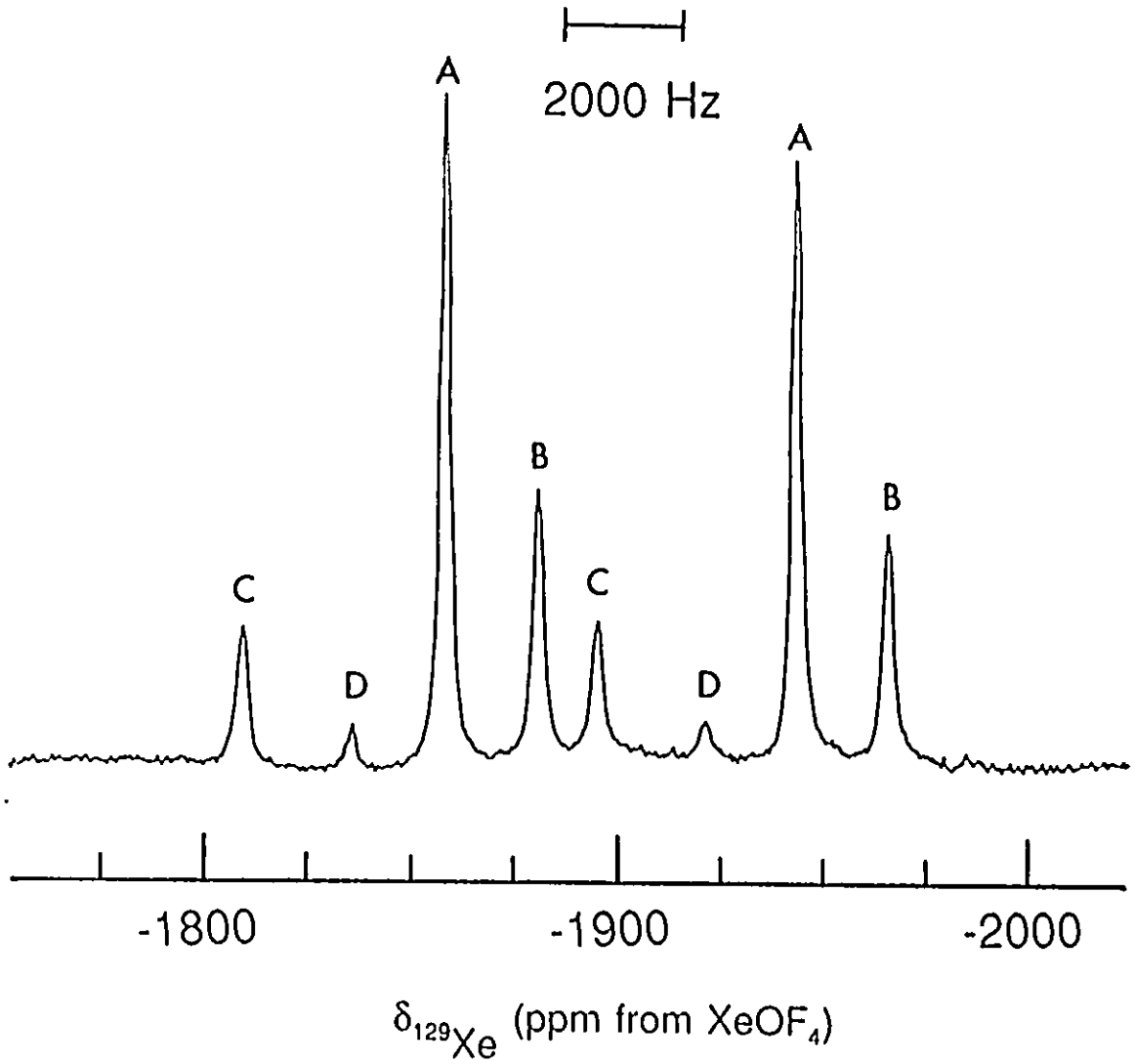
2000 Hz
A
A
B
B
C
C
D
D
-1800
-1900
-2000
$\delta_{^{129}Xe}$ (ppm from $XeOF_4$)

Table 7.2

Reduced Coupling Constants, $^1K_{Xe\text{-}N}$, for XeF^+ Coordinated to Nitrogen that is Formally sp or sp^2 Hybridized

Molecule/Cation	$^1K_{Xe\text{-}N} \times 10^{22}$ ($NA^{-2}m^{-3}$)	%s Character of Xe-N σ-bond
$RC{\equiv}N\text{-}XeF^+$	1.297 - 1.383	50%
$FXe\text{-}N(SO_2F)_2$	0.913	33.3%
$R_FC_5F_4N\text{-}XeF^+$	1.016 - 0.929	33.3%
$FXe\text{-}N_{sp3}$	(0.52 ± 0.05)	25%

a comparison of the Xe-N reduced coupling constants [Table 7.2, $^1K\ (Xe\text{-}N)_F = 0.983 \times 10^{22}\ NA^{-2}m^{-3}$, $^1K(Xe\text{-}N)_{4\text{-}CF_3} = 0.991 \times 10^{22}\ NA^{-2}m^{-3}$, $^1K(Xe\text{-}N)_{2\text{-}CF_3} = 0.929 \times 10^{22}\ NA^{-2}m^{-3}$ and $^1K(Xe\text{-}N)_{3\text{-}CF_3} = 1.016 \times 10^{22}\ NA^{-2}m^{-3}$] with those in which the xenon atom is σ-bonded to sp hybridized nitrogens [$RC{\equiv}N\text{-}XeF^+ = (1.297 - 1.393) \times 10^{22}\ NA^{-2}m^{-3}$] and an sp^2-hybridized nitrogen [$FXe\text{-}N(SO_2F)_2 = 0.913 \times 10^{22}\ NA^{-2}m^{-3}$] is consistent with bonding between the sp^2 hybridized nitrogen of the perfluoropyridines and xenon.

(C) CHARACTERIZATION OF $R_FC_5F_4N\text{-}XeF^+AsF_6^-$ (R = F, 2-CF_3/3-CF_3 AND 4-CF_3) IN THE SOLID STATE BY LOW-TEMPERATURE RAMAN SPECTROSCOPY

The low-temperature Raman spectra of the solid compounds, $R_FC_5F_4N\text{-}XeF^+AsF_6^-$ (R = F, 2-CF_3, 3-CF_3 and 4-CF_3), isolated from BrF_5 solution, are also consistent with the formation of AsF_6^- salts in which the xenon atoms are σ-bonded to the aromatic perfluoropyridine rings through nitrogen.

The Raman spectrum of the isolated product of the reaction of $C_5F_5NH^+AsF_6^-$ with XeF_2 in BrF_5 was studied at -196 °C (Figure 7.6, Table 7.3). The $C_5F_5N\text{-}XeF^+$ cation would be expected to possess C_{2v} symmetry and therefore a total of 3N - 6 = 33 normal modes are predicted for the cation. With the exception of A_2, which is infrared inactive, the representations of the normal vibrations for the $C_5F_5N\text{-}XeF^+$ cation (choosing xz as the molecular plane) are all Raman and infrared active, and given by

$$\Gamma_{vib}(C_{2v}) = 12A_1 + 11B_1 + 3A_2 + 7B_2 \qquad (7.4)$$

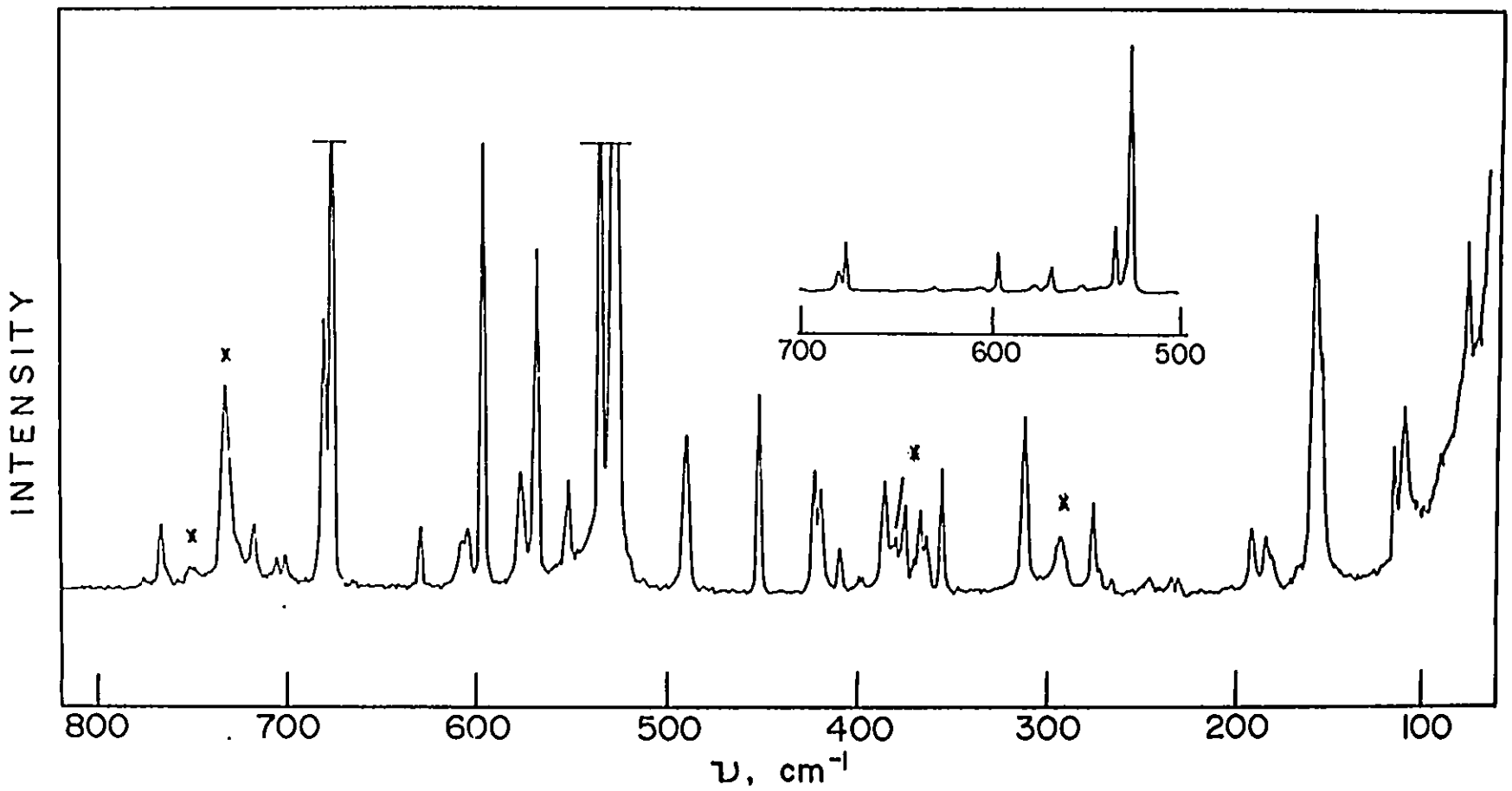

Figure 7.6 Raman spectrum of C_5F_5N-$XeF^+AsF_6^-$ recorded at -196 °C in an FEP sample tube. Asterisks (*) denote FEP bands.

Table 7.3

Raman Frequencies for C_5F_5N, $C_5F_5NH^+AsF_6^-$ and C_5F_5N-$XeF^+AsF_6^-$ and Their Tentative Assignments.[a]

Frequency, cm^{-1}			Approximate
C_5F_5N[b]	$C_5F_5NH^+AsF_6^-$[c]	C_5F_5N-$XeF^+AsF_6^-$	Description
	3002(1)		N-H Str.
1650(4)		1670(1)	A_1 (C-C ring str.) and B_1 (C-C str).
1619(<1)			428 + 1172 = 1600
1561(<1)			273 + 1285 = 1558
1529(4)		1552(1)	A_1 (ring str.)
1492(1)		1528(<1)	B_1 (ring str.)
1473(1)			174 + 1285 = 1459
1420(5)		1451(6)	A_1 (C-F str.)
1363(1)			620 + 736 = 1356
1347(<1)		1331(1)	?
1285(5)	1290 (1)	1288(1), 1274(1)	A_1 (C-F str.) and B_1 (ring str.)
1243(1)	1217(1)	1260(1)	184 + 1077 = 1261
1172(5)		1205(2)	B_1 (C-F str.)
1154(2)			457 + 694 = 1157
1077(<1)		1115(1)	A_1 (C-F str.)
983(<1)		1005(<1)	B_1 (C-F str.)
857(1)		812(3)	273 + 593 = 860
736(2)	736(2) [730(100)]	767(3)	B_2 (C-C twist.)
706(3)		705(1)	B_1 (i.p. C-F def.)
694(5)		701(1)	A_1 (ring def.)
	[694(8)]	680(9), 677(24)	$\nu_1(a_{1g})$ AsF_6^-
620(3)		629(2)	B_2 (C-C twist.)
593(9)	[593(10)]	605(2)	A_1 (ring str.)

continued ...

Table 7.3 (continued)

Frequency, cm^{-1}			Approximate
$C_5F_5N^a$	$C_5F_5NH^+AsF_6^-$	C_5F_5N-$XeF^+AsF_6^-$	Description
570(<1)		577(4)	A_2 (C-C twist)
	527(1) [525(13)]	569(12), 559(4)	$\nu_2(e_g)$ AsF_6^-
555(<1)			2 X 272 = 544
		535(28), 528(100)	A_1 (Xe-F)
476(7)	478(2)	490(5)	A_1 (ring def.)
457(<1)	446(3)	452(7)	B_1 (ring def.)
428(7)	410(2)	423(4)	A_2 (o.p. C-F def.)
398(<1)		419(4),410(2), 399(1)	184 + 231 = 415
379(<1)			?
	370(1) [384(32)]	386(4), 375(3), 370(1)	$\nu_3(t_{1g})$ AsF_6^-
		367(3), 364(2)	A_1 (Xe-N)
353(6)	354(1)	355(4)	B_2 (o.p. C-F def.)
310(1)	349(1)	275(3)	A_1 (i.p. C-F def.)
273(2)	270(1) [272(10)]	272(1)	A_1 (i.p. C-F def.) and
			B_1 (i.p. C-F def.)
		266(1), 235(1)	B_1 δ(XeNC)
224(<1)	291(1)	231(1)	B_1 (i.p. C-F def.) and
			B_2 (o.p. C-F def.)
		191(2)	B_2 δ(XeNC)
174(<1)		184(2)	B_2 (o.p. C-F def.) and
			A_2 (o.p. C-F def.)
		158(13), 154sh	B_1 and B_2 δ(FXeN)
		110(5)	Lattice modes
		76(5)	

continued ...

Table 7.3 (continued)

a The Raman spectrum was recorded at -196 °C using an FEP sample tube and 514.5 nm excitation. Lines due to FEP have not been deleted from the spectrum. Values in parentheses denote intensities; sh denotes a shoulder. Data given are for the spectrum depicted in Figure 7.6.

b Recorded in the liquid-phase.[220]

c From Ref. (221), values in square brackets are from the present work.

In addition, three Raman-active modes associated with the octahedral AsF_6^- anion, $\nu_1(a_{1g})$, $\nu_2(e_g)$ and $\nu_5(t_{2g})$ are also expected. An analysis of the Raman spectrum of the C_5F_5N-XeF^+ cation can be given in terms of the modes of the C_5F_5N and F-Xe-N moieties.

A total of 27 normal modes of vibration for the planar pentafluoropyridine group are expected and are given by the irreducible representations $10A_1 + 9B_1 + 3A_2 + 5B_2$ and correspond to in-plane vibrations, $10A_1$ and $9B_1$ (Raman and infrared active) and out-of-plane vibrations, $3A_2$ (Raman active) and $5B_2$ (Raman and infrared active).

The linear N-Xe-F moiety will give rise to 3N - 5 = 4 modes belonging to the irreducible representations $2A_1 + B_1 + B_2$ corresponding to ν(XeF), A_1; ν(XeN), A_1; δ(FXeN) in-plane, B_1 and δ(FXeN) out-of-plane, B_2. In addition, an in-plane F-Xe-ring wagging mode, B_1, and out-of-plane F-Xe-ring rocking mode, B_2, are also expected.

The vibrational modes of the C_5F_5N- group in the C_5F_5N-XeF^+ cation can be readily assigned by comparison with previous assignments for C_5F_5N[220-224] and $C_5F_5NH^+AsF_6^-$.[221] Long and Bailey [220] studied the liquid-phase Raman spectrum for C_5F_5N (Table 7.3) and have done a complete normal coordinate analysis and assignments for C_6F_5H upon which their assignments for C_5F_5N are based. The vibrational assignments for C_5F_5N-$XeF^+AsF_6^-$ are given in Table 7.3. This Table also includes tentative assignments of overtones and combinations for all bands observed up to 1700 cm^{-1}.

The pentafluoropyridine ring in the C_5F_5N-XeF^+ cation would be expected to have a spectrum similar to that of C_5F_5N. Consequently, the frequencies of C_5F_5N are useful in making assignments for the fundamental frequencies of the C_5F_5N-XeF^+ cation. The descriptions of the A_1, B_1, B_2 and A_2 vibrational modes of the pentafluoropyridine ring

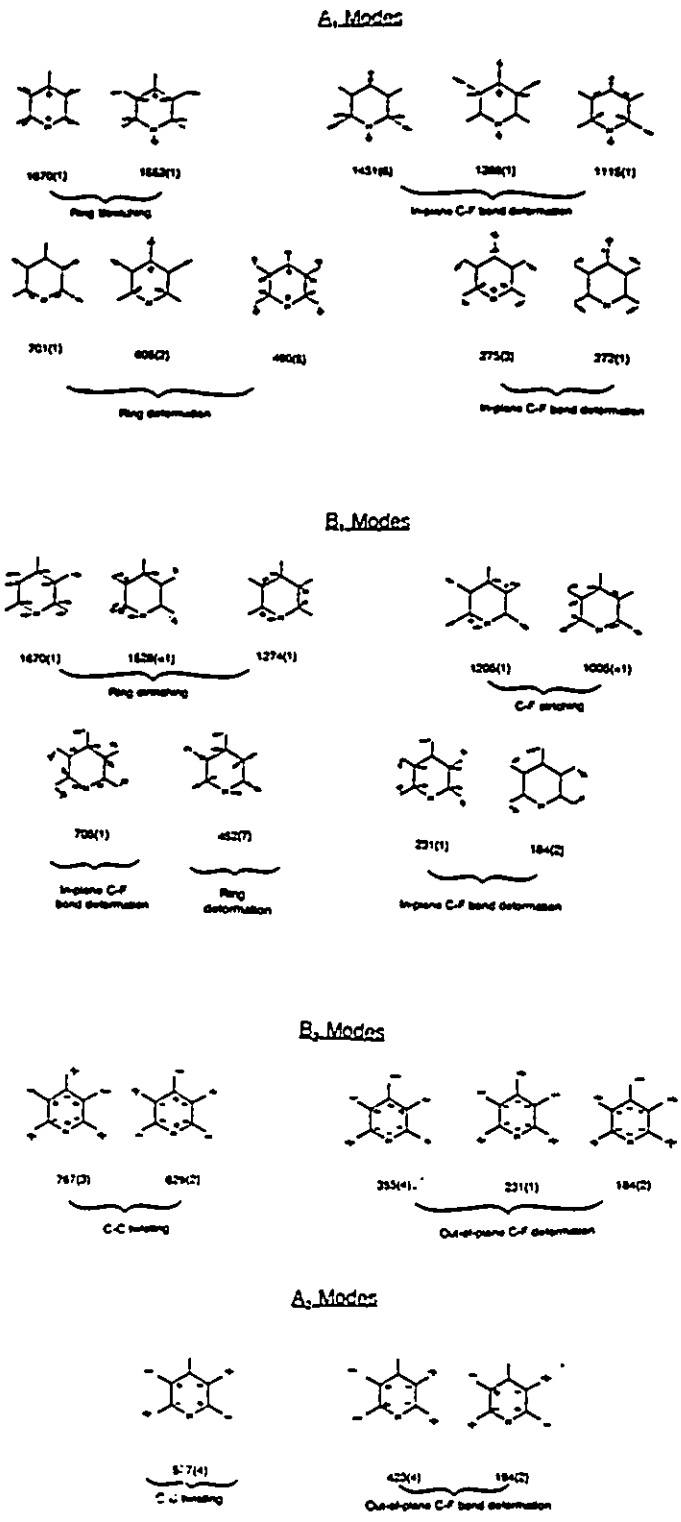

Figure 7.7 The in-plane and out-of-plane atomic displacements of the C_5F_5N ring in the C_5F_5N-XeF^+ cation.

in the C_5F_5N-XeF^+ cation are depicted in Figure 7.7. The atomic displacements are based on the descriptions of the vibrational analysis in reference (217).

Five of the expected ten fundamental vibrations belonging to the A_1 symmetry class are readily assigned for the C_5F_5N-XeF^+ cation: 1552(1), 1451(6), 1115(1) and 701(1) and 605(2) cm^{-1}. These frequencies are shifted to higher frequencies than the corresponding Raman lines in C_5F_5N,[220] as might be expected for the C_5F_5N-XeF^+ cation. The line observed at 1670(1) cm^{-1} is assigned to A_1 symmetry and belongs to the C-C stretching mode. This would be compatible with the assignment of this frequency to both the A_1 and the B_1 C-C stretching modes as has been done for C_5F_5N. The line at 1285(5) cm^{-1} is assigned to the C-F stretching modes in the spectrum of C_5F_5N and again is assigned to two bands having A_1 and B_1 symmetries. The corresponding two bands are better separated in the Raman spectrum of C_5F_5N-XeF^+ to produce the two lines observed at 1288(1) and 1274(1) cm^{-1}, which are assigned to the A_1 and B_1 modes, respectively. The remaining three A_1 modes of C_6F_5N ring have lines close to 273, 310 and 476 cm^{-1} of C_6F_5N. Two Raman lines are observed close to the latter line at 490(5) and at 452(7) cm^{-1}. The 490 (5) cm^{-1} line, which is shifted to higher frequency, has been assigned to the A_1 class and it is also close to the A_1 value of 476(7) in the C_5F_5N spectrum. The lower frequency line at 452(7) cm^{-1} is assigned to the B_1 fundamental. Raman lines observed at 275(3) and 272(1) cm^{-1} can be assigned to the two remaining A_1 fundamentals. Either of these frequencies could also be associated with a B_1 mode whose predicted value from the spectrum of C_5F_5N is in the 291 - 304 cm^{-1} region.

Assignments for four of the nine fundamentals having B_1 symmetry have already been dealt with; these are occur at 1670(1), 1274(1), 452(7) and 272(1) cm^{-1}. The Raman lines at 1528(<1), 1205(2) and 1005(<1) cm^{-1} can also be assigned to B_1 fundamentals by comparison with the frequencies of C_5F_5N in the liquid phase. The remaining two B_1 fundamental modes are both associated with C-F deformations. One band is observed at 705(1) cm^{-1} and the last mode is likely to be the Raman line at 231(2) cm^{-1}, although this may also be assigned to a B_2 mode.

The Raman line at 767(3) cm^{-1} has been assigned to a torsional mode (B_2 symmetry). The Raman band at 231(2) cm^{-1} (224(<1) cm^{-1} for C_5F_5N), is also assigned to B_2 and B_1 modes. The remaining three fundamental bands assignable to B_2 modes are (corresponding assignments for C_5F_5N are given in parentheses): 629(2) cm^{-1} (620(3) cm^{-1}), 355(4) cm^{-1} (353(6) cm^{-1}) and 184(2) (174(<1) cm^{-1}).

The three A_2 fundamental bands of the C_5F_5N ring have been assigned to 577(4), 423(4) and 184(2) cm^{-1} by comparison with C_5F_5N, i.e., 577(4) cm^{-1} (570(<1) cm^{-1}), 423(4) cm^{-1} (428(7) cm^{-1}) and 184(2) cm^{-1} (174(<1) cm^{-1}).

Formation of the C_5F_5N-XeF^+ cation introduces to the vibrational spectrum six extra degrees of freedom in addition to those of the C_5F_5N- group which, after subtracting the fundamental modes of C_5F_5N ($10A_1 + 9B_1 + 3A_2 + 5B_2$) from equation (7.4), leaves $2A_1 + 2B_1 + 2B_2$ to be accounted for. For the linear F-Xe-N group, four fundamental modes of vibration can be described: the N-Xe, Xe-F stretches, which are assigned to the remaining two A_1 modes; and in-plane (B_1) and out-of-plane (B_2) N-Xe-F bends, which have already been taken into account. The remaining two fundamental modes can be

described as an in-plane F-Xe-ring wagging mode, B_1, and an out-of-plane F-Xe-ring rocking mode, B_2. Of these six modes, the four deformation modes ($2B_1$ and $2B_2$) are expected to have low frequencies, probably less than 250 cm^{-1}.

The Xe-F stretching (A_1) mode of the C_5F_5N-XeF^+ cation is readily assigned by comparison with the Xe-F stretching frequencies of the other L-Xe-F species (see Table 3.3 in Chapter 3), which is usually the most intense band in the Raman spectrum and is consequently assigned to intense bands at 528(100) and 535(28) cm^{-1}; the splitting can only be attributed to coupling of vibrational modes within the unit cell.

The Xe-F stretching frequency of the C_6F_5N-XeF^+ cation is higher than that of FXe-$N(SO_2F)_2$ (506 cm^{-1}),[64] and lower than in the nitrile cations $RC{\equiv}N$-XeF^+ (565 - 541 cm^{-1} for R = H, CH_3, CH_2F, CH_2Cl, C_2H_5, $(CH_3)_2CH$ and $(CH_3)_3C$, respectively), reflecting the intermediate base strength of C_5F_5N with respect to the Lewis acid XeF^+. In the absence of ^{15}N isotopic enrichment experiments, the Xe-N stretching frequency (A_1 mode) can only be tentatively assigned to weak bands at 367(3) cm^{-1} and 364(2) cm^{-1}.

Based on the stretching frequencies of ν(Xe-F) and ν(Xe-N), an approximate assessment of the relative covalent character of the Xe-N bond in C_5F_5N-XeF^+ can also be made. It is noteworthy that the Xe-F stretching frequencies are lower than those of $FXe^+...FMF_5^-$ and $(FXe)_2F^+$,[25] but are higher in frequency than those of the $RC{\equiv}N$-$XeF^+AsF_6^-$ cations. Parallel trends have also been noted for the ^{19}F chemical shifts and ^{129}Xe-^{19}F coupling constants. This increase in the covalent character of the Xe-F bond relative to that of C_5F_5N-XeF^+ leads to a corresponding decrease in the covalent character of the Xe-N bond and a corresponding decrease in the Xe-N stretching

frequency. The in-plane (B_1) and out-of-plane (B_2) bending modes δ(F-Xe-N) are expected to occur at lower frequencies than the rocking and wagging F-Xe-ring modes and are assigned to bands at 158(13) and 154 (sh) cm^{-1}, respectively, by comparison with F-Xe-$N(SO_2F)_2$, where δ(F-Xe-N) is 200 cm^{-1} (average), and $HC{\equiv}N\text{-}XeF^+$, where δ(F-Xe-N) is 146 cm^{-1} (average). The δ(F-Xe-N) bend of $C_5F_5N\text{-}XeF^+$ reflects the relative covalent character of the Xe-N bond and is expected to be lower than that of F-Xe-$N(SO_2F)_2$, but higher than that of $HC{\equiv}N\text{-}XeF^+$.

The bands at 235(1) and 266(1) cm^{-1} are tentatively assigned to the B_1 in-plane F-Xe-ring bending. This assignment is supported by the assignments of the in-plane C-C-I deformation of iodobenzene and its derivatives, [224] which occur in the range 200 - 250 cm^{-1}. The B_2 F-Xe wagging (out-of-plane F-Xe-ring bending) mode is expected, by comparison with the iodobenzene, to occur at lower frequency than the in-plane F-Xe-ring bending mode and is tentatively assigned to a weak band at 191(2) cm^{-1}.

In addition, more than the expected three Raman-active bands due to the AsF_6^- anion are observed. The additional bands are attributed to site symmetry lowering and have been assigned under O_h symmetry to $\nu_1(a_{1g})$ (677(24), 680(9) cm^{-1}), $\nu_2(e_g)$ (559(4), 569(12) cm^{-1}), and $\nu_5(t_{2g})$ (370(1), 375(3), 386(4) cm^{-1}), respectively. Lines occurring below 112 cm^{-1} have been assigned to lattice modes.

The laser Raman spectrum of the product resulting from the reaction of $4\text{-}CF_3C_5F_4NH^+AsF_6^-$ with XeF_2 in BrF_5 (equation (7.3)) was studied at low-temperature (-196 °C) and supports the conclusion that this compound can be formulated as $4\text{-}CF_3C_5F_4N\text{-}XeF^+AsF_6^-$. The Raman spectrum at -196 °C showed signs of

decomposition when the solid was exposed to the laser beam at high power levels, resulting in a deep blue color. It is, however, possible to assign a number of bands in the 4-$CF_3C_5F_4N$-XeF^+ cation which are consistent with the proposed structure of the cation in the solid state. Table 7.4 lists some of the key Raman frequencies and their assignments for 4-$CF_3C_5F_4N$-$XeF^+AsF_6^-$ as well as a comparison with the corresponding frequencies in the C_5F_5N-$XeF^+AsF_6^-$ salts. The Xe-N stretching frequency can only be tentatively assigned to a weak band at 367 cm^{-1}, but this is in good agreement with the tentative assignment for the C_5F_5N-XeF^+ cation (367 cm^{-1}). The most intense band in the Raman spectrum of the salt occurs at 524 cm^{-1} and is assigned to Xe-F stretching frequency. The δ(F-Xe-N) bending frequency can also be tentatively assigned to a weak band at 162 cm^{-1}. In addition, lines arising from the AsF_6^- anions (677, 680 cm^{-1}, $\nu_1(a_{1g})$; 577 cm^{-1}, $\nu_2(e_g)$; 375 cm^{-1}, $\nu_5(t_{2g})$) are readily assigned. The low-temperature Raman spectra of the isolated mixture of $R_FC_5F_4N$-$XeF^+AsF_6^-$ (R_F = F, 2-CF_3, 3-CF_3 and 4-CF_3) was also obtained in the Xe-F stretching frequency region, and showed the most intense lines in the range (538 - 576 cm^{-1}), which are assigned to the Xe-F stretching frequencies.

Table 7.4

Some Key Frequencies and Assignments for C_5F_5N-$XeF^+AsF_6^-$ and 4-$CF_3C_5F_5N$-$XeF^+AsF_6^-$

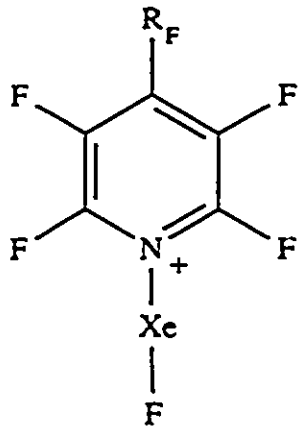

R_F = F, CF_3

Frequency (cm^{-1})[a]		Assignments
C_5F_5N-$XeF^+AsF_6^-$	4-$CF_3C_5F_4N$-$XeF^+AsF_6^-$	
528(100)	524(100)	ν(Xe-F)
367(2)	367(12)	ν(Xe-N)
158(13)	162(13)	δ(F-Xe-N)
677, 680		$\nu_1(a_{1g})$ } AsF_6^-
569		$\nu_2(e_g)$ } AsF_6^-
375		$\nu_5(t_{2g})$ } AsF_6^-

a Spectra recorded in FEP sample tubes at -196 °C and excited using the 514.5 nm line of an argon ion laser.

CHAPTER 8

SUMMARY, CONCLUSIONS AND DIRECTIONS FOR FURTHER RESEARCH

(A) SUMMARY

The present work represents a significant extension of noble-gas chemistry, and in particular, the synthesis of compounds containing noble-gas nitrogen bonds. This has been achieved by taking advantage of the Lewis acid properties of noble-gas cations and has given rise to several novel examples of xenon-nitrogen bonds. Moreover, this work has laid the ground work for the discovery of krypton-nitrogen bonds, namely, $HC{\equiv}N\text{-}KrF^{+}AsF_6^{-}$ [122] and $R_FC{\equiv}N\text{-}KrF^{+}AsF_6^{-}$ ($R_F = CF_3$, C_2F_5, $n\text{-}C_3F_7$).[123] The adduct salts, which have stabilities ranging from explosive at -60 °C for $HC{\equiv}N\text{-}KrF^{+}AsF_6^{-}$ [122] to stable at room temperature for $s\text{-}C_3F_3N_2N\text{-}XeF^{+}AsF_6^{-}$,[123] have donor-acceptor bonds which are among the weakest bonds that still deserve to be called bonds.

This Thesis has been concerned with the syntheses, structural characterization and bonding of the Lewis acid cation, XeF^{+}, to a variety of organic nitrogen base centers. Examples of Xe-N bonds have been relatively rare prior to this work. Several new adduct cations have resulted and have been characterized which represent novel Xe-N bonding

situations for xenon in its +2 oxidation state. The systems described in the present work were derived from the interaction of XeF^+ with appropriate electron pair donors, nitriles or perfluoropyridines, resulting in two new classes of xenon-nitrogen bonded compounds in which the Xe-N bonds are among the most ionic Xe-N bonds characterized to date. These studies have resulted in the preparation and characterization of nitrile cations $RC{\equiv}N\text{-}XeF^+$, where R = H, CH_3, FCH_2, $ClCH_2$, C_2H_5, CH_2FCH_2, *n*-C_3H_7, CH_3CHFCH_2, $CH_3CF_2CH_2$, $CH_2FCH_2CH_2$, $CHF_2CH_2CH_2$, $(CH_3)_2CH$, $ClCH_2C(CH_3)H$, $FCH_2C(CH_3)H$, $(CH_3)_3C$, *n*-C_4H_9, $CH_3CHFCH_2CH_2$ and C_6F_5 and the perfluoropyridinium cations $R_FC_5F_4N\text{-}XeF^+$, where R_F = F, 2-CF_3, 3-CF_3 and 4-CF_3. These cations have been characterized in HF and/or BrF_5 solutions by ^{129}Xe, ^{19}F, ^{14}N, ^{15}N, ^{13}C and ^1H NMR spectroscopy and in the solid state by low-temperature Raman spectroscopy. Furthermore, the perfluoropyridine derivatives of xenon represent the first examples in which a noble-gas atom serves as an aromatic substituent. The $HC{\equiv}N\text{-}XeF^+$, $CH_3C{\equiv}N\text{-}XeF^+$, $FCH_2C{\equiv}N\text{-}XeF^+$, $ClCH_2C{\equiv}N\text{-}XeF^+$, $C_2H_5C{\equiv}N\text{-}XeF^+$, $(CH_3)_2CHC{\equiv}N\text{-}XeF^+$, $(CH_3)_3CC{\equiv}N\text{-}XeF^+$, $C_5F_5N\text{-}XeF^+$ and 4-$CF_3C_5F_4N\text{-}XeF^+$ cations have also been isolated and characterized in the solid state by low-temperature Raman spectroscopy.

(i) <u>A Rational Understanding of the Approaches Used in the Syntheses of Nitrogen Base Adducts of XeF^+</u>

In view of the propensity of the XeF^+ cation to form strong fluorine bridges to counter anions in the solid state,[3] the XeF^+ cation may be regarded as having a significant

Lewis acid strength. Based on considerations of the high electron affinities of the cations (ArF^+, 13.7 eV[225]; KrF^+, 13.2 eV[190]; XeF^+, 10.9 eV[155]) and first adiabatic ionization potentials of selected bases, where the first adiabatic ionization potential, IP_1 (usually determined from photoelectron spectroscopy) is equal to or greater than the estimated electron affinity, EA, of the noble-gas cation; it has been possible to single out specific nitrogen bases and classes of nitrogen bases which offer reasonable promise for preparing noble-gas adduct cations in which the strongly oxidizing noble-gas cations are bound to organic and perfluoro-organic fragments through the nitrogen of the base.

Up to the present studies, there were two general synthetic approaches to forming bonds to xenon(II) which had been used:

The first approach involved the direct interaction of XeF_2 with the corresponding ligand group's protonic acid leading to HF displacement, which is generalized by equation (8.1).

$$XeF_2 + n\ RH \rightleftharpoons F_{2-n}XeR_n + n\ HF \qquad (8.1)$$

The second approach involved ligand exchange, and can be illustrated by the reaction of XeF_2 and $B(OTeF_5)_3$ in an inert solvent (equation (8.2)).

$$XeF_2 + \tfrac{2}{3}\ B(OTeF_5)_3 \longrightarrow Xe(OTeF_5)_2 + \tfrac{2}{3}\ BF_3 \qquad (8.2)$$

In the present work, the interaction of the Lewis acid XeF^+ with the neutral organic

Lewis bases represents a new synthetic approach. Interestingly, in the former two synthetic approaches, the ligand group must meet a set of criteria in order to form stable bonds to noble-gas centers. Among these criteria the most important is that the ligand group must possess a high effective electronegativity. In the present work, this criterion may also be seen to be operative as a requirement in forming stable Xe-N bonded compounds. Among the nitrogen electron donor centers investigated, namely those having formal hybridizations sp and sp^2, the effective electronegativity of the nitrile base center is expected to be higher than that of the pyridine base center. This is reflected in the relative stabilities of those adduct cations where the nitrile cations were found to be thermally more stable than the pyridine cations. These differences in stability and effective electronegativity are also reflected in the spectroscopic measurements (*vide infra*).

(ii) Fluoro(hydrogen cyanide)xenon(II) Hexafluoroarsenate:

$HC{\equiv}N\text{-}XeF^+AsF_6^-$

Hydrogen cyanide is oxidatively among the most resistant ligands investigated thus far, having a first adiabatic ionization potential of 13.80 eV. The estimated electron affinity of XeF^+ (10.9 eV[155]) suggested that $HC{\equiv}N$ would be resistant to oxidative attack by the XeF^+ cation and that $HC{\equiv}N\text{-}XeF^+$ might have sufficient thermal stability to permit its spectroscopic characterization in solution and in the solid state.

The reaction of XeF^+ with $HC{\equiv}N$ and the subsequent isolation of $HC{\equiv}N\text{-}XeF^+AsF_6^-$

and its characterization have indeed been realized in Chapter 3. The compound, $HC{\equiv}N\text{-}XeF^{+}AsF_6^{-}$, has been isolated as a white microcrystalline solid and characterized by multi-NMR and Raman spectroscopy. The vibrational assignments of the ν(Xe-N) stretching and δ(XeNC) and δ(FXeN) bending modes have been aided by obtaining Raman spectra for natural abundance, ^{15}N and ^{13}C-enriched $HC{\equiv}N\text{-}XeF^{+}AsF_6^{-}$.

Multinuclear magnetic resonance (multi-NMR) spectroscopy has proven essential for the characterization of the $HC{\equiv}N\text{-}XeF^{+}$ cation. Every element in the $HC{\equiv}N\text{-}XeF^{+}$ cation possesses at least one nuclide which is suitable for observation by NMR spectroscopy, namely, the spin-½ nuclei ^{1}H, ^{13}C, ^{15}N, ^{129}Xe and ^{19}F, and the spin-1 nucleus ^{14}N. Multinuclear magnetic resonance spectra were recorded for $HC{\equiv}N\text{-}XeF^{+}AsF_6^{-}$ in HF and BrF_5 solvents for all five spin-½ nuclei of the cation using natural abundance and ^{13}C and ^{15}N enriched compounds. All possible nuclear spin-spin couplings have been observed, unambiguously establishing the solution structure of the $HC{\equiv}N\text{-}XeF^{+}$ cation. Included among these scalar couplings are $^{1}J(^{129}Xe\text{-}^{14}N)$, $^{2}J(^{129}Xe\text{-}^{13}C)$ and $^{3}J(^{129}Xe\text{-}^{1}H)$, representing the first time scalar couplings have been observed between these nuclides.

An interesting feature of the NMR spectroscopy of the $HC{\equiv}N\text{-}XeF^{+}$ cation is the ready observation of the directly bonded $^{129}Xe\text{-}^{14}N$ and $^{14}N\text{-}^{13}C$ scalar couplings. The observation of both couplings and the relative ease of observing $^{1}J(^{129}Xe\text{-}^{14}N)$ in the alkyl nitrile and perfluoropyridine adducts of XeF^{+} (*vide infra*) is attributed to several factors which minimize quadrupole relaxation of the $^{129}Xe\text{-}^{14}N$ and $^{14}N\text{-}^{13}C$ couplings; the low electric field gradient at the ^{14}N nucleus of the adduct cations, low viscosity of the HF solvent leading to a short molecular correlation time and the small line width factor for

^{14}N.[22] However, in the higher viscosity solvent BrF_5 (-58 °C), the ^{129}Xe-^{14}N and ^{14}N-^{13}C couplings are quadrupole collapsed into single lines. Because they are generally obscured owing to quadrupolar relaxation caused by the ^{14}N nucleus, ^{15}N enrichment was required for the observation of scalar couplings between nitrogen and non-directly bonded nuclei where the magnitudes of the couplings are small.

(iii) Fluoro(nitrile)xenon(II) Hexafluoroarsenates; $RC{\equiv}N\text{-}XeF^+AsF_6^-$

Reactions of $XeF^+AsF_6^-$ with alkyl nitriles, $RC{\equiv}N$, and $C_6F_5C{\equiv}N$ have also been carried out by combining stoichiometric amounts of the reactants in anhydrous HF. The reactions proceed by analogy with equation (3.1). In the case of the alkyl nitriles and $HC{\equiv}N$, equilibrium (5.4) is significant so that equilibrium amounts of XeF_2, $RC{\equiv}NH^+$ and $HC{\equiv}NH^+$ were observed in the ^{129}Xe, ^{19}F, $^{14/15}N$, ^{13}C and ^1H NMR spectra but XeF_2 frequently was not observed in the ^{19}F and ^{129}Xe NMR spectra. The apparent absence of XeF_2 in the NMR spectra is attributed to chemical exchange involving free XeF^+ arising from equilibrium (5.5) and $Xe_2F_3^+$ as an exchange intermediate (equilibrium (5.7)).

Multi-NMR spectra (^{129}Xe, ^{19}F, ^{14}N, ^{15}N, ^{13}C and ^1H) have provided unambiguous proof for the structures of the $RC{\equiv}N\text{-}XeF^+$ cations in HF solution. Several alkyl nitrile adducts of the XeF^+ cation have also been isolated and characterized in the solid state by low-temperature Raman spectroscopy. The Xe-F stretching frequencies are consistent with weak covalent bonding between xenon and nitrogen.

(iv) Fluoro(perfluoropyridine)xenon(II) Hexafluoroarsenates: $R_FC_5F_4N\text{-}XeF^+AsF_6^-$

The fluoro(perfluoropyridine)xenon(II) cations, $R_FC_5F_4N\text{-}XeF^+$ (R_F = F or 4-CF_3), have been observed in HF and BrF_5 solutions and are stable in both media up to -30 °C. The salts $R_FC_5F_4N\text{-}XeF^+AsF_6^-$ have been isolated at -30 °C from BrF_5 solutions initially containing equimolar amounts of $R_FC_5F_4NH^+AsF_6^-$ and XeF_2. The resulting white solids were stable to -25 °C. Low-temperature Raman and ^{129}Xe, ^{19}F and ^{14}N NMR spectroscopic results are consistent with planar cations (Structure 8.1) in which the xenon atom is coordinated to the aromatic ring.

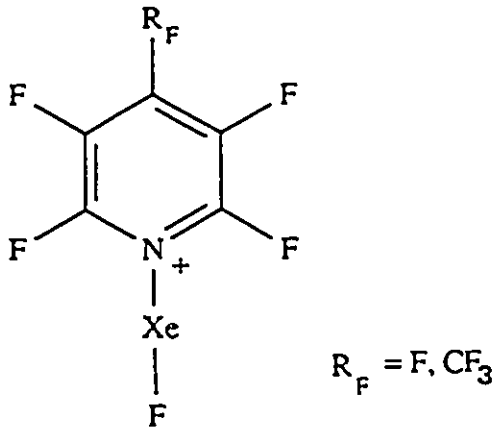

8.1

Equimolar amounts of $XeF^+AsF_6^-$ and the perfluoropyridine, $R_FC_5F_4N$ (R_F = F or 4-CF_3), react in anhydrous HF at -30 to -20 °C according to equation (7.1) and equilibria

(7.2) and (7.3) to give the novel Xe-N bonded cations, $R_FC_5F_4N\text{-}XeF^+$, as the AsF_6^- salts in solution.

At -30 °C these solutions consisted of equilibrium mixtures of XeF_2, $R_FC_5F_4NH^+AsF_6^-$ and $R_FC_5F_4N\text{-}XeF^+AsF_6^-$ as determined by NMR spectroscopy. Removal of HF solvent by pumping at -50 °C resulted in white solids which Raman spectroscopy at -196 °C also showed to be mixtures of $R_FC_5F_4N\text{-}XeF^+AsF_6^-$, XeF_2 and $R_FC_5F_4NH^+AsF_6^-$.

An alternative approach, which led to isolation of the Xe-N bonded cations, allowed stoichiometric amounts of XeF_2 and the perfluoropyridinium cations, as their AsF_6^- salts, to react in HF and BrF_5 solvents at -30 °C according to equilibrium (7.4). The equilibria in both solvents were monitored by ^{129}Xe, ^{19}F and ^{14}N NMR spectroscopy. In the case of BrF_5, formation of $R_FC_5F_4N\text{-}XeF^+AsF_6^-$ was strongly favored over that in HF solvent. Consequently, removal of BrF_5 solvent under vacuum at -30 °C yielded white solids corresponding to the salts $R_FC_5F_4N\text{-}XeF^+AsF_6^-$. The CF_3-derivatives substituted at the 2- and 3-positions have also been synthesized from their perfluoropyridinium salts in BrF_5 solvent and characterized by NMR spectroscopy. The $^{129}Xe\text{-}^{14}N$ coupling was quadrupole collapsed, as has also been observed for $4\text{-}CF_3\text{-}C_5F_4N\text{-}XeF^+AsF_6^-$ and $C_5F_5N\text{-}XeF^+AsF_6^-$ in BrF_5 at low temperatures. In HF solvent, however, $^1J(^{129}Xe\text{-}^{14}N)$ = 235 - 238 Hz was observed at -30 °C. The coupling between the ortho-ring fluorine and terminal fluorine on xenon $^4J(F_1\text{-}F_2)$ has also been observed for the perfluoropyridine cations $4\text{-}CF_3\text{-}C_5F_4N\text{-}XeF^+$ and $C_5F_5N\text{-}XeF^+$ and provides strong support for the proposed structures.

(v) Assessment of the Relative Ionic Characters of Xe-F and Xe-L (L = F, O or N) Bonds in F-Xe-L Type Compounds

Previous NMR studies of xenon(II) derivatives containing XeF groups bonded to oxygen or fluorine have shown that the NMR parameters measured in the ^{19}F and ^{129}Xe spectra can generally be used to assess relative covalent characters of the Xe-O, Xe---F bridge and terminal Xe-F bonds. In general, as the ionic character of the Xe-L (L = ligand) bond increases, the covalent character of the terminal Xe-F bond increases, increasing the formal charge on xenon. These trends are paralleled by decreases in $\delta(^{129}Xe)$ and increases in both $^1J(^{129}Xe\text{-}^{19}F)$ and $\delta(^{19}F)$ for the terminal XeF group. Table 8.1 provides the ^{129}Xe and ^{19}F chemical shifts and $^1J(^{129}Xe\text{-}^{19}F)$ coupling constants for a number of xenon(II) compounds containing terminal Xe-F bonds for comparison with some xenon-nitrogen bonded species.

Trends in ^{129}Xe and ^{19}F chemical shifts and $^1J(^{129}Xe\text{-}^{19}F)$ coupling constants show the variation in NMR parameters can be related to the ionic character of the Xe(II)-ligand atom bond. The terminal Xe-F group may be regarded as being bridged in either a fluoride, as in XeF_2 and $Xe_2F_3^+$, or to an oxygen, as in *trans*-FXe-$OIOF_4$ and *cis*-FXe-$OIOF_4$, or to a nitrogen, as in $HC{\equiv}N\text{-}XeF^+$, $4\text{-}CF_3C_5F_4N\text{-}XeF^+$, $s\text{-}C_3F_3N_2N\text{-}XeF^+$, $C_5F_5N\text{-}XeF^+$ and $FXe\text{-}N(SO_2F)_2$. In the specific case of XeF^+, the cation is not regarded as totally free, but is weakly bonded to a solvent fluorine or oxygen atom. The ^{129}Xe chemical shifts and $^1J(^{129}Xe\text{-}^{19}F)$ coupling constants show a decrease while ^{19}F chemical

Table 8.1

Comparison of Xe-F Stretching Frequencies and the Chemical Shifts and Coupling Constants in the F-Xe-L Derivatives

		NMR Parameters[b]				
Species[a]	ν(Xe-F) cm^{-1}	$^1J(^{129}Xe-^{19}F)$[c] Hz	$\delta(^{129}Xe)$[c,d] ppm	$\delta(^{19}F)$[c,d] ppm	T, °C	Ref.
$XeF^+...FSb_2F_{10}^-$	619	7230	-574	-290.2	23[f]	20,27,171,172
$XeF^+...FAsF_5^-$	610	6892	-869		-47	122,165,166,173,174
$(FXe)_2F^+$	593	6740	-1051	-252.0	-62	20,27,165,171
HC≡N-XeF$^+$	564	6181	-1569	-198.4[g]	-58	156
F_3S≡N-XeF$^+$	554	6248	-1661	-180.5	-60	228
CF_3C≡N-XeF$^+$		6397	-1337	-210.4	-63	123
C_2F_5C≡N-XeF$^+$		6437	-1294	-212.9	-63	123
n-C_3F_7C≡N-XeF$^+$		6430	-1294	-213.2	-63	123
CH_3C≡N-XeF$^+$[h]	560	6020	-1708	-185.5	-10	156
s-$C_3F_3N_2N$-XeF$^+$	548	5932	-1862	-145.6	-50	123
		5909	-1808	-154.9	-5	
FO_2SO-XeF	528	5830	-1666		-40	20,27,71,175
cis/trans-						
F_4OIO-XeF	527	5803/ 5910	-1824/ -1720	-161.7' -170.1'	0 0	60
C_5F_5N-XeF$^+$	528	5926	-1922	-139.6	-30	157
4-$CF_3C_5F_4N$-XeF$^+$	524	5963	-1853	-144.6	-50	157
F_5TeO-XeF	520		-2051	-151.0[k]	26	176,177
$(FO_2S)_2N$-XeF	506	5586 5664[k]	-1977 -2009[k]	-126.1' -126.0[k]	-58 -40	64,67
F_4S=N(H)-XeF$^+$		[l]	-2672[m]	[l]	-20	228
F_5S-N(H)-Xe$^+$		[l]	-2886[m]	[l]	-20	228
F_5Te-N(H)-Xe$^+$		[l]	-2903 -2841[m]	[l] [l]	-50 -45	229
XeF_2	496	5621	-1685	-184.3	-52	65,158,178

Continued...

Table 8.1 (continued)

a Unless otherwise indicated, all cations have AsF_6^- as the counterion.

b Spectra were obtained in BrF_5 solvent unless otherwise indicated.

c The NMR parameters of XeF groups are very sensitive to solvent and temperature conditions; it is therefore important to make comparisons in the same solvent medium at the same or nearly the same temperature.

d Referenced with respect to the neat liquids $XeOF_4$ (^{129}Xe) and $CFCl_3$ (^{19}F) at 24 °C; a positive sign denotes the chemical shift of the resonance in question occurs to higher frequency of (is more deshielded than) the resonance of the reference substance.

e Table entries refer to the terminal fluorine on the noble-gas atom.

f Recorded in SbF_5 solvent.

g $\delta(^{19}F)$ measured in anhydrous HF solvent at -10 °C.

h NMR parameters measured in HF solvent at -15 °C.

i $\delta(^{19}F)$ measured in SO_2ClF solvent at -40 °C.

j NMR parameters measured in SO_2ClF solvent.

k NMR parameters measured in SO_2ClF solvent at -50 °C.

l Not observed; Xe-F is relatively ionic and readily undergoes exchange in HF solvent.

m $\delta(^{129}Xe)$ measured in HF solvent.

shifts show an increase with increasing ionic character of the terminal Xe-F bond. This is consistent with valence bond structures 8.2 and 8.3,

$F\text{-}Xe^{+}\ \cdot L$ $\qquad\qquad$ $F^{-}\ {}^{+}Xe\text{-}L$

8.2 $\qquad\qquad$ 8.3

where the bonding electron pair of the terminal Xe-F bond becomes increasingly more localized with increasing ionic character of the Xe-L (L = F, O or N) bond. The results suggest the group electronegativies increase in the order: $-N(SO_2F)_2 < C_5F_5N < s\text{-}C_3F_3N_2N < 4\text{-}CF_3C_5F_4N <$ *cis*-$OIOF_3$ < *trans*-$OIOF_3$ < $CH_3C{\equiv}N < -OSO_2F < F_3S{\equiv}N < HC{\equiv}N < R_fC{\equiv}N$. Thus, the Xe-F bond of $HC{\equiv}N\text{-}XeF^{+}$ is among the weakest xenon-ligand bonds observed thus far.

Furthermore, if one considers the Xe-F stretching frequency of these derivatives to reflect the ionic character of the Xe-F bond, then the frequency is expected to increase as the xenon-ligand atom bond becomes more ionic and the terminal Xe-F bond becomes more covalent, i.e., develops more XeF^{+} character. The stretching frequency of the terminal Xe-F bond does indeed increase in the order of anticipated increasing group electronegativity, i.e., $-N(SO_2F)_2$, 506 cm^{-1} < $4\text{-}CF_3C_5F_4N$, 524 cm^{-1} < C_5F_5N, 528 cm^{-1} < *cis*/*trans*-$OIOF_3$, 527 cm^{-1} < HCN, 564 cm^{-1}, further supporting the proposed trend.

(vi) The Solvolytic Behaviors of $HC{\equiv}N\text{-}XeF^{+}AsF_6^{-}$ and $HC{\equiv}N$ in Anhydrous HF Solvent

The decomposition products of $HC{\equiv}N\text{-}XeF^{+}/HF$ reactions have been characterized using natural abundance, 99.2% ^{13}C and 99.5% ^{15}N-enriched $HC{\equiv}N\text{-}XeF^{+}AsF_6^{-}$, which are characterized as CF_4, CF_3H, $CF_3NH_3^{+}$, $CF_2{=}NH_2^{+}$, $CHF{=}NH_2^{+}$, Xe gas and several unidentified minor products. The first two products, CF_4 and CF_3H, were well known prior to this work while $CF_3NH_3^{+}$, $CF_2{=}NH_2^{+}$ and $CHF{=}NH_2^{+}$ have been characterized for the first time by ^{19}F, ^{14}N, ^{15}N, ^{13}C and ^{1}H NMR spectroscopy in the course of the present studies. The $CF_3NH_3^{+}$ cation represents one of the major products resulting from the decomposition of $HC{\equiv}N\text{-}XeF^{+}AsF_6^{-}$ in HF solvent. The $HC{\equiv}N\text{-}XeF^{+}$ cation was shown to exist for up to 14 hours at room temperature. The NMR spectra of HF solutions of $HC{\equiv}N$ recorded at -15 °C after warming for 7 days at room temperature indicate that one species, namely, the difluoromethylammonium cation, $CHF_2NH_3^{+}$, was formed. The $CHF_2NH_3^{+}$ cation has also been characterized in HF solution by ^{19}F, ^{14}N, ^{13}C and ^{1}H NMR spectroscopy. No other products were observed to form after 7 days at room temperature, conflicting with the earlier work,[189] which reported subsequent polymerization to give polymers whose structures were uncertain. In contrast with the related $RC{\equiv}N$ systems in HF solvent, the $RCF_2NH_3^{+}$ cations were shown to be intermediates, dimerizing to form *E*- and *Z*-$RCF_2N(H)C(R)NH_2^{+}$ (R = CH_3, C_2H_5, *n*-C_3H_7 and *n*-C_4H_9) cations (see Chapter 6, Structures 6.1 and 6.2). Reaction Schemes for the formation of the fluorinated decomposition/solvolysis products resulting from the $HC{\equiv}N\text{-}XeF^{+}/HF$ and $HC{\equiv}N/HF$

systems have been proposed in this Thesis.

(vii) The Solvolytic Behaviors of $RC{\equiv}N\text{-}XeF^{+}AsF_6^{-}$ and $RC{\equiv}N$ in Anhydrous HF Solvent

The solvolytic behaviors of the novel adduct salts, $RC{\equiv}N\text{-}XeF^{+}AsF_6^{-}$, have been studied in anhydrous HF solvent. The decompositions of the nitrile adduct cations $CH_3(CH_2)_nC{\equiv}N\text{-}XeF^{+}$ (n = 0 - 3) have been monitored in HF solution by multi-NMR spectroscopy. The rate of fluorination of the alkyl chain was shown to increase with increasing chain length, where the degree of fluorination increases at the alkyl carbons in the order $\beta < \gamma < \delta$, with no fluorination being observed at the α-carbon.

The thermal stabilities of the $RC{\equiv}N\text{-}XeF^{+}AsF_6^{-}$ salts have been examined by warming HF solutions of $RC{\equiv}N$ (R = CH_3, C_2H_5, *n*-C_3H_7 and *n*-C_4H_9) and $XeF^{+}AsF_6^{-}$ for several hours at room temperature. The stabilities of the $RC{\equiv}N\text{-}XeF^{+}AsF_6^{-}$ salts with respect to the chain length of the alkyl group decrease in the order *n*-$C_4H_9C{\equiv}N$ > *n*-$C_3H_7C{\equiv}N$ > $C_2H_5C{\equiv}N$ > $CH_3C{\equiv}N$.

A parallel study of the free nitriles in anhydrous HF concluded that the mechanism is dramatically different. In the former case, fluorination occurred on the alkyl group, while the neutral alkyl nitriles invariably add HF to the $C{\equiv}N$ bond and dimerize to form the *E*- and *Z*-$RCF_2N(H)C(R)NH_2^{+}$ (R = CH_3, C_2H_5, *n*-C_3H_7 and *n*-C_4H_9) cations (see Chapter 6. Structures 6.1 and 6.2). These reactions involve the $RCF_2NH_3^{+}$ cations as intermediates.

(B) CONCLUSIONS

Significant progress has been made in noble-gas chemistry by way of developing a new synthetic approach which leads to the formation of Xe(II)-N bonded adduct cations. This work has demonstrated that organic nitrogen bases are capable of stabilizing Xe(II), including several examples of the first compounds in which a noble-gas atom serves as an aromatic substituent. The key to this approach has been the choice of a neutral Lewis base, e.g., HC≡N, RC≡N and $R_FC_5F_4N$, such that the first ionization potential, IP_1, of the base is equal to or greater than the estimated electron affinity, EA, of the Lewis acid cation, XeF^+.

The overall significance and impact of this work is summarized below:

(1) The first examples of Xe-N bonded compounds, containing sp-hybridized nitrogen have been synthesized, namely, $HC{\equiv}N\text{-}XeF^+AsF_6^-$ and $RC{\equiv}N\text{-}XeF^+AsF_6^-$.

(2) The first examples of the Xe-N bonded species in which a noble-gas atom serves as an aromatic substituent have been synthesized, namely, $R_FC_5F_4N\text{-}XeF^+AsF_6^-$.

(3) A new synthetic approach to the formation of Xe-N bonds has spawned several novel developments not included in this Thesis:

   (i) The synthesis of $HC{\equiv}N\text{-}XeF^+$ has laid the ground work for the synthesis of the first Kr-N bonds,[122,123] by the interaction of KrF_2 (the estimated electron affinity of KrF^+ is 13.2 eV) with the $HC{\equiv}NH^+$ ($HC{\equiv}N$, IP_1 = 13.80 eV[133]), $CF_3C{\equiv}NH^+$ ($CF_3C{\equiv}N$, IP_1 = 13.90 eV[131]), $C_2F_5C{\equiv}NH^+$ and *n*-$C_3F_7C{\equiv}NH^+$.

(ii) Novel xenon-nitrogen bonds derived from perfluoroalkylnitriles, $R_FC{\equiv}N$-XeF^+ (R_F = CF_3, C_2F_5 or n-C_3F_7) have been characterized in BrF_5 solvent by ^{19}F and ^{129}Xe NMR spectroscopy.[123]

(iii) The adduct cation salt, s-$C_3F_3N_2N$-$XeF^+AsF_6^-$, which is stable at room temperature has been synthesized and characterized.[123]

(iv) The $F_3S{\equiv}N$-$XeF^+AsF_6^-$ cation, which undergoes solvolysis in HF at low-temperature to produce the novel $F_4S{=}N$-Xe^+ and F_5S-$N(H)Xe^+$ cations has recently been characterized by ^{19}F and ^{129}Xe NMR spectroscopy.[227] The F_5S-$N(H)Xe^+$ cation represents the first example of Xe-N bonded species where the nitrogen atom has formal sp^3-hybridization.

(v) Novel examples of xenon compounds containing N-Xe-O linkages, e.g., s-$C_3F_3N_2N$-Xe-$OMF_5^+AsF_6^-$ and $F_3S{\equiv}N$-Xe-$OMF_5^+AsF_6^-$ [227] (M = Te or Se) have been synthesized using the Lewis acid properties of the $XeOMF_5^+$ cations[228] (M = Te or Se). The synthesis of $XeOTeF_5^+Sb(OTeF_5)_6^-$ [228] and its high solubility in SO_2ClF allowed the formation of the $CH_3C{\equiv}N$-Xe-$OTeF_5^+$ and C_5F_5N-Xe-$OTeF_5^+$ adduct cations in this low polarity solvent.[228]

(C) DIRECTIONS FOR FUTURE RESEARCH

The successful preparation of xenon(II)-nitrogen bonded species by taking advantage of the Lewis acid behaviors of XeF^+, $XeOTeF_5^+$ and $XeOSeF_5^+$ has been

achieved by choosing nitrogen bases having first ionization potentials higher than the estimated electron affinity of the noble-gas Lewis acid cations. Several other bases not investigated in the present work which have potential and should also be investigated include N≡C-C≡N (IP_1 = 13.9), ClC≡N (IP_1 = 12.49 ± 0.4) and FC≡N.

$$X\text{-}C{\equiv}N + XeF^+AsF_6^- \xrightarrow{HF \text{ or } BrF_5} X\text{-}C{\equiv}N\text{-}XeF^+AsF_6^- \qquad (8.3)$$

$$X\text{-}C{\equiv}N + XeOTeF_5^+Sb(OTeF_5)_6^- \xrightarrow{SO_2ClF} X\text{-}C{\equiv}N\text{-}Xe\text{-}OTeF_5^+Sb(OTeF_5)_6^- \qquad (8.4)$$

(X = C≡N, Cl or F)

To date several examples of xenon(II)-nitrogen bonds have been synthesized where the nitrogen atom has formal sp and sp^2 hybridization. More recently, two examples containing xenon(II)-N_{sp3} bonded species, $F_5TeN(H)\text{-}Xe^+$ and $F_5SN(H)\text{-}Xe^+$, have been characterized by multi-NMR in solution.[229] Trifluoromethyl amine, CF_3NH_2, is a considerably weaker base than CH_3NH_2 due to the high effective electronegativity of the CF_3 group. The formation of $CF_3N(H)\text{-}Xe^+$ by the reaction of $CF_3NH_3^+$ and XeF_2 in BrF_5 (equation 8.5) should be feasible and would serve to extend the range of xenon(II)-N_{sp3} bonded species.

$$CF_3NH_3^+AsF_6^- + XeF_2 \xrightleftharpoons{BrF_5} CF_3N(H)\text{-}Xe^+AsF_6^- + 2HF \qquad (8.5)$$

Many of the adduct cations discussed in this Thesis have been isolated as

crystalline solids. Growing crystals of $HC{\equiv}N\text{-}XeF^{+}AsF_6^{-}$, $FCH_2C{\equiv}N\text{-}XeF^{+}AsF_6^{-}$, $(CH_3)_2CHC{\equiv}N\text{-}XeF^{+}AsF_6^{-}$, $(CH_3)_3CC{\equiv}N\text{-}XeF^{+}AsF_6^{-}$, $C_5F_5N\text{-}XeF^{+}AsF_6^{-}$ and $4\text{-}CF_3C_5F_4N\text{-}XeF^{+}AsF_6^{-}$ suitable for single crystal X-ray structure determinations would be a worthwhile extension of this work, but is complicated by the thermal instability of these compounds which necessitates both low-temperature mounting of suitable crystals, the most formidable problem, and low-temperature data acquisition.

Presently, XeF^{+}, $XeOTeF_5^{+}$, $XeOSeF_5^{+}$ and KrF^{+} have been used as noble-gas Lewis acids in adduct formation with organic and inorganic nitrogen Lewis bases. The success of this approach suggests that organic and inorganic oxygen Lewis bases, e.g., hexafluoroacetone, CF_3COCF_3, and carbonylfluoride, CF_2O, should interact with these noble-gas Lewis acids in a similar manner.

$$(R_F)_2CO + XeL^{+}AsF_6^{-} \longrightarrow (R_F)_2CO\text{-}XeL^{+}AsF_6^{-} \qquad (8.6)$$

$$(R_F = F \text{ or } CF_3 \text{ and } L = F, OTeF_5 \text{ or } OSeF_5)$$

In addition, the interaction of high-valent noble-gas Lewis acids, e.g., XeF_3^{+}, $XeOF_3^{+}$, XeO_2F^{+} and XeF_5^{+} should be attempted with nitrogen (equations (8.7) - (8.10)) and oxygen (equations (8.11) and (8.12)) base centers having appropriately high IP_1 values. However, in order to assesss the viability of these experiments it is desirable to have estimates of the electron affinities of these cations, which are expected to be significantly greater than that of XeF^{+}.

$$X\text{-}C{\equiv}N + XeF_3^+SbF_6^- \longrightarrow X\text{-}C{\equiv}N\text{-}XeF_3^+SbF_6^- \quad (8.7)$$

$$X\text{-}C{\equiv}N + XeOF_3^+SbF_6^- \longrightarrow X\text{-}C{\equiv}N\text{-}XeOF_3^+SbF_6^- \quad (8.8)$$

$$X\text{-}C{\equiv}N + XeO_2F^+SbF_6^- \longrightarrow X\text{-}C{\equiv}N\text{-}XeO_2F^+SbF_6^- \quad (8.9)$$

$$X\text{-}C{\equiv}N + XeF_5^+SbF_6^- \longrightarrow X\text{-}C{\equiv}N\text{-}XeF_5^+SbF_6^- \quad (8.10)$$

(X = H, C≡N, Cl or F)

$$(R_F)_2CO + XeF_3^+SbF_6^- \longrightarrow (R_F)_2CO\text{-}XeF_3^+SbF_6^- \quad (8.11)$$

$$(R_F)_2CO + XeOF_3^+SbF_6^- \longrightarrow (R_F)_2CO\text{-}XeOF_3^+SbF_6^- \quad (8.12)$$

$$(R_F)_2CO + XeO_2F^+SbF_6^- \longrightarrow (R_F)_2CO\text{-}XeO_2F^+SbF_6^- \quad (8.13)$$

$$(R_F)_2CO + XeF_5^+SbF_6^- \longrightarrow (R_F)_2CO\text{-}XeF_5^+SbF_6^- \quad (8.14)$$

(R_F = F or CF_3)

The reactions of $R_FC_5F_4NH^+AsF_6^-$ with XeF_2 and $HC{\equiv}NH^+AsF_6^-$ with KrF_2 in HF and BrF_5 solvents strongly suggest that this approach could be extended to interaction of neutral high-valent, coordinately unsaturated noble-gas compounds, e.g., XeO_2F_2 and $XeOF_4$, with nitrogen (equations (8.15)-(8.16)) and oxygen bases leading to the formation of new high-valent xenon compounds containing xenon-nitrogen and xenon-oxygen bonds.

$$X\text{-}C{\equiv}N + XeO_2F_2 \longrightarrow X\text{-}C{\equiv}N\text{-}XeO_2F_2 \quad (8.15)$$

$$X\text{-}C{\equiv}N + XeOF_4 \longrightarrow X\text{-}C{\equiv}N\text{-}XeOF_4 \quad (8.16)$$

(X = H, C≡N, Cl, F)

REFERENCES

1. N. Bartlett, Proc. Chem. Soc. 218 (1962).
2. K. Seppelt and D. Lentz, In "Progress in Inorganic Chemistry", S.J. Lippard, Ed.; John Wiley & Sons, Inc.: New York, 1982, Vol. 29, pp. 167 - 202.
3. H. Selig and J.H. Holloway, In "Topics in Current Chemistry", F.L. Boschke, Ed.; Springer-Verlag: New York, 1984, pp. 33 - 90.
4. H.H. Classen, In "The Noble Gases", D.C. Health and Company: Boston, 1966.
5. J.H. Holloway, In "Noble-Gas Chemistry", Methuen & Co.: Bungay, Suffolk, 1968.
6. H.H. Hyman, In "Noble-Gas Compounds", The University of Chicago: Chicago, 1963.
7. N. Bartlett and F.O. Sladky, In "Comprehensive Inorganic Chemistry", J.C. Bailar, H.J. Emeleus, R. Nyholm and A.F. Trotman-Dickenson, Eds.; Pergamon Press: New York, 1973, Vol. 1, Chapt. 6.
8. K. Seppelt and N. Bartlett, Z. Anorg. Allg. Chem., 436, 122 (1977).
9. B. Weintock, E.E. Weaver and C.P. Knop, Inorg. Chem., 5, 2189 (1966).
10. K.O. Christe, E.C. Curtis, D.A. Dixon, H.P. Mercier, J.C.P. Sanders and G.J. Schrobilgen, J. Am. Chem. Soc., 113, 3351 (1991).
11. (a) K.O. Christe, J.C.P. Sanders, G.J. Schrobilgen and W.W. Wilson, J. Chem. Soc., Chem. Commun., 837 (1991). (b) A. R. Mahjoub and K. Seppelt, J. Chem. Soc., Chem. Commun., 840 (1991).

12. W.J. Adams, H.B. Thompson and L.S. Bartell, J. Chem. Phys., 53, 4040 (1970).

13. W.E. Falconer and W.A. Sunder, J. Inorg. Nucl. Chem., 29, 1380 (1967).

14. J.G. Malm and C.L. Chernick, Inorg. Synth., 8, 254 (1966).

15. Ref. (13), p. 258.

16. R.J. Gillespie and G.J. Schrobilgen, J. Chem. Soc., Chem. Commun., 595 (1977).

17. K.O. Christe and W.W. Wilson, Inorg. Chem., 27, 3763 (1988).

18. N. Bartlett and M. Wechsberg, Z. Anorg. Allg. Chem., 385, 5 (1971).

19. F. Sladky, P.A. Bulliner and N. Bartlett, J. Chem. Soc., Dalton Trans., 2179 (1969).

20. G.J. Schrobilgen, J.H. Holloway, P. Granger and C. Brevard, Inorg. Chem., 17, 290 (1978).

21. R.J. Gillespie and G.J. Schrobilgen, Inorg. Chem., 13, 765 (1974).

22. J.H. Holloway and J.G. Knowles, J. Chem. Soc. (A), 756 (1969).

23. V.M. McRae, R.D. Peacock and D.R. Russell, J. Chem. Soc., Chem. Commun., 62 (1969).

24. F.O. Sladky, P.A. Bulliner and N. Bartlett, J. Chem. Soc. (A), 2179 (1969).

25. R.J. Gillespie and B. Landa, Inorg. Chem., 12, 1383 (1973).

26. B. Frlec and J.H. Holloway, J. Chem. Soc., Dalton Trans., 535 (1975).

27. R.J. Gillespie, A. Netzer and G.J. Schrobilgen, Inorg. Chem., 13, 1455 (1974).

28. N. Bartlett, M. Gennis, D.D. Gibler, B.K. Morrell, Inorg. Chem., 12, 1717 (1973).

29. C.J. Adams and N. Bartlett, Isr. J. Chem., 17, 114 (1978).

30. N. Bartlett, F. Einstein, D.F. Stewart and J. Trotter, J. Chem. Soc. (A), 1190

(1967).

31. K. Leary, D.H. Templeton, A. Zalkin and N. Bartlett, Inorg. Chem., 12 1726 (1973).

32. J. Slivnik, B. Frlec, B. Žemva and M. Bohinc, J. Inorg. Nucl. Chem., 32, 1397 (1970).

33. N. Bartlett and F.O. Sladky, J. Am. Chem. Soc., 90, 5316 (1968).

34. M.J. Rothman and L.S. Bartell, J. Chem. Phys., 73, 375 (1980).

35. K. Leary, A. Zalkin and N. Bartlett, Inorg. Chem., 13, 775 (1974).

36. J.H. Holloway and G.J. Schrobilgen, J. Che. Soc., Chem. Commun., 623 (1975).

37. K. Leary and N. Bartlett, J. Chem. Soc., Chem. Commun., 903 (1972).

38. K.E. Pullen and G.H. Cady, Inorg. Chem., 6, 2267 (1967).

39. B. Žemva, K. Lutar, A. Jesih, W.J. Casteel, Jr., and N. Bartlett, J. Chem. Soc., Chem. Commun., 346 (1989).

40. D.E. McKee, C.J. Adams, A. Zalkin and N. Bartlett, J. Chem. Soc., Chem. Commun., 26 (1973).

41. D.E. McKee, A. Zalkin and N. Bartlett, Inorg. Chem., 12, 1713 (1973).

42. R.J. Gillespie and G.J. Schrobilgen, Inorg. Chem., 13, 2370 (1974).

43. R.J. Gillespie, B. Landa and G.J. Schrobilgen, J. Inorg. Nucl. Chem., Suppl., 179 (1976).

44. R.J. Gillespie, D. Martin and G.J. Schrobilgen, J. Chem. Soc., Dalton Trans., 1898 (1980).

45. N. Bartlett, M. Wechsberg, F.O. Sladky, P.A. Bulliner, G.R. Johns and R.D.

Burbank, J. Chem. Soc., Chem. Commun., 703 (1969).

46. M. Wechsberg, P.A. Bulliner, F.O. Sladky, R. Mews and N. Bartlett, Inorg. Chem., 11, 3063 (1972).

47. F. Sladky, Angew. Chem., Int. Ed. Engl., 8, 373 (1969).

48. F. Sladky, Angew. Chem., Int. Ed. Engl., 8, 523 (1969).

49. F. Sladky, Monatsh. Chem., 101, 1559 (1970).

50. F. Sladky, Monatsh. Chem., 101, 1571 (1970).

51. D. Lentz and K. Seppelt, Angew. Chem., Int. Ed. Engl., 17, 356 (1978).

52. D. Lentz and K. Seppelt, Angew. Chem., Int. Ed. Engl., 15, 66 (1976).

53. E. Jacob, D. Lentz, K. Seppelt and A. Simon, Z. Anorg. Allg. Chem., 472, 7 (1981).

54. G.A. Schumacher and G.J. Schrobilgen, Inorg. Chem., 23, 2923 (1984).

55. M. Eisenberg and D.D. DesMarteau, Inorg. Chem., 11, 1901 (1972).

56. K. Seppelt, Angew. Chem., Int. Ed. Engl., 11, 723 (1972).

57. K. Seppelt and D. Nothe, Inorg. Chem., 12, 2727 (1973).

58. J.J. Musher, J. Am. Chem. Soc., 90, 7371 (1968).

59. M. Eisenberg and D.D. DesMarteau, Inorg. Nucl. Chem. Lett., 6, 29 (1970).

60. R.G. Syvert and G.J. Schrobilgen, Inorg. Chem., 28, .1564 (1989).

61. F.A. Cotton and G. Wilkinson, Eds., In "Advanced Inorganic Chemistry", Wiley Interscience, J. Wiley & Sons: New York (1980), pp. 555.

62. D.R. Lide, "CRC Handbook of Chemistry and Physics"; CRC Press Inc., Boca Raton, Florida, 72th Edition (1991-1992).

63. H. Meinert and S. Rüdiger, Z. Chem., 9, 35 (1969).

64. J.F. Sawyer, G.J. Schrobilgen and S.J. Sutherland, Inorg. Chem., 21, 4064 (1982).

65. D.D. DesMarteau, R.D. LeBlond, S.F. Hossian, D. Nothe, J. Am. Chem. Soc., 103, 7734 (1981).

66. R.D. LeBlond and D.D. DesMarteau, J. Chem. Soc., Chem. Commun., 555 (1976).

67. G.A. Schumacher and G.J. Schrobilgen, Inorg. Chem., 22, 2178 (1983).

68. J. Foropoulos and D.D. DesMarteau, J. Am. Chem. Soc., 104, 4260 (1982).

69. R. Faggiani, D.K. Kennepohl, C.J.L. Lock and G.J. Schrobilgen, Inorg. Chem., 25, 563 (1986).

70. D.D. DesMarteau, J. Am. Chem. Soc., 100, 6270 (1978).

71. T.A. Carlson and R.M. White, J. Chem. Phys., 36, 2883 (1962).

72. V.D. Nefedov, M.A. Toropova and A.V. Levchenko, Radiokhimiya, 9, 138 (1967): C.A. 67, 59841 (1967).

73. M.A. Toropova, V.D. Nefedov, A.V. Levchenko and O.G. Matveev, Radiokhimiya, 10, 613 (1968); C.A. 70, 24701 (1969).

74. M.A. Toropova, V.D. Nefedov, A.V. Levchenko and Yu.P. Saikov, Radiokhimiya, 10, 611 (1968); C.A. 70, 24889 (1969).

75. T.O. Tiernan and P.S. Gill, J. Chem. Phys., 50, 5042 (1969).

76. L.P. Theard and W.H. Hamill, J. Am. Chem. Soc., 84, 1134 (1962).

77. D. Holtz and J.L. Beauchamp, Science, 173, 1237 (1971).

78. M. Karplus, C.W. Kern and D. Sazdins, J. Chem. Phys., 40, 3738 (1964).

79. F.H. Field and J.L. Franklin, J. Am. Chem. Soc., 83, 4509 (1961).

80. L.J. Turbini, R.E. Aikman and R.J. Lagow, J. Am. Chem. Soc., 101, 5833 (1979).

81. M. Schmeisser, R. Walter and D. Naumann, Z. Anorg. Allg. Chem., 464, 233 (1980).

82. D.D. DesMarteau, private communication.

83. R.L. Lagow, W., -H. Lin, W.D. Clark and M.M. Brezinski, American Chemical Society, 9th Winter Fluorine Conference, St. Petersburg Beach, Florida, January 29 - February 3 1989.

84. W. Tötsch and N. Bartlett, private communication.

85. D.R. Stull and H. Prophet, JANAF Thermochemical Tables, 2nd Ed., NSRDS-NBS # 37 (1971), 1/1141.

86. V.I. Pepekin, Y.A. Lebedev and A.Y. Apin, Zh. Fiz. Khem., 43, 869 (1969).

87. (a) J.K. Hovey and T.B. McMahon, J. Am. Chem. Soc., 108, 528 (1986). (b) G.R. Hertel and W.S. Koski, J. Am. Chem. Soc., 87, 1686 (1965). (c) M.S.B. Munson, F.H. Field and J.L. Franklin, J. Chem. Phys., 37, 1790 (1962).

88. G. Klöter, H. Pritzkow and K. Seppelt, Angew. Chem., Int. Ed. Engl., 19, 942 (1980).

89. L. Turowsky and K. Seppelt, Inorg. Chem., 27, 2135 (1988).

90. G.J. Schrobilgen, unpublished work.

91. D. Naumann and W. Tyrra, J. Chem. Soc., Chem. Commun., 47 (1989).

92. H. J. Frohn and S. Jakobs, J. Chem. Soc., Chem. Commun., 625 (1989).

93. H.J. Frohn, S. Jakobs and G. Henkel, Angew. Chem., Int. Ed. Engl., 28, 1506

(1989).

94. H.J. Frohn, J. Helber and A. Richter, Chem. Ztg. 107, 169 (1983).

95. R.D. Willett, S.D. Petersen and B.A. Coyla, J. Am. Chem. Soc., 99, 6202 (1977).

96. G.J. Perlow and M.R. Perlow, J. Chem. Phys., 48, 955 (1968).

97. H. Meinert, Z. Chem., 6, 71 (1966).

98. L.Y. Nelson and G.C. Pimentel, Inorg. Chem., 6, 1758 (1967).

99. W.F. Howard, Jr. and L. Andrews, J. Am. Chem. Soc., 96, 7864 (1974).

100. L. Stein, J.R. Norris, A.J. Downs and A.R. Minihan, J. Chem. Soc., Chem. Commun., 502 (1978).

101. L. Stein and W.W. Henderson, J. Am. Chem. Soc., 102, 2856 (1980).

102. W.F. Howard, Jr. and L. Andrews, J. Am. Chem. Soc., 97, 2956 (1975).

103. R.S. Mulliken, J. Chem. Phys., 52, 5170 (1970).

104. W.R. Wadt, J. Chem. Phys., 68, 402 (1978).

105. C.T. Goetschel and K.R. Loos, J. Am. Chem. Soc., 94, 3018 (1972).

106. N.N. Greenwood and A. Earnshaw, Eds., In "Chemistry of The Elements", Pergamon Press: Oxford (1984), Chapter 18.

107. F. Schreiner, J.G. Malm and J.C. Hindman, J. Am. Chem. Soc., 87, 25 (1965).

108. J.J. Turner and G.C. Pimental, Science, 140, 974 (1963).

109. D.R. MacKenzie, Science, 141, 1171 (1963).

110. J. Slivnik, A. Šmalc, K. Lutar, B. Žemva and B. Frlec; J. Fluorine Chem., 5, 273 (1975).

111. L.V. Streng and A.G. Streng, Inorg. Chem., 5, 328 (1966).

112. A.A. Arlyukhov, V.A. Lagasov, G.N. Makeev, L.A. Palkina, B.M. Smirnov and B.B. Chaivanov, Khim. Vys. Energ., 11, 88 (1977); C.A. 86 : 163520j (1977).

113. V.N. Bezmel'nitsyn, V.A. Legasov and B.B. Chaivanov, Dokl. Alkad. Nauk SSSR, 235, 96 (1977); C.A. 87 : 110631k (1977).

114. G.J. Schrobilgen, Ph.D. Thesis, McMaster University, Hamilton, Ontario, Canada (1973).

115. R.J. Gillespie and G.J. Schrobilgen, Inorg. Chem., 13, 1230 (1974).

116. A.V. Grosse, A.D. Kirshenbaum, A.G. Streng and L.V. Streng, Science, 139, 1047 (1963).

117. E.N. Sloth and M.H. Studier, Science, 141, 528 (1964).

118. T.A. Carlson and R.M. White, J. Chem. Phys., 39, 1748 (1963).

119. G.R. Hertel and W.S. Koski, J. Am. Chem. Soc., 87, 1686 (1965).

120. F.H. Field, H.N. Head and J.L. Franklin, J. Am. Chem. Soc., 84, 1118 (1962).

121. J.K. Hovey and T.B. McMahon, J. Phys. Chem., 91, 4560 (1987).

122. G.J. Schrobilgen, J. Chem. Soc., Chem. Commun., 863 (1988).

123. G.J. Schrobilgen, J. Chem. Soc., Chem. Commun., 1506 (1988).

124. N. Keller and G.J. Schrobilgen, unpublished work.

125. T.R.G. Syvret, Ph.D. Thesis, McMaster University, Hamilton, Ontario, Canada (1987).

126. J.C.P. Sanders and G.J. Schrobilgen, unpublished work.

127. J.C.P. Sanders and G.J. Schrobilgen, J. Chem. Soc., Chem. Commun., 1576 (1989).

128. H. Meinert, Z. Chem., 9, 389 (1969).

129. (a) K. Seppelt, Angew. Chem., Int. Ed. Engl., 21, 877 (1982). (b) F. Sladky, H. Kropshofer and O. Leitzke, J. Chem. Soc., Chem. Commun., 134 (1973).

130. Ref. (7), pp. 250 - 252.

131. H. Bock, R. Dammel and D. Lentz, Inorg. Chem., 23, 1535 (1984).

132. F.H. Field and J.L. Franklin, In "Electron Impact Phenomena and the Properties of Gaseous Ions", Academic Press, New York, 1957, Chapter 4, p. 113.

133. V.H. Dibeler and S.K. Liston, J. Chem. Phys., 48, 4765 (1968).

134. J.T. Herron and V.H. Dibeler, J. Res. Nat. Bur. Stand., Sect A, 65, 405 (1961).

135. G.P. van der Kelen and P.J. DeBievre, Bull. Soc. Chim. Belg., 69, 379 (1960).

136. D.B. Beach, W.L. Jolly, R. Mews and A. Waterfeld, Inorg. Chem., 23, 4080 (1984).

137. J.T. Herron and V.H. Dibeler, J. Am. Chem. Soc., 82, 1555 (1960).

138. D.M. Rider, G.W. Ray, E.J. Darland and G.E. Leroi, J. Chem. Phys., 74, 1652 (1981).

139. J.T. Herron and V.H. Dibeler, J. Chem. Phys., 33, 1595 (1960).

140. B.W. Levitt, H.F. Widing and L.S. Levitt, Chem. Ind. (London), 793 (1973).

141. H. Neuert, Z. Naturforsch, A 7, 293 (1952).

142. C.R. Brundle, M.B. Robin and N.A. Kuebler, J. Am. Chem. Soc., 94, 1466 (1972).

143. V.H. Dibeler, R.M. Reese and J.L. Franklin, J. Am. Chem. Soc., 83, 1813 (1961).

144. P. Rosums, H. Stafast and H. Bock, Chem. Phys. Lett., 34, 275 (1975).

145. S.R. Prasad and A.N. Singh, Indian J. Phys., Sect. B, 59, 1 (1985).

146. J. Collin, Can. J. Chem., 37, 1053 (1959).

147. I. Omura, H. Baba, K. Higasi and Y. Kanaoka, Bull. Chem. Soc. Jpn., 30, 633 (1957).

148. J.R. Majer and C.R. Patrick, Trans. Far. Soc., 58, 17 (1962).

149. C. Lifshitz and W.A. Chupka, J. Chem. Phys., 47, 3439 (1967).

150. J.E. Huheey, In "Inorganic Chemistry, Principles of Structure and Reactivity", Harper & Row: New York (1978), Chapter 4.

151. C.J. Hoffman, Inorg. Synth., 4, 150 (1953).

152. C.M. King and E.R. Nixon, J. Chem. Phys., 48, 1685 (1968).

153. Pure Appl. Chem., 29, 627 (1972); 45, 217 (1976).

154. G.J. Schrobilgen, In "Synthetic Fluorine Chemistry"; G.A. Olah, R.D. Chambers, and G.K.S. Prakash, Eds.; Wiley, in press.

155. $EA(XeF^{\bullet}) = IP(Xe) + BE(XeF\cdot) - BE(XeF^{\bullet}) = 12.1 + 0.86 - 2.1 = 10.9$ eV.

156. A.A.A. Emara and G.J. Schrobilgen, J. Chem. Soc., Chem. Commun., 1646 (1987).

157. A.A.A. Emara and G.J. Schrobilgen, J. Chem. Soc., Chem. Commun., 257 (1988).

158. P.J. MacDougall, G.J. Schrobilgen and R.F.W Bader, Inorg. Chem., 28, 763 (1989).

159. G.J. Schrobilgen, In "NMR and the Periodic Table", R.K. Harris and B.E. Mann, Eds.; Academic Press: London, 1978, Chapter 14, pp. 439-454.

160. C.J. Jameson, In "Multinuclear NMR", J. Mason, Ed.; Plenum Press: New York, 1987, Chapter 18, pp. 463 - 475.

161. G.A. Olah and T.E. Kiovsky, J. Am. Chem. Soc., 90, 4666 (1968).

162. M. Tsuboi, Spectrochim. Acta, 16, 505 (1960).

163. H.C. Allen, Jr., E.D. Tidwell and E.K. Plyler, J. Chem. Phys., 25, 302 (1956).

164. C. Naulin and R. Bougon, J. Chem. Phys., 64, 4155 (1976).

165. This work.

166. A. Zalkin, D.L. Ward, R.N. Biagioni, D.H. Templeton and N. Bartlett, Inorg. Chem., 17, 1318 (1978).

167. I.H. Hillier and M.A. Vincent, J. Chem. Soc., Chem. Commun., 30 (1989).

168. W. Koch, J. Chem. Soc., Chem. Commun., 215 (1989).

169. M.W Wong and L. Radom, J. Chem. Soc., Chem. Commun., 719 (1989).

170. D.A. Dixon and A.J. Arduengo, Inorg. Chem., 29, 970 (1990).

171. R.J. Gillespie and G.J. Schrobilgen, Inorg. Chem., 15, 22 (1976).

172. J. Burgess, C.J.W. Fraser, V.M. McRae, R.D. Peacock and D.R. Russell, J. Inorg. Nucl. Chem., Suppl., 183 (1976).

173. G.J. Schrobilgen, unpublished work.

174. N. Bartlett, B.G. DeBoer, F.J. Hollander, F.O. Sladky and D.H. Templeton, A. Zalkin, Inorg. Chem., 12, 780 (1974).

175. N. Bartlett, M. Wechsberg, G.R. Jones and R.D. Burbank, Inorg. Chem., 11, 1124 (1972).

176. T. Birchall, R.D. Myers, H. deWaard and G.J. Schrobilgen, Inorg. Chem., 21, 1068 (1982).

177. J.C.P. Sanders and G.J. Schrobilgen, unpublished work.

178. P.A. Agron, G.M. Begun, H.A. Levy, A.A. Mason, G. Jones and D.F. Smith, Science, 139, 842 (1963).

179. G. Herzberg, "Infrared and Raman Spectra of Polyatomic Molecules"; Van Nostrand: New York, 1945; p 174.

180. G.J. Schrobilgen and N. Valsdóttir, unpublished work.

181. (a) J. Mason, In Multinuclear NMR; Mason, J., Ed.; Plenum Press: New York, 1987; Chapter 2, pp. 11 - 13, 19. (b) O. Howarth, ibid.; Chapter 5, pp. 151 - 152.

182. J.A. Pople and D.P. Santry, Mol. Phys., 8, 1 (1964).

183. (a) C.J. Jameson, In "Multinuclear NMR"; J. Mason, Ed.; Plenum Press: New York, 1987; Chapter 4, pp 116-118. (b) C.J. Jameson and H.S. Gutowsky, J. Chem. Phys., 51, 2790 (1969). (c) R.W. Kunz, Helv. Chim. Acta, 63, 2054 (1980). (d) J. Mason, Polyhedron, 8, 1657 (1989). (e) B. Wrackmeyer and K. Horchler, In "Annual Reports on NMR Spectroscopy"; G.A. Webb, Ed.; Academic Press: London, 1989; Vol. 22, p. 261.

184. T. Schaefer, H.M. Hutton and S.R. Salman, Can. J. Chem., 57 1877 (1979).

185. G. Klöter, W. Lutz, K. Seppelt and W. Sundermeyer, Angew. Chem., Int. Ed. Engl., 16, 707, (1977).

186. H. Bürger and G. Pawelke, J. Chem. Soc., Chem. Commun., 105 (1988).

187. H. Henle, M. Geisel and R. Mews, J. Fluorine Chem., 26, 133 (1984).

188. (a) C.J. Jameson, A.K. Jameson, D. Oppusunggu, S. Wille, P.M. Burrell and M. Mason, J. Chem. Phys., 74, 81 (1981). (b) K.T. Schmidt, Ph.D. Thesis, University of Calgary, Calgary, Alberta, Canada (1990).

189. R.J. Gillespie and R. Hulme, J. Chem. Soc., Dalton Trans., 1261 (1973).

190. $EA(KrF^{+}) = IP(Kr) + BE(KrF^{\cdot}) - BE(KrF^{+}) = 14.0 + 0.8 - 1.6 = 13.2$ eV.

191. N. Muller and D.E. Prichard, J. Chem. Phys., 31, 768 (1959).

192. N. Muller and D.E. Prichard, J. Chem. Phys., 31, 1471 (1959).

193. J.N. Shoolery, J. Chem. Phys., 31, 1427 (1959).

194. N. Muller, J. Chem. Phys., 36, 359 (1962).

195. G. Binsh, J.B. Lambert, B.W. Robert and J.D. Robert, J. Am. Chem. Soc., 86, 5564, (1964).

196. J.A. Pople, W.G. Schneider and H.J. Bernstein," High-Resolution Nuclear Magnetic Resonance", McGraw-Hill: New York, 1959, pp. 184 -190.

197. M. Karplus and D.M. Grant, Proc. Natl. Acad. Sci., U.S., 45, 1269 (1959).

198. (a) N.F. Ramsay and E.M. Purcell, Phys. Rev., 85, 143, 1952; (b) N.F. Ramsay, ibid., 91, 303 (1953).

199. R.A. DeMarco, W.B. Fox, W.B. Moniz and S.A. Sojka, J. Mag. Res., 18, 522, (1975).

200. J. M. Lehn and J.P. Kintzinger, In "Nitrogen NMR", M. Witanaowski and G.A. Webb, Eds., Plenum Press: London, 1973, Chapter 3, p. 108.

201. A. Bruylants, M. Tits, C. Dieu and R. Gauthier, Bull, Soc. Chim. Belg., 61, 366 (1952).

202. (a) J.R. Durig and D.W. Wertz, Spectrochim. Acta, Part A, 24, 21 (1968). (b) R.J. Jones and W.J. Orville-Thomas, J. Chem. Soc., 4632 (1965).

203. N.E. Duncan and G.J. Janz, J. Chem. Phys., 23, 434 (1955).

204. V.M. Baryshev, V.V. Ryabova and R. sh. Frenkel, Opt. Spectrosco., 3, 35 (1973).

205. R. Yamadera and S. Krimm, Spectrochim. Acta, Part A, 24, 1677 (1968).

206. K. Kumar, Spectrochim. Acta, Part A, 28, 459 (1972).

207. A.L. Smith, "Applied Infrared Spectroscopy", John Wiley & Sons: New York, 1979, p. 146.

208. J.R. Durig, "Vibrational Spectra and Structure", Elsevier Scientific Publishing: New York , 1977, Vol. 6, pp. 329 - 345.

209. J.E. Bertie and S. Sunder, Spectrochim. Acta, Part A, 30, 1373 (1974).

210. J.R. Durig, K.J. Kanes and J.F. Sullivan, J. Mol. Str., 99, 61 (1983).

211. J.R. Durig, G.A. Guirgis and D.A.C. Compton, J. Chem. Phys., 83, 1313 (1979).

212. T. Klapötke, J. Passmore and E.G. Awere, J. Chem. Soc., Chem. Commun., 1426 (1988).

213. K. Wiechert, H., -H. Heilmann and P. Mohr, Z. Chem., 3, 308 (1963).

214. S. Yanagida, T. Fujita, M. Ohaka, I. Katagiri and S. Komori, Bull. Chem. Soc. Jpn., 46, 292 (1973).

215. (a) F.C. Schaefer, In "The Chemistry of the Cyano Group", Z. Rappoport, Ed., Interscience Publishers: New York, 1970; Chapter 6, pp. 239 - 246. (b) E.N. Zil'berman, Russ. Chem. Rev., 31, 615 (1962).

216. (a) E. Allenstien and A. Schmidt, Spectrochim. Acta, 20, 1451 (1964). (b) S.W. Peterson and J.M. Williams, J. Am. Chem. Soc., 88, 2866 (1966).

217. J.J. Katz and I Sheft, J. Inorg. Nucl. Chem., Supplement, 37 (1976).

218. E. Allenstein, A. Schmidt and V. Beyl, Chem. Ber., 99, 431 (1966).

219. M. Clark and J.S. Thrasher, J. Chem. Educ., 67, 235 (1990).

220. D.L. Long and R.T. Bailey, Trans. Far. Soc., 59, 599 (1963).

221. K. Zuchner, T.J. Richardson, O. Glemser and N. Bartlett, Angew. Chem., Int. Ed. Engl., 19, 944 (1980).

222. D.A. Long and S. Steele, Spectrochim. Acta, Part A, 19, 1791 (1963).

223. J.H.S. Green and D.J. Harrison, Spectrochim. Acta, Part A, 33, 81 (1977).

224. J. Jullien, J. Martin and R. Ramanadine, Bull. Soc. Chim. Fr., 171 (1964).

225. G. Frenking, W. Koch, C.A. Deakyne, J.F. Liebman and N. Bartlett, J. Am. Chem. Soc., 1989, 111, 31.

226. J.C.P. Sanders and G.J. Schrobilgen, In "A Methodological Approach to Multinuclear in Liquids and Solids-Chemical Applications"; NATO Advanced Study Institute, Magnetic Resonance; P. Granger and R.K. Harris, Eds., Kluwer Academic Publishers: Dordrecht, 1990, pp. 157 - 186.

227. N.T. Arner, J.C.P. Sanders, G.J. Schrobilgen and J.S. Thrasher, Proceedings of the Fourth United States Air Force High-Energy Density Matter (HEDM) Conference, Long Beach, California, February 25 - 28, 1990.

228. A.A.A. Emara, D. Hutchinson, A. Paprica, J.C.P. Sanders and G.J. Schrobilgen, Proceedings of the Third United States Air Force High-Energy Density Materials (HEDM) Conference, New Orleans, Louisiana, March 12 - 15, 1989.

229. J.C.P. Sanders, G.J. Schrobilgen and J.M. Whalen, Proceedings of the Fifth United States Air Force High-Energy Density Matter (HEDM) Conference, Albuquerque, New Mexico, February 24 - 27, 1991.